Open Research Online

The Open University's repository of research publications
and other research outputs

# Creep behaviour of the ternary lead-free solder alloy : Sn-3.8wt.%Ag-0.7wt.%Cu

## Thesis

How to cite:

Cooper, Shellene (2002). Creep behaviour of the ternary lead-free solder alloy : Sn-3.8wt.%Ag-0.7wt.%Cu. PhD thesis The Open University.

For guidance on citations see FAQs.

© 2002 The Author

https://creativecommons.org/licenses/by-nc-nd/4.0/

Version: Version of Record

Link(s) to article on publisher's website:
http://dx.doi.org/doi:10.21954/ou.ro.0000d491

Copyright and Moral Rights for the articles on this site are retained by the individual authors and/or other copyright owners. For more information on Open Research Online's data policy on reuse of materials please consult the policies page.

oro.open.ac.uk

UNRESTRICTED

# CREEP BEHAVIOUR OF THE TERNARY LEAD-FREE SOLDER ALLOY: Sn-3.8wt.%Ag-0.7wt.%Cu

A THESIS

SUBMITTED TO THE MATERIALS ENGINEERING DISCIPLINE

OF THE OPEN UNIVERSITY

FOR THE DEGREE OF DOCTOR OF PHILOSOPHY

By

SHELLENE COOPER
(BEng)

November 2002

AUTHOR NO: T206429X
Submission date: 8 November 2002
Award date: 13 October 2003

**ABSTRACT**

Electronic equipment is facing the challenge of both miniaturisation and the need to replace lead in interconnections. In service, interconnections generally fail by thermomechanical fatigue, and this behaviour is strongly affected by the creep process. This thesis examines the creep behaviour of a popular lead-free replacement alloy, Sn-3.8wt.%Ag-0.7wt%Cu (Sn-Ag-Cu), in joint and bulk form. Experimental work involved the determination of the creep properties of this alloy at various temperatures, over a range of stresses.

Over the regions tested, the creep behaviour is best described by the Norton power law constitutive equation. The stress exponent for bulk Sn-Ag-Cu ranged between 10 and 18 (at 125 to −10°C respectively) and indicates that a dispersion-strengthened mechanism is dominant in the creep process. The activation energy for creep in the bulk Sn-Ag-Cu is approximately 120kJ/mol and falls in the region similar to that observed for the self-diffusion of tin. In joint form the stress exponent is greater than 10 at high stresses but a change in mechanism is indicated at lower stress where the creep exponent falls to 3. The activation energy for creep in Sn-Ag-Cu when used in joint form is approximately 70kJ/mol and falls in the region similar to that observed for the short-circuit diffusion of tin.

Results obtained from the ternary alloy were directly compared to those from Sn-37wt.%Pb (Sn-Pb) and other prospective lead-free alloys in bulk form. The creep resistance of the ternary lead-free alloy at 75°C is superior to the conventional Sn-Pb alloy and the possible replacement alloys (tin-copper and tin-silver). This superiority is retained when tested at similar homologous temperatures. However, the Sn-3.8Ag-0.7Cu alloy is less ductile but generally possesses strains to failure above 10 percent in comparison to the 25 to 50 percent ductility of Sn-Pb.

## DECLARATION

This thesis is submitted for the degree of Doctor of Philosophy of the Open University. It is an account of research performed in the Materials Engineering Department, Technology Faculty between June 1999 and October 2002 under the supervision of Professor William Plumbridge and Dr. Ray Matela. The work reported is original and has been performed without collaboration. None of this work has been submitted for a degree or other qualifications at this or any other University. Where the work of other authors has been included in the text, this has been acknowledged in the List of References. Some parts of the work have been presented at an International Conference, during a course presented in Taiwan (May 2001) and will be used in an academic publication in the near future:

W.J Plumbridge, C.R. Gagg and S. Peters. The Creep of Lead-free Solders at 75°C. in 2001 TMS Annual Meeting and Exhibition Lead-free Solder Materials and Soldering Technologies. 2001. New Orleans, Louisiana.

W.J Plumbridge and S. Peters, Methods and Training for Reliability Testing and Data Analysis Week 1: Current Status, Basic Processes, Materials Properties, Course held in Taiwan, May 2001. (to be published as Open University Postgraduate course material)

S. Cooper and W. J. Plumbridge, Creep of Sn-3.8Ag-0.7Cu and Sn-37Pb at 75°C, Presented at symposium on Pb-Free and Pb-Bearing solders at 2002 TMS Fall Meeting, Columbus Ohio, October 2002.

## ACKNOWLEDGEMENTS

I would like to express my sincere gratitude to my supervisor, Professor W.J. Plumbridge, for his invaluable support and guidance throughout this project. Also, the help and advice kindly offered by C. Gagg and N. Williams is gratefully acknowledged.

I appreciate the generous technical assistance supplied by all members of the research laboratories and workshop at the Materials Engineering Department. In particular, I would like to thank P. Ledgard, C. Haynes, and J. Jones for their considerable help in sample manufacture and metallographic preparation.

The author would also like to acknowledge Alpha Metals and Multicore solders for the supply of the solder materials for this research.

Finally, I would like to express my deepest appreciation to my family, friends and most importantly my husband, Mark, for all their support and encouragement throughout the last three years.

*For my gorgeous baby boy, Joshua Ethan, who was born three weeks after the viva voce for this thesis.*

## TABLE OF CONTENTS

## LIST OF TABLES

## LIST OF FIGURES

# CREEP OF THE TERNARY LEAD-FREE SOLDER ALLOY:

# Sn-3.8wt.%Ag-0.7wt.%Cu

# CHAPTER ONE

## 1 INTRODUCTION

The electronics industry currently uses soldering as the primary method of component attachment to printed circuit boards (PCBs). Solder alloys are required to provide mechanical strength as well as both electrical and thermal conductivity to the assembly. Until recently, tin-lead alloys were the preferred choice of solder in this industry. However, at present there is a transition from conventional to 'newer, environmentally friendly' alloys. After describing the factors driving this change, this thesis considers the behaviour of a new, lead-free alloy, in bulk and joint form, during creep, which is a major source of damage in service. The influences of stress, temperature and microstructure on these properties will also be examined.

This introductory chapter provides a background understanding of the current status of lead-free soldering in the electronics industry. It highlights the role of the solder alloy, the factors influencing the transition from conventional to 'new generation' alloys and the legislation affecting this. Some of the major industry and academic participants in the development and implementation of lead-free technology are introduced. The prospective lead-replacement alloys will also be discussed.

### 1.1 Background

Soldering is the joining of two surfaces using a molten filler metal, which leads to the formation of metallurgical bonds (intermetallic compounds) between the filler

and the respective components [1]. This method is used to produce permanent electrical, thermal and mechanical connections between metals.

The project focuses upon solders used within the electronics industry (for example in television sets, mobile phones and computers). The majority of solders used in this industry are referred to as 'soft solders'; they melt below approximately 350°C [2]. Industry currently favours a conventional tin-lead alloy, usually of the eutectic composition tin-37wt.%lead (Sn-37Pb), which has a melting point of 183°C.

Soft solders date back nearly 5,000 years, when Mesopotamians used pure lead to join copper plates together [3]. However, tin-lead solder compositions and their uses in the ancient cultures are obscure. This is because the tin component in the solder reduces to stannic acid, which makes solder identification quite difficult [3]. Soldering entered into the electronics industry in the $20^{th}$ century, providing a reliable way of connecting conducting wires for power and signal generation.

## 1.2 Drivers Towards Lead-free Soldering

Although tin-lead alloys are a common choice for electronic solder, it is well known that lead is a toxic metal and can cause many serious health problems, particularly in children. It has, in the past, been the target of several environmental campaigns; for example, legislation in 1986 (The Safe Drinking Water Act in the United States [4]) was enforced banning lead-containing solder alloys from use in plumbing. Concerns are now arising about the use of lead in industries such as electronics. Lead can contaminate the environment during the disposal of 'end of life' electronic products in either landfill or by incineration. When disposed of into landfill, lead can be leached from the soldered boards under the action of acid rain. Lead leachant can enter into ground water and eventually contaminate domestic water supplies. If equipment is disposed of by incineration, airborne particles of lead

may be released into the atmosphere contaminating surrounding farmland. Lead can be ingested into the body during the consumption of contaminated crops. Those opposed to lead-free soldering have argued that only a small amount of lead is used in electronics with respect to other industries, table 1.1. However, lead emission from landfill waste disposal sites (to which electronics wastes contribute) is quite significant, table 1.2. This can have an effect on both the environment and human health. Various legislative actions, which will be covered later in the chapter, have been initiated to eliminate or reduce lead in electronic equipment. This may be described as the 'environmental push' towards lead-free soldering.

| **Product** | **Consumption (%)** |
|---|---|
| Storage | 80.81 |
| Other oxides (paint, glass etc) | 4.78 |
| Ammunition | 4.69 |
| Sheet lead | 1.79 |
| Cable covering | 1.40 |
| Casting Metals | 1.13 |
| Brass and Bronze billets and ingots | 0.72 |
| Pipes and other extruded products | 0.72 |
| Solder (excluding electronic grade) | 1.70 |
| *Electronic Solder* | *0.49* |
| Miscellaneous | 2.77 |

Table 1.1: Lead Consumption (Fukuda, 1995 [5])

| **Source** | **Emission Level (million metric tonnes)** |
|---|---|
| Transportation | 1.4 |
| Fuel Consumption | 0.4 |
| Industrial Processes | 2.1 |
| *Solid Waste Disposal* | *0.7* |
| Miscellaneous | 0.1 |
| *TOTAL* | *4.7* |

Table 1.2: Lead Emission (Napp, 1996 [6])

In contrast, there are various factors providing a more 'commercial pull' and are proving to be more significant in driving the transition away from conventional soldering materials. As printed circuit technology advances, the requirement of a solder joint is changing, the sizes of components and hence 'end products' are

reducing (miniaturisation). Figure 1.1 shows the miniaturisation of mobile phones since 1996. Surface mount technology (SMT) is replacing the traditional through-hole (TH) wave-soldering method of manufacture (see appendix 1.1). SMT allows attachment of smaller components to both surfaces of a printed circuit board, facilitating miniaturisation. Figure 1.2 shows the types of joints commonly formed in SMT and TH technology. Joint geometries and solder joint volumes vary from joint to joint. This may affect the overall properties. Failure modes may change with type of joint technology and service conditions. SMT joints are expected to support the entire weight of components, conduct electricity and conduct heat produced during service away from the component. This places a greater emphasis on the role and reliability of the modern solder joint. In preliminary studies evaluating the properties of alternative alloys, some lead-free solders such as tin-silver and tin-silver-copper, have proven to be superior in relation to conventional alloys under specific conditions [7-9], especially in creep resistance.

Many companies in Japan are already using lead-free alloys in their production lines. The sales of a (Matsushita) mini disc player manufactured with lead-free solder highlights the potential commercial gain by manufacturers. Once a 'green leaf – lead-free' label was added to the product its market share rose from 4 to 14 per cent [10]. In this case, industry has utilised the consumers' environmental awareness and growing intolerance of lead to its advantage. Hence, countries wanting to compete and export to those already manufacturing using lead-free solders will also have to convert. A combination of all these influences has encouraged a substantial amount of research. Significant research and recommendations concerning alloy choice are highlighted in this section.

Although the driving forces for the transition to lead-free soldering materials have changed, the goal remains the same and the main justification is a commercial one.

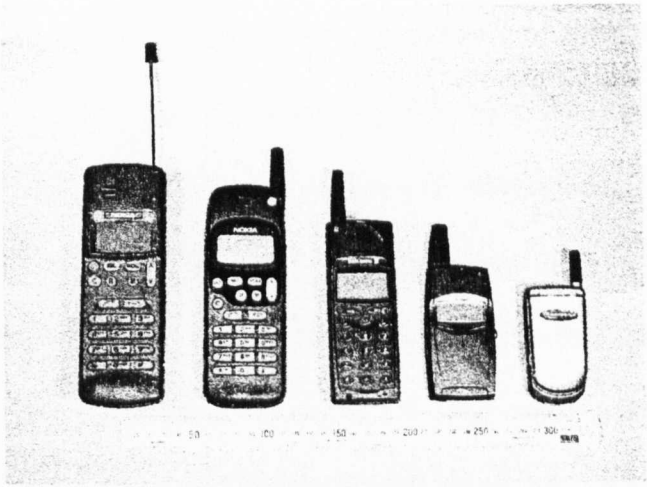

Figure 1.1: An illustration of the miniaturisation of electronic equipment (since 1996)

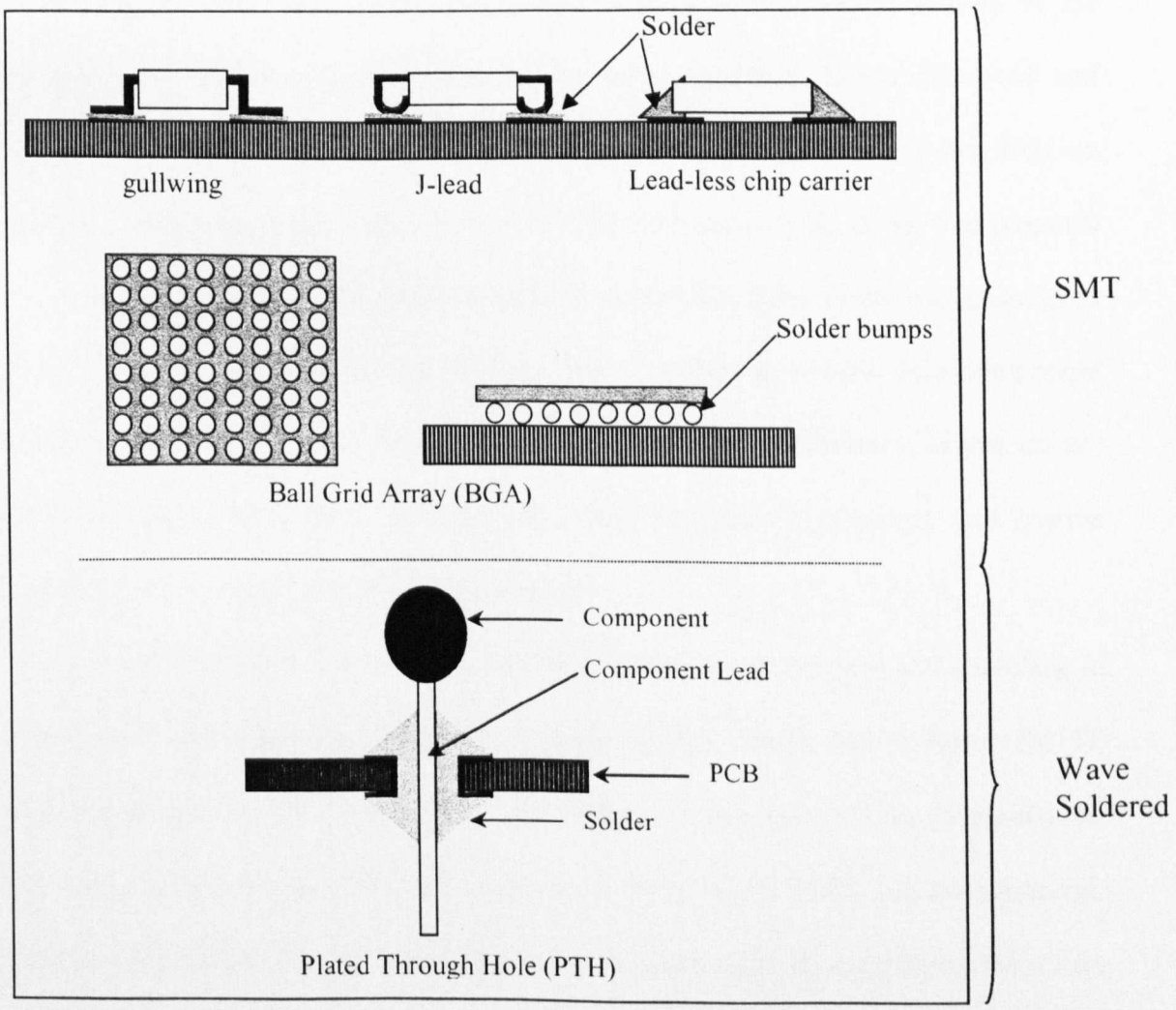


Figure 1.2: Types of joints formed during the manufacture of electronic equipment

### *1.2.1 Summary of Lead-free Legislation*

The initial driving force towards lead-free electronics began in the United States during the 1990s. This was the result of the introduction of the Reid Bill S.391 – Lead Reduction Act in 1991. Another bill emerged in the US in 1993, S.729 – Lead Exposure Reduction Act. However, the electronics industry fought against these claiming that manufacturing with lead-free solders was not possible, and both legislative efforts were dropped. There have since been no further attempts in the US to legislate against lead in solders. Nevertheless, the Environmental Protection Agency (EPA)[11] has recently proposed a crack down on lead emissions from industrial plants. This may in turn impact on the electronics industry.

The biggest challenge to the electronics industry is the current activity in the European Commission. Draft proposals have been published (Waste Electrical and Electronic Equipment (WEEE)) [12] concerning the introduction of restrictions on hazardous material being disposed of in landfill from as early as 2006. The proposal also bans lead (along with other hazardous materials) from electronic assemblies from 1$^{st}$ January 2008. This will not only impact solder alloys but also component finishes, board finishes and flame retardancy issues. These directives, as yet, do not have any legal force, but if adopted, the entire European Community and anyone supplying to it would be required to comply.

The only legislative activity in Japan deals with the reclamation and recycling of electronics. The Japanese Ministry of International Trade and Industry (MITI) introduced this in May 1998 [13]. According to the law, which promotes the recycling of household electrical appliances, from April, 2001[14] manufacturers will be responsible for the reclamation of all lead used in equipment they have produced. Therefore, all household electrical appliance manufacturers are working

towards the creation of completely lead-free products. Many of the major electronics producers have announced time scales in which lead will be phased out of their products. Most companies, that have announced their environmental polices and release dates, expect to be producing lead-free products by 2003. These announcements in Japan have encouraged other nations, particularly the US, to develop lead-free technologies.

## 1.3 Lead-free Solders

### *1.3.1 Solder Alloy Requirements*

Utilisation of SMT and the continuing miniaturisation of electronic equipment have put a greater focus on the role of a solder joint. A solder alloy must offer mechanical support and both thermal and electrical conductivity to a joint. The main considerations for the selection of a new alloy are its processability and performance in service. It is therefore important to consider both.

Processing Requirements

Soldering involves the melting of a small quantity of solder and allowing it to solidify in the correct location to form a metallurgical bond with the components being joined and to provide electrical and thermal conduction. A suitable replacement solder alloy should possess the following attributes. The solder should have a low melting point (similar to that of tin-lead); this will allow energy conservation in production and avoids heat damage to either the board material or component. The liquid solder should solidify quickly allowing rapid production and preventing the movement of components during the soldering process. The alloy constituents should have a lower toxicity to lead. Finally, the solder constituents should be readily available and economically priced.

All solder alloys have a common feature; they are based upon metallic elements of low melting point. In attempting to identify potential alternative alloys, such elements were the obvious starting point. Alloys such as cadmium, mercury and lead were excluded from consideration due to their toxicity. Gallium, bismuth and indium are quite rare elements and therefore cannot be used in significant quantities. Numerous studies [15-22] indicated that on the basis of availability, costs, melting point, toxicity and reactivity, tin-based alloys are the most likely replacement for lead-containing solders. Tin has excellent wetting/spreading properties, is considered non-toxic and is readily available [15]. Alloying tin with a second or third element improves the properties of this alloy and will lower the melting point. Most solder alloys, whether they are binary, ternary or quarternary alloys are of eutectic composition. This implies that there is a single melting temperature i.e. no pasty range. A eutectic will have a have a lower melting temperature than its components (e.g. tin and lead in the conventional electronic grade solder) or any other composition in the system, figure 1.3. The determination of possible alloys was the basis for the preliminary research within the industry, however, work is now more focused on the properties of the major alloys that were identified [23].

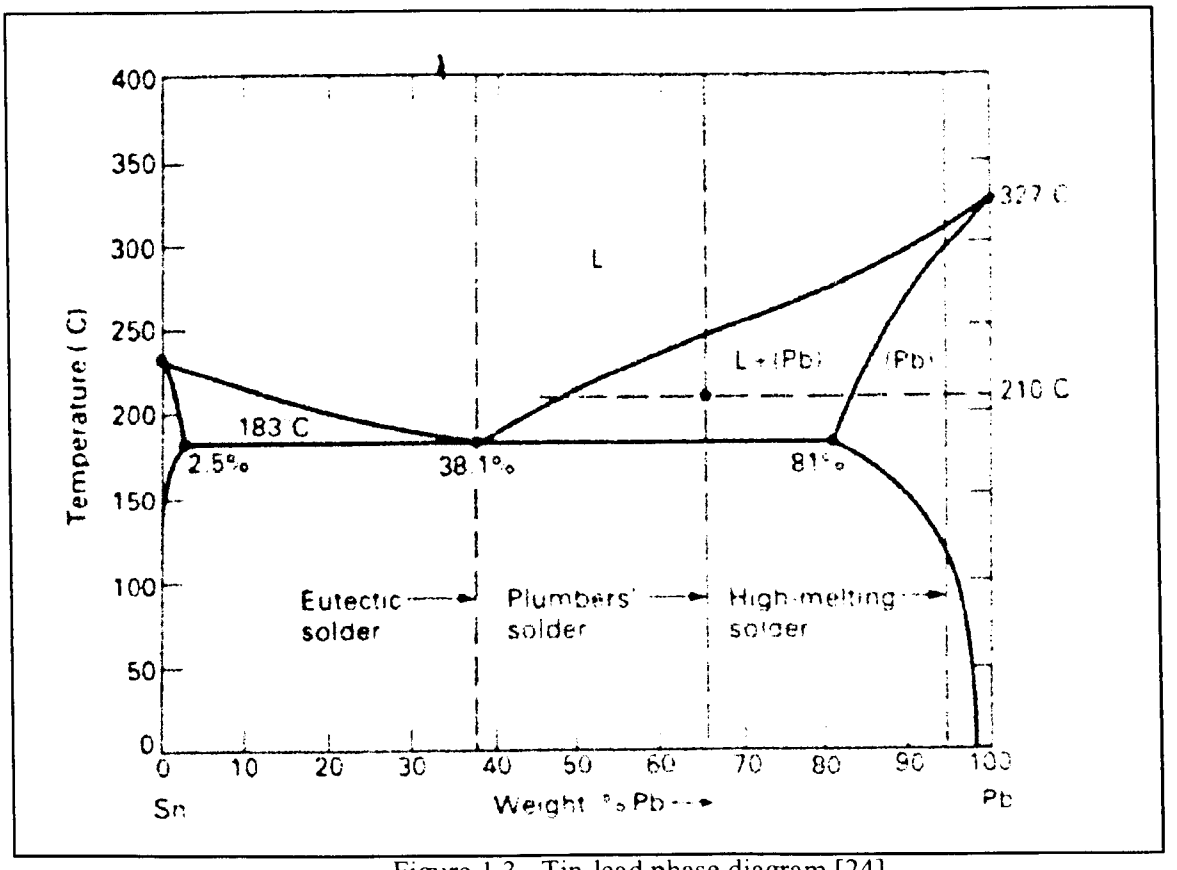


Figure 1.3 Tin-lead phase diagram [24]

Performance Properties

The conditions under which electronic assemblies are required to operate vary dramatically with application. Assemblies may experience elevated temperatures, temperature cycles and dwells caused by power switching and external factors. Temperature is frequently the biggest variant in service and depending on application can range from –55 °C to 180°C.

Modern electronic materials can have widely different coefficients of thermal expansion (CTEs), table 1.3, and this can result in thermo-mechanical fatigue (TMF). As the 'softest' material in the assembly, solders absorb most of the varying stresses/strains created by the CTE mismatch during the heating and cooling of the materials that constitute the joint. The mismatch created is illustrated in figure 1.4, where $\alpha_s$ and $\alpha_c$ are the coefficients of thermal expansion for the two materials, and

'h' is the height of the solder joint. $T_{min}$, $T_0$ and $T_{max}$ are the minimum, equilibrium and maximum temperatures. If the CTE of the lower bar ($\alpha_s$) is greater than the CTE of the upper bar ($\alpha_c$), the lower bar contracts more on cooling and expands more on heating. The respective relative displacements are:

On cooling to $T_{min}$ $$(\alpha_s - \alpha_c)(T_o - T_{min})L/2 \quad (1.1)$$

and on heating to $T_{max}$ $$(\alpha_s - \alpha_c)(T_{max} - T_0)L/2 \quad (1.2)$$

The shear strain, $\gamma$, is displacement/height, so, for a complete thermal cycle between $T_{min}$ and $T_{max}$, the shear strain range, $\Delta\gamma_t$, is given by:

$$\Delta\gamma_t = \frac{(\alpha_s - \alpha_c)(T_{max} - T_{min})L}{2h} \quad (1.3)$$

indicating that the height of the solder is influential in TMF and consequently the failure of the joint.

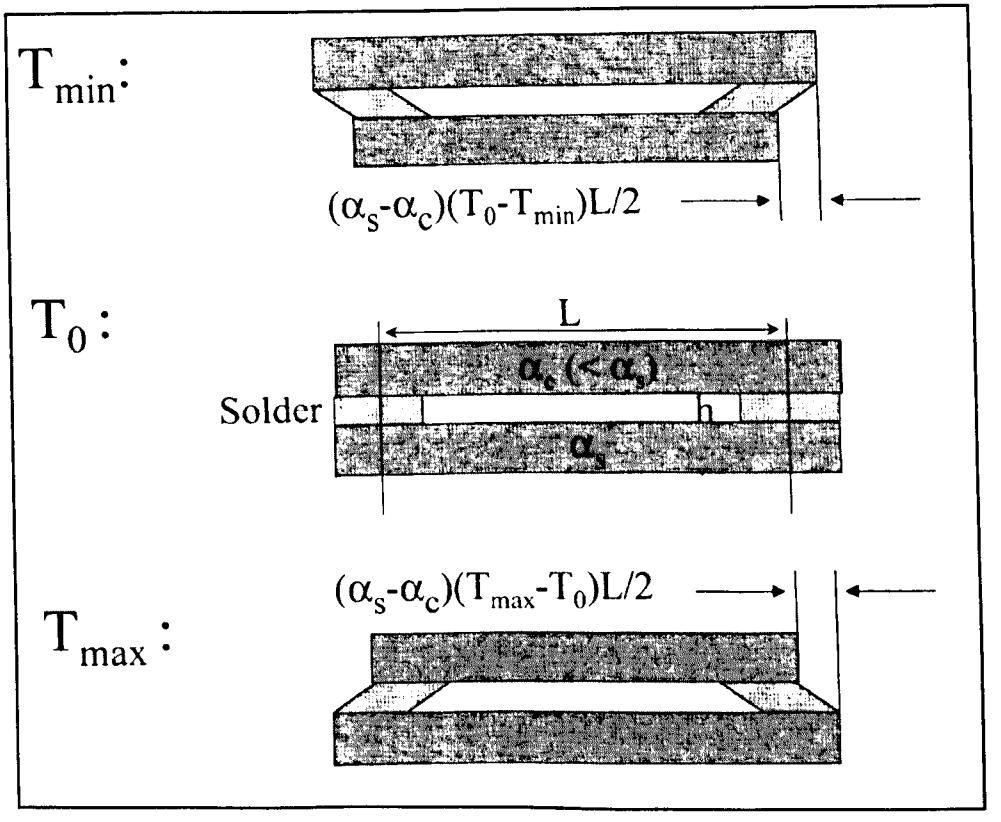


Figure 1.4 Schematic of shear strain due to thermal mismatch in solder joints

TMF is a concern to the electronics industry, but it is complicated and difficult to replicate under laboratory conditions. So, for the purpose of accelerated testing, TMF is often split into two components – creep and fatigue.

In addition to temperature cycles during service, there may be periods of time where the temperature remains constant (dwells) and the material is 'held' at a high homologous temperature. The homologous temperature, $T_h$, is the temperature at which a material operates relative to its melting point in degrees Kelvin ($T_h = T/T_m$). At homologous temperatures greater than 0.4, materials are susceptible to creep (or stress relaxation). For the Sn37Pb and SnAgCu alloys, room temperature is equivalent to an homologous temperature of 0.66 and 0.62 respectively, indicating that creep is always a potential problem in service. It is therefore necessary to understand the creep, in addition to fatigue, mechanisms that can occur.

| Material | Young's Modulus (GPa) | Poisson's Ratio | Yield Stress (MPa) | Coefficient of Thermal Expansion (ppm/K) |
|---|---|---|---|---|
| Ceramic Package | 250 | 0.30 | | 5.0 |
| Alloy 42 (Fe-42Ni) | 140 | 0.30 | 380 | 4.4 |
| Copper | 120 | 0.35 | 380 | 17.7 |
| Solder | 35 | 0.28 | 30 | 20.0 |
| Plastic Package | 14 | 0.30 | | 18.6 |
| FR-4 board | 11 | 0.28 | | 14.7 |

Table 1.3 Typical material properties in electronics components (Schmidt *et al*, 1995[25])

### *1.3.2 Development of Lead-free Solders*

To meet both the legislative and commercial demands described, replacement solder alloys for tin-lead are required.

Preliminary studies (for example by the National Centre for Manufacturing Sciences [26] and a collaboration between the Department of Trade and Industry,

International Tin Research Institute, Multicore and GEC-Marconi in 1991 [15]) show that there is not an ideal 'drop in' replacement for the conventional Sn-37Pb alloy. Therefore, a compromise of properties is necessary. Possible alternative alloys, recommended in the Department of Trade and Industry publication [20], are based upon one of the following five groups: tin-copper (Sn-Cu), tin-silver (Sn-Ag), tin-silver-copper (Sn-Ag-Cu), tin-silver-bismuth (Sn-Ag-Bi) and tin-zinc-bismuth (Sn-Zn-Bi) (table 1.4). Zinc containing alloys tend not to be considered due to the reactive and corrosive nature of zinc, which may cause processing concerns. The alternative alloys can have a wide range of melting temperatures, from 110°C up to 365°C [27]. The choice of alloy will depend on the service temperature and conditions of specific applications.

| Alloy System | Composition (wt %) | Melting Range (°C) |
|---|---|---|
| Sn-Bi | Sn-58Bi | 138 (e) |
| Sn-Bi-Zn | Sn-8Zn-3Bi | 189-199 |
| Sn-Ag | Sn-3.5Ag | 221 (e) |
| Sn-Cu | Sn-0.7Cu | 227 (e) |
| Sn-Ag-Bi | Sn-3.5Ag-3Bi | 206-213 |
| Sn-Ag-Cu | Sn-3.8Ag-0.7Cu | 217 |

(e) denotes the eutectic composition

Table 1.4: Solder compositions and melting points (Richards *et al*, 1999[20])

### *1.3.3 Alloy Compositions*

The characteristics of each of the most common alloy compositions highlighted above are now considered.

**Sn-Cu (Sn-0.7Cu):** This is an attractive alloy as it is one of the cheapest lead-free alloys available. Cost is particularly significant when filling a wave solder bath for the first time (for example, the capacity of a bath can be 400kg of Sn-Pb). However, Sn-0.7Cu has the highest melting temperature. This would probably incur greater manufacturing costs, as processing temperatures would have to be raised. In addition, Sn-Cu possesses poor mechanical properties relative to the other lead-free candidates

[7], so the range of potential applications is restricted. It has been recently demonstrated that the alloy is susceptible to the formation of tin-pest when subjected to temperatures below 12°C for prolonged periods of time [28].

**Sn-Ag (Sn-3.5Ag):** This is a eutectic alloy with a melting point of 221°C and amongst the lead-free alloys it has been extensively investigated. Mechanical testing has shown that the silver-containing alloys have superior properties to Sn-Cu and Sn-Pb [7] particularly in respect of creep resistance.

**Sn-Ag-Bi (Sn-3.5Ag-3Bi):** This alloy has a lower melting point than other lead-free alternatives and minor composition variations melt in the range 200-210°C. The solderability of these alloys was found to be the best of the replacement alloys [20] as confirmed by Matsushita [10]. However, particularly when in contact with Sn-Pb component finishes, the alloy shows a tendency to exhibit fillet lifting or hot tearing during solidification [29].

**Sn-Zn-Bi (Sn-8Zn-3Bi):** Alloys based on Sn-Zn have not proven to be as successful as other candidate alloys, although they can be produced with melting temperatures very close to that of the Sn-Pb eutectic. The presence of zinc causes many problems related to its reactivity, such as: potential corrosion, excess drossing and oxidation, requirement for relatively active fluxes, and very short shelf lives of pastes produced using this alloy [20].

**Sn-Ag-Cu (Sn-3.8Ag-0.7Cu):** This alloy has been developed more recently as an improvement on the basic Sn-Ag alloy. It produces a ternary eutectic at 217°C, a lower melting point than the binary Sn-Ag alloy, although the actual ternary eutectic composition is still a matter of debate. The Sn-3.8Ag-0.7Cu alloy was recommended for general-purpose use by the Brite-Euram IDEALS project [30, 31]. Studies have

shown that the ternary alloy has superior properties and solderability than other alternatives such as Sn-Ag and Sn-Cu [7].

Iowa State University patented a Sn-4.7Ag-1.7Cu alloy as the ternary eutectic composition in June 1996 (Patent Number 5,527,628) [32]. The patent covered any alloy in the range of Sn-3.5-7.7Ag-1.0-4Cu, (using at least 89 percent tin). A licensing agreement was made by Ames Laboratory, Iowa State with Multicore Solders, Johnson Manufacturing and Nihan Superior Company for the manufacture and supply of this alloy [33, 34]. To explore compositions outside of the patent, Sn-3.8Ag-0.7Cu and Sn-4.0Ag-0.5Cu were developed. The electronics industry can now use an alternative ternary composition to that patented and hence, not be forced to buy solder from a limited number of suppliers or pay '*royalties*' to the patent holders. The alternative alloys have proven to be just as good as the patented composition [35, 36].

Of the several lead-free alternatives suggested as replacement alloys, the ternary Sn-Ag-Cu alloy is emerging to be the favourite for general-purpose applications. For low temperature use, Sn-58Bi is a likely candidate. While the favourites have been identified, it must be appreciated that little is known about their more complex mechanical behaviour, which will influence service performance.

### *1.3.4 Research Activities at the Open University*

The Solder Research Group at the Open University (SRG) is currently running an EPSRC funded programme concentrating on solder alloys for use in electronics. Focus is placed upon the performance of a sound joint, i.e. one with no defects. Many mechanical properties have been evaluated along with examination of the effects of strain rate, temperature and ageing. In conjunction with mechanical testing, extensive metallography of tested samples has been performed to provide a better

understanding of the mechanisms of failure. The overall strategy of this research is to compare the behaviour of bulk solders, model joints and printed circuit boards under similar conditions. Therefore, allowing the determination of any correlation between bulk and board behaviour [8]. To date, the SRG has established an extensive base of bulk mechanical properties for the conventional alloy (Sn-37Pb) and the more popular lead-free replacements. In addition to mechanical testing, computational modelling is under investigation. It has been shown that employing incorrect values for mechanical properties can render sophisticated computations useless. Therefore, the SRG has materials engineers and computer modellers working in close conjunction to establish reliable computer models. An important fact arising from the SRG work is that the relative performance of alloys may change if the assessment conditions change. Therefore, alloy selection must be determined under conditions appropriate to service. The work completed for this project 'slots' into the overall objectives of the SRG. Results obtained for this project will be compared with other data collated from the SRG work later in the discussion section.

## 1.4 Project Outline

Despite significant research, there is still insufficient understanding of the behaviour of lead-free alloys. Since solders operate at high temperatures relative to their melting point, creep behaviour is a major consideration. The project examines the creep of a lead-free solder alloy (Sn-3.8Ag-0.7Cu) which is one of the favourites to replace the lead-containing alloys and was identified by IDEALS and NEMI as the most likely general-purpose replacement alloy [9, 37]. The work focuses on the microstructure which most closely resembles that found in actual, soldered joints.

A combination of testing and extensive metallography provides a better understanding of the creep behaviour of this alloy. Data collected from the creep

testing of bulk alloys allows the relationships between applied stress, time to rupture, temperature and minimum strain rate to be established. The properties of this alloy are also compared with tin-lead and other potential lead-free alternative alloys.

Phase two of the programme uses the Sn-3.8Ag-0.7Cu alloy in simple copper 'pin in ring' joints to determine the effects of intermetallic compounds and loading in shear. Mechanical testing and metallography allows a comparison to be made between bulk and joint behaviour, enabling the determination of possible correlation.

The next two chapters of the thesis present a review relevant to the research objectives, starting with the fundamentals of creep deformation (chapter two). The chapter describes the quantitative evaluation of creep data (for example, the effects of temperature and stress) followed by the mechanisms of creep deformation. Chapter three highlights the microstructural changes occurring when solders are used in joint form. Also, the importance of joint geometry is reviewed along with various manufacturing methods of a chosen joint geometry. The materials, sample manufacture and testing techniques used in this research are introduced in chapter four. Chapter five presents the creep response of the bulk ternary alloy over a range of temperatures. The second part of this chapter describes the equivalent behaviour of joints. In chapter six, the results are analysed, discussed and compared with data obtained from various other alloys. The quantitative results are examined alongside the microscopy findings to explore relationships between creep properties and microstructure. In this chapter, a correlation between joint and bulk behaviour is investigated. Finally, this chapter compares the bulk behaviour of Sn-Ag-Cu with the findings from other alloys examined during the SRG research programme. The main conclusions and recommendations for further work are summarised in chapter seven.

# CHAPTER TWO

## 2 FUNDAMENTALS OF CREEP

This research focuses upon the creep component of thermo-mechanical fatigue in solders. Creep is the time dependent deformation of a material under constant load or stress and occurs at homologous temperatures greater than 0.4. The following chapter explains the quantitative aspects of creep and describes various creep mechanisms that can occur. Due to a limited quantity of data specifically on the ternary alloy, published literature relating to tin-lead, tin-silver and tin-silver-copper alloys is discussed.

### 2.1 Quantitative Aspects of Creep

The principal objective of a creep test is to study the effects of temperature and stress on the minimum creep rate and time to rupture. Figure 2.1 shows an idealised curve obtained from a test measuring strain as a function of time under constant load or stress. The curve itself can be separated into three individual regions (not including the instantaneous strain): primary; secondary; and tertiary creep. It should be noted that the extent of primary, secondary and tertiary creep vary, depending on the material and test conditions.

On the application of a load, an instantaneous strain, $\varepsilon_0$, occurs. After this, further deformation occurs at a diminishing (strain) rate, 'primary creep'. Following primary creep a linear portion of the curve occurs, where creep strain rate is essentially constant and at a minimum i.e. 'secondary (or steady state) creep'. After reaching a minimum during secondary creep, the creep rate increases with time until failure 'tertiary' creep.

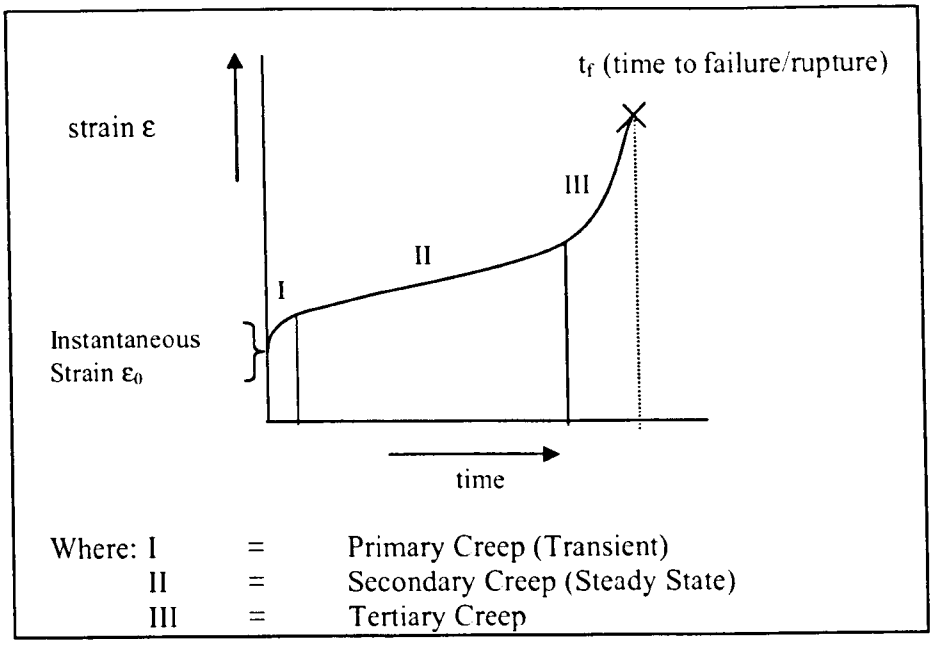


Figure 2.1: An idealised strain vs. time curve for a pure metal

Primary creep is sometimes referred to as transient creep and can follow a $t^{1/3}$ law:

$$\varepsilon_{pc} = at^{1/3} \qquad (2.1)$$

where: a = constant
t = time

Generally, at high temperatures primary and steady state creep occur together and obey the relationship:

$$\varepsilon_{p\&s} = at^{1/3} + bt \qquad (2.2)$$

where: bt represents steady state creep (b is a constant).

Some attempts have been made to incorporate tertiary creep into equation (2.2) to represent the strain – time behaviour throughout a creep test [38], equation 2.3:

$$\varepsilon_{all} = at^{1/3} + bt + ct^3 \qquad (2.3)$$

where: a, b and c are constants

However, the estimation of the entire creep curve is difficult due to the varying deformation and damage processes that may occur. Generally, when the creep

process has been considered in the past, most emphasis has been placed on the steady state creep behaviour. Steady state creep is now considered in the following sections.

### *2.1.1 Temperature Dependence of Secondary Creep Rate*

Creep rate increases exponentially with temperature and an increase in temperature of 20°C can double the creep rate [24]. At higher temperatures, more vacancies are present allowing diffusion to occur more rapidly and dislocations to climb more freely. Therefore, higher temperatures lead to a decrease in creep life as illustrated by figure 2.2. Dislocation movement in creep is considered in section 2.2.1.

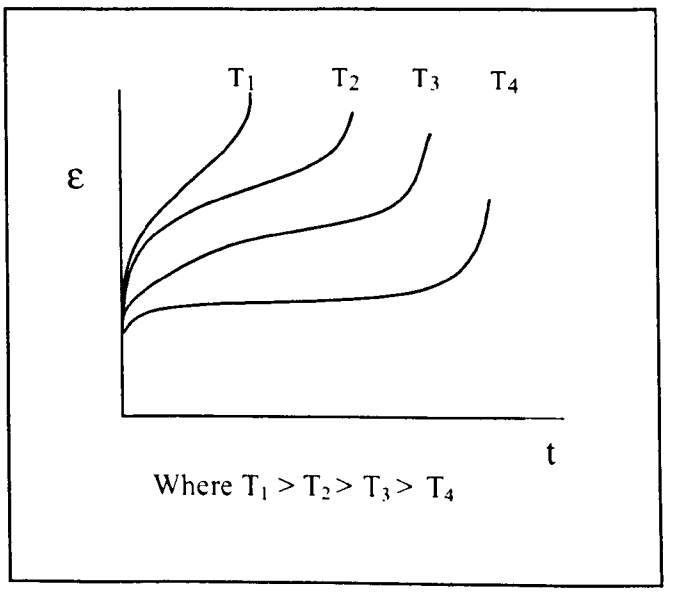


Figure 2.2: Schematic diagram showing the temperature dependence of creep

The following Arrhenius equation illustrates the relationship between steady state creep rate and temperature. Steady state creep rate ( $\dot{\varepsilon}_{ss}$ ) is proportional to exp. $^{-(Q\,RT)}$

$$\text{i.e. } \dot{\varepsilon}_{ss} = A_2 . \exp.^{-(Q\,RT)} \qquad (2.4)$$

Where: $A_2$ = constant
R = Universal Gas Constant
Q = Activation Energy for creep

To determine the activation energy 'Q', an Arrhenius plot of natural logarithm (ln) of $\dot{\varepsilon}_{ss}$ versus reciprocal of the absolute temperature and universal gas constant (1/RT) is used. A straight line with a gradient of –Q is expected, see figure 2.3 [24]. Alternatively, a plot of $\ln \dot{\varepsilon}_{ss}$ versus 1/T can be used which produces a gradient of $-Q_c/R$.

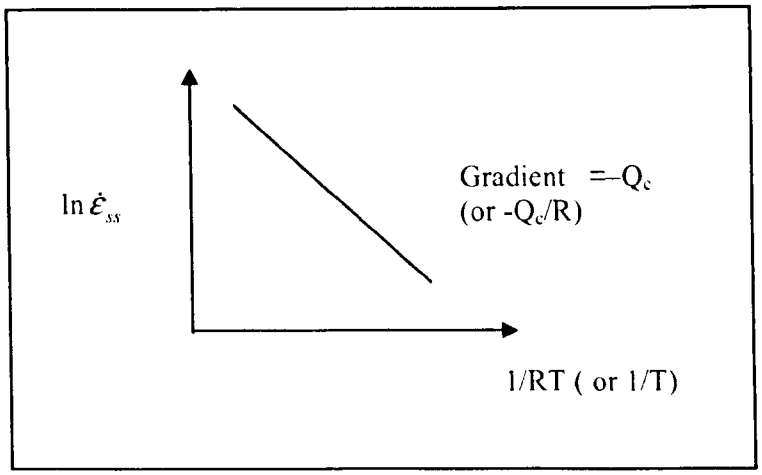


Figure 2.3: Idealised diagram showing the determination of activation energy

### *2.1.2 Stress Dependence of Secondary Creep Rate*

Figure 2.4 illustrates the stress dependence of creep. As the stress increases, the time to rupture decreases and the proportion of steady state creep appears to decrease. These observations are investigated with relation to the ternary alloy in chapter five.

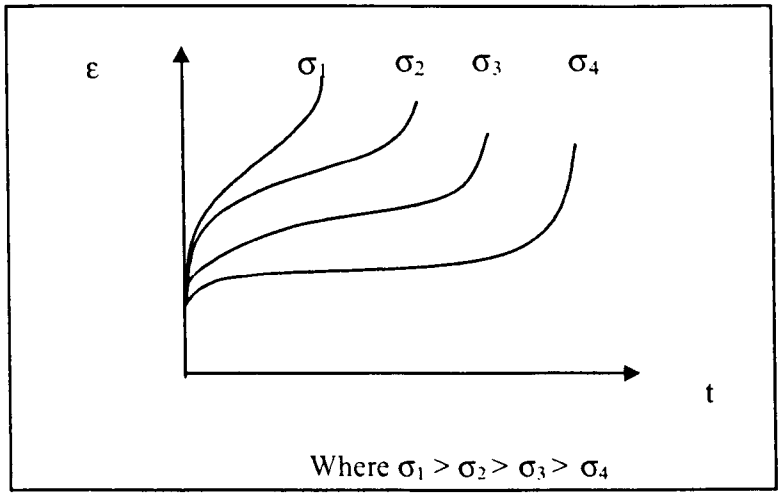


Figure 2.4: The influence of applied stress on creep

The minimum creep rate is generally related to the applied stress by a series of equations depending on the dominant creep mode. Equation 2.5 demonstrates the power law relationship between steady state creep rate and stress. By plotting $\log \dot{\varepsilon}_{ss}$ against log σ at constant temperature, a value of creep (or stress) exponent 'n' can be determined, from the gradient of the line produced, figure 2.5. This tends to be one of the most widely used equations when describing the creep behaviour of solders (section 2.3)

$$\dot{\varepsilon}_{ss} = A_1 \sigma^n \qquad (2.5)$$

Where: $A_1$ = constant
n = creep/stress exponent.

Other relationships include

$$\dot{\varepsilon}_{ss} = A_3 \exp(a\sigma) \qquad (2.6)$$

and $$\dot{\varepsilon}_{ss} = A_4 \sinh(\alpha\sigma) \qquad (2.7)[40]$$

Where: $A_3$, $A_4$, a and α = constants

Here, equation 2.6 represents exponential creep and 2.7 combination creep. The combination creep relationship is generally used where a transition between two or more dominant creep mechanisms is suggested by a change in gradient of the log $\dot{\varepsilon}_{min} = n.\log\sigma + A_1$ relationship, figure 2.5. This is discussed in greater detail when describing the model joint data in section 5.2.5.

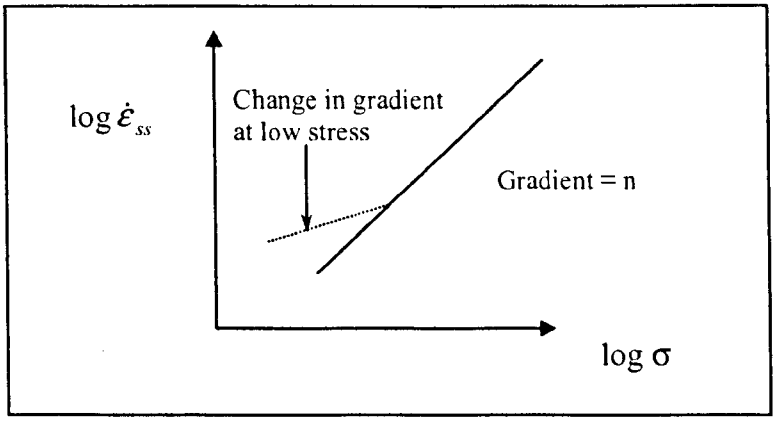


Figure 2.5: Idealised diagram to show the determination of creep exponent

Since steady state creep is a function of both stress and temperature i.e.

$$\dot{\varepsilon}_{ss} = u(\sigma).v(T)$$

The resulting equation relating to $\dot{\varepsilon}_{ss}$ (by combining equations 2.4 and 2.5) is as follows:

$$\dot{\varepsilon}_{ss} = A_5\sigma^n exp.^{-(Q/RT)} \qquad (2.8)$$

Where: $A_5$ = constant

$A_5$, n and Q will vary from material to material and are all determined experimentally. The values of both creep exponent 'n' and activation energy 'Q' are important as, generally, they provide an indication of the dominant mechanisms occurring in creep under specific conditions [38].

The creep/stress exponent 'n' can range from 1, at low stresses, to around 18 in solders at higher stresses, (see literature review at the end of this chapter for

examples). Typically, 'n' lies between 3 and 8 at high stresses and this type of creep is termed power law creep [24]. Values higher than 8 are usually found for dispersion strengthened alloys, where a dispersion of second phase particles inhibits dislocation motion [41], increasing creep resistance.

### *2.1.3 Monkman-Grant Relationship*

Another relationship utilising steady state creep rate is the Monkman-Grant relationship [42]. Here, the product of steady state creep rate ($\dot{\varepsilon}_{min}$) and time to rupture ($t_r$) is constant and by plotting $\log \dot{\varepsilon}_{min}$ versus $\log t_r$ a straight line is produced (see chapter five). This relationship may be used to predict the lifetime of a sample once steady state creep has been achieved. However, care must be taken as a change in dominant creep mechanism (particularly at low stresses) will cause a change in the trend slope, leading to an overestimation of lifetime.

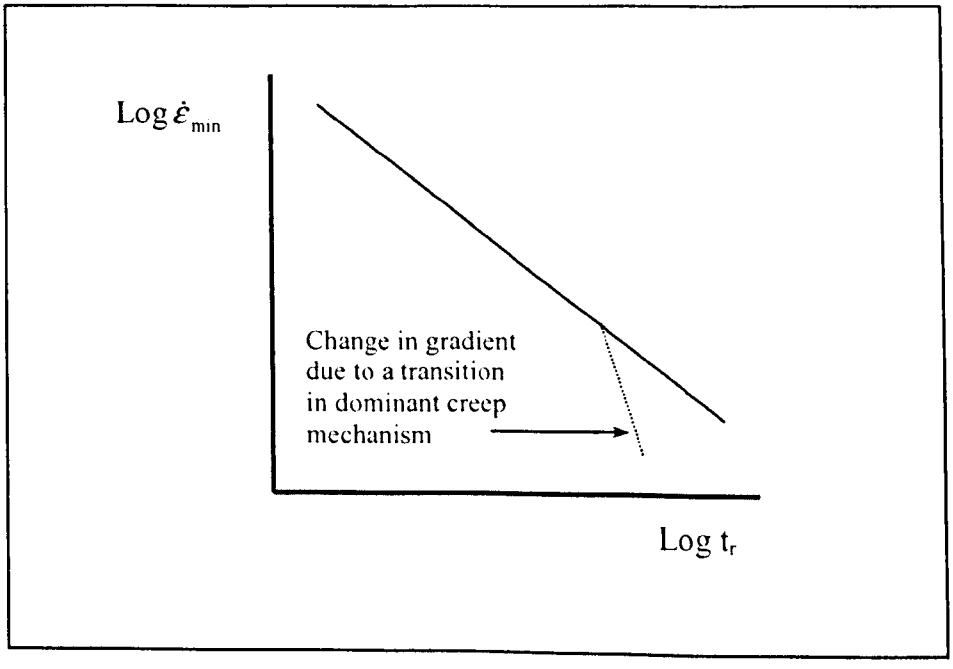


Figure 2.6 Schematic of Monkman-Grant relationship to illustrate possible discrepancies during creep life prediction

## 2.2 Creep Mechanisms

Either dislocation or diffusional mechanisms can dominate creep deformation. The rates of both mechanisms are dependent upon diffusion and follow an Arrhenius type relationship. Diffusion is the mass transport by atomic motion and can occur using different 'paths' e.g. lattice/self diffusion or short circuit diffusion, and these terms may be used in the description of the creep process. Diffusion mechanisms rely on vacancies present within the structure for atoms to move into. 'Lattice or self diffusion' is a process that takes place through the bulk lattice of the crystal and excludes such mechanisms as short circuit diffusion [43]. 'Short circuit diffusion' is any diffusion process occurring via grain boundaries (grain boundary diffusion), surfaces or dislocations (core or pipe diffusion). Since the ternary alloy is tin-based, the activation energies for tin are of most interest. In general, the activation energy for short circuit diffusion in tin (≈60kJ/mol) is half that of self-diffusion (≈120kJ/mol) examples of which are referred to in [44] [45]), although there is a wide variation of data in the published literature. Diffusion occurring within an alloy is significant above a homologous temperature of 0.4. Consequently, creep is an important consideration when service temperatures rise above this value [46].

During this research, the creep behaviour of a solder was examined and, given their low melting points, solders can be referred to as high temperature alloys i.e. homologous temperatures in excess of 0.4 are seen in service. Although not classed as a conventional high-temperature material, in comparison to those materials usually associated with high temperature applications, such as nickel-based alloys, solders operate at equivalent or higher homologous temperatures (figure 2.7). Therefore, creep is an important factor in the life of a solder joint, emphasising the importance of

understanding creep behaviour and mechanisms. The following three sub-sections consider the individual creep mechanisms in more detail.

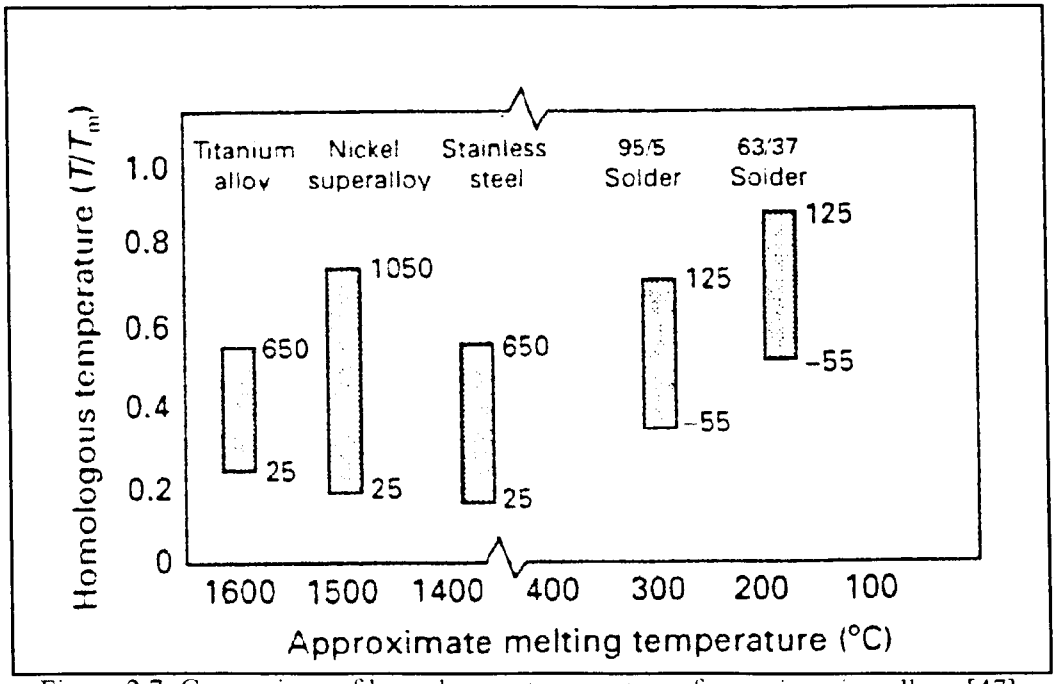

Figure 2.7: Comparison of homologous temperatures for engineering alloys [47]

### *2.2.1 Dislocation Creep*

A dislocation is a line defect; and movement of these within a crystal is the principal mechanism for creep deformation at high stresses. When they move through a crystal, dislocations produce plastic, permanent strain [24]. A shear stress must be applied to a crystal in order to force the dislocation through it, 'slip'. For yielding to occur, this force must be great enough to overcome any resistance to dislocation motion. Resistance can be due to alloying precipitates, grain boundaries, lattice friction or dislocation tangles (work hardening).

Diffusion can enable dislocations to free themselves from obstructions, which is termed 'recovery'. When a vacancy arrives at the end of the half plane, the dislocation will climb [48]. Dislocation climb is the movement of an edge dislocation in a direction normal to its slip plane. Once climb has occurred, the dislocation will be free to move (i.e. is no longer pinned on precipitates, solute atoms or other

dislocations). When the 'free' dislocations start to glide, they may become tangled again with other obstacles. The process will then start again. Dislocation density can be reduced by a combination of slip and climb. Each dislocation will undergo climb until both lie on the same slip plane. Since edge dislocations of opposite sign attract, they move together by slip and annihilate one another.

Dislocations can also overcome obstacles by the process of 'cross slip'. This is the switching of a moving dislocation from one slip plane to another, which occurs whenever it changes its direction of glide [39]. Cross slip is promoted by a 'back stress' produced by dislocations trapped by obstacles. This 'back stress' exerts a force on other dislocations, which lie within that slip plane. These are then forced to find alternative routes to overcome the obstruction, i.e. by using secondary slip planes. Figure 2.8 shows the process of cross slip where the alternative route taken by the dislocation is highlighted by bold arrows.

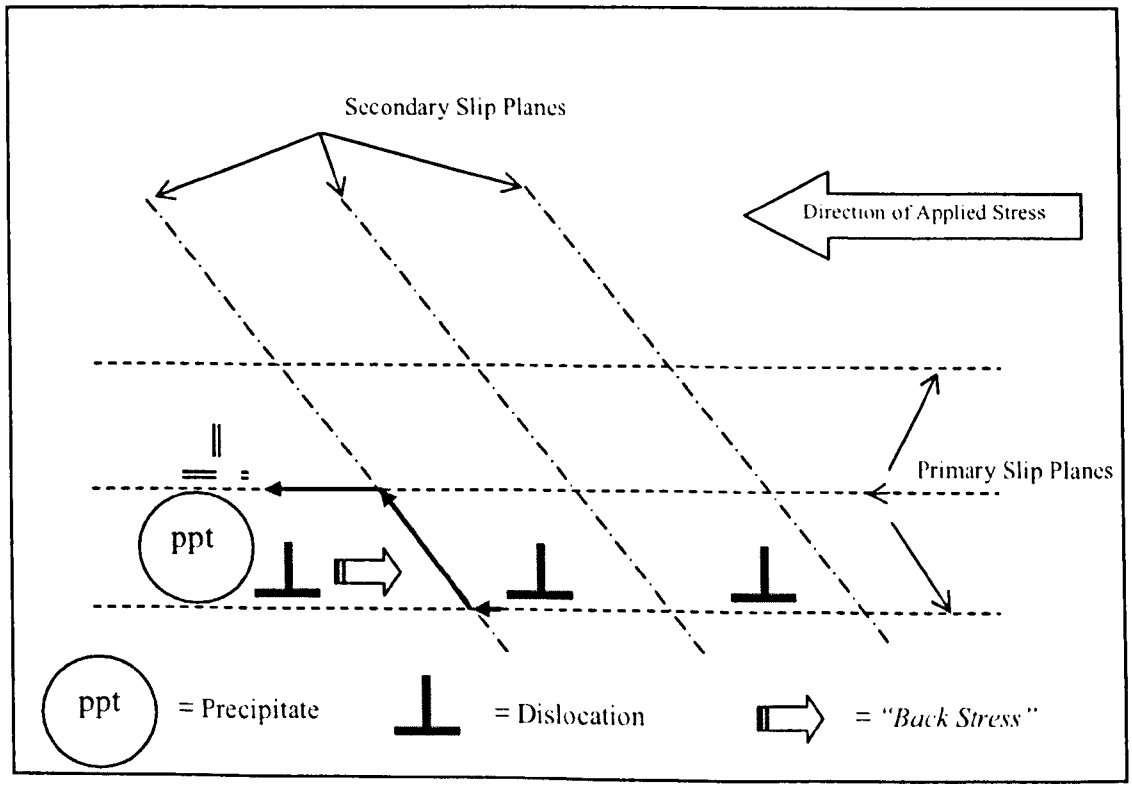


Figure 2.8: An illustration of the process of cross slip

Description of a Typical Creep Curve for Sn-3.8Ag-0.7Cu

This sub-section describes the mechanisms behind the creep curve seen in figure 2.1 with relation to the dislocation motion described above. An elastic instantaneous strain occurred on loading. The creep strain rate then decreases (primary creep) due to dislocations present within the alloy gliding in their slip plane until they encounter other dislocations or obstacles. They become tangled and are more resistant to further movement, leading to work hardening. Work hardening and recovery processes take place most of the time. However, during primary creep, work hardening occurs more rapidly than recovery and during secondary creep, work hardening is balanced by recovery. The balance of work hardening and recovery produces the straight part of the curve – steady state creep.

After reaching a minimum during secondary creep, the creep strain rate '$\dot{\varepsilon}$' increases with time and strain, becoming tertiary creep. This is associated with various structural changes occurring within the alloy. These could be the onset of recrystallization, coarsening of the microstructure or other damage such as the formation of internal cracks or voids. Strain occurs at an increasing rate until failure. In solder alloys, failure frequently occurs in a ductile manner, typically associated with 'necking'. Immediately prior to failure, necking takes place and cracks grow by the coalescence of voids. During necking, the plastic flow becomes localised across one section of the specimen producing a reduction in cross-sectional area. Therefore, as the cross-section shrinks, the stress within the neck increases above that of the other cross-sections. If straining continues, a point is reached where the stress in the neck exceeds the work hardening [48]. In which case the neck deforms at an accelerating rate until failure occurs.

### 2.2.2 *Diffusional Creep*

Diffusional creep involves the stress-directed flow of vacancies that takes place in order to restore an equilibrium condition. It can occur either by lattice or grain boundary diffusion, Nabarro-Herring and Coble creep respectively.

The Nabarro-Herring mechanism [49, 50] dominates the creep process at low stress levels and high temperatures and is accomplished by diffusional mass transport [51] in the bulk of the material [52]. This mechanism occurs at temperatures greater than $T_h = 0.7$ (approximately 70°C for the Sn-Ag-Cu alloy), when there are more diffusional paths in the bulk than in the grain boundary.

Figure 2.9(a) illustrates the diffusion process occurring during Nabarro-Herring creep. There is a higher vacancy concentration in the regions of a material experiencing a tensile stress in comparison to those subjected to a compressive stress [51]. This produces a vacancy flux from the regions of material under tension to those subjected to compression. Therefore, there will be a migration of atoms in the opposite direction resulting in an elongation of the individual grains along the tensile axis and this is equivalent to a creep strain, (see figure 2.9b and figure 2.10).

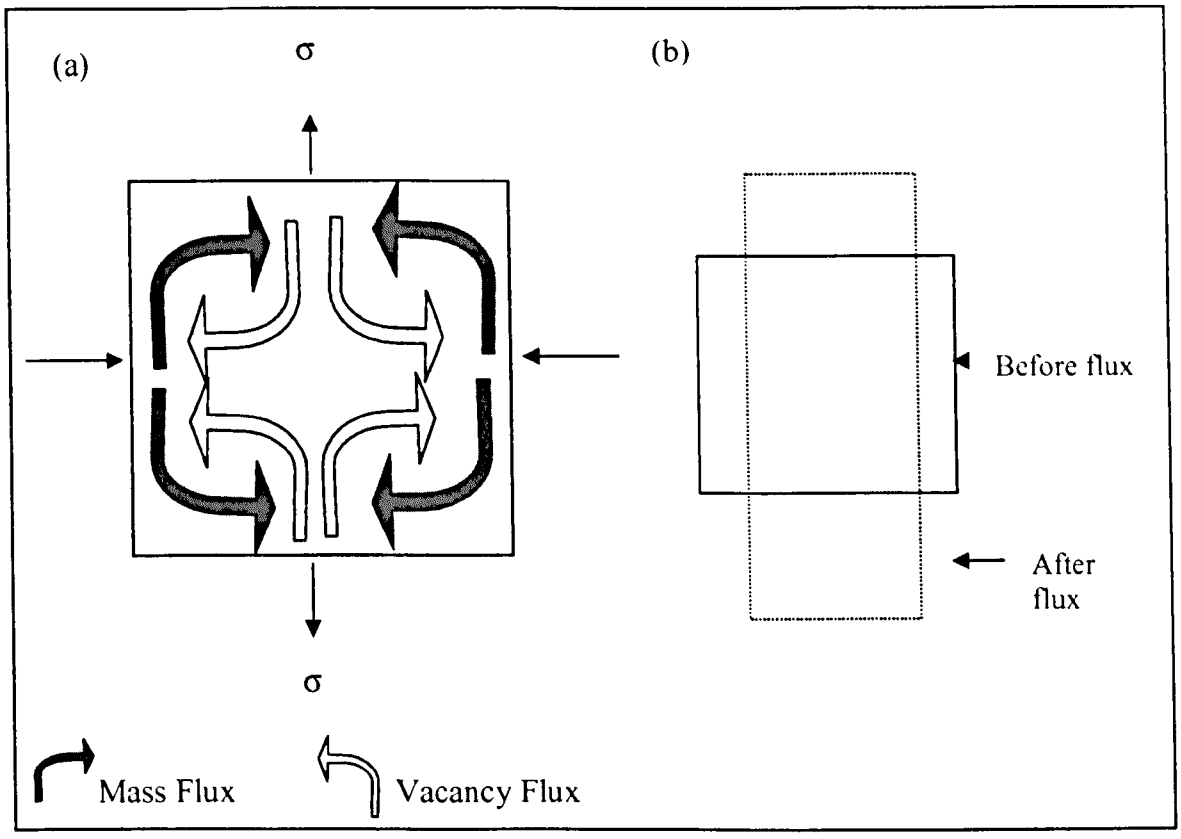


Figure 2.9(a): Illustration of the process and (b): change in grain dimensions occurring during Nabarro-Herring creep.

Coble creep [53] is driven by the vacancy concentration gradient arising from the same tension/compression regions as in Nabarro-Herring creep. However, mass transport occurs by diffusion along the grain boundaries in a polycrystalline material or along the surface of a single crystal [54] as opposed to through the lattice.

Coble creep is dominant at temperatures lower than that for Nabarro-Herring creep but still above $T_h = 0.7$. In this case, the temperature is low enough so bulk diffusion is limited relative to the diffusion activated in the grain boundary [46]. Both Nabarro-Herring and Coble mechanisms are favoured by high temperatures and lower stress values. As diffusion in Coble creep occurs along the grain boundaries rather than in the bulk, more diffusion paths are available when the grain size is small. Therefore, Coble creep will dominate in very fine-grained materials. Coble and Nabarro-Herring mechanisms are parallel processes and the creep rate due to diffusional flow is considered to be the sum of both processes.

Figure 2.10 illustrates both the Nabarro-Herring and Coble mechanisms of diffusion creep.

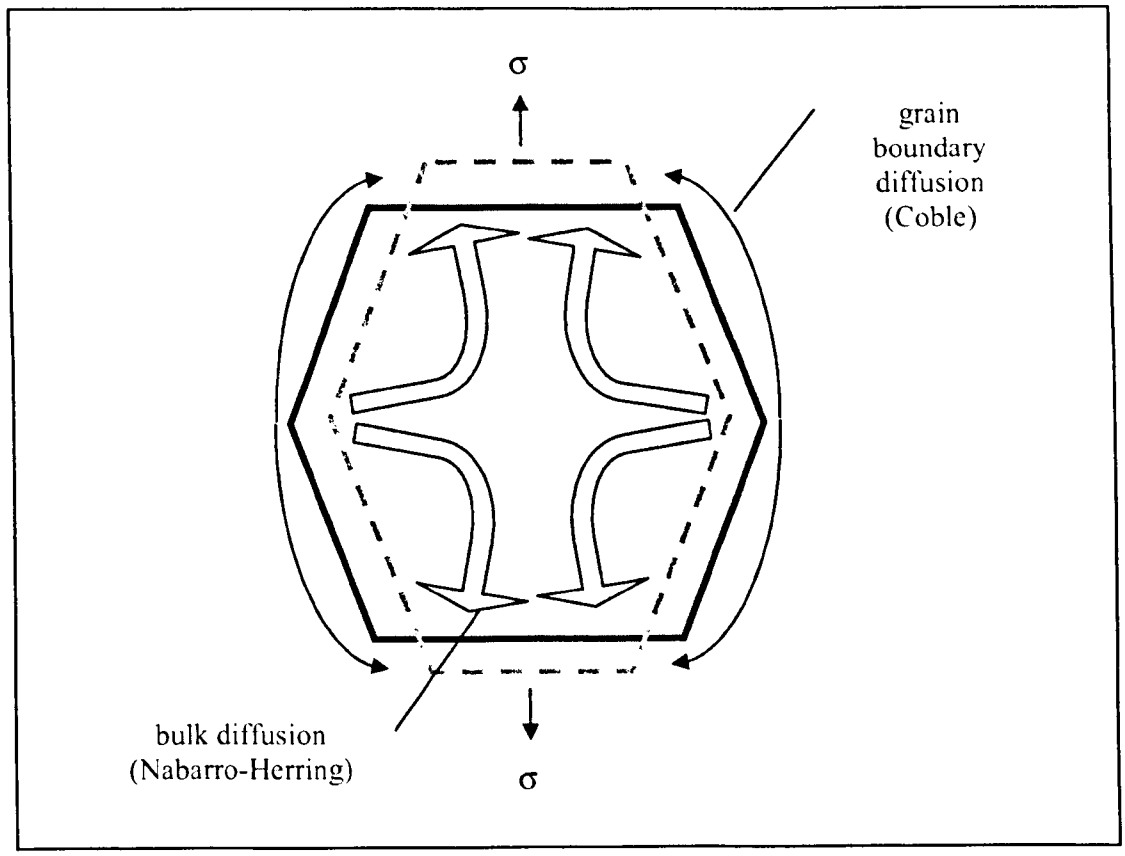


Figure 2.10: Mechanisms of diffusion creep

### *2.2.3 Grain Boundary Sliding*

Grain boundary sliding can also occur at low stresses. This is a process where grains become displaced with respect to each other but exhibit no significant elongation. This results in an increase in the number of grains lying along the tensile axis. This behaviour is termed Rachinger sliding [55] and occurs in high temperature creep in materials with a large grain size and in super-plasticity when the grain size is very small (<10μm). A sliding process also occurs in diffusion creep, this is called Lifshitz sliding [56] and is an accommodation process. It is different from Rachinger sliding as the grains retain their positions, so that there is not a net increase in their number lying in the tensile axis.

### 2.2.4 *Creep Constants*

As previously mentioned, values of creep exponent and activation energy are important in the determination of dominant creep mechanisms occurring in particular materials under specific conditions. Table 2.1 below shows typical examples of creep exponent 'n' and activation energy 'Q' for various creep mechanisms.

| Creep Process | Temperature | σ | n | $Q_c$ |
|---|---|---|---|---|
| High Temperature Dislocation Creep | Above 0.7 $T_m$ (>70°C for SAC) | Intermediate/High | >3 | ~$Q_{SD}$ |
| Low Temperature Dislocation Creep | ~ 0.4 – 0.7 $T_m$ (-77 to 70°C for SAC) | Intermediate/High | >3 | $Q_{short\ circuit}$ |
| High Temperature Diffusional Creep | Above 0.7 $T_m$ (>70°C for SAC) | Low | ~ 1 | $Q_{SD}$ |
| Low Temperature Diffusional Creep | ~ 0.4 – 0.7 $T_m$ (-77 to 70°C for SAC) | Low | ~ 1 | $Q_{GB}$ |

(Taken from [57]) Where $Q_{SD}$ = Activation for self diffusion, $Q_{short\ circuit}$ = pipe diffusion and $Q_{GB}$ = grain boundary diffusion. SAC = tin-silver-copper alloy

Table 2.1: Variation of creep exponent and activation energy with stress and temperature

The applied stresses utilised within this research were not sufficiently low enough to activate diffusional creep in solder and values of creep exponent obtained were generally above '3', hence most emphasis in this and the discussion chapter was placed upon dislocation creep mechanisms.

### 2.2.5 *Deformation Mechanism Maps*

Creep occurs by different mechanisms according to the temperature and applied stress. It is useful to determine which mechanism is most likely to occur under particular conditions. Deformation mechanism maps are used to illustrate the dominant creep mechanisms for specific circumstances by plotting either strain rate or stress versus homologous temperature. When selecting materials for engineering purposes, which operate under 'creep' conditions, it is helpful to consult these

diagrams. Figure 2.11 shows an example of a map for a pure metal. As a limited amount of work has been performed on the 'newer' solder alloys, there isn't as yet a deformation mechanism map available for the ternary alloy in published literature.

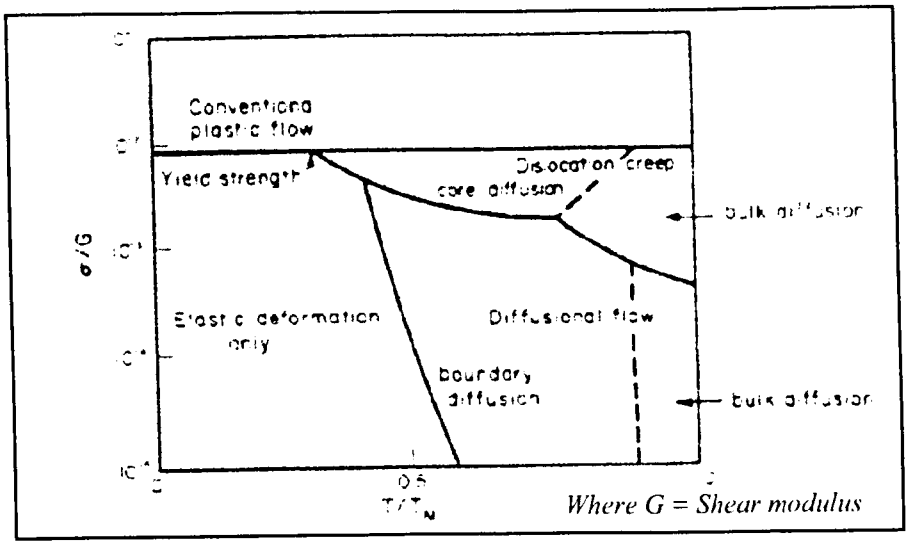


Figure 2.11 Deformation mechanisms at different stresses and temperatures [24]

## 2.3 Literature Survey

### *2.3.1 Creep of Tin-lead Solders*

Extensive research has been performed on the mechanical properties of tin-lead solder, including creep. This section examines some of the available creep data for Sn-37Pb (or Sn-40Pb), and describes the difficulties in comparing data from different authors. Figure 2.12 (courtesy of Colin Gagg, Open University [59]) demonstrates the large scatter that is often observed when comparing creep data from various sources, highlighting the problem facing engineers when deciding upon which data to select for their analysis. Figure 2.12 indicates that at low stress levels (e.g. 3MPa), equivalent to what may be found in service, the scatter in the measured minimum strain rate values may be up to four orders of magnitude. This large scatter in data may be due to the many variables introduced in manufacture or test regimes. Thus

making a direct comparison of data obtained between different laboratories and with different alloy batches difficult. As solders operate at high homologous temperatures, they are very sensitive to past history and testing conditions. Factors influencing their properties may include initial microstructure, strain rate, temperature and manufacturing methods. Machining, ageing and polishing the sample prior to testing may alter the microstructure, which can in turn influence the material properties. Gagg and Williams [58] determined that bulk solder microstructures and hence properties were altered once the sample gauge length had been machined and polished prior to testing. They also concluded that 'as cast' solder samples were most representative of the microstructures found in service.

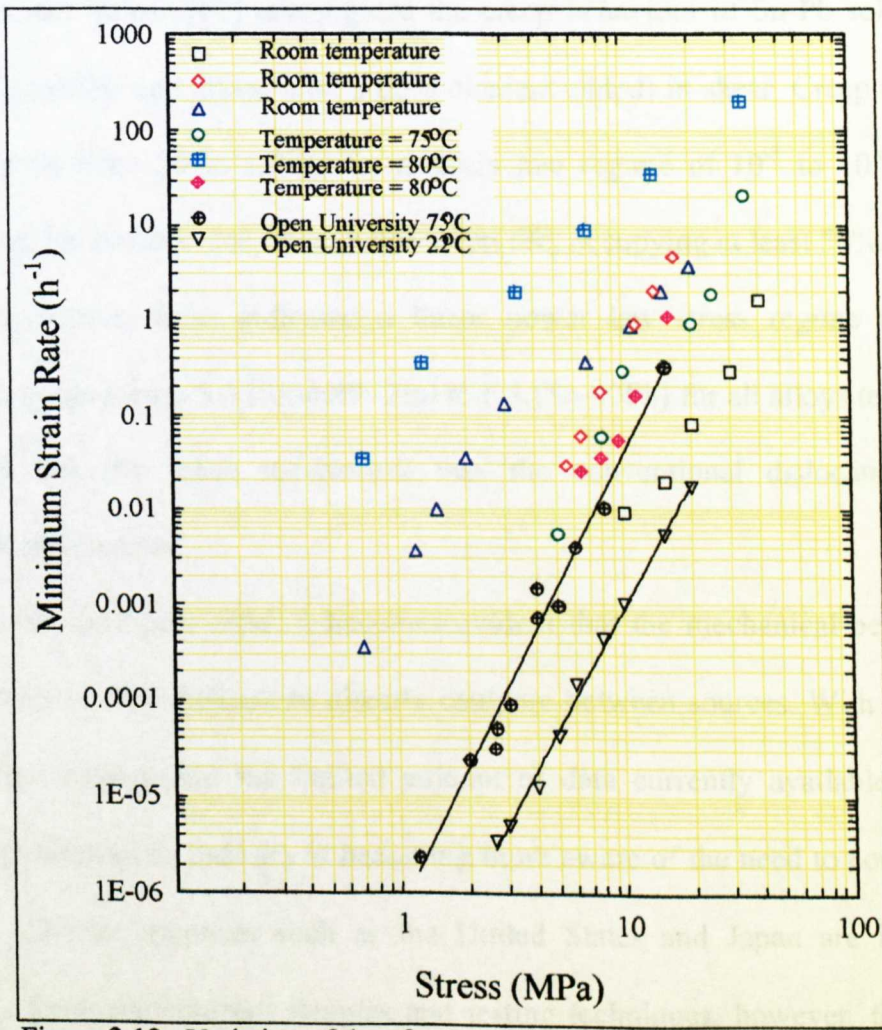


Figure 2.12 Variation of data for Sn-37Pb solder from different sources (courtesy of Colin Gagg, Open University [59])

Much of the available tin-lead data has been performed in the high stress regime and therefore is not representative of what would necessarily occur in service. At these levels, the creep mechanisms activated may not be those occurring under service conditions and therefore extrapolation to longer lifetimes would be unsafe.

Two examples are now presented to illustrate the variations in the methods of data collation from assorted authors. Stephens and Frear [60] investigated the compressive creep behaviour of Sn-40Pb between –55 to 125°C. For the applied stress levels studied (5 to 80MPa) the stress exponents range from 3 to 5 at 125°C suggesting that creep is dominated by climb. While the stress exponents range from 10.75 to 15.79 at –55°C, suggesting plasticity dominated power law breakdown.

Tribula and Morris [61] investigated the creep behaviour of Sn-Pb solder joints (Sn37Pb, Sn-40Pb and alloys with a third element added) in shear. Creep tests were performed between 20 to 125°C for a strain rate regime of $10^{-3}$ to $10^{-6}$ $s^{-1}$, they determined that tertiary creep dominated creep life, occupying at least 50%. A plot of strain rate versus stress indicated a linear power law stress regime and creep exponents ranged from 3.8 (Sn-40Pb-2In) to 6.3 (Sn-40Pb) for all alloys tested. They suggested that the creep mechanism was the conventional dislocation climb-controlled mechanism.

Given the examples cited, it becomes evident that the mechanical behaviour of solder alloys is very difficult to directly compare between sources. With the advent of lead-free solders and the limited amount of data currently available for these alloys, the electronics industry is becoming more aware of the need to compare data reliably. Various countries such as the United States and Japan are introducing standards for manufacturing samples and testing techniques, however, these as yet are not universal and comparison is still problematic. For the purpose of this research

the discussion of creep behaviour in solder alloys is limited to samples manufactured and tested at the Open University so that comparisons and observations can be made reliably.

### *2.3.2 Creep of Lead-free Solders*

Published literature on the deformation of the Sn-3.8Ag-0.7Cu solder alloy is limited. However, more research has been performed on the binary Sn-3.5Ag alloy, as until recently it was one of the favourites for replacing Sn-37Pb in electronics. Therefore, published data are reviewed for tin (as both alloys are tin-based), Sn-3.5Ag and Sn-3.8Ag-0.7Cu, assuming that their properties are broadly similar.

The following section lists published data and the conditions under which the data were collated. This demonstrates the wide-ranging manufacturing techniques, test parameters and therefore, 'constants' obtained from different sources, again emphasising the difficulty of direct data comparison. These data will be summarised by author and any trends identified at the end of the section.

Mathew *et al.* [62] reviewed the published data on tin and established that there was no clear agreement on the self-diffusion data reported. However, as the homologous temperature is decreased, a transition (around $T_h$ = 0.5 - 0.6) from 'lattice-diffusion controlled creep' to 'pipe-diffusion controlled creep' occurred. They determined the creep exponent of Sn-3.5Ag to be five, and under the testing conditions (temperature range of 23 to 200°C) the activation energy was similar to that of the creep activation energy obtained for tin (60.7kJ/mol). They suggested that lattice-diffusion controlled dislocation climb was the rate controlling mechanism for creep in both tin and the Sn-Ag alloy. However, other authors believe that an activation energy of 60kJ/mol indicates short circuit diffusion (pipe (core) diffusion) in tin [44] [36] [45].

At moderate to high stresses and at temperatures lower than 100°C, McCabe and Fine [45] found that the creep of tin is dominated by 'pipe-diffusion controlled dislocation climb'. They suggest that a small value of activation energy (<90kJ/mol) and a higher 'n' (>10) often indicates that dislocation climb is controlled by short-circuit diffusion mechanism e.g. pipe-diffusion. Activation energies greater than 90kJ/mol would suggest self-diffusion in tin. Guo *et al.* [63] investigated the creep of Sn3.5Ag and Sn4Ag0.5Cu and obtained activation energies also indicating short circuit diffusion.

Grivas *et al.* [64] obtained creep exponents, 'n', for the Sn-3.5Ag alloy, of 2 at low stresses and 7 in the higher stress region. The low value was attributed to grain boundary sliding and the higher value to the dominance of dislocation climb.

Mavoori *et al.* [65, 66] examined creep under constant load for both Sn-Ag and Sn-Zn alloys. After casting, the samples were machined and heated to 150°C for 25 hours and then held at room temperature for 6-10 days. From these three preliminary tests at 25°C (10MPa, 15MPa and 20MPa) an estimate of the creep exponent for Sn-Ag was obtained, n = 7.34. Mavoori *et al.* [65] examined the constant load creep behaviour (between 10-22MPa) of these alloys further at 25°C and also at 80°C, to determine values for creep exponent and activation energy. According to Norton's Law, the creep exponent in this instance was found to be 11.3, an average taken of the values obtained at 25 (n = 10.9) and 80°C (n=13), and activation energy was 82.3kJ/mol. They offer no explanation to the differences in values of 'n' obtained at room temperature between the two sets of data.

Hwang and Vargas [67] performed constant load creep tests at room temperature on twenty-two different solder alloys, including Sn-3.5Ag and Sn-5Ag. Prior to testing, samples were lightly polished along the longitudinal direction to alleviate

any gross surface defects. In comparison to other alloys, the silver-containing solders possessed a higher creep resistance. This was attributed to solution hardening i.e. when a load is applied deformation is hindered by the interaction of dislocations with solute atoms in the microstructure. Dislocation movement and structure in relation to temperature and stress was believed to be the fundamental theory responsible for the creep behaviour of the solder alloys examined.

Igoshev *et al* [68] reviewed the available data obtained for the Sn-Ag alloy, values of stress exponent ranged between 5 and 12. They suggest that grain boundary sliding and/or dislocation motion accounts for the high values of 'n' in the silver-containing alloys. A change in the fracture mode of Sn-3.5Ag in creep at an applied stress of 7.5MPa was also observed [69]. A creep mechanism change is believed to occur in this stress range leading to a change in creep exponent.

Kariya, Atsumi and Otsuka [70] tested Sn-3.5Ag-1Cu in creep. They obtained an activation energy of 83.7kJ/mol and a creep exponent of 6.2. Prior to testing, samples were heat-treated for one hour at 100°C and the gauge lengths polished to a 1μm finish using diamond paste. In comparison to the binary alloy, the copper-containing solder possessed higher creep strength. Kariya and Plumbridge [36] compared Sn3.0Ag0.5Cu with both Sn3.8Ag-0.7Cu and Sn3.5Ag in a rapidly cooled, 'as cast' state. Creep tests were performed at 75°C at a constant load. The creep resistances of the two ternary alloys were comparable and were both higher than the binary alloy. The ductilities of all three alloys were similar. The Norton power law equation best described the creep behaviour and resulted in a creep exponent of 13. A value of 61kJ/mol was obtained for the activation energy (from tensile tests) and suggested that pipe-diffusion controlled dislocation climb is the dominant mechanism in tensile tests. The high creep exponent indicates that a dispersion-strengthened mechanism is

dominant in the creep process. This may be attributed to the presence of fine $Ag_3Sn$ particles in the microstructure.

It has been suggested that the creep exponent was greatly effected by the precipitation of $Ag_3Sn$ [68]. When the intermetallic was finely dispersed throughout the microstructure the minimum strain rate was three orders of magnitude lower at room temperature than solder with large rod-like particles of $Ag_3Sn$. Sn-3.5Ag with finely dispersed particles has a high activation energy (~100kJ/mol), whereas Sn-3.5Ag with rod-like particles has a lower activation energy (<100kJ/mol).

Plumbridge [47] investigated the creep behaviour of various lead-free alloys and the conventional tin-lead alloy. At 75°C, the Sn-3.5Ag alloy has a creep resistance a hundred times superior to both tin-copper and tin-lead, it can also withstand stress levels of an order of magnitude greater. Work performed by the Solder Research Group (Open University) is covered in greater depth in the discussion chapter, where results obtained for the ternary alloy are compared to other lead-free and the lead-containing alloys. This is possible because the same workers in the same laboratory have collated the data, thus eliminating some of the 'variables' first mentioned in the beginning of this section.

Generally, values of creep exponent for the silver-containing alloys range from 2 (at low stresses) to 13. A transition in gradient in the Norton's law plot, occasionally seen at low stresses, has been attributed to a change in dominant creep mechanism. It was suggested that a low value of creep exponent corresponds to grain boundary sliding and a higher 'n' (>5) relates to dislocation climb. The reported activation energies for creep range between 60 to 84kJ/mol and relate to dislocation pipe diffusion in tin. However, the values of creep activation energy and exponent were shown to depend on microstructure, particularly on the shape and distribution of

$Ag_3Sn$ particles. The change in microstructure and the resultant effect on 'constants' due to specific manufacturing and ageing techniques have not been reported in the individual pieces of literature.

Clech [71] recently reviewed data relating to the creep behaviour of the tin-lead, tin-silver and tin-silver-copper alloy, which included some data obtained at the Open University. The tin-silver and tin-silver-copper data collated from eight authors, in the Clech review, confirmed the scatter in data first observed within this thesis review. The author also suggested that there are limited data available at applied stresses below 10MPa. However it is these data that are most representative of conditions observed in service and require consideration. Clech also suggested that the discrepancies seen among the data sets require solving before a reliable constitutive model can be developed for small solder joints of electronic assemblies. On comparison of tensile and shear creep data, it was illustrated that different trends were followed, this also requires further investigation. The general conclusions drawn from the Clech review stated that although there was a large scatter of data some trends were observed. Ternary alloy data collated for this research is compared with the review alloy in chapter six. A comparison is also made between the SnAg model joint data from the review and data obtained during this research for SnAgCu model joints.

### *2.3.3 Creep in Soldered Joints*

This section looks at the creep behaviour of lead-free solders in joints (model and actual). Each authors work has been described individually because of the difficulty in the comparison of properties due to the utilisation of different joint geometries and manufacturing/testing procedures.

Darveaux and Banerji [72] performed creep tests using actual Sn-Ag 'Ball Grid Array' joints. They suggested that the rate controlling creep mechanism is dislocation climb. However, their value for activation energy was low in comparison to values previously observed for lattice-diffusion and pipe-diffusion in tin. It was therefore proposed that activation energy was stress dependent since the data were obtained in the power law breakdown regime.

Cho*i et al.* [44] performed creep tests on both eutectic tin-silver and composite tin-silver alloys reinforced with $Cu_6Sn_5$. It was discovered that the 'as made' joints with reinforcement particulate show a higher creep resistance than the eutectic alloy by two to three orders of magnitude. The Sn-3.5Ag alloy possesses an activation energy in the region of 60kJ/mol suggesting that grain boundary or pipe diffusion may control the deformation. Whereas the joint reinforced with $Cu_6Sn_5$ particles had an activation energy similar to the self-diffusion of tin (120kJ/mol) [44].

Hua *et al.* [73] examined the creep behaviour at 60, 95 and 130°C of four lead-free alloys; Sn-3.5Ag, Sn-0.7Cu, Sn-3.0Ag-0.5Cu and Sn-10In-3.1Ag. Creep testing was performed using lap joints manufactured from copper coupons plated with gold over electro-less nickel. Soldering was carried out in a reflow oven using a nitrogen atmosphere, with two rates of cooling (2.7°C/s and 3.5°C/min). At 130°C, SnAgCu (with a cooling rate of 2.7°C/s) has the longest rupture time and a creep exponent of 6.6. The creep exponent increases to 7.8 at 95°C. An activation energy of 115kJ/mol was established for the ternary alloy, agreeing with the activation energy for the self-diffusion of tin. All the lead-free alloys show two creep mechanisms at each temperature, indicated by a change in creep exponent, 'n'. Table 2.2 shows the change in 'n' for the ternary alloy subjected to a cooling rate of 2.7°C/sec. The change in gradient is particularly evident at 60°C (although the authors suggest that

more work is required). They conclude that the creep behaviour of solder joints in shear is a complex function of stress and temperature, which is not entirely understood. They recommend that until this complex behaviour can be understood metallurgically, and therefore treated analytically, tests should use geometries and conditions as near as possible to those anticipated in service [74].

| 130°C | | 95°C | | 60°C | |
|---|---|---|---|---|---|
| High σ | Low σ | High σ | Low σ | High σ | Low σ |
| 9.2 | 5.0 | 9.9 | 6.0 | 12.7 | 4.4 |

Table 2.2 Change in creep exponent for the ternary alloy, with a cooling rate of 2.7°Cs$^{-1}$, for all test temperatures [73]

Wiese *et al.* [75] investigated the constitutive behaviour of Sn3.5Ag, Sn-4Ag-0.5Cu and Sn-37Pb of ultra small flip chip solder joints. They discovered that the lead-free solders exhibit a very high dependence on stress while the SnPb alloy showed a low stress dependence. The ternary alloy possessed a creep exponent of n = 18, which was significantly higher than that of the binary alloy (n = 11). The ternary had lower creep rates than the binary alloy and it was assumed that this was the result of the fine dispersion of intermetallic particles acting as obstacles for dislocation movement, therefore increasing the creep resistance. The activation energy was also higher in the ternary alloy, 83.1 kJ/mol, which also may be caused by the fine dispersion of $Ag_3Sn$ and $Cu_6Sn_5$ within the matrix [75].

It is again evident from the published data that varying methods of testing and manufacture have been utilised producing a wide range of 'constants'. This variation makes it very difficult to compare data or decide which data to use when establishing reliable computer models. Data obtained from the published literature produced a wide scatter of data making it difficult to establish reliable trends. In general, activation energy for creep in soldered joints falls in a similar range to that for the bulk material, between 60 to 120kJ/mol. Creep exponent values ranged between 6.6

up to 18, showing a high dependence of creep on stress. In addition to testing and manufacturing conditions other factors that should be investigated include the effects of joint geometry, intermetallic thickness, solder volume and solder area in contact with copper lands/leads.

# CHAPTER THREE

## 3 SOLDERED JOINTS

### 3.1 Introduction

Data acquired from bulk mechanical testing may be used in computer models to predict the behaviour of solders during service. However, several details should first be considered. First, laboratory testing may not always replicate the processes occurring in operation and using these data may lead to an inaccurate estimation of lifetime. Secondly, although it is necessary to test bulk material to gain an understanding of fundamental properties, such as creep, solders may behave differently in joint form. In comparison to the bulk material, a soldered joint is a complex structure and this will have an effect on properties. A joint consists of not only solder and substrate materials but also intermetallic compounds. Model joints can be mechanically tested to determine the effects of microstructure, soldering process and shear loading, providing an indication of how actual joints may behave in service. This chapter focuses on the second issue. It describes the structure of a joint, the importance of selecting a suitable joint configuration for testing and evaluates published information relating to manufacturing techniques and joint strength.

### 3.2 The Soldered Joint

In electronics, solders are required to attach components to printed circuit boards (PCBs) and provide electrical and thermal conductivity. It is important that a sound joint is produced i.e. one with good wetting and without voiding or cracks. 'Wetting' implies that a specific interaction takes place between the liquid solder and the base

material being soldered [76], forming a reaction product or intermetallic compound (IMC).

A typical solder joint comprises of solder, the substrate material (commonly copper) and IMCs. Electronic grade solders are generally tin-based and the compounds formed during soldering are commonly $\eta$-$Cu_6Sn_5$ and $\varepsilon$-$Cu_3Sn$. IMCs tend to be harder and more brittle than the solder alloy due to their ionic bonding. The thickness of the IMC layer increases with temperature and contact time between the substrate and molten solder during joint formation. If the layer becomes too thick, it can have an embrittling effect, and the strength of a joint may be reduced. Figure 3.1 shows the microstructure observed in a model joint made with tin-copper solder for the preliminary joint manufacturing trials used in this research. At present, very few manufacturers are using lead-free solders, therefore the structure of an actual joint is not well established.

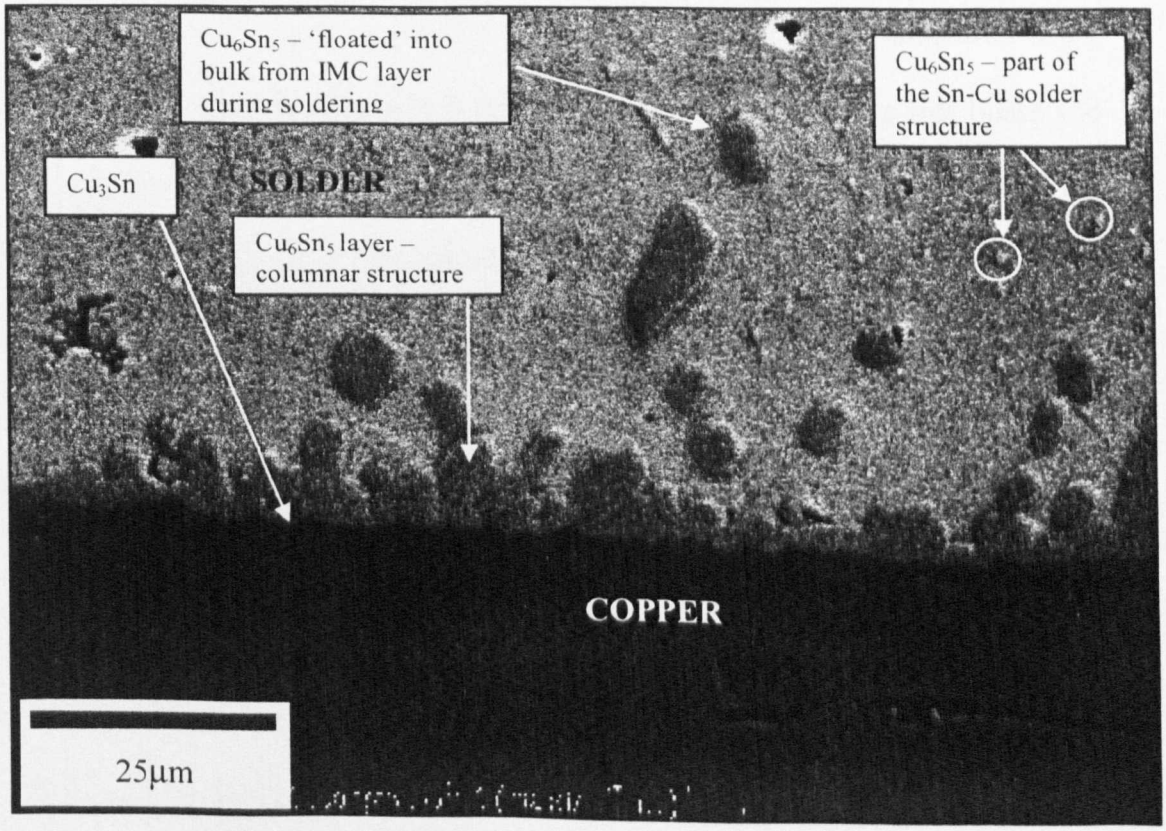


Figure 3.1: The structure of a model joint manufactured using the technique devised for this research

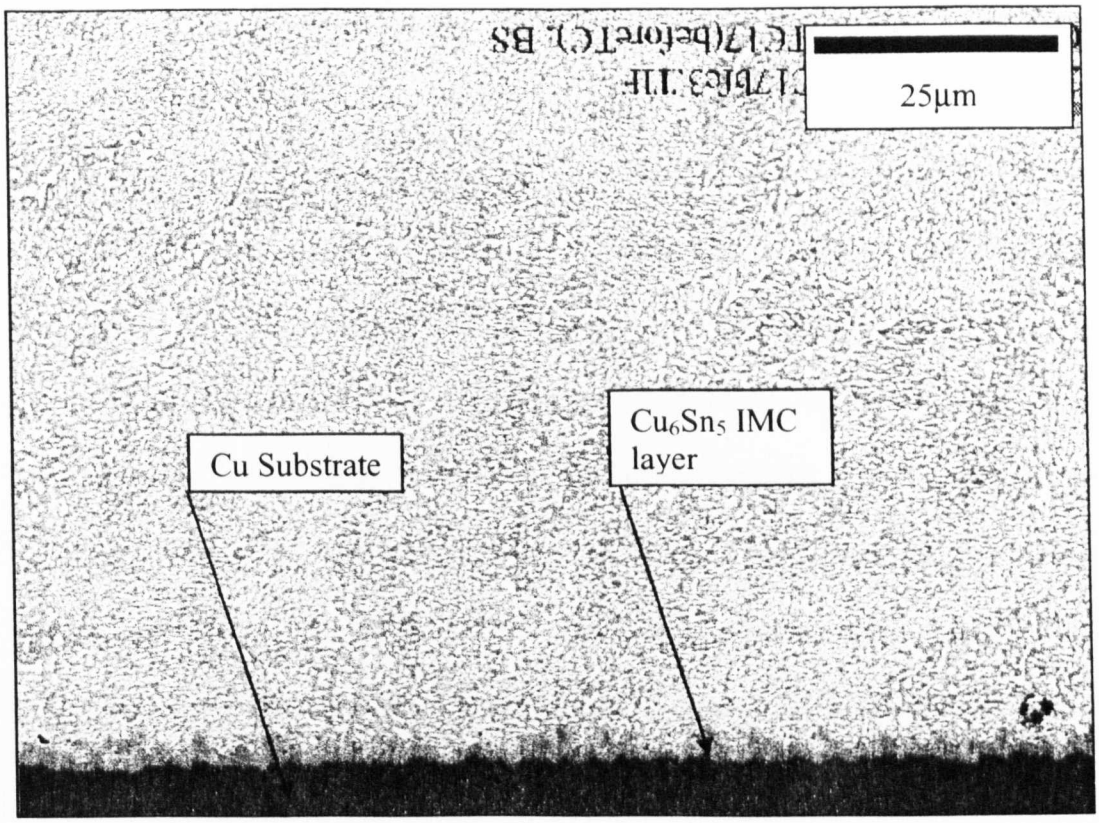


Figure 3.2 Structure of a Sn40Pb/Cu model joint used for thermal cycling tests at the Open University (courtesy of Xian Wei Lui, Solder Research Group)

Figure 3.2 illustrates the vast difference in microstructure, in comparison to the lead-free 'pin in ring' joint, produced when a model joint is manufactured using Sn40Pb solder. The dark areas within the microstructure above are tin-rich phase and the light areas lead-rich phase. However, the joint dimensions and manufacturing technique were different to those used in the manufacture of the lead-free 'pin in ring' joint and therefore, the two can not be directly compared. The lead-containing joint, pictured in figure 3.2, was manufactured using Sn-40Pb paste sandwiched between the copper parts, which are then heated in a furnace. Work to evaluate the creep behaviour of the SnPb/Cu 'pin in ring' joint in creep is planned for the future, a direct comparison between lead-containing and lead-free solder model joints could then be performed.

During soldering, $Cu_6Sn_5$ grows first and extends into the solder. It is thicker than the $Cu_3Sn$ layer, which lies between the copper substrate and $Cu_6Sn_5$. $Cu_3Sn$ is

formed through solid state diffusion. While the solder is molten, $Cu_6Sn_5$ particles may break off from the initial layer and 'float' into the bulk solder.

The amount of IMC formed during soldering is dependent on many factors. Harris and Chaggar [77] indicated that the quantity is a direct function of the soldering time and temperature as well as the joint volume and alloy composition.

IMCs also possess different coefficients of thermal expansion (CTE) to the other materials found in an assembly [78]. This mismatch of CTEs is a concern to the electronics industry, as previously mentioned. Significant research has been performed to determine the effect of IMC thickness on the strength of the solder joint. Tu *et al.* [79] examined the fatigue failure of actual, Sn-37Pb soldered joints during cyclic thermal ageing. Using two cycles per hour, between –35°C and 125°C, they determined that thermal history, including thermal test cycles, affects the IMC thickness and consequently the fatigue lifetime of surface mount joints. Their results indicate that the fatigue lifetime depends on the thickness of the IMC. The fatigue lifetime of solder joints decreases rapidly with increasing IMC thickness, but decreases more slowly once the thickness exceeds 1.4 μm, as shown in figure 3.3. The morphology of the IMC layer also effects the joint lifetime. A smooth layer can degrade the fatigue lifetime more than an uneven one. This degradation occurs because the smooth layer is less resistant to shearing, which is most common in service. During thermal cycling, the fatigue failure occurs mainly at the IMC/solder interface.

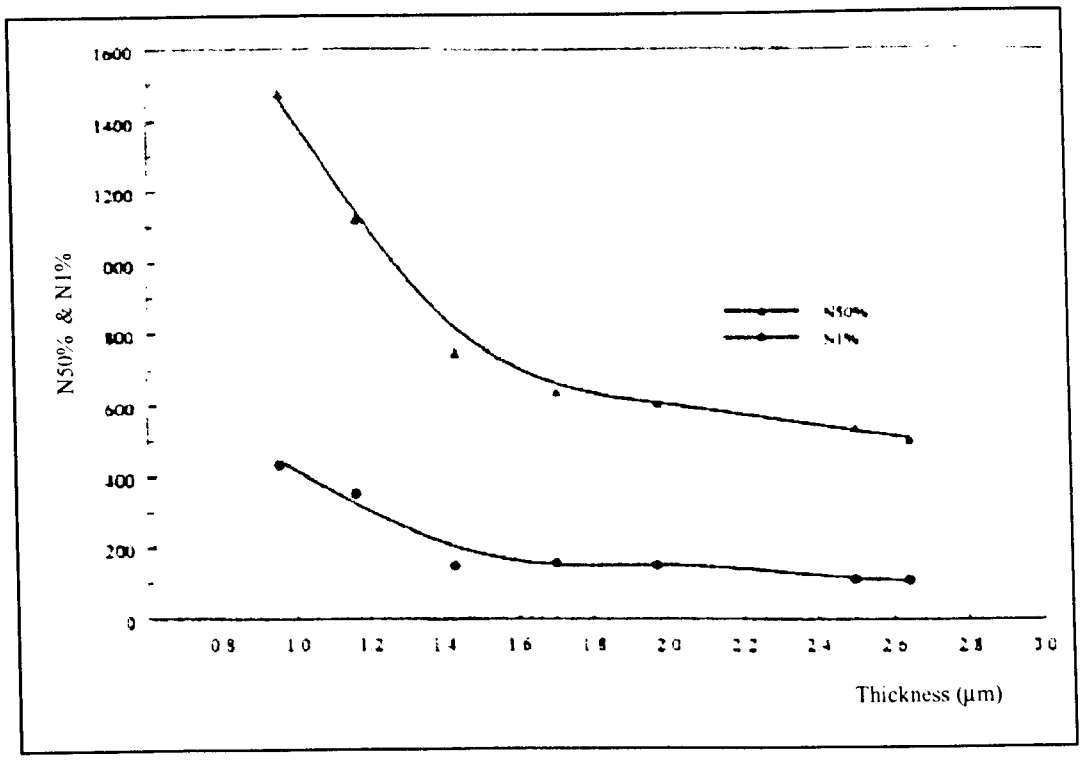


Figure 3.3 IMC thickness versus number of cycles to failure at 50% (N50%) and 1% (N1%) failure [79]

Frear and Vianco [80] studied six common solder alloys, including Sn-37Pb and Sn-3.5Ag, and deduced that joints comprising solders with low strengths failed in the bulk by plastic deformation, whereas joints with higher strength solders (greater than 20MPa, e.g. Sn-3.5Ag) were dependent upon the IMC thickness. In the higher strength alloys, when the IMC layer was thin, fracture occurred in the solder or at the solder/IMC interface. As the interfacial IMC thickened the fracture path was contained within the intermetallic layer.

Dirnfeld and Ramon performed tests on Sn-40Pb 'pin in ring' model joints [81] and suggest that there is an optimum thickness of IMC. For tin-lead 'pin in ring' soldered joints with a solder layer thickness of 0.7mm, this is typically about 1.3µm. Here, failure is believed to occur at the interface between the solder and intermetallic interface as the strength achieved is greater than that for the bulk solder. Above this thickness the joint strength deteriorates, figure 3.4.

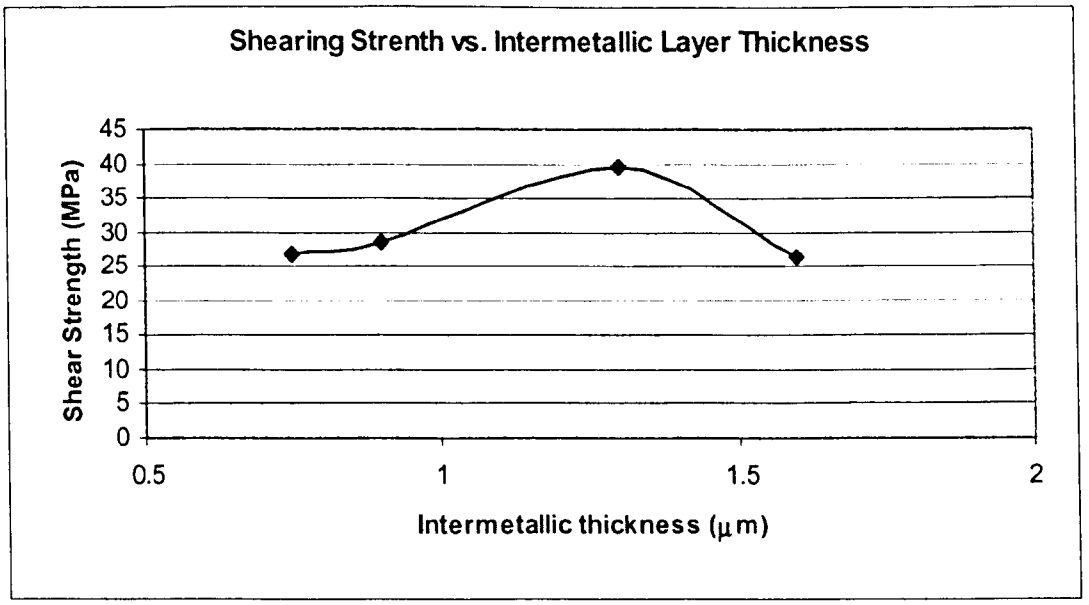


Figure 3.4 The effect of IMC thickness on the shear strength of joints [81].

Unfortunately, the work of Dirnfeld and Ramon cannot be directly compared with that of Tu *et al.* Tu *et al.* examined thermally cycled actual joints and Dirnfeld and Ramon determined how IMC thickness effects the shear strength of model joints.

It is the effect of intermetallic compounds, joint microstructure and loading in shear on creep, which is the focus of phase two of this investigation. The ultimate goal is the correlation of bulk and joint behaviour.

## 3.3 The Role of Mechanical Testing

With many 'day to day' systems now relying on electronics to function, more focus is being placed on predicting how long soldered joints will last. Establishing reliability and lifetime prediction of soldered joints during service is a challenging task. Here, reliability is defined as a measure of the equipment's ability to perform a function for a specified time under given conditions, without exceeding acceptable failure limits [82] and failure is any inability to carry out a specified function. It is impossible to calculate the exact period of time for which an item will work without

failure. In electronics, the failure of a single solder joint could render a piece of equipment useless. If the equipment can be repaired, the likely period of time an item will function without failure is often represented by the 'mean time between failures'. However, there is no certainty that the equipment will fail at this specified time. An estimation of reliability and hence life prediction, is difficult to establish. The probability of failure should, ideally, be made on an understanding of deformation and failure mechanisms. However, data for computational methods of life prediction are generally obtained through mechanical or empirical testing, where tests do not necessarily relate to actual service conditions.

During laboratory testing it is important to activate the deformation mechanisms occurring in service [83]. Sample microstructures and testing conditions should also be considered, as these too will affect joint properties. Mechanical testing is significant in the design and manufacture of electronic assemblies. Before manufacture, testing can be used to determine material and system properties by the use of 'dummy' boards or model joints. These properties can include elastic, yield and fracture properties, bond strengths, thermal properties, fatigue and creep behaviour. During manufacture, methods may be used for quality testing specific batches of boards and the results used to modify the process, making it more reliable.

### *3.3.1 Model Joints*

Due to their size, it is very difficult to test actual joints under controlled and monitored conditions of stress, strain and temperature. A compromise is made and larger, 'model' joints are used. Before testing can commence, determination of a suitable joint configuration and hence, stressing condition is necessary. A model joint should simulate the most commonly encountered stress situation in service, be made under easily controlled conditions, which are similar to those in practical soldering

and finally, give reproducible test results [84]. Before deciding on a configuration for a model joint in this research, a review of the most common model joints and manufacturing methods was performed and this is now presented.

The following joint designs are those most commonly used for mechanical testing; single lap joint, double lap joint, butt joint, pin in ring joint and peel (or Chadwick) tests. In 1976, Thwaites and Duckett performed a detailed evaluation of each joint configuration [84]. They determined that single lap joints (figure 3.5a), although easy to manufacture, produced peeling stresses on loading. This is because the two component pieces cannot both lie in the axis of load. The solder is only initially subjected to shear and then the non-linearity of loading produces rotational forces, which invariably bend the component pieces.

The double lap joint (figure 3.5b) has a similar configuration to that of the single lap joint, with two component pieces soldered at either side of a central one. This balances out the rotational forces and bending is eliminated. However, the resultant stressing condition is not pure shear, the configuration is a device for compensating for non-axial loading. The solder film will still be subjected to stresses other than those of pure shear. The manufacturing technique for this joint was complicated.

The butt joint is the simplest type of joint, figure 3.5c. The solder film is theoretically stressed in a direction at right angles to the joint interfaces, providing tensile stressing of the joint. The equivalence between tensile and shear strengths is given by:

$$\sigma_u = \gamma_u \sqrt{3}$$

where: $\gamma_u$ = shear strength
$\sigma_u$ = tensile strength

Any non-axiality of loading leads to peeling stresses and hence a reduced value for strength. The risk of non-axial stresses increases with joint area, therefore it is necessary to use small rods in manufacture. However, this type of configuration was found to be difficult to manufacture. Machining is required to produce a uniform rod specimen of the required diameter and this may alter the microstructure and properties of the joint, giving unrepresentative values for joint strength.

Thwaites and Duckett [84] believed the 'pin in ring' joint (figure 3.5d) to be the most representative of those found in service, since it most closely represents the in-service stressing situation. However, as with the double lap joint, the solder is not in line with the loading axis and any bending stresses due to non-axial loading are internally balanced, but not eliminated. The breaking load of this joint configuration can be determined either by applying tension to the assembly or by pushing the pin through the ring.

Peel tests (figure 3.5e) were specifically designed to measure the resistance to tearing or peeling of the weakest interface of a solder joint [84]. Narrow strips of metal are soldered parallel over a length, using spacers to control the gap width. The two unsoldered ends of the component are bent away from each other to form a 'T' shape and are pulled apart in a tensile testing machine. The load per unit width of a joint is continuously recorded, while a mean value is taken. This test effectively applies tensile stresses to the solder film at the point of peeling but two values may be recorded; the load required for crack initiation and the load required for crack propagation, which is usually lower. Usually the initial peak value is ignored and a mean peeling value is measured.

Alternative solder joint configurations, which subject the solder layer to shear stresses have also been investigated [85]. The Iosipescu joint is currently a preferred

method for polymers and ceramics and the asymmetrical four-point bend test (AFPB) is used due to its smaller specimen requirement. However, for the evaluation of solder the pin in ring configuration is most widely favoured.

*Single lap joint (3.5a)*

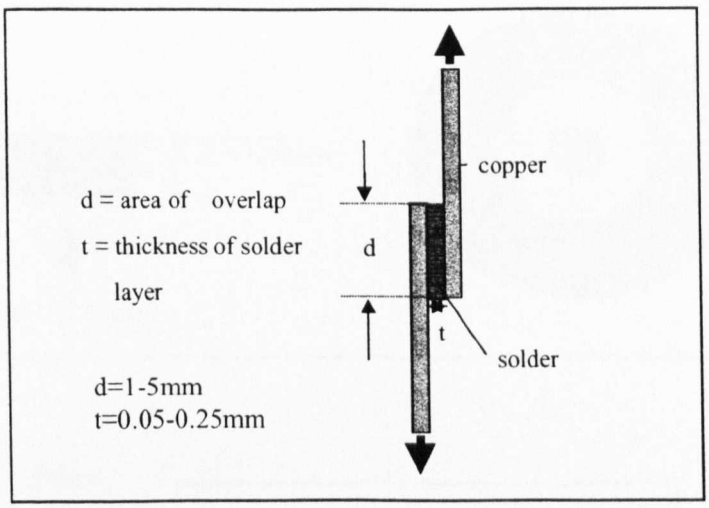


*Double Lap Joints (3.5b)*

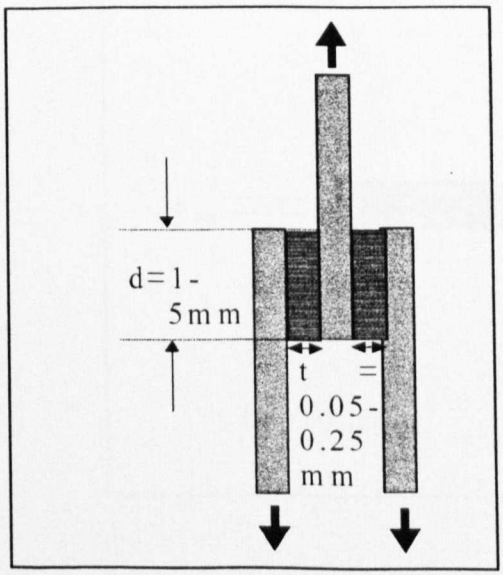


*Butt Joint (3.5c)*

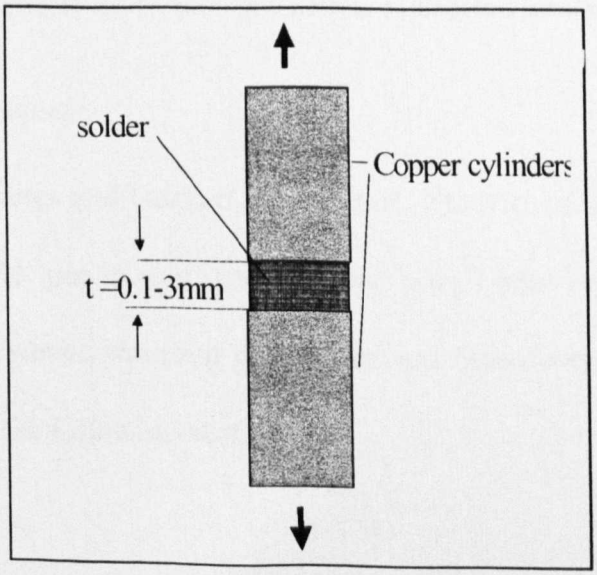

*Ring and pin joint (3.5d)*

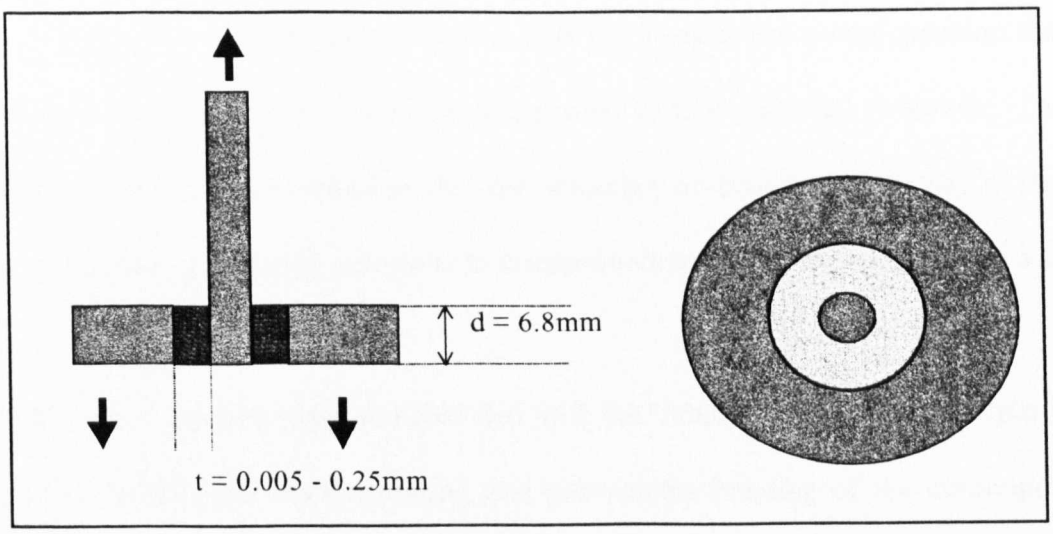


*Peel (Chadwick) Tests (3.5e)*

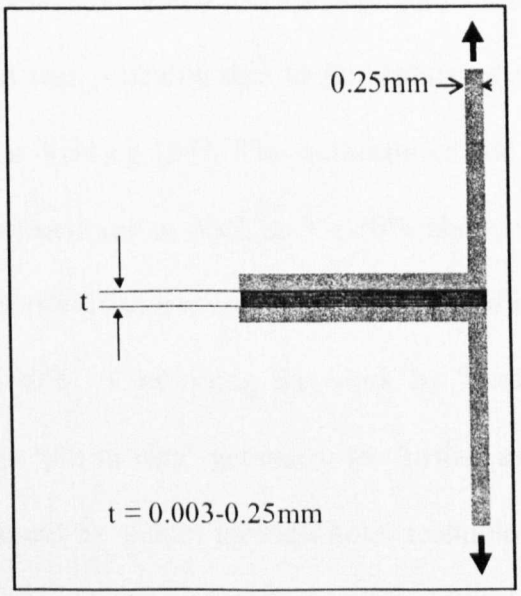


Figure 3.5 (a-e) Possible model joint geometries considered for this research

### *3.3.2 Choice of Joint Geometry*

Ramon, Dirnfeld, Thwaites and Duckett, Foley *et al.*, Stone *et al.* and Gillot [81, 84, 86-89] all selected the 'pin in ring' (or 'ring and plug') joint configuration for their work on solders. However, the joint geometries and manufacturing techniques vary and are discussed in the following section.

Ramon and Dirnfeld [86] measured the strength of small Sn-40Pb 'pin in ring' soldered joints, at room temperature and at 100°C. They chose a configuration that subjected the solder layer to shear stresses, similar to that observed in service. The mass of the joint was kept small so that the soldering procedure was similar to that found in practice, producing comparable microstructures between actual and model joints.

Thwaites and Duckett [84] predicted that both the 'double overlap' and the 'pin in ring' joints would give shear stressing and prevent the bending of the component members as experienced in the 'single lap' joint for which they anticipated lower strength values. However, strengths obtained for the 'double lap' joint were in fact lower than the 'single lap' joint. This was probably due to the failure of one joint before the other leading to non-linear loading [84]. The variation of the strength values of the double lap joints was sometimes as high as +/- 20% about the mean value. Whereas the 'pin in ring' joints provided a more repeatable method of testing with a variation of no more that +/-10%. Continuing the work by Thwaites and Duckett, Stone *et al.* [88] selected the 'pin in ring' geometry for further evaluation. The configuration is similar to that found in 'plated through-hole' technology and is comparable to capillary joints used in plumbing. They determined that the 'pin in ring' joint presented the fewest practical difficulties and could be made easily and reproducibly to give uniform joint gaps with minimum sensitivity to the manufacturing conditions. Work was performed on both lead-containing and lead-free alloys (including Sn-3.5Ag) in bulk and joint forms. The results are discussed in section 3.4. They commented that there was a little correlation between joint and bulk behaviour [88].

Foley *et al.* [87] chose the 'pin in ring' configuration for their work as it has been accepted that, as a shear test, it provides reliable and consistent results. Some variation in shear strength results have been observed, even for similar conditions. They suggested that this may be due to voids or porosity formed in the joint. Twenty-one solder alloys were tested including Sn-3.8Ag-0.7Cu. Results obtained from this work are discussed later in the chapter.

On the basis of past work, the author determined that the chosen geometry should subject the solder layer to shear stresses, as observed in service, be easily manufactured and produce consistent results on testing. Of the shear type joints considered, the 'pin in ring' configuration was favoured. This is due to the balancing of the bending stresses, which are seen in 'single lap' joints, without the complications associated with the 'double lap' joints. Also, the manufacturing technique (once established) was simple and consistent, providing samples with reproducible dimensions, microstructures and strength.

### *3.3.3 Manufacturing Methods for 'Pin in Ring' Joints*

Having identified a suitable joint geometry, a reliable method of manufacturing was determined. The following section highlights techniques described in the literature and explains the fundamentals behind the method selected.

Thwaites and Duckett [84] devised a method of producing 'pin in ring' joints (figure 3.6), which was later used by Stone *et al* [88]. Prior to soldering, three 0.13mm nickel-chromium alloy 'spacer' wires were inserted at 120° intervals in the joint. These were not wetted by the solder in the joint and simply reduced the joint area by a theoretical maximum of 2%, the effect was neglected for their work. Thwaites and Duckett had previously tested joint gap widths of 0.03mm up to 0.26 mm, but little difference was found in the joint strengths. The mass of the assembled

joint was kept sufficiently low so the rate of heating during solder dipping was nearly the same as that in practical soldering operations. Once constructed, the assembly was preheated in a bath of fused $ZnCl_2 - NH_4Cl$ (the flux) followed by a brief dip in a solder bath of Sn-40Pb, held at a constant temperature of 235°C. Here, the solder was drawn into the gap by capillary action.

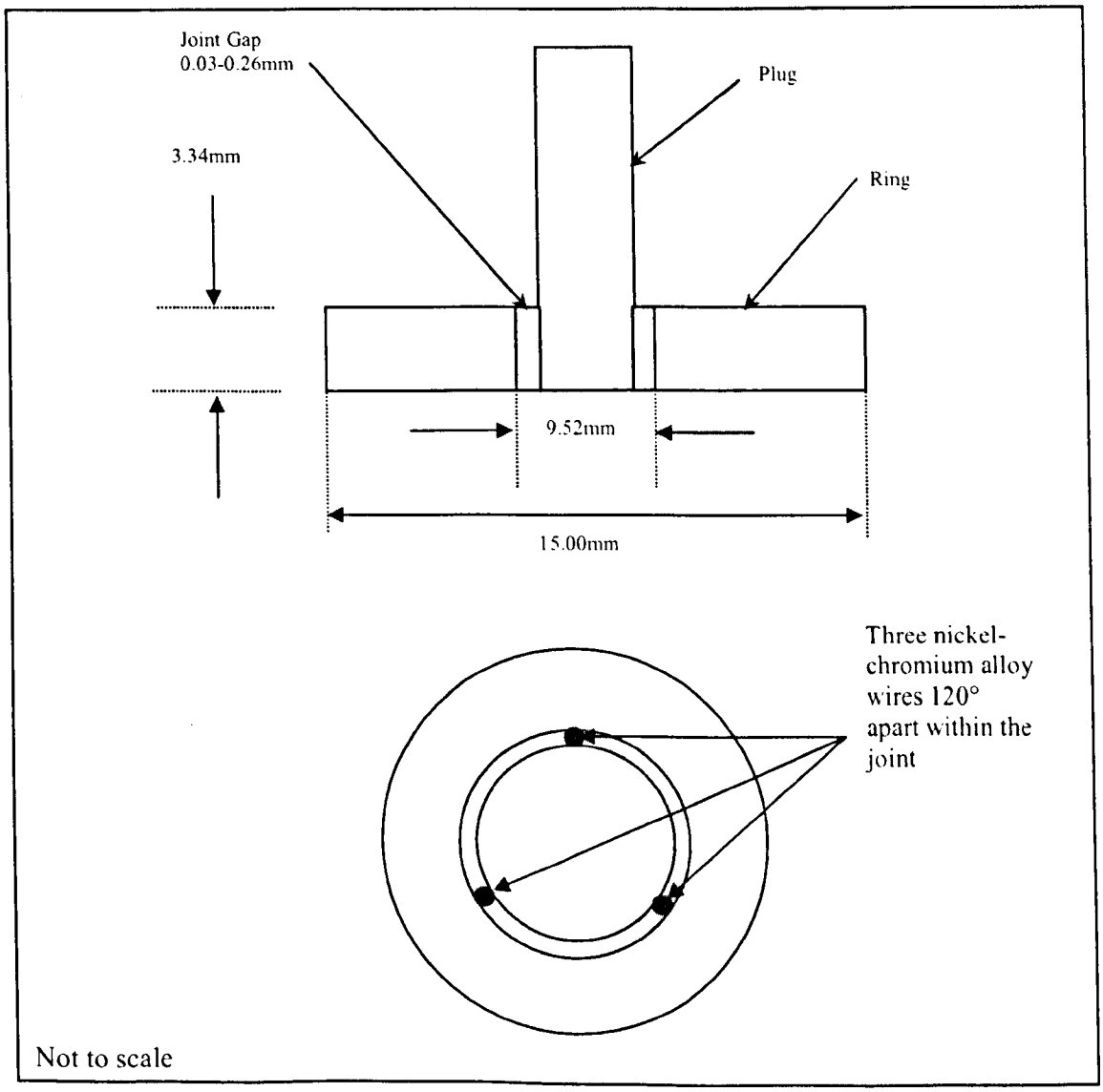


Figure 3.6 Schematic of the pin in ring assembly [88] [84]

The breaking load of the joint was determined by applying tension to the pin. Strengths were comparable to that of bulk solder, suggesting failure was occurring within the solder rather than the in IMC layer or at the solder/IMC interface. As the

soldering time and hence the IMC layer thickness increased there was a progressive fall in joint strength as discussed previously.

Rynemark *et al.* [90] used a 'pin in ring' joint configuration and soldering took place in a vacuum in order to minimise the occurrence of porosity. Figure 3.7 shows the dimensions of their model joint.

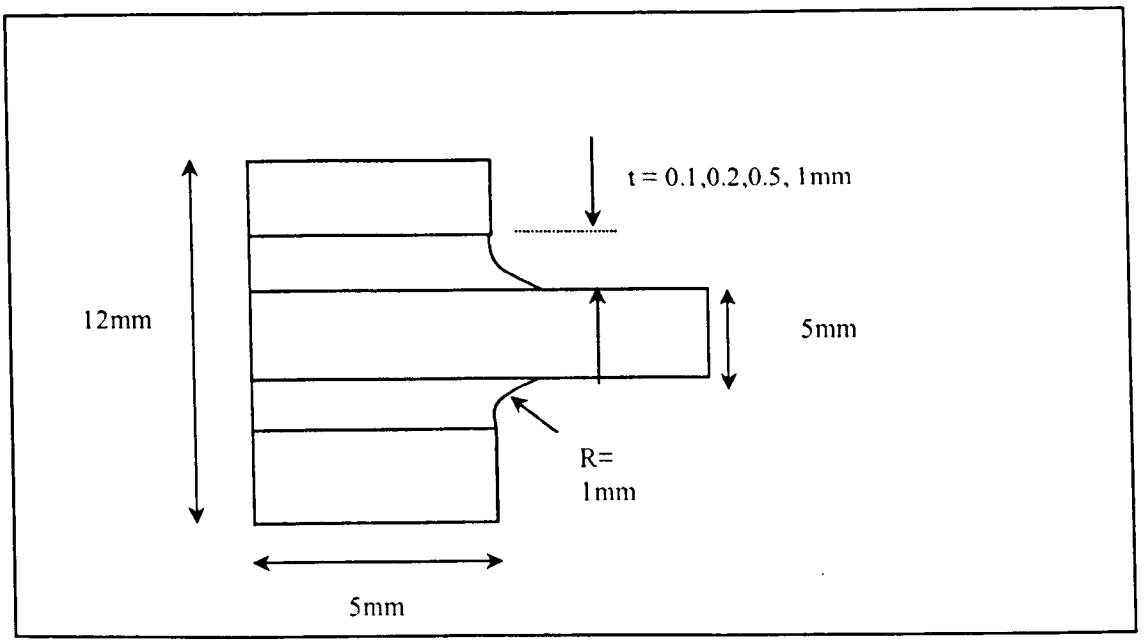


Figure 3.7 The 'pin in ring' sample used by Rynemark *et al.*

Ramon and Dirnfeld [86] manufactured 'ring and plug' specimens from lengths of electrical copper wire, figure 3.8. Rings were made from 3.2mm-diameter copper tubing, which was re-drilled with an internal diameter of 1.8mm after straightening. Slices 1mm thick were cut using a diamond blade. They were mounted onto the plugs, which were cut into 12 to 15cm lengths, and the ends crimped to prevent the rings falling off. The specimens were fluxed and a soldering iron placed to the crimped end for three seconds. The assembly was then left to solidify. Any excess wire and solder was removed by grinding, first with a stone grinder and then with increasing mesh sizes of wet grinding paper. The upper shoulder of the joint was simply cut with a sharp knife.

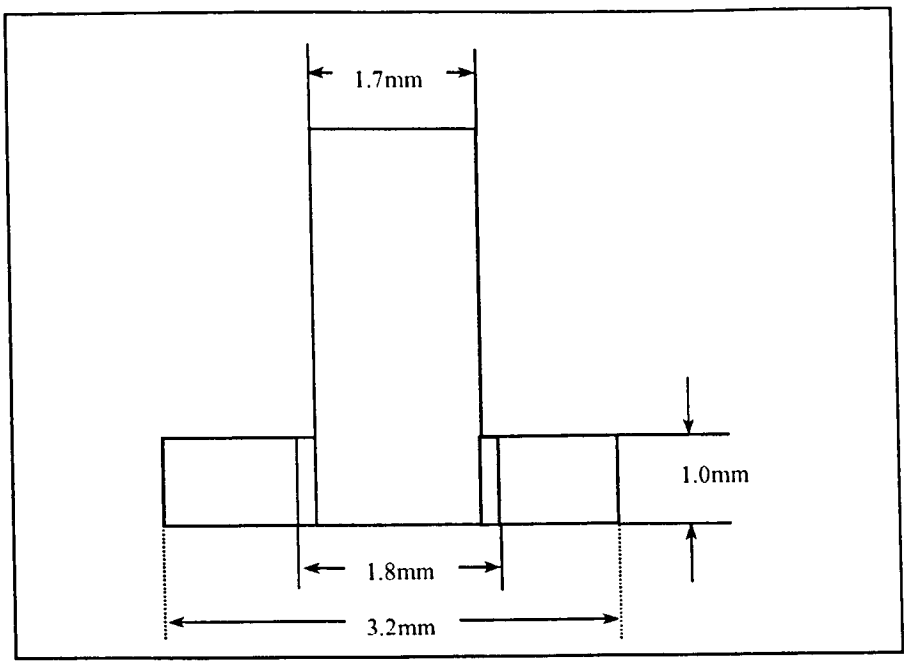


Figure 3.8 Ramon and Dirnfeld 'ring and plug' design [86]

Foley *et al.* [87] also analysed the shear strengths of 'ring and plug' samples using lead-free solders. They used a modified version of the manufacturing method first used by Thwaites and Duckett, omitting the spacing wires. A joint gap of 175μm was produced, see figure 3.9, as Johnson Manufacturing had shown that this was the least likely to produce micro-porosity in the alloys. Wires of both 'nichrome' [84, 88] and copper [91] appeared to induce problems in the sample joint integrity. The lack of spacing wires did produce some joints with varying thicknesses (non-concentrical plugs). However, it was claimed that the results were relatively consistent suggesting that by not using spacer wires, better wetting and less voiding were achieved.

Samples were tested using a plunger mechanism and the pin was pushed through the ring. The testing rig reduced the risk of any off-axis loading. Samples were tested at room temperature and at 125°C and the results are discussed in section 3.4.

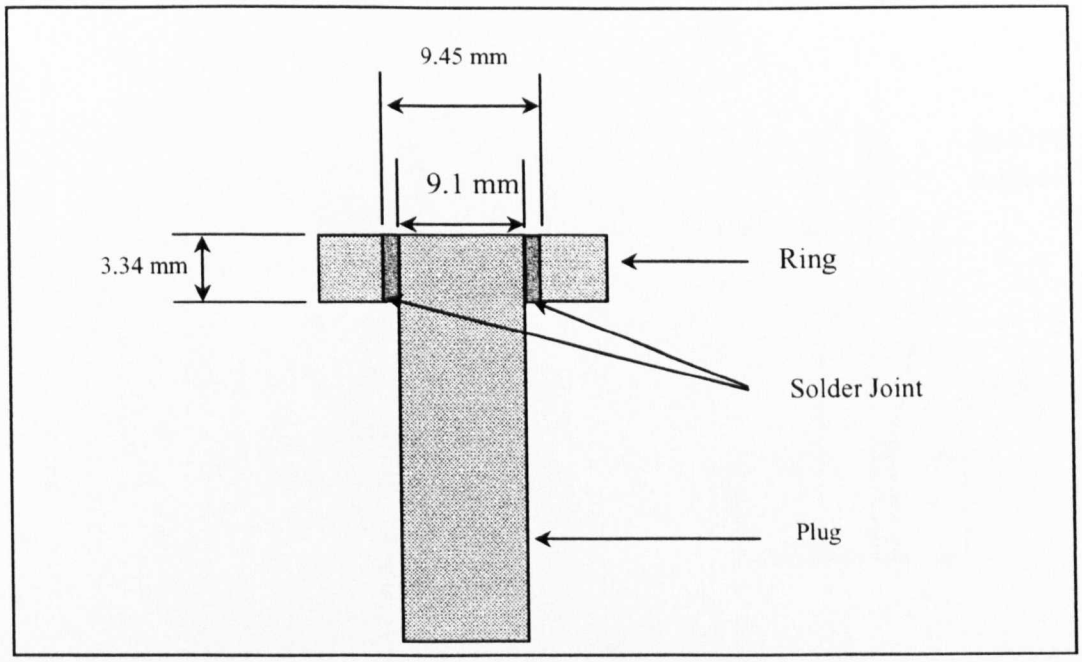


Figure 3.9 Diagram of the ring and plug sample configuration used (Foley *et al.*).

A manufacturing technique devised at the Swedish Institute for Metals Research [89, 92] also involves producing the ring and pin from pure copper and soldering together using conventional Sn-40Pb solder. The pin fitted into a gap machined into the ring component to ensure correct positioning of the pin prior to soldering, figure 3.10a. Before soldering, both components were cleaned using an ultrasonic bath and hydrochloric acid. They were dried, fluxed and a solder sheet was rolled around the pin and slid into the gap between the pin and ring. Soldering was performed by dipping the whole assembly into a solder bath held at 250°C. Any excess solder and copper were removed by machining to obtain the geometry shown in figure 3.10b.

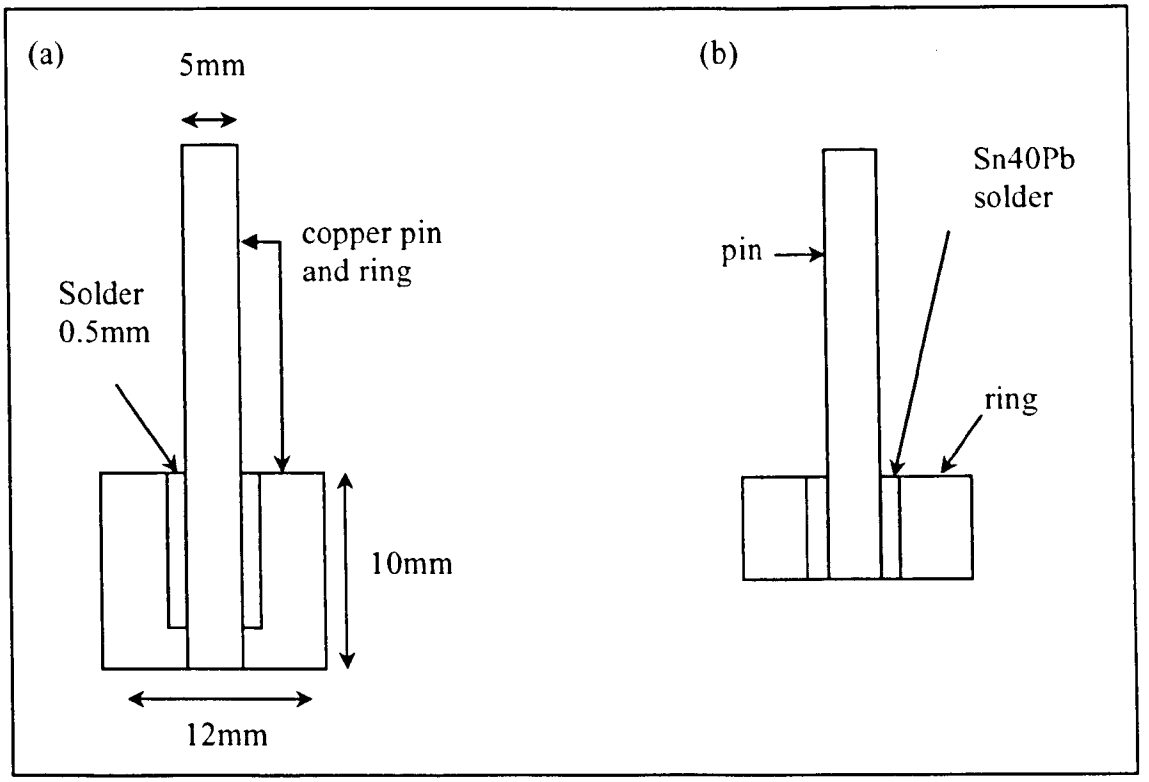


Figure 3.10 Pin in ring configuration used by Gillot and Rod.

On the authors' evaluation of these methods of production, several areas of concern arose. In particular, the possible change of joint microstructure due to heat being produced or strain hardening occurring during the machining step of production. Samples previously examined at the Open University indicate that there may be damage and property changes induced by surface machining [58]. The effects of spacer wires in manufacture, possible non-concentrical positions of the components and testing discrepancies were also areas of concern when devising a suitable and reliable manufacturing method.

Apparent advantages of using 'pin in ring' specimens include ease of preparation and convenience for loading in shear. These joints are considered most relevant to the design of engineering applications [84]. Work was performed to determine a suitable manufacturing method eliminating the areas of concern seen above. The manufacturing technique devised is described in chapter four.

## 3.4 Published Results on Joint Strength

The following section examines published data obtained from the testing of model joints. The majority of published data refer to the conventional Sn40Pb alloy. There is limited data for the lead-free alloys Sn-Cu and Sn-Ag, and at present there is very little data for the ternary Sn-Ag-Cu alloy.

Figure 3.11 summarises some of the data obtained from mechanical tests on joints [86-88, 93-99]. It demonstrates the difficulty in directly comparing results from different sources, reiterating a point first introduced in chapter two. There are many factors that influence joint properties. These include strain rate, temperature, joint geometry, test method, joint manufacture and microstructure. It is also necessary to take into account the slightly varying alloy compositions, substrate material and testing methods utilised by each researcher. Generally, when both lead-containing and lead-free alloys have been tested under similar conditions, the lead-free alloys are comparable or superior to the lead-containing alloys. The large 'bands' usually indicate that a significant number of alloys were tested (especially for references [94], [95] and [87]), and demonstrate the spread of the data obtained (a factor of two is not uncommon).

Figure 3.12 shows data for the three alloys about which most information is available [86, 88, 93-95], [87], [98, 99]. It should be noted that the alloys were tested at nominal room temperature and strain rates (as crosshead speeds) are shown on the graph for each data group. Although results obtained from different sources cannot be directly compared, there are some general trends apparent. Sn-0.7Cu joints have shear strengths similar or less than joints manufactured with Sn-40Pb. Also, the silver-containing lead-free alloy, Sn-3.5Ag, possesses superior shear strength to both the Sn-40Pb and Sn-0.7Cu alloys.

Figure 3.13 illustrates the effect of strain rate on the shear strength of 'pin in ring' joints for several alloys [88]. Again, strain rate here is deduced from crosshead speed, and its absolute value is governed by the specimen geometry. Increasing the strain rate by three orders of magnitude produces greater shear strengths for all nine alloys tested. A factor of two increase in shear strength typically results, apart from in the high lead alloys where the strengthening effect is smaller. Figure 3.14 demonstrates that all these alloys exhibit a higher shear strength at room temperature than at 100°C. The increase is generally less than a factor of two, and the high lead-silver containing alloys are much less sensitive to temperature. Both figures 3.13 and 3.14 show that alloys with a high tin and silver content (Sn-3.5Ag and Sn-36Pb-2Ag) possessed superior shear strengths. High lead alloys (lead content is greater or equal to 90 per cent) produced the poorest results of the nine alloys tested. Figure 3.15 shows that the shear strength of Sn-40Pb decreases with increasing temperature and decreasing strain rate. The same trends are observed for Sn-3.5Ag.

Figure 3.16 illustrates the effect of different joint geometries, pin in ring joint [87] and a butt joint tested in a asymmetrical four point bend test (AFPB) [95]. Shear strengths for the 'butt' joint configuration are consistently higher than those for the pin in ring joints, especially for the silver-containing alloy.

## 3.5 Summary

It is necessary to examine how microstructural changes, caused by the soldering procedure, determine the strength of joints. For the purpose of this work, the 'pin in ring' configuration was selected as a suitable model joint. Reliable methods of manufacture and testing were determined and are discussed in the following chapter.

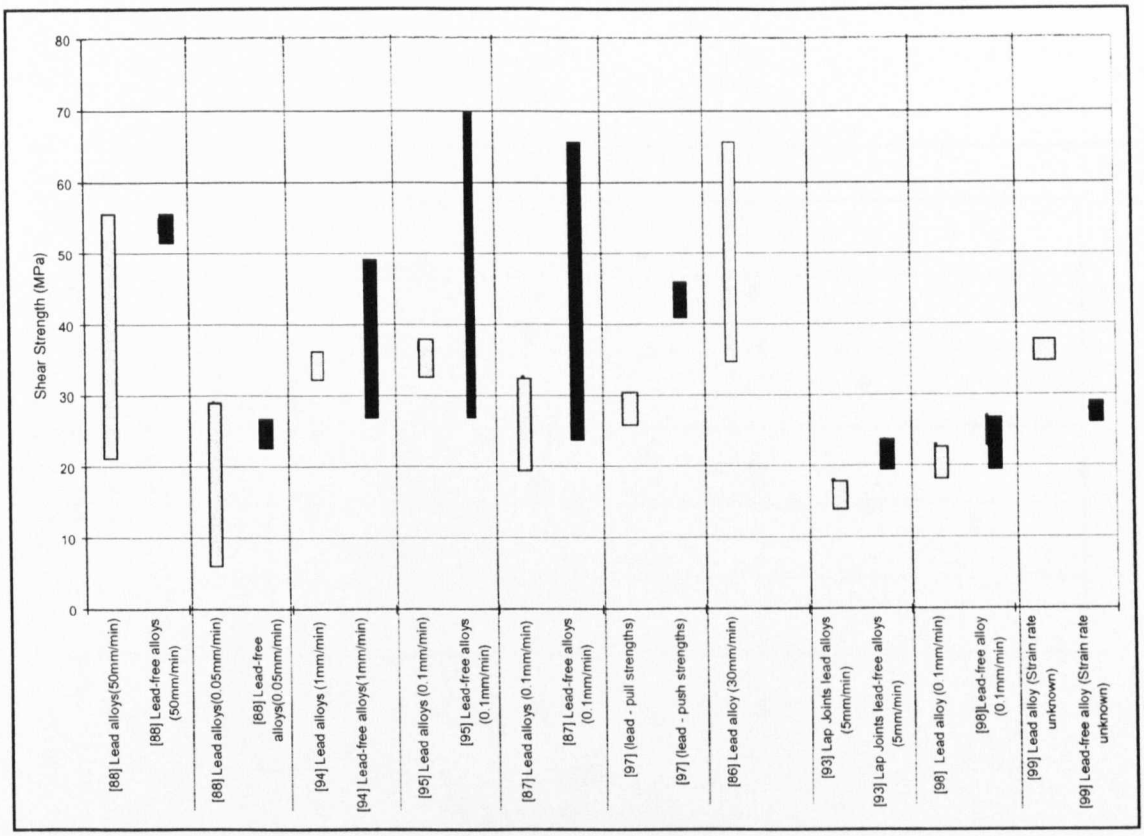


Figure 3.11 Data overview for the shear testing of lead-containing and lead-free model solder joints at nominal room temperature.

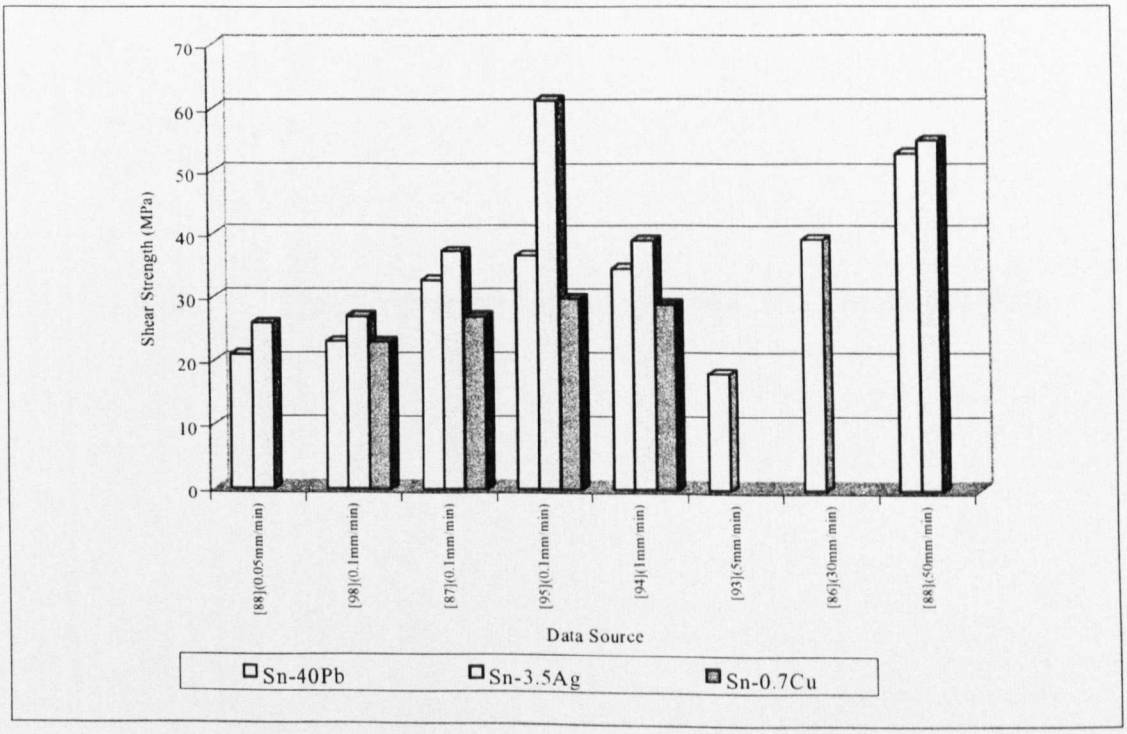


Figure 3.12 Groups of data for the shear testing of Sn-40Pb, Sn-3.5Ag and Sn-0.7Cu model solder joints at room temperature.

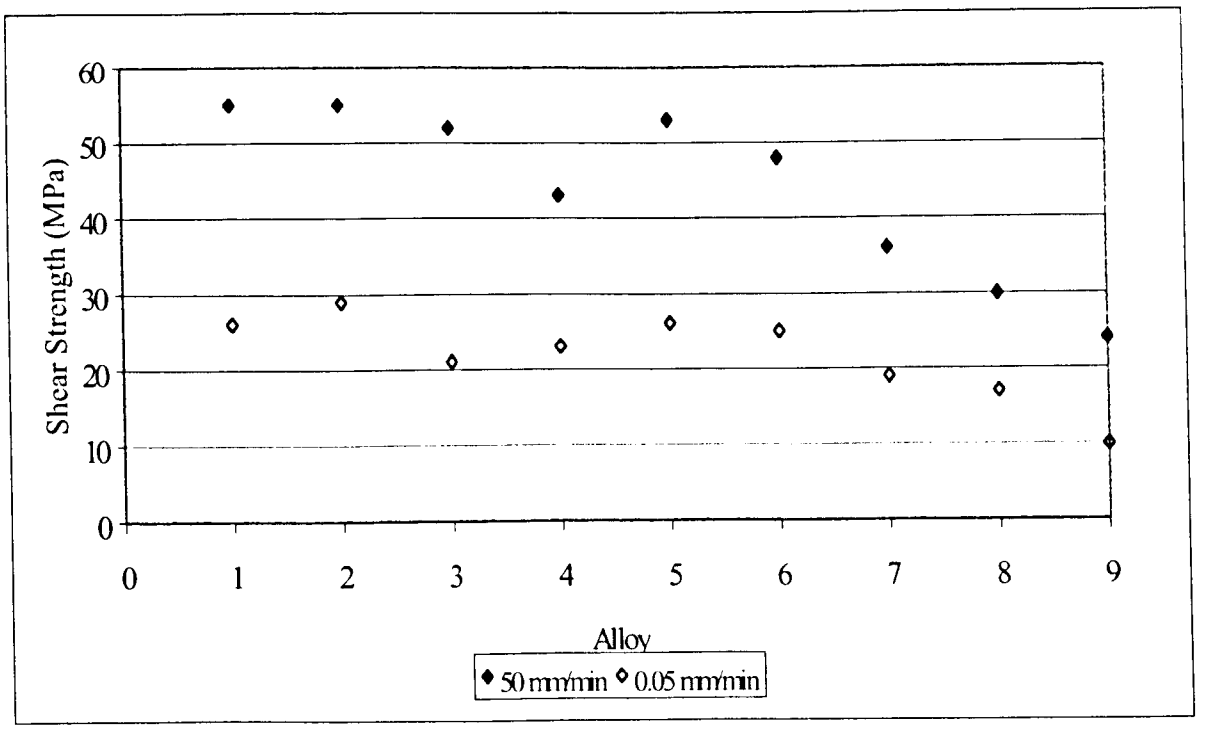


1- Sn-3.5Ag
2- Sn-36Pb-2Ag
3- Sn-40Pb
4- Sn-58Pb-2Sb
5- Sn-5Sb
6- Sn-60Pb
7- Sn-90Pb
8- Sn-93.5Pb-1.5Ag
9- Sn-97.5Pb-1.5Ag

Figure 3.13 Effect of strain rate on shear strength at 20°C (Stone *et al* [88]).

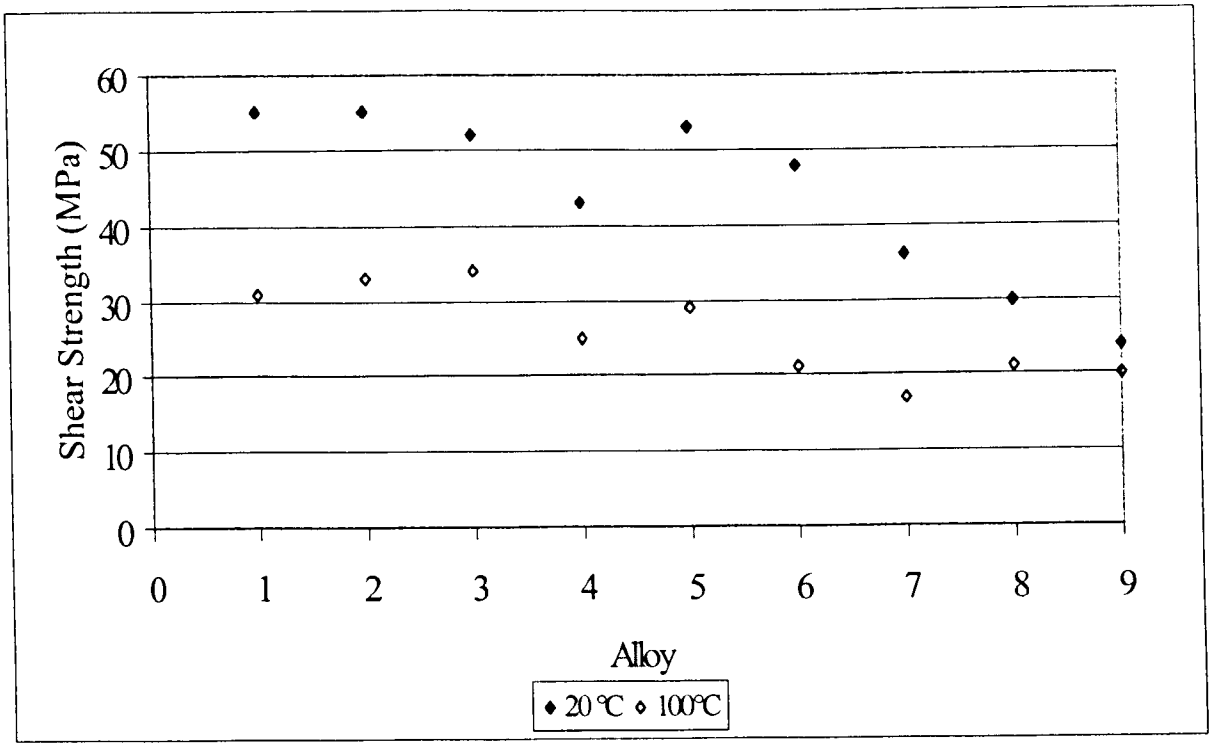


1- Sn-3.5Ag
2- Sn-36Pb-2Ag
3- Sn-40Pb
4- Sn-58Pb-2Sb
5- Sn-5Sb
6- Sn-60Pb
7- Sn-90Pb
8- Sn-93.5Pb-1.5Ag
9- Sn-97.5Pb-1.5Ag

Figure 3.14 Effect of temperature on shear strength (strain rate of 50mm/min)(Stone *et al* [88] ).

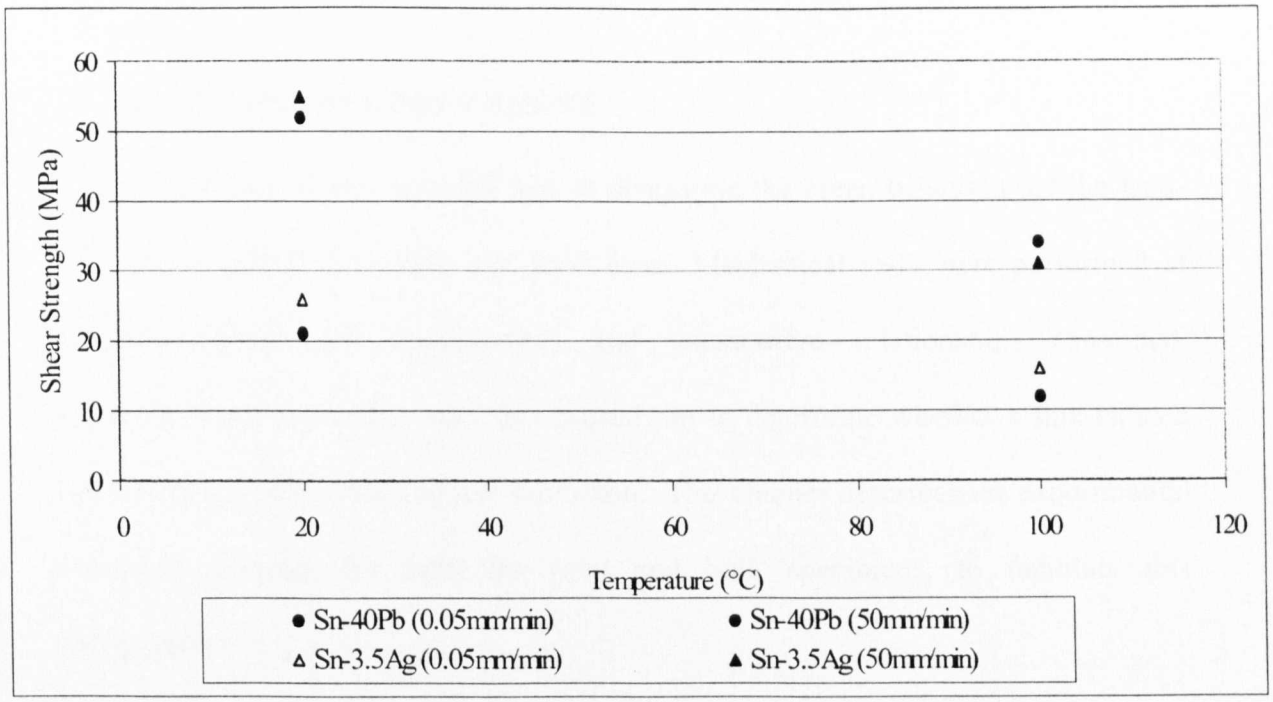


Figure 3.15 Variation of shear strength of Sn-40Pb and Sn-3.5Ag 'pin in ring' joints with temperature and strain rate (Stone *et al* [88]).

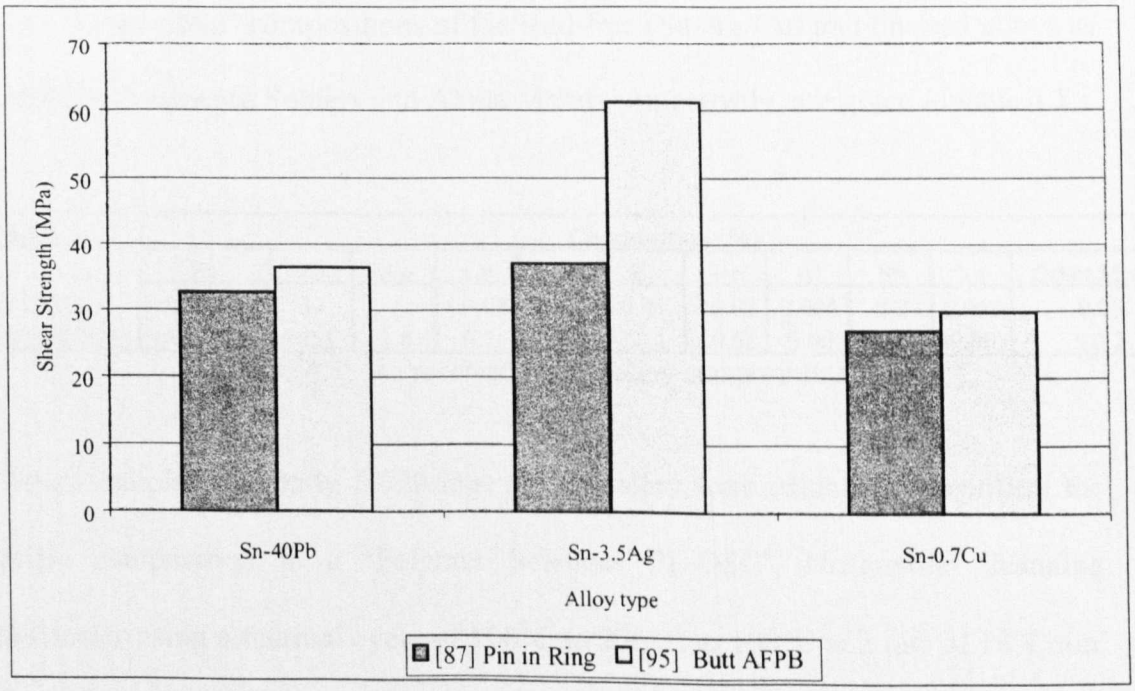


Figure 3.16 Variation of shear strength with joint geometry (Anderson et al [95]) and Foley et al [87]).

# CHAPTER FOUR

## 4 EXPERIMENTAL PROCEDURE

The objective of this research was to determine the creep behaviour of the lead-free Sn-3.8Ag-0.7Cu in bulk and joint form. Mechanical tests were performed at various stresses and temperatures and constitutive relationships examined. Microstructural evaluation was also carried out to determine whether a link existed between creep properties and microstructure. This chapter describes the experimental procedure utilised, for both the joint and bulk specimens, to facilitate this investigation.

### 4.1 Bulk Solder Specimens

#### *4.1.1 Materials*

The 'as specified' compositions of the lead-free (Sn-Ag-Cu) and tin-lead alloys as supplied by Multicore Solders and Alpha Metals respectively, are given in table 4.1.

| Alloy | Composition (%) | | | | | | | | | | |
|---|---|---|---|---|---|---|---|---|---|---|---|
| | Sn | Pb | Ag | Cu | As | Bi | Fe | Al | Sb | Zn | Other Metals |
| Sn-37Pb | BALANCE | 37 | - | <0.08 | <0.02 | 0.25 | <0.02 | 0.005 | 0.2 | 0.005 | 0.08 |
| Sn-3.8Ag-0.7Cu | BALANCE | <0.1 | 3.8 | 0.7 | <0.03 | <0.1 | <0.02 | <0.001 | <0.1 | <0.001 | <0.2 |

Table 4.1: 'As received' solder alloy compositions

Small samples (typically 10-20 mg) of each alloy were examined to confirm the specific composition in a 'Polymer Sciences PL-DSC', Differential Scanning Calorimeter using a thermal cycle of 100°C to 270°C to 100°C at a rate of 10°Cmin$^{-1}$. By comparing with alloys of known compositions, the scan identified whether the new material was a true eutectic or not. If the compositions were not true eutectic there would be an additional melting peak. The materials supplied were confirmed to be of the correct composition.

### *4.1.2 Sample Manufacture*

Samples were manufactured by melting the alloys in dedicated ceramic crucibles to avoid contamination. The molten alloys were then cast into a pre-heated cylindrical aluminium mould. Three samples, with a gauge length of 60mm and a cross-sectional area of $100mm^2$, were produced from each casting (appendix 4.1, plate 4.1). When casting, the molten alloy pours from beneath the oxide layer, leaving the dross at the base of the crucible. Immediately after casting, samples were water-quenched by lowering the mould into a basin of water and then placing them under cold running water. 'Water quenching' (which yields a cooling rate of 20°C/sec) produces a fine microstructure, which closely resembles that found in actual, manufactured solder joints. Once manufactured, samples were stored in a freezer at −18°C, to inhibit any microstructural evolution prior to testing. Only the water cast microstructure was examined for this project, examination of 'air cooled' and 'furnace cooled' microstructures had already been performed within the Solder Research Group [100].

### *4.1.3 Bulk Creep Testing*

The Open University creep facility houses approximately thirty constant load creep frames (appendix 4.1, plate 4.2). Six of these are capable of testing at temperatures as low as −50°C. Testing involved the application of a load to a bulk solder sample by the means of a lever arm. Each frame had a specific lever arm ratio, see figure 4.1. The load caused the sample to extend at a constant temperature. Testing was performed in the temperature range −10 to 125°C, (giving homologous temperatures between 0.54 to 0.81, see table 4.2). Extension was measured by a LVDT (linear voltage displacement transducer) and data were recorded both on an X-Y chart recorder and Pico computer software. Temperature was monitored using

'K' type thermocouples at two positions along the sample gauge length and was also logged using Pico software.

| Alloy | Melting Temp (K) | Test Temp (°C) | Test Temp (K) | Homologous Temperature |
|---|---|---|---|---|
| Sn-37Pb | 456 | 75 | 348 | 0.76 |
| Sn-3.8Ag-0.7Cu | 490 | -10 | 263 | 0.54 |
| Sn-3.8Ag-0.7Cu | 490 | 29 | 302 | 0.62 |
| Sn-3.8Ag-0.7Cu | 490 | 75 | 348 | 0.71 |
| Sn-3.8Ag-0.7Cu | 490 | 99.4 | 372.4 | 0.76 |
| Sn-3.8Ag-0.7Cu | 490 | 125 | 398 | 0.81 |

Table 4.2 Homologous temperatures at specified test conditions

Before use, both transducers and temperature recording equipment were calibrated and any errors were noted on the chart. Temperature recording capabilities were confirmed by comparing readings with data obtained using a hand held thermocouple. The furnaces maintained a constant temperature to within ±0.3°C (Appendix 4.2).

The sample was placed into split collets and attached to the rig using pins, (figure 4.1). With the sample, transducer and thermocouples in place, the furnace was switched on and the system was allowed to equilibriate at the test temperature for one hour and the load was then applied. Data recording during short-term tests was continuous for both strain and temperature. For longer term tests, the temperature recording was constant, but strain measurements on the chart recorder were monitored once or three times daily (due to the long lifetimes of the samples), until near failure when recording was continuous.

Testing was performed on the tin-lead alloy at 75°C to complete the series of other tin-lead data collated within the research group. Results at 75°C presented in chapter six are a mix of data obtained by the author and an additional member of the research group.

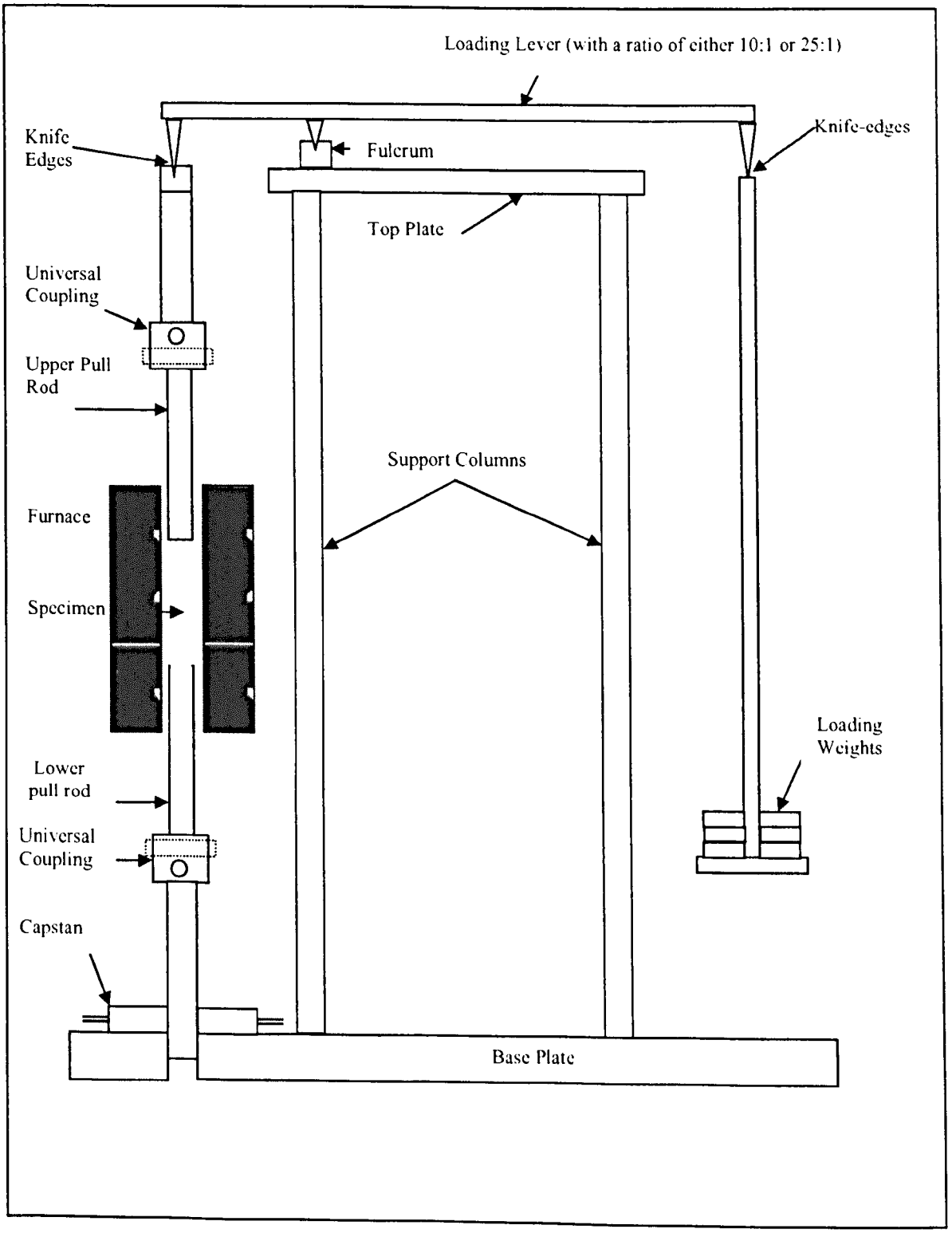


Figure 4.1: Constant load creep frame

### *4.1.4 Metallography*

Examination of bulk solder microstructure plays a valuable role in the determination of creep mechanisms and the effect of temperature and strain. Samples were examined using both a MEF3 Optical Microscope and a JEOL JSM-820 Scanning Electron Microscope. Metallography was performed on both lead-containing and lead-free solder alloys. Small sections of crept samples were made using electric discharge machining as this minimises specimen damage. Sections were taken to examine: the microstructure after heating (specimen head); the effect of heat and strain (gauge length); severe straining/deformation (necked area); and the as cast structure, see figure 4.2. Fracture surfaces were also examined using the scanning electron microscope.

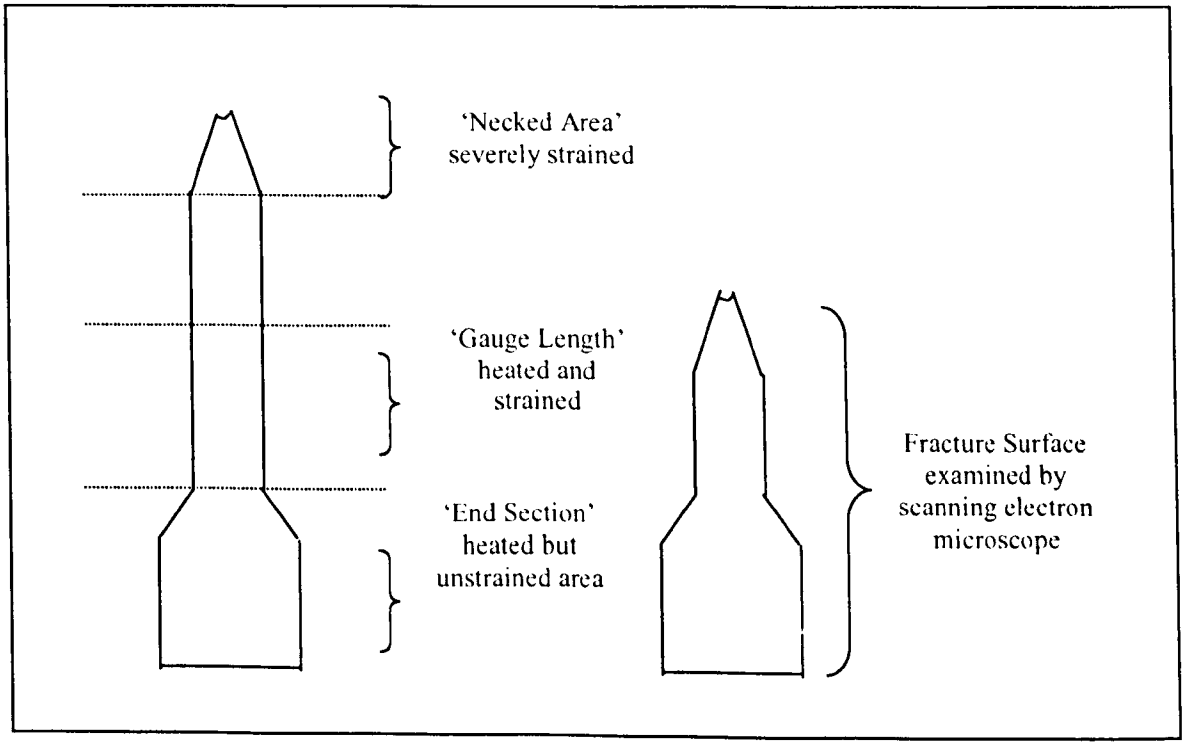


Figure 4.2: Sections of creep specimens required for metallography

Once sectioned, samples were placed into pre-greased mounting cups and submersed in Epofix resin. This resin produces little heat on curing minimising the temperature increase, which may have an effect on the microstructure. Grinding and polishing were performed on a Buehler Autopol and a Struers RotoPol-35 respectively (automated grinding and polishing machines).

The metallographic procedure for each type of alloy was as follows (see figure 4.3); Sn-Pb alloys were wet ground to a 1200 grit finish using silicon carbide paper (SiC), polished to 1μm using diamond followed by a final polish with 0.05μm colloidal silica (Masterprep). An ammonium acetate etchant was added to the final polishing step to emphasise the difference in phases. The ternary alloy was wet ground using SiC paper from 1200 to a 4000 grit finish, followed by diamond polishing to a 1μm finish and with a final stage using 0.05μm colloidal silica. To emphasise intermetallic compounds dilute ammonium persulphate solution was added to the 0.05μm polishing cloth. To enhance the examination of grain sizes and boundaries, the samples were repolished using the above method (omitting the ammonium persulphate) and etched using HCl vapour. Both Sn-37Pb and lead-free samples were examined under an optical microscope between polishing steps and stages were repeated if necessary. Samples were stored in a dessicator prior to microscopic examination.

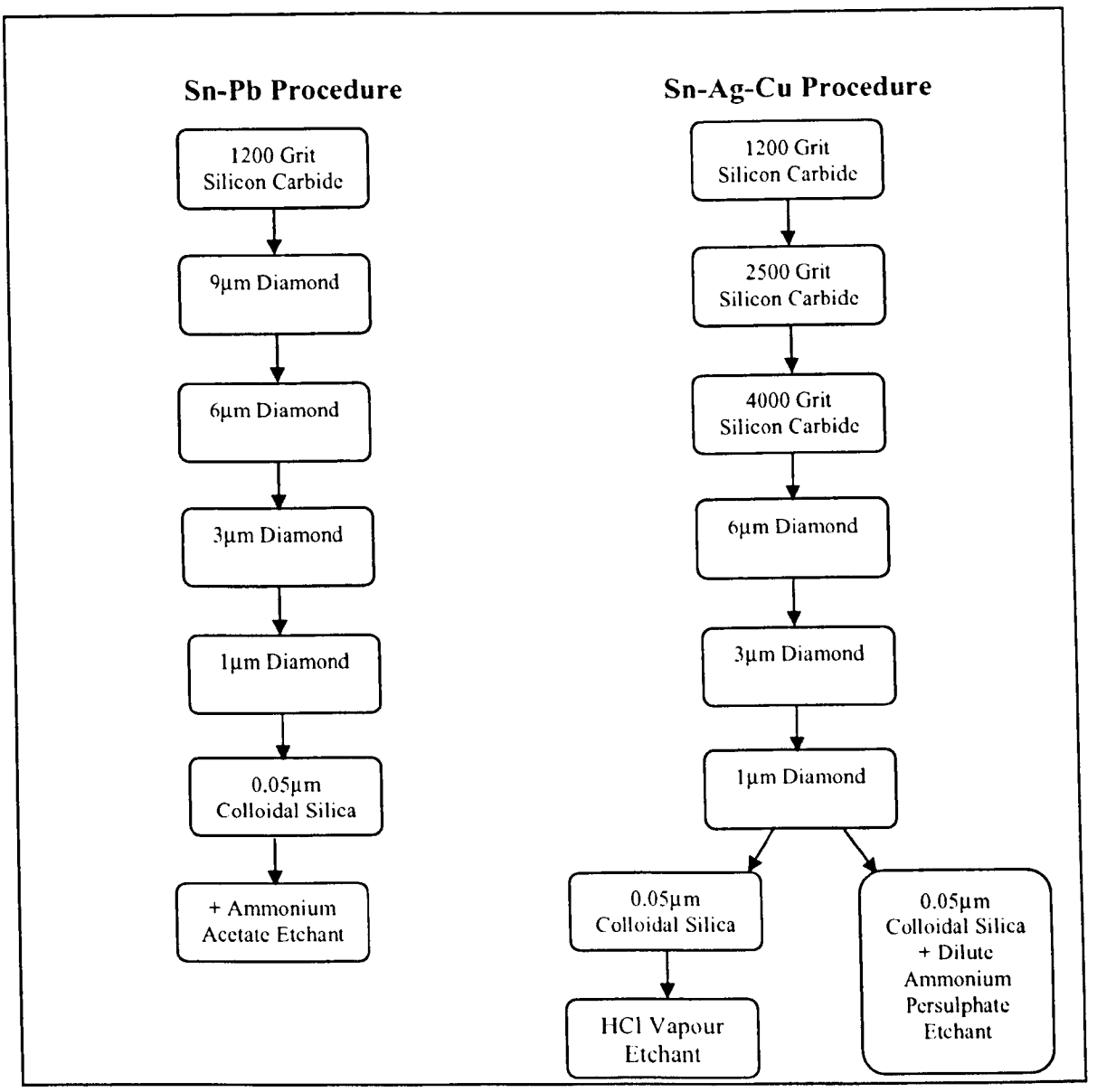


Figure 4.3 Metallographic techniques for solder alloys

## 4.2 Joint Testing

### *4.2.1 Materials*

For the production of joints, pure copper (for the pin and ring components), Sn-3.8Ag-0.7Cu solder (supplied by Multicore Solder) and a liquid flux were used. Both solder and copper were supplied in ingot form. Copper rings were machined to a 12mm outer diameter and the pins to a 6mm diameter. The copper rings were produced with an 8mm inner diameter producing a solder gap of 1mm between the ring and pin. Solder sleeves were produced from the solder ingot to fit around the ring and provide adequate solder to sufficiently fill the gap.

### *4.2.2 Sample Manufacture*

The method devised to manufacture the pin in ring joints, see figure 4.4 involved mounting the pin, spacer ring and copper ring into a small aluminium rig that ensured gap width and concentricity of the pin. The spacer ring was required to allow air around the joint permitting the flow of solder into the gap. Prior to assembly, the pin component was ground to a 1200-grit finish using silicon carbide paper and coated in the liquid flux. During trials this was found to reduce voiding at the pin surface. Once assembled, the solder barrel was pinched against the pin so that it sat just above the ring. Approximately 0.5ml of flux was injected into the solder gap using a hypodermic syringe. Flux is required to 'clean' the surfaces being soldered and to prevent re-oxidisation during the soldering procedure. The assembly was heated using a handheld gas burner for approximately 30 seconds, until the solder flowed into the gap. The time and temperature of soldering was measured using Pico software (an example of a heating profile can be seen in appendix 4.3). Once soldering was complete, the assembly was water quenched by plunging into a basin

of cold water. Water quenching produced a fine microstructure and inhibited intermetallic growth. This represents similar cooling rates as found in service, therefore producing a structure representative of that found in actual joints. However, solder joints commercially manufactured with the ternary alloy, for the purpose of comparison, have been extremely difficult to obtain.

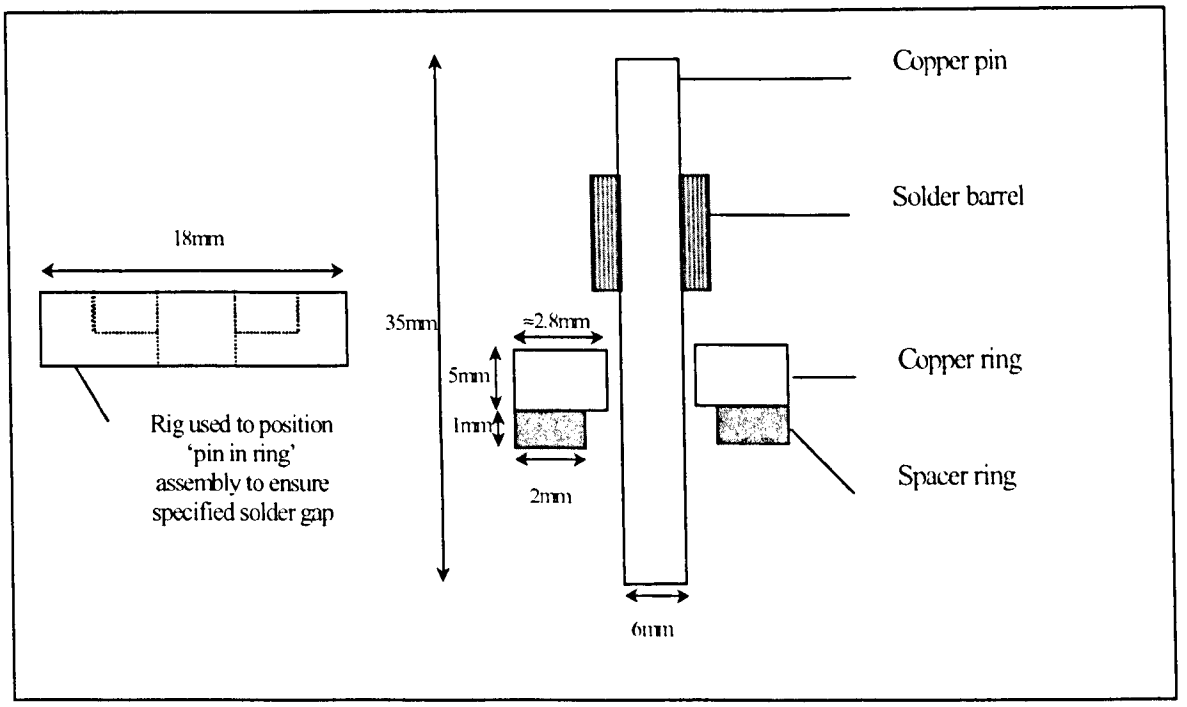


Figure 4.4 Assembly used for the manufacture of a pin in ring model joint specimen
(Appendix 4.4 Photograph of a manufactured pin in ring specimen used in this research)

### *4.2.3 Shear Strength Measurement*

The manufactured joints were first tested using a screw driven Instron machine to obtain a representative value for shear strength (cross head displacement rate: 0.5cm/min). This provided an indication of the loads to be used in creep testing and also probable failure locations within the joint. Joints were held in a simple jig with both the pin and the jig held in grips. During the test the pin was pulled down through the ring. Testing was performed at room temperature.

### 4.2.4 *Joint Creep Testing*

After establishing a representative value for shear strength, manufactured joints were tested in creep. Joints were mounted into standard creep frames (as used for bulk testing) using a modified loading rig (see figure 4.5). Testing was performed in the temperature range 29-125°C, (giving homologous temperatures between 0.62-0.81) using the same procedure as described for bulk testing.

By comparison of the moduli for both the copper and solder it was assumed that the joint would fail in the solder (5.6GPa for solder and 130GPa in copper, see appendix 4.7). It was shown by calculation that shear stress would be concentrated at the solder/pin interface, where the cross sectional area is smallest. Therefore the calculated shear stress values are determined using 94.2mm$^2$ as the cross sectional area (as the sample was loaded in shear), appendix 4.5.

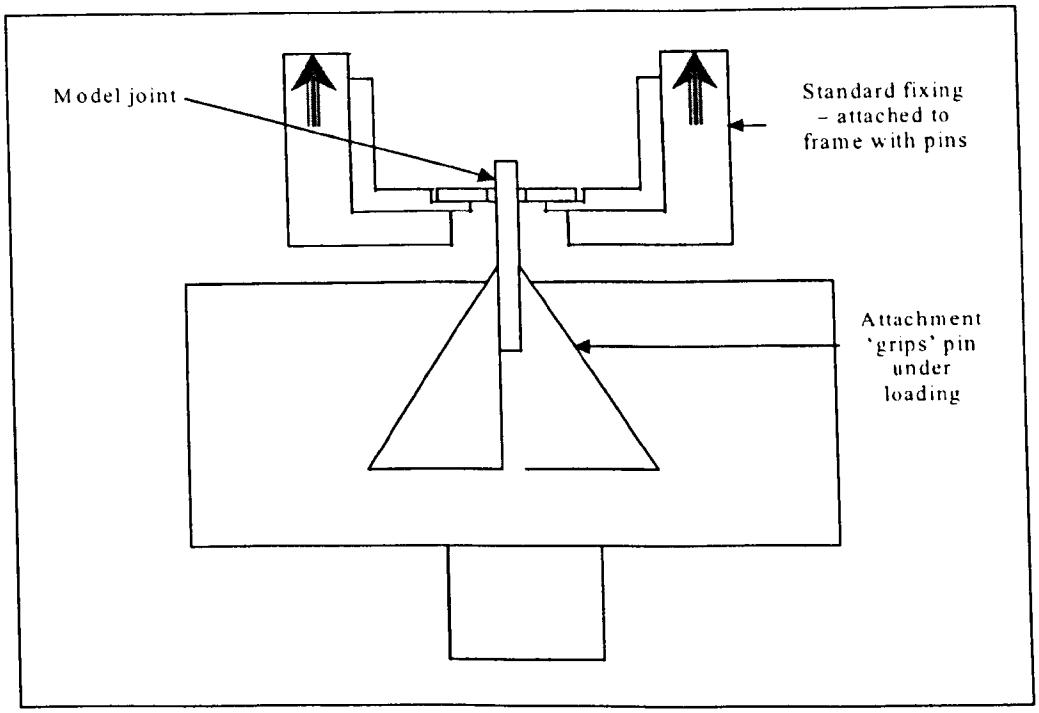


Figure 4.5 Attachment for loading 'pin in ring' model joints into a standard creep frame (Appendix 4.6 shows a more detailed drawing including dimensions)

During the testing of the model joint samples, it was observed that large instantaneous strains occurred on loading. These were uncharacteristically large and

their origins were investigated, appendix 4.7. It was thought that large displacements may be caused by the slipping and gripping mechanism of the rig deforming the copper, slipping of the specimen in the gripping mechanism or displacement in either the copper or loading assembly. Solid copper specimens were used in the creep rigs to identify a machine constant under typical test conditions.

### *4.2.5 Metallography*

To determine failure location, intermetallic layer thickness and the influence of test conditions on microstructure, joints were examined using both optical and scanning electron microscopy. Sectioning and mounting followed the same procedure as that described for the bulk material. Grinding and polishing were performed on Buehler Autopol and Struers RotoPol machines, using a similar procedure as for bulk lead-free solders but omitting the HCl etching stage. Polished specimens and fracture surfaces were examined using optical (MEF3 Optical Microscope) and scanning electron microscopy (using a JEOL JSM-820 Scanning Electron Microscope.)

Energy dispersion spectroscopy (EDS) was performed using a Noran Vantage X-ray microanalyser in conjunction with the JEOL scanning electron microscope. This was used for both spot analysis of the microstructure and for detailed line scanning across the samples. Spot analysis was performed to identify specific particles within the structure and the line scanning determined the composition of the structure across the copper solder interface and within the bulk solder.

## 4.3 Possible Sources of Experimental Error

Although the topic of experimental error has been touched upon throughout the thesis, this section brings together many of the sources of error discovered and the methods utilised for eliminating or reducing it.

Creep is temperature dependent and any temperature change over the life of a creep test may provide a source of some error in strain recording. In order to determine whether errors were introduced in this manner, temperature was monitored continually during the entire creep test (using Pico log software). Any changes in temperature were compared with the 'strain versus time' plots to determine whether the observed variation in temperature had an effect on the creep curve. There may also be some inaccuracy of this measured temperature and it was necessary to compare and, if necessary, calibrate the thermocouples and data logging equipment with a standard (usually a handheld thermocouple).

Thermal gradients may occur over the gauge length of the specimen, therefore it was important to measure temperature at various locations along the gauge length to determine whether the sample had an even temperature distribution. In this research temperature was measured at two points along the sample gauge length. Generally, the furnaces enabled temperature control to ±0.3°C as measured at each point on the sample.

The microstructure of samples was an important consideration during manufacture as it was previously discovered that differences in microstructure would effect overall mechanical properties [58]. Although great care was taken during sample production, slight differences may occur such as small variations in quench rates and thermal history. All samples for this research were water quenched from casting and stored at −18°C in a freezer prior to test. Due to careful preparation

microstructures were assumed to be similar. It was difficult to confirm this assumption, as samples would require sectioning i.e. destructive analysis, which was not performed during this research.

It is possible that due to surface finishing in manufacturing the gauge length of samples contains work hardening effects or is not parallel. Therefore, for the purpose of this research, samples were tested 'as cast' eliminating any inaccuracies that may be introduced by machining and surface finishing.

Before commencement of the creep testing of bulk SnAgCu in this research, the author determined a feedback check on the accuracy of recording by superimposing the authors Sn-Pb data onto a Sn-Pb data set obtained by another member of the Solder Research Group.

## 4.4 Summary

During this research, the lead-free ternary solder alloy, Sn-3.8Ag-0.7Cu was examined both in its bulk and joint form. Alongside mechanical testing, metallographic analysis was performed to determine the role of microstructure in the creep behaviour of SnAgCu. The quantitative results for bulk and model joint behaviour are now presented in the following chapter and are discussed in conjunction with microstructural findings in chapter six.

# CHAPTER FIVE

## 5 RESULTS

This chapter examines results obtained from the mechanical testing of Sn-3.8Ag-0.7Cu in bulk and joint form. The author performed the testing between 29°C and 125°C and a colleague within the SRG collated additional 'bulk' results at −10°C. The chapter has been divided into two sub-sections, 'bulk data' and 'model joint data', and the information is evaluated separately. Analysis was performed to determine the best-fit creep relationship for the ternary alloy in each circumstance. Results are presented along with microstructural evaluation. Discussion of quantitative data and microstructural findings to substantiate quantitative data is presented in chapter six. Comparison between bulk and model joint behaviour and the performance of the bulk ternary alloy with respect to other lead-free and lead-containing alloys are also considered in the following chapter.

### 5.1 Bulk Sn-3.8Ag-0.7Cu Solder Alloy

#### *5.1.1 Individual Creep Test Analysis*

A typical strain versus time curve obtained from a constant load creep test (at constant temperature) is illustrated in figure 5.1. The data were obtained for the ternary alloy at -10°C (263K) with an initial applied stress of 38MPa. It is evident that even at temperatures as low as '−10°C' ($T_h$ = 0.54), the homologous temperature is still sufficiently high for creep to occur. This specimen possesses a creep life greater than 2,000 hours and exhibits all creep regimes (primary, secondary and tertiary creep). Values, which are useful for comparing creep data from different sources, can be established from this information, for example 'time to rupture',

'minimum strain rate' and 'strain to failure'. It is also useful to plot this data as strain rate versus life fraction to produce a bathtub shape curve, figure 5.2.

Here, strain rate is defined as

$$\frac{\varepsilon_{t_2} - \varepsilon_{t_1}}{t_2 - t_1}, \qquad (5.1)$$

and life fraction as

$$\frac{t}{t_r}, \qquad (5.2)$$

where $\varepsilon$ = strain (at $t_2$ and $t_1$)
$t$ = time
$t_r$ = time to rupture.

This plot provides an understanding of strain rate variation during creep life. By defining steady state creep parameters, measurements of each creep regime can be made. This method of analysis is described in greater depth in section 5.1.7 and was utilised for all bulk specimens. A table summarising the obtained data, strain versus time and strain rate versus life fraction plots for all tests performed during this research can be found in appendix 5.1.

### *5.1.2 Time to Rupture*

Figures 5.3a and b show stress versus time to rupture plots (semi-log and log scales) incorporating all test temperatures from –10 to 125°C. These plots demonstrate the effect of both stress and temperature on the creep life of the ternary alloy. By increasing either test temperature or initial applied stress, the resulting creep life is reduced. In terms of creep strength (in MPa) at 10, 100 and 1000-hour lives at each temperature, the values are shown in table 5.1. At all temperatures, the

creep strengths at 1,000 hours are approximately eighty percent of those at 100hrs and between sixty to seventy-five percent of those at 10 hours. Due to the nature of long term creep testing it is difficult to incorporate precise error calculations and error bars onto plots. Therefore, only errors for this and the Norton's Law plot have been examined and are discussed in appendix 5.2.

| **Temperature °C** | **Creep strength (MPa) at 10 hrs** | **Creep strength (MPa) at 100 hrs** | **Creep strength (MPa) at 1,000hrs** |
|---|---|---|---|
| -10 | 52.9 | 46 | 40 |
| 29 | 36.2 | 31 | 27 |
| 75 | 23.5 | 19 | 15 |
| 99.4 | 20.6 | 17 | 14 |
| 125 | 15.6 | 12 | 10 |

Table 5.1 Creep strengths at 10, 100 and 1,000 hours

Creep life is greatly effected by initial applied stress and strain to failure appears to decrease with reducing stress. Ratio of creep life is shown in table 5.2. Stress values were chosen to represent high, medium and low stress levels for each data set.

| **Temperature °C** | **Initial Applied Stress** */Creep Life Ratio* | | |
|---|---|---|---|
| -10 | **38MPa** *70* | **45MPa** *4* | **50MPa** *1* |
| 29 | **26MPa** *3,200* | **28MPa** *1,200* | **45MPa** *1* |
| 75 | **12MPa** *1,700* | **19.5MPa** *40* | **27MPa** *1* |
| 99.4 | **15MPa** *75* | **17MPa** *30* | **25MPa** *1* |
| 125 | **8MPa** *14,100* | **12MPa** *600* | **25MPa** *1* |

Table 5.2 Effect of stress on creep life at each test temperature

In calculating the following creep life ratios at three different temperatures, (table 5.3), some of the results were extrapolated. Data extrapolation cannot guarantee accurate predictions of life because creep mechanisms may change.

| At 20MPa | **125°C** | **75°C** | **29°C** |
|---|---|---|---|
| Ratio | 1 | 60 | 10,000* |
| At 30MPa | **75°C** | **29°C** | **-10°C** |
| Ratio | 1 | 200 | 50,000* |

Table 5.3: Creep life ratios at various test temperatures (* extrapolated data)

A reduction in ductility is also apparent as temperature is reduced. This ductility trend is not obvious for all data (as illustrated in section 5.1.3).

Equations for the best fit lines in figure 5.3b (logarithmic plot of stress vs. time to rupture) were established, paying particular attention for any bi-linearity occurring at low stresses, as this may indicate a change in dominant creep mechanism. The general form of the equation is as follows;

$$\sigma = C.t_r^m \qquad (5.3)$$

by taking logarithms of equation 5.3, the relationship expands to:

$$\log\sigma = m.\log t_r + \log C \qquad (5.4)$$

where $\sigma$ = stress
$t_r$ = time to rupture
C = constant

Lines and resulting equations were obtained using 'excel software' to fit a trend to all the available data. Table 5.4 shows the gradients and intercepts obtained for each of the test temperatures.

| Temperature °C | Gradient | Intercept (MPa) |
|---|---|---|
| -10 | 0.0597 | 60.65 |
| 29 | 0.0644 | 41.99 |
| 75 | 0.1005 | 29.56 |
| 99.4 | 0.0792 | 24.67 |
| 125 | 0.1073 | 19.94 |

Table 5.4 Constants obtained from time to rupture lines

With the exception of 75°C, the gradient of the slopes generally increase slightly with increasing temperature. At all test temperatures the creep response is highly stress dependent (the gradient is shallow) i.e. a small change in applied stress will significantly affect the time to rupture. The intercept indicates creep strength at one hour (Log 1 = 0).

There is no apparent bi-linearity of the lines at any of the test temperatures, although there is a large scatter of data at the lower stress levels (longer life times) at 75 and 99.4°C. This may suggest a change of dominant creep mechanism. Further work is required in this area, and compared to the minimum strain rate versus stress plots. However, due to extended lifetimes and limited testing resources, repeat testing was impractical given the specified time scale of this research.

### *5.1.3 Creep Ductility*

Figures 5.4a and b show 'strain to failure' as both a function of time to rupture and of stress. Failure strain appears to decrease with increasing lifetime, however, given the wide scatter of data is difficult to quantify. No clear trend exists between strain to failure and stress. Generally, ductility values range between 0.1 (10%) to 0.4 (40%), with the majority falling below 0.3 (30%).

### *5.1.4 Monkman-Grant Relationship*

Figure 5.5 shows the relationship between minimum strain rate and lifetime. The data fall in a straight line in agreement with Monkman-Grant's empirical law:

$$\dot{\varepsilon}_{min} t_r = C, \qquad (5.5)$$

where $\dot{\varepsilon}_{min}$ = minimum strain rate ($h^{-1}$)
$t_r$ = time to rupture (h)
C = constant.

This relationship allows the creep life of a sample to be estimated from its steady-state creep rate. However, similar to the time to rupture data there is a scatter of data at the longer times to rupture. Table 5.5 shows the best fit relationship at each test temperature using the equation below (5.6) and establishing trends using computer software (Excel):

$$\log \dot{\varepsilon}_{min} = m. \log t_r + \log C \qquad (5.6)$$

| Temperature °C | Equation | Constant C | Gradient m |
|---|---|---|---|
| All | $\dot{\varepsilon}_{min} t_r^{1.13} = 2.3\times10^{-2}$ | $2.3 \times 10^{-2}$ | 1.13 |
| -10 | $\dot{\varepsilon}_{min} t_r^{1.09} = 6.2\times10^{-2}$ | $6.2 \times 10^{-2}$ | 1.09 |
| 29 | $\dot{\varepsilon}_{min} t_r^{1.23} = 2.4\times10^{-2}$ | $2.4 \times 10^{-2}$ | 1.23 |
| 75 | $\dot{\varepsilon}_{min} t_r^{1.18} = 1.7\times10^{-2}$ | $1.7 \times 10^{-2}$ | 1.18 |
| 99.4 | $\dot{\varepsilon}_{min} t_r^{1.17} = 3.5\times10^{-2}$ | $3.5 \times 10^{-2}$ | 1.17 |
| 125 | $\dot{\varepsilon}_{min} t_r^{1.12} = 2.1\times10^{-2}$ | $2.1 \times 10^{-2}$ | 1.12 |

Table 5.5 Constants obtained from the Monkman-Grant relationship

### *5.1.5 Minimum Creep Rate – Stress Relationships*

Figure 5.6 shows minimum creep strain rate as a function of applied stress over a range of temperatures (-10 to 125°C) according to Norton's Law. Of the creep rate versus stress relationships examined including the 'sinh' relationship (see chapter 2), Norton's Law best described the bulk creep data. At each temperature, power law relationships between minimum strain rates and stresses were observed. The Norton power law is described as:

$$\dot{\varepsilon}_{min} = A_1 \sigma^n \qquad (2.5)$$

where $\dot{\varepsilon}_{min}$ = minimum creep strain rate
$\sigma$ = applied stress
$A_1$ = constant.
n = creep exponent

Best-fit lines in figure 5.6 were obtained using the expression:

$$\log \dot{\varepsilon}_{min} = n.\log\sigma + \log A_1. \qquad (5.7)$$

Lines were fitted using 'excel' computer software. In order to get the best-fit at 75°C the low stress data point (12MPa) was omitted. Minimum strain rate shows a high sensitivity to the applied stress at all temperatures. The creep exponent, 'n', and constant, $A_1$, at each temperature, are shown in table 5.6. It can be seen that values for creep exponent range from 10 to 18, decreasing with increasing temperature. Estimated minimum strain rate ratios at 20MPa for 29°C:75°C:99°C are approximately 1:1,000:10,000. The creep rate is greatly effected by temperature. Again, note that data at 29°C have been extrapolated to obtain the strain rate ratios.

| **Temperature °C** | **Constant $A_1$** | **Creep Exponent n** |
|---|---|---|
| -10 | $6 \times 10^{-34}$ | 18 |
| 29 | $4 \times 10^{-30}$ | 17 |
| 75 | $5 \times 10^{-23}$ | 14 |
| 99.4 | $1 \times 10^{-20}$ | 13 |
| 125 | $2 \times 10^{-15}$ | 10 |

Table 5.6 Calculation of creep exponent from Norton's Law

### *5.1.6 Determination of Activation Energy*

Apparent activation energy values (not taking into account the temperature dependence of elastic modulus) were determined for both data sets using values of strain rate obtained from Norton's Law plots at three values of applied stress. For the

bulk samples values of 15, 20 and 35MPa were used. Logarithmic (ln) minimum strain rates were plotted against the inverse of the product of the gas constant, R (8.314 $JK^{-1}mol^{-1}$), and absolute temperature, T (K), (figure 5.7) according to the relationship:

$$\dot{\varepsilon}_{min} = A_2 e^{-(Q/RT)} \qquad (2.4)$$

where $A_2$ = constant
Q = activation energy for creep

Table 5.7a shows the values of apparent creep activation energy and the constants obtained at each stress level. It is evident that as applied stress is increased the activation energy decreases. At 20MPa, the activation energy derived corresponds to values observed for the self-diffusion of tin (120kJ/mol [44]). As the alloy is tin-based, a high value of activation energy (greater than 100kJ/mol) would usually suggest that a process such as self-diffusion is occurring and a lower activation energy, of approximately 60kJ/mol, would indicate short circuit diffusion [45]. Values for activation energy decrease with increasing stress levels, although all values obtained were high (> 90kJ/mol).

| Stress (MPa) | Activation Energy (kJ/mol) | ln $A_2$ | $A_2$ |
|---|---|---|---|
| 15 | 136 | 33.9 | $5.28 \times 10^{14}$ |
| 20 | 120 | 32.2 | $9.64 \times 10^{13}$ |
| 35 | 97 | 31.6 | $2.29 \times 10^{13}$ |

Table 5.7 Apparent activation energy and constants

The matrix of the ternary alloy is principally tin and the elastic modulus of tin, E, is dependent on temperature, decreasing on heating. Therefore, to provide a more precise description of the deformation mechanism, Young's modulus can be incorporated into equation 2.8 i.e.

$$\dot{\varepsilon}_{ss} = A\left(\frac{\sigma}{E}\right)^{n} \exp\left(-\frac{Q}{RT}\right) \quad (5.8)$$

This equation was used to determine a value for true activation energy. Normalised stress, σ/E was plotted as a function of minimum strain rate and temperature, figure 5.7b. The temperature dependence of the elastic modulus of tin follows the following equation:

$$E(MPa) = 76087 - 109 \times T(K) \qquad (5.9)\ [36]$$

True activation energy for creep was derived using the method previously described where values of minimum strain rate at a selected normalised stress were determined at each temperature using trends established from figure 5.7b. Then logarithmic (ln) minimum strain rates were plotted against the inverse of the product of the gas constant and absolute temperature. Values of 123 $kJmol^{-1}$, 88$kJmol^{-1}$ and 79 $kJmol^{-1}$ were obtained at $\sigma/E \times 10^{-4} = 2.5$, 5 and 6 respectively, which are slightly lower but comparable to those values previously obtained for the apparent activation energy for creep. The author believes these values still to be in the region representing the self-diffusion of tin.

### *5.1.7 Factors Affecting Strain Rate*

*Effect of Stress*

Strain rate versus life fraction graphs (as first described in section 5.1.1) were used to illustrate the effect of stress on strain rate. In total five plots were made, one for each test temperature, where selected stress values (high, medium and low) were used to illustrate the testing extremes. Figure 5.8 demonstrates the effect of stress at 75°C, plots for −10, 29, 99.4 and 125°C can be found in appendix 5.3. Minimum strain rate is greatly affected by applied stress as shown in table 5.8. Here, data were

selected to give the widest spread of available data (including a mid-value of stress) for each data set.

| **Temperature** °C | **Initial Applied Stress** */Minimum Strain Rate Ratio* | | |
|---|---|---|---|
| -10 | **38MPa** *1* | **45MPa** *20* | **50MPa** *110* |
| 29 | **26MPa** *1* | **28MPa** *4* | **45MPa** *25,000* |
| 75 | **12MPa** *1* | **19.5MPa** *25* | **27MPa** *2,200* |
| 99.4 | **15MPa** *1* | **17MPa** *20* | **25MPa** *50* |
| 125 | **8MPa** *1* | **12MPa** *40* | **25MPa** *28,000* |

Table 5.8 Effect of stress on minimum strain rate at each test temperature

*Effect of Temperature*

Selecting a constant stress and varying the test temperature produced a similar plot demonstrating the effect of temperature on strain rate. Figure 5.9 illustrates this effect when the stress is held constant at 20MPa. Unfortunately, no data at 29°C or lower were available (at 20MPa) due to the impracticality of testing for such long periods of time. The strain rate ratio between 75°C: 99.4°C: 125°C is approximately 1: 40: 50.

*Using Strain Rates to Determine Creep Regime.*

Most life prediction methodologies are based upon secondary creep behaviour. Therefore, it was of interest to determine the extent of secondary creep throughout the creep life of a sample. Using strain rate versus life fraction plots (as discussed in section 5.1.1) and by defining steady state creep as the time spent below 'minimum

strain rate plus ten per cent' ($1.1\dot{\varepsilon}_{min}$) estimates can be made concerning the proportions of life spent in each creep regime, figure 5.10.

Table 5.9 shows the percentage of life-time spent in each creep regime for every test specimen. There is no obvious trend between the proportions of creep regime and applied stress or temperature. Primary creep generally accounts for less than twenty-five percent of the entire creep life. Between twenty to forty percent of life is spent in steady state creep, with a couple of exceptions at 99.4°C where the proportion of primary creep was very small and secondary creep larger. There is a wide scatter of data for the set obtained at 99.4°C, the author obtained these data using the same method as for the other data, and therefore, at present, cannot offer an explanation. Given infinite time it would be beneficial to repeat this testing regime. Tertiary creep tended to dominate creep lifetime, ranging from approximately forty up to seventy-five percent of life. However, very few life prediction models take tertiary creep into account. The question now arises as to how reliable these relationships and therefore, how accurate life-predictions are.

| Temperature °C | Stress MPa | Primary % | Secondary % | Tertiary % |
|---|---|---|---|---|
| -10 | 38 | 21 | 26 | 53 |
| -10 | 40 | 21 | 30 | 49 |
| -10 | 45 | 28 | 24 | 48 |
| -10 | 50 | 22 | 39 | 39 |
| 29 | 26 | 15 | 24 | 61 |
| 29 | 28 | 14 | 40 | 46 |
| 29 | 30 | 20 | 38 | 42 |
| 29 | 32 | 2 | 23 | 75 |
| 29 | 35 | 9 | 22 | 69 |
| 29 | 40 | 11 | 32 | 57 |
| 29 | 41 | 6 | 25 | 69 |
| 29 | 42.5 | 9 | 37 | 54 |
| 29 | 45 | 16 | 40 | 44 |
| 75 | 12 | 23 | 24 | 53 |
| 75 | 16 | 19 | 34 | 47 |
| 75 | 19 | 26 | 27 | 47 |
| 75 | 19.5 | 4 | 28 | 68 |
| 75 | 21 | 22 | 23 | 55 |
| 75 | 23.5 | 8 | 25 | 67 |
| 75 | 24 | 17 | 21 | 62 |
| 75 | 27 | 8 | 29 | 63 |
| 75 | 33 | 15 | 38 | 47 |
| 99.4 | 14 | 13 | 42 | 45 |
| 99.4 | 15 | 8 | 55 | 37 |
| 99.4 | 17 | 23 | 37 | 40 |
| 99.4 | 20 | 10 | 45 | 45 |
| 99.4 | 25 | 27 | 23 | 50 |
| 99.4 | 25.25 | 23 | 20 | 57 |
| 99.4 | 27 | 0 | 43 | 57 |
| 125 | 8 | 19 | 37 | 44 |
| 125 | 10 | 26 | 32 | 42 |
| 125 | 12 | 20 | 40 | 40 |
| 125 | 18 | 8 | 40 | 52 |
| 125 | 20 | 8 | 31 | 61 |
| 125 | 22.5 | 16 | 29 | 55 |
| 125 | 25 | 24 | 22 | 54 |

Table 5.9 Proportions of each creep regime (in terms of life time)

### *5.1.8 Creep Strain*

*Extent of Creep Strain Occurring in Each Regime*

Some applications are strain rather than fracture limited, therefore it is important to have information concerning the accumulation of strain during a creep test. The proportions of each regime in relation to strain rate were determined in section 5.1.7, this section now determines how much strain is occurring in each regime (primary, secondary and tertiary). Figures 5.11 and 5.12 show how creep strains were obtained separately and accumulatively.

Tables of both types of analysis performed on all data can be found in appendix 5.4. Determination of the proportion of creep strain in each regime with respect to ductility, table 5.10, proved to be the most informative as it provides a better indication of the proportions of creep regime throughout the creep life (as determined by strain). This type of analysis is relevant when considering life prediction methods as most appear to be based on secondary creep.

| Temp °C | Stress MPa | % $\varepsilon_0$ (=$\varepsilon_0/\varepsilon_f$ x 100) | %$\varepsilon_p$ (=$\varepsilon_p/\varepsilon_f$ x 100) | %$\varepsilon_s$ (=$\varepsilon_s/\varepsilon_f$ x 100) | %$\varepsilon_t$ (=$\varepsilon_t/\varepsilon_f$ x 100) |
|---|---|---|---|---|---|
| -10 | 38 | 3 | 6 | 11 | 80 |
| -10 | 40 | 3 | 4 | 11 | 82 |
| -10 | 45 | 10 | 8 | 16 | 67 |
| -10 | 50 | 6 | 6 | 10 | 78 |
| 29 | 40 | 3 | 3 | 7 | 88 |
| 29 | 41 | 5 | 2 | 5 | 89 |
| 29 | 30 | 5 | 4 | 4 | 87 |
| 29 | 45 | 4 | 6 | 9 | 81 |
| 29 | 35 | 4 | 1 | 6 | 89 |
| 29 | 42.5 | 4 | 6 | 10 | 79 |
| 29 | 32 | 3 | 1 | 7 | 90 |
| 29 | 28 | 1 | 7 | 7 | 84 |
| 29 | 26 | 5 | 4 | 8 | 83 |
| 75 | 12 | - | - | - | - |
| 75 | 21 | 1 | 3 | 2 | 93 |
| 75 | 23.5 | 6 | 1 | 5 | 89 |
| 75 | 27 | 3 | 1 | 5 | 91 |
| 75 | 24 | 8 | 5 | 5 | 82 |
| 75 | 16 | 4 | 1 | 1 | 95 |
| 75 | 19.5 | 2 | 1 | 3 | 94 |
| 75 | 19 | 5 | 5 | 3 | 87 |
| 75 | 33 | 9 | 6 | 6 | 79 |
| 99.4 | 25 | 2 | 3 | 7 | 87 |
| 99.4 | 27 | 4 | 0 | 12 | 84 |
| 99.4 | 25.25 | 8 | 4 | 6 | 81 |
| 99.4 | 20 | 3 | 3 | 6 | 88 |
| 99.4 | 15 | 7 | 9 | 19 | 65 |
| 99.4 | 17 | 5 | 7 | 22 | 66 |
| 99.4 | 14 | 3 | 1 | 3 | 94 |
| 125 | 10 | 1 | 3 | 4 | 92 |
| 125 | 20 | 2 | 3 | 6 | 90 |
| 125 | 25 | 9 | 4 | 9 | 77 |
| 125 | 22.5 | 4 | 0 | 6 | 90 |
| 125 | 18 | 14 | 1 | 3 | 81 |
| 125 | 12 | 6 | 8 | 11 | 75 |
| 125 | 8 | 3 | 12 | 6 | 79 |

Table 5.10 Proportion of creep strain occurring in each creep regime with respect to ductility (analysis has also been completed by omitting instantaneous strain, appendix 5.5)

The majority of creep strain occurring during a lifetime is tertiary creep, ranging between sixty-five to ninety-five percent strain. Very little strain is apparent during secondary creep, generally between one to sixteen percent. Although, an anomaly to this occurs at 99.4°C (15 and 17MPa) where larger strains are observed (up to twenty-two percent). In general, there doesn't appear to be any correlation of creep strain with applied stress and temperature.

*Using Strain During Creep Life to Determine Failure Definitions*

Often when considering a material for design purposes, failure definitions based upon strain are used as an alternative to time to rupture. In gas turbines, for example, a certain amount of deformation in the turbine blades will cause failure of the equipment, even though the material hasn't ruptured. In situations such as this, time to reach a specified strain is used i.e. a failure definition.

For this research, times to reach 2%, 5% and 10% strain have been calculated and compared with time to rupture. Table 5.11 shows the time to attain 2%, 5% and 10% strain for the ternary alloy at each test temperature and stress. This table also shows the percentage of life elapsed to reach these failure criteria. It is important to note that SnAgCu is not a particularly ductile material and the majority of life has elapsed by the time ten percent strain is reached, in some cases five percent strain accounts for more that ninety-five percent of life. Such behaviour may have important repercussions in engineering design as the material may be in tertiary creep where strain and ultimately failure occurs rapidly.

Figures 5.13a to e show the time at each failure definition (time at 2,5,10% strain and time to rupture) for each test temperature. These plots produce a narrow band of

data with little distinction between each criteria. This suggests that little strain is occurring throughout the creep test until tertiary creep.

| Temperature | Stress (MPa) | $t_{2\%,cc}$ (h) | $t_{5\%,cc}$ (h) | $t_{10\%,cc}$ (h) | $t_r$ (h) | %life 2%strain | %life 5%strain | %life 10%strain |
|---|---|---|---|---|---|---|---|---|
| -10°C | 50 | 0.98 | 19.84 | 28.69 | 29.5 | 3% | 67% | 97% |
| -10°C | 45 | - | 47.33 | 103 | 115.2 | 0% | 41% | 89% |
| -10°C | 40 | 192.3 | 953.8 | 1392.3 | 1485 | 13% | 64% | 94% |
| -10°C | 38 | 226.2 | 1214.3 | 1857.1 | 2027.67 | 11% | 60% | 92% |
| 29°C | 26.0 | 369.5 | 752.2 | 775.6 | 775.6 | 48% | 97% | 100% |
| 29°C | 28.0 | 166.2 | 279.4 | 284.02 | 284.02 | 59% | 98% | 100% |
| 29°C | 30.0 | 256 | 616 | 694 | 694.25 | 37% | 89% | 100% |
| 29°C | 32.0 | 28.3 | 36.1 | 40 | 40 | 71% | 90% | 100% |
| 29°C | 35.0 | 2 | 4.53 | 5.8 | 6.21 | 32% | 73% | 93% |
| 29°C | 40.0 | 0.708 | 1.22 | 1.392 | 1.42 | 50% | 86% | 98% |
| 29°C | 41.0 | 2.84 | 6.36 | 7.12 | 7.29 | 39% | 87% | 98% |
| 29°C | 42.5 | 0.36 | 1.5 | 1.779 | 1.779 | 20% | 84% | 100% |
| 29°C | 45.0 | 0.007 | 0.1 | 0.176 | 0.242 | 3% | 41% | 73% |
| 75°C | 12.00 | 714.30 | 1988.00 | 2121.00 | 2121.00 | 34% | 94% | 100% |
| 75°C | 16.00 | 400.00 | 435.00 | 443.00 | 443.36 | 90% | 98% | 100% |
| 75°C | 19.00 | 309.60 | 355.53 | 355.53 | 355.53 | 87% | 100% | 100% |
| 75°C | 19.50 | 38.45 | 42.90 | 43.30 | 43.31 | 89% | 99% | 100% |
| 75°C | 21.00 | 15.73 | 19.15 | 20.25 | 20.25 | 78% | 95% | 100% |
| 75°C | 23.50 | 4.00 | 5.93 | 6.33 | 6.40 | 63% | 93% | 99% |
| 75°C | 24.00 | 20.77 | 32.70 | 34.30 | 34.30 | 61% | 95% | 100% |
| 75°C | 27.00 | 0.67 | 1.12 | 1.24 | 1.25 | 54% | 90% | 99% |
| 75°C | 33.00 | - | 0.24 | 0.42 | 0.43 | 0% | 56% | 99% |
| 99.4°C | 25.25 | - | 2.214 | 2.764 | 2.82 | 0% | 79% | 98% |
| 99.4°C | 25.0 | 2.152 | 4.065 | 4.22 | 4.22 | 51% | 96% | 100% |
| 99.4°C | 20.0 | 1.66 | 5.2 | 6 | 6.07 | 27% | 86% | 99% |
| 99.4°C | 15.0 | 6.66 | 283 | 306.95 | 306.95 | 2% | 92% | 100% |
| 99.4°C | 17.0 | 16.9 | 128.5 | 136.13 | 136.13 | 12% | 94% | 100% |
| 99.4°C | 14.0 | 744.44 | 788.42 | 788.42 | 788.42 | 94% | 100% | 100% |
| 99.4°C | 27.0 | - | 0.0395 | 0.0686 | 0.0885 | 0% | 45% | 78% |
| 125°C | 8.0 | 615.38 | 3346.14 | 3528.03 | 3528.03 | 17% | 95% | 100% |
| 125°C | 10.0 | 544.1 | 555.88 | 558.8 | 558.8 | 97% | 99% | 100% |
| 125°C | 12.0 | 13.2 | 140.75 | 147.77 | 147.77 | 9% | 95% | 100% |
| 125°C | 18.0 | - | 0.268 | 0.587 | 0.653 | 0% | 41% | 90% |
| 125°C | 20.0 | 1.31 | 3.42 | 3.56 | 3.56 | 37% | 96% | 100% |
| 125°C | 22.5 | 0.005 | 0.126 | 0.174 | 0.196 | 3% | 64% | 89% |
| 125°C | 25.00 | - | 0.113 | 0.238 | 0.244 | 0% | 46% | 98% |

Table 5.11 Failure criterion for bulk SnAgCu

### *5.1.9 Metallographic Examination of Bulk Specimens*

Metallographic examination is important to obtain microstructural information to identify mechanisms of deformation and failure. Both examination of sectioned samples and fractured surfaces was performed and the findings are now presented.

Figure 5.14 illustrates damage that has accumulated near the fracture surface in a necked sample tested at 75°C and 18MPa. It shows coarsening of the grains and

intermetallics around the fracture surface (in comparison to the grains in the central region of the neck) and cracking at some grain boundaries.

Fractography may be used to determine the type of creep rupture experienced in a sample; for example, figures 5.15a and b show both a ductile and a mixed-mode (sharing some brittle and ductile failure characteristics) type failure observed during SnAgCu creep testing. Samples appeared to fail in a ductile manner at high stresses and possess a mixed-mode mechanism at lower stress values, this was observed at all test temperatures. Typical ductile fracture dimples can be seen to have originated around small particles of intermetallic compound, figure 5.15ai, as identified by energy dispersive spectroscopy (EDS) analysis. The small inclusions contained within the dimples suggest that during deformation the ductile Sn-matrix material pulls away from the undeforming intermetallic particle. A hole nucleates around each inclusion and grows until it meets neighbouring voids (void coalescence). The mixed mode failure site exhibits areas of ductile dimples and regions where the material appears to have failed along colony boundaries (β-Sn and eutectic boundaries). Figure 5.15bii clearly shows this type of boundary, as they are too big to be individual grain boundaries.

Figure 5.16a illustrates the 'as cast' microstructure of water quenched Sn-3.8Ag-0.7Cu. This initial microstructure consists of a mixture of precipitate free β-Sn globules and eutectic regions of $Ag_3Sn$ intermetallic finely dispersed within a tin matrix. The grain size of the β-Sn region (approximately 5μm) is larger than that of the eutectic region (approximately 2 μm). The $Ag_3Sn$ intermetallic particles are sub-micron as are the $Cu_6Sn_5$ particles, which are indistinguishable in the 'as cast' condition. Quantities of those elements present within the microstructure were identified using EDS.

Figure 5.16 illustrates the extent of coarsening from the 'as cast' condition when exposed to 75°C and 125°C. Sections were taken to illustrate the effect of temperature, the effect of both temperature and strain and also the combination of temperature and severe straining (necked area). Figures 5.16 b to d show the microstructure of the ternary alloy after exposure to 75°C for approximately 800 hours. Figure 5.16b illustrates that both types of intermetallic compound coarsen under the action of temperature, although those containing copper grow much more rapidly (to approximately 4μm). The addition of stress to temperature, figure 5.16c, has little additional effect on the $Ag_3Sn$ particles, however, a larger quantity of $Cu_6Sn_5$ particles is evident, although they are smaller than those observed in the specimen head (approximately 1 to 2 μm). The highly strained area adjacent to the fracture surface is densely populated with $Cu_6Sn_5$ particles, figure 5.16d, reinforcing the suggestion of strain assisted coarsening. In contrast, the central portions of the necked area, which experience much lower levels of deformation, exhibit few such particles.

Figures 5.16 e to g show a similar set of micrographs for a sample exposed to 125°C for approximately 3,500 hours. In comparison to figures 5.16 b to d, these show a more severe coarsening. Under the action of temperature, both types of particle coarsen leaving only a little of the finely dispersed eutectic structure remaining. Strain, in combination with temperature, causes additional coarsening particularly in the $Cu_6Sn_5$ particles (to approximately 2 to 3μm). In contrast to the gauge length, slightly more coarsening is observed in the severely strained, necked region of the sample and no finely dispersed region is apparent.

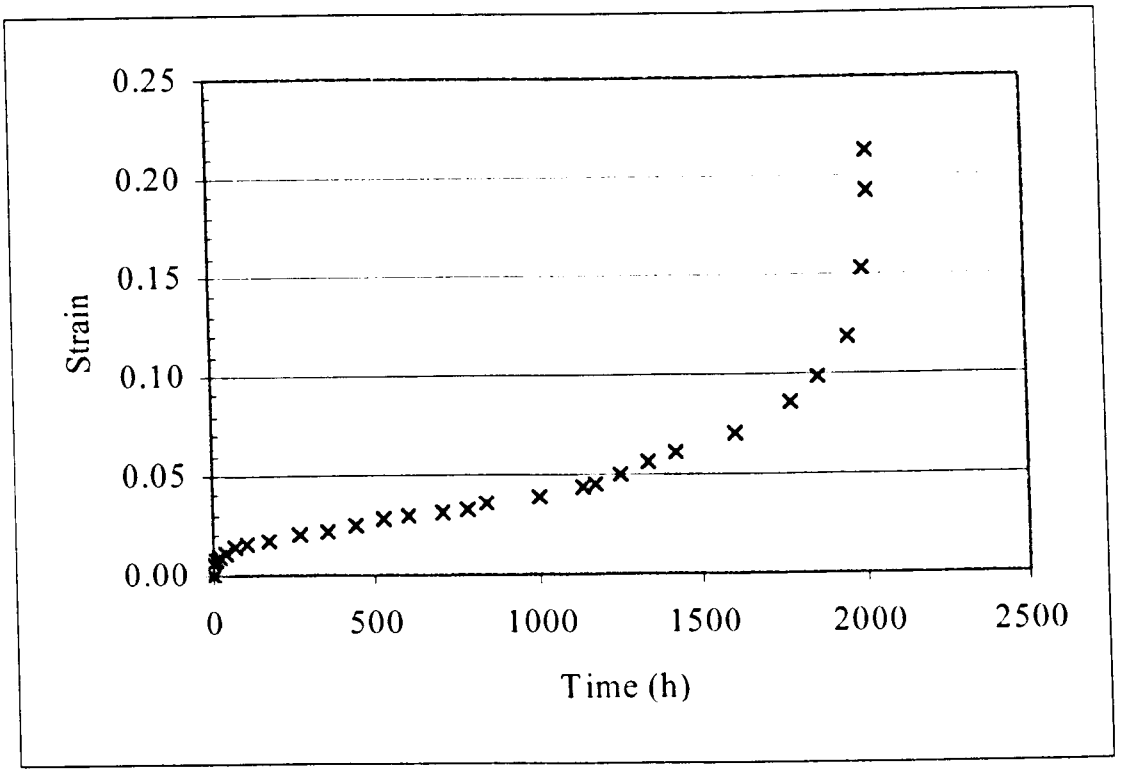


Figure 5.1 Strain vs time curve for SnAgCu tested at -10°C and 38MPa

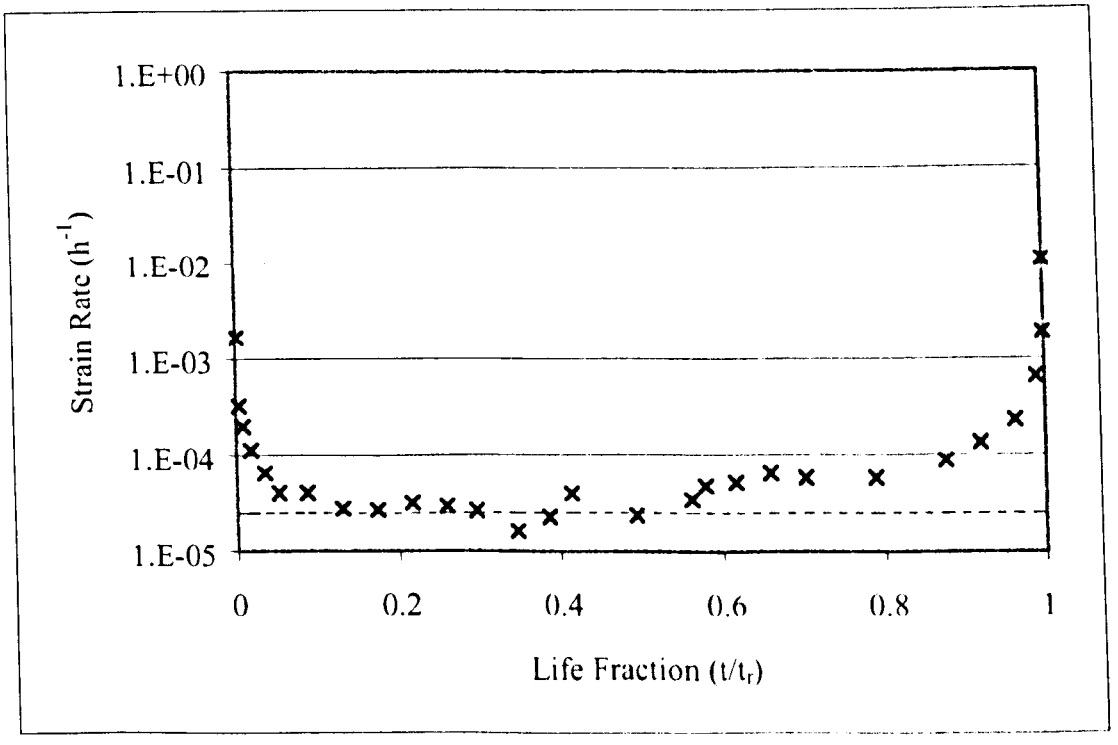


Figure 5.2 Strain rate vs life fraction for SnAgCu tested at -10°C and 38MPa

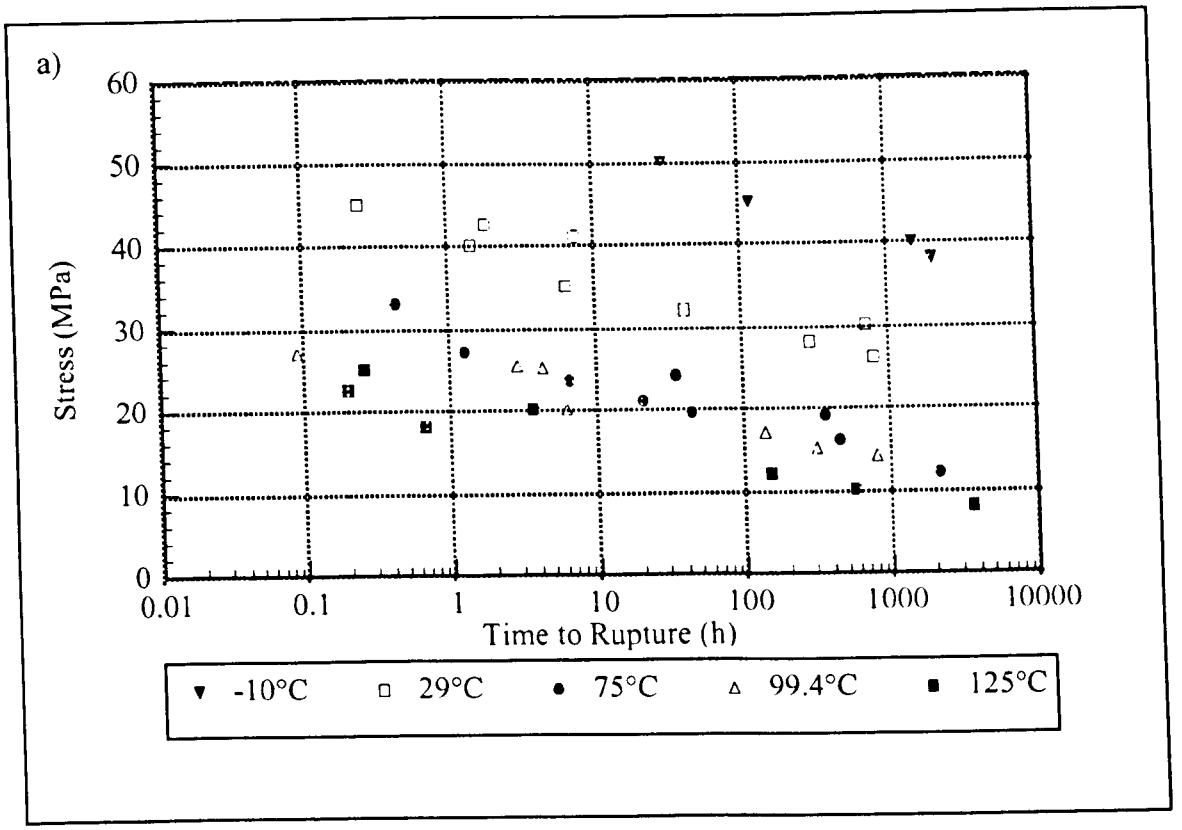


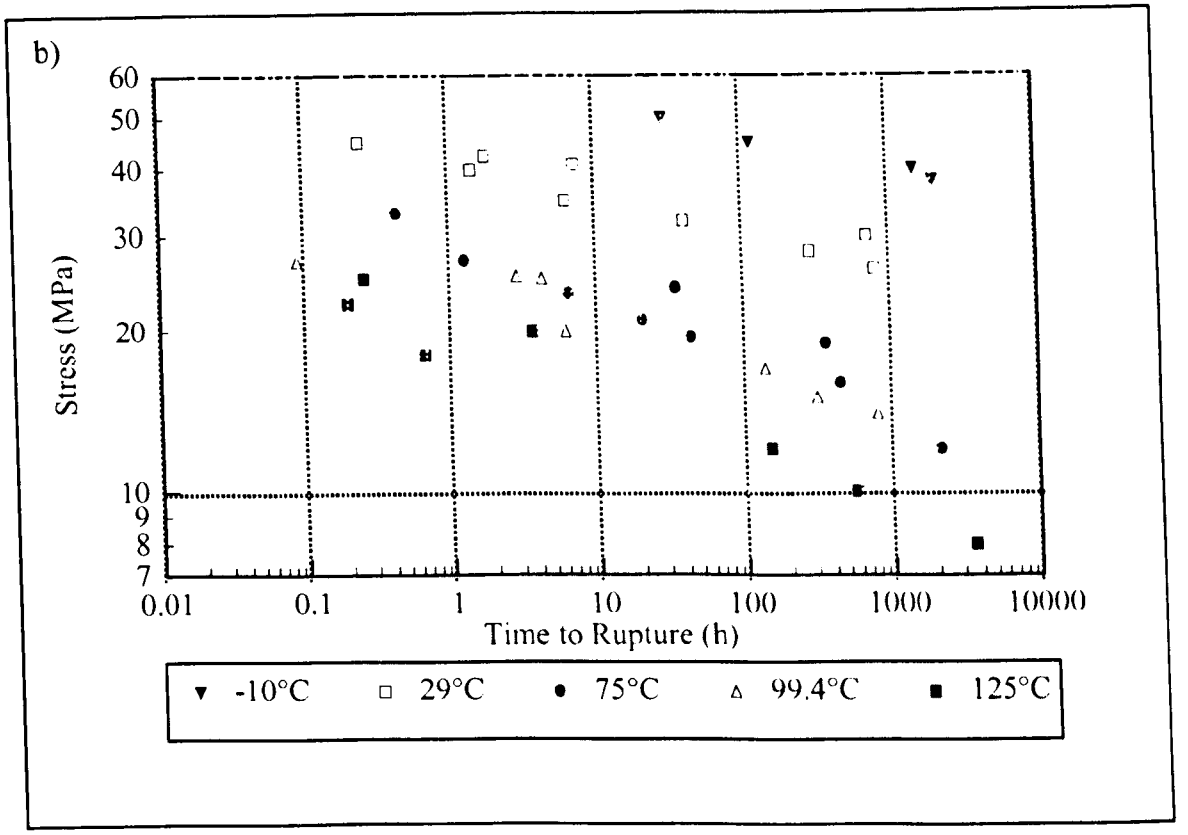


Figure 5.3 a & b Stress vs. time to rupture a) semi-log scale b) log-log scale

(See Appendix 5.2 for trend lines and error calculation)

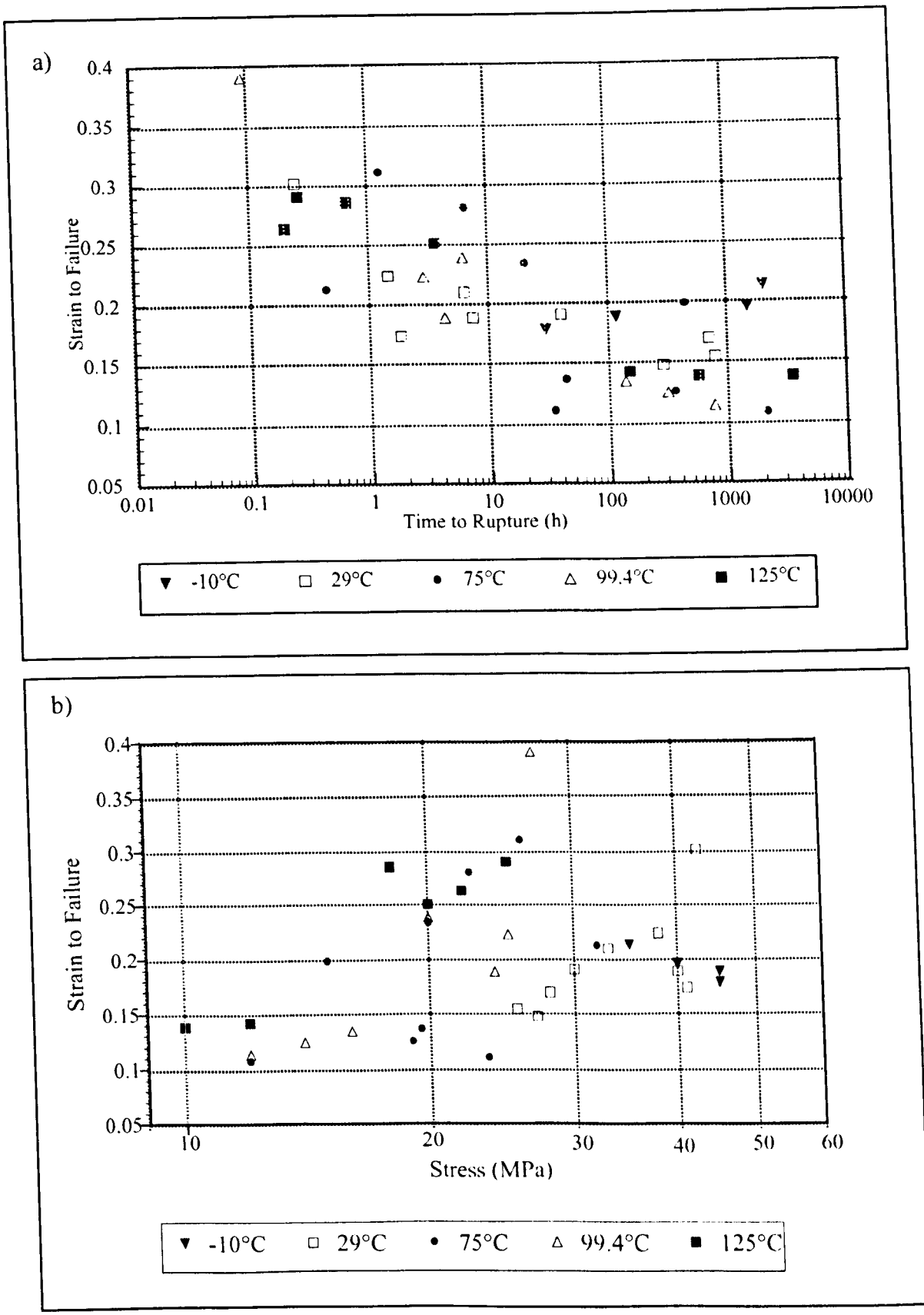


Figure 5.4 a & b Ductility of SnAgCu in creep a) vs. time to rupture b) vs. stress

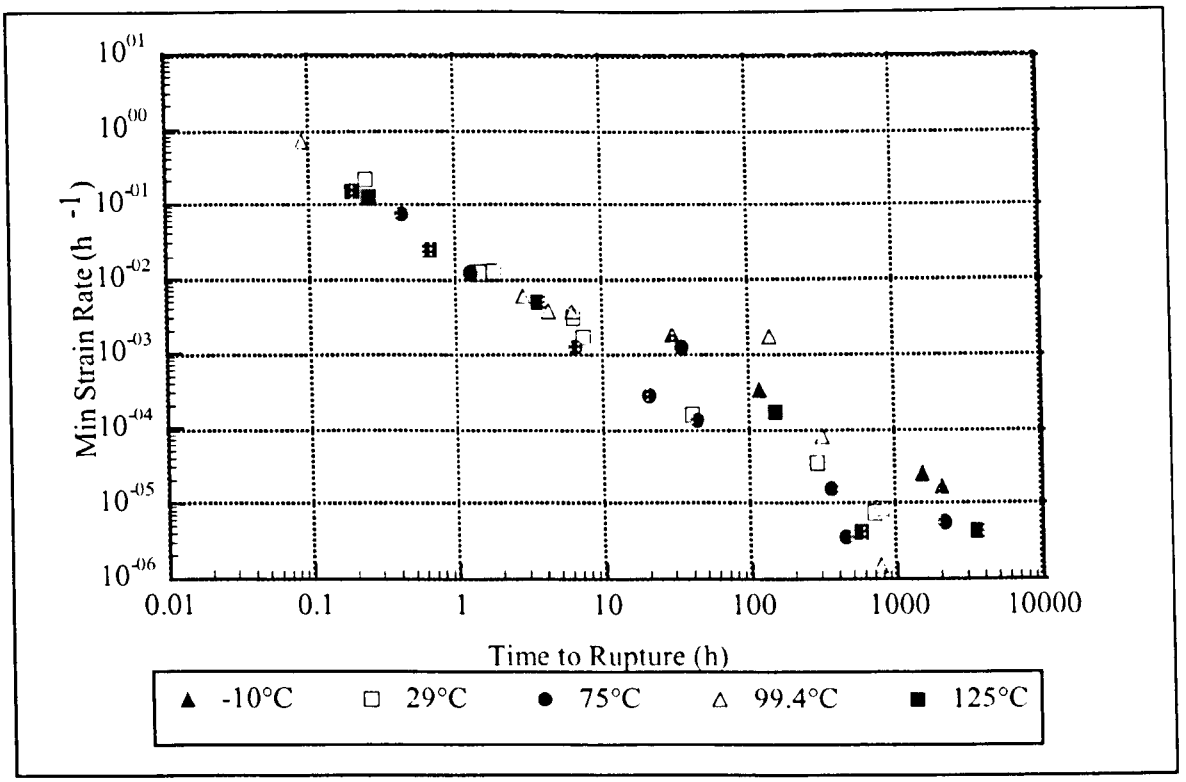


Figure 5.5 Monkman-Grant relationship at all temperatures
(See Appendix 5.2b for trend lines)

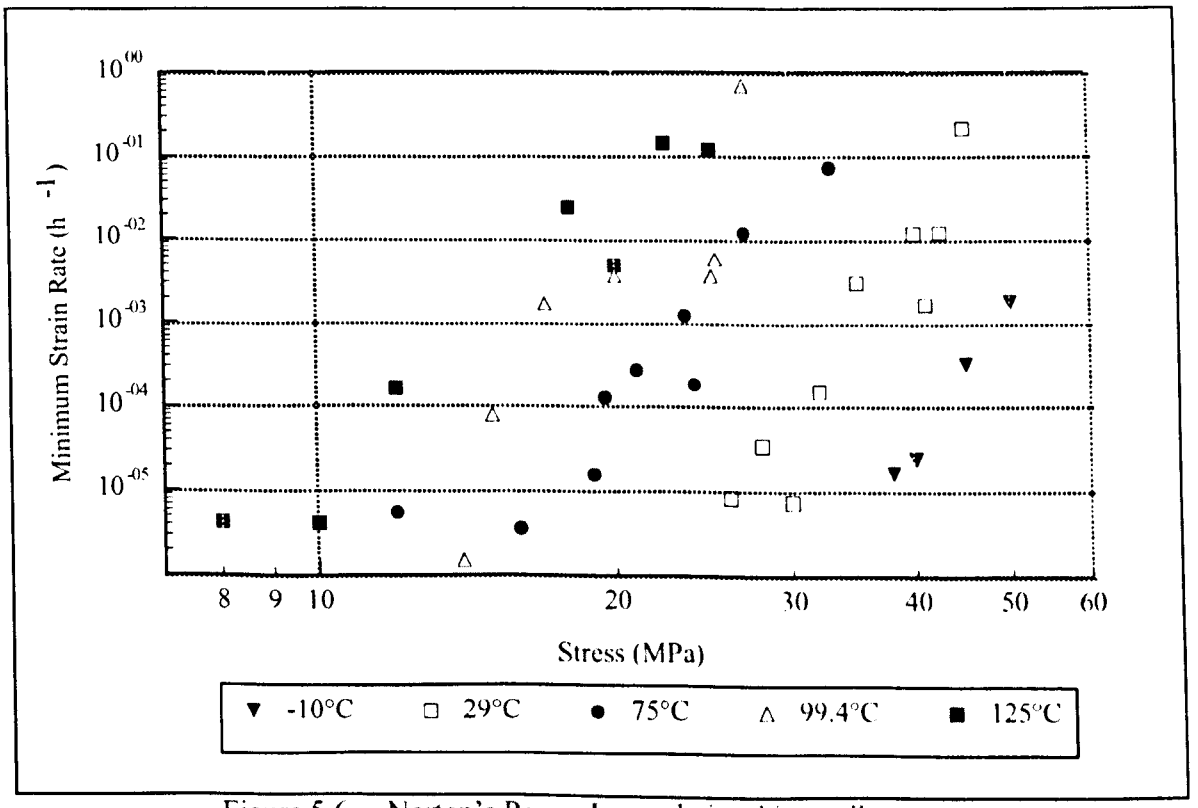


Figure 5.6 Norton's Power Law relationship at all temperatures

(See Appendix 5.2 for trend lines and error calculation)

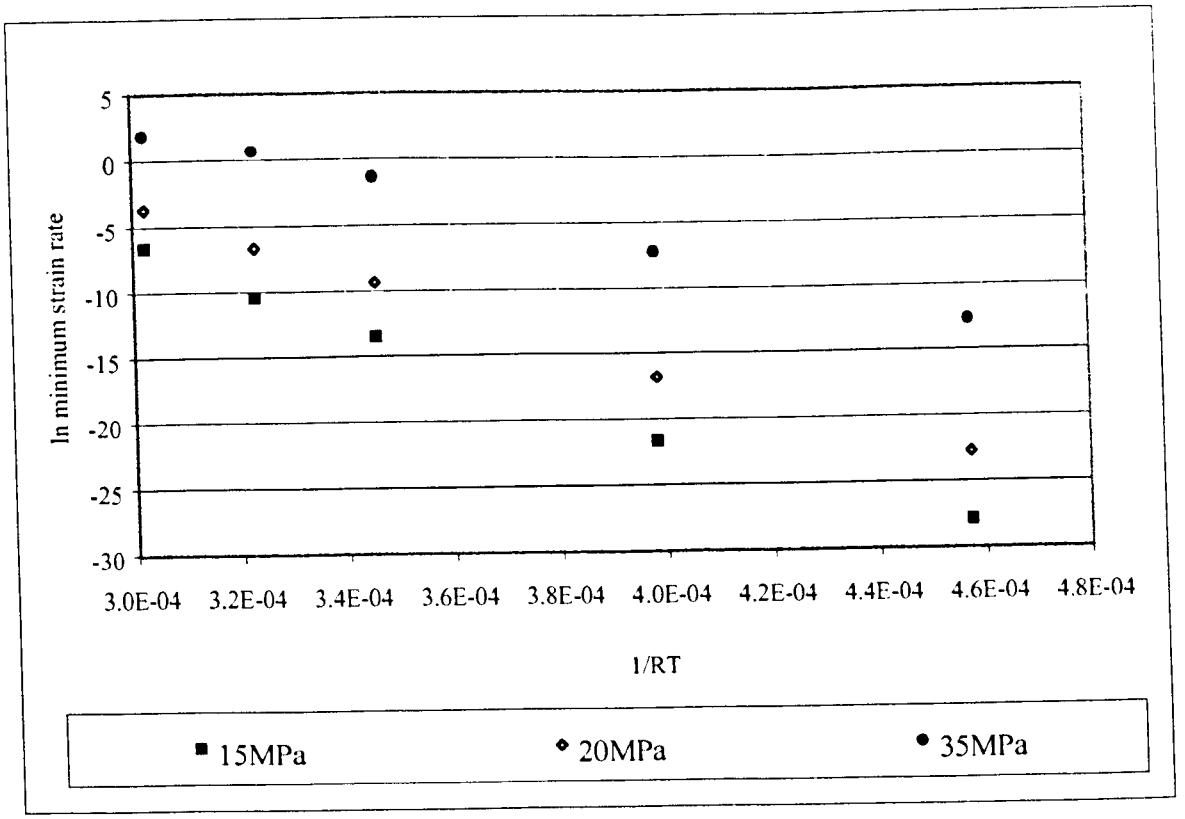


Figure 5.7a Determination of apparent activation energy for creep

(See Appendix 5.2b for trend lines)

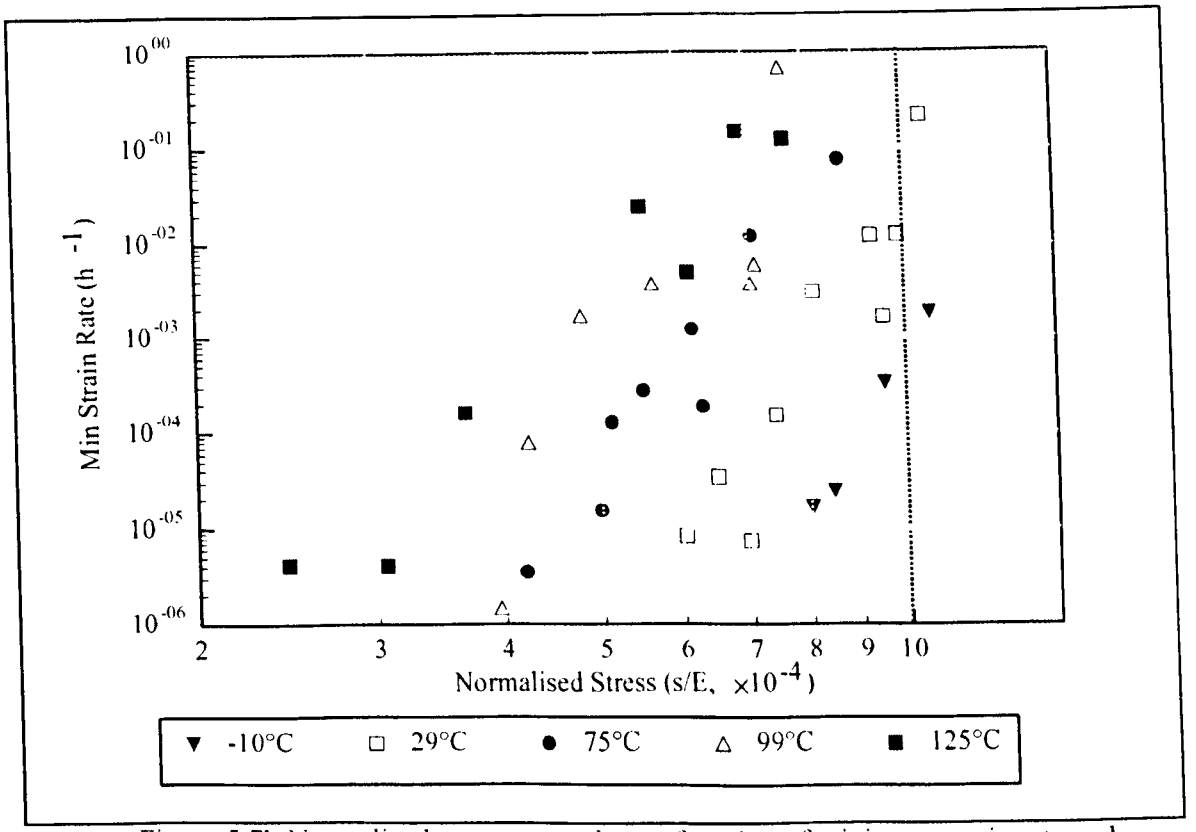


Figure 5.7b Normalised creep strength as a function of minimum strain rate and temperature – used in the determination of true activation energy
(See Appendix 5.2b for trend lines)

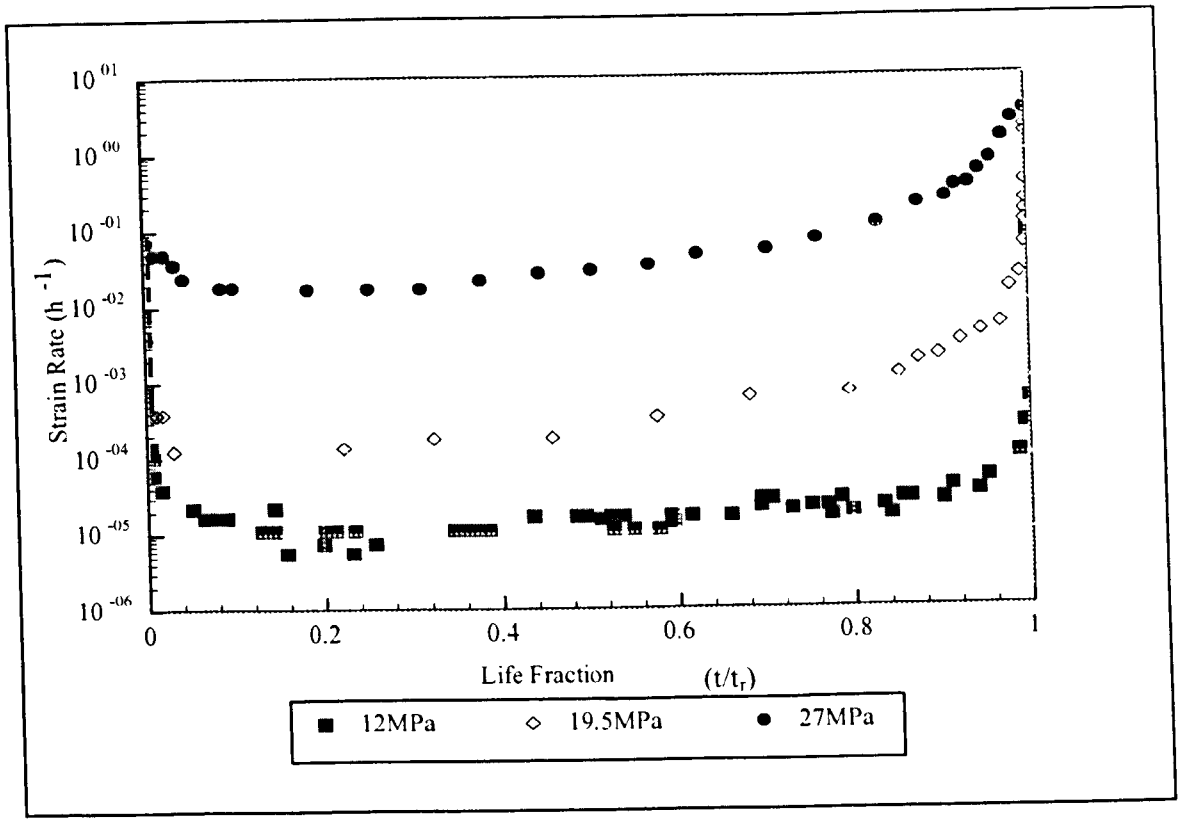


Figure 5.8 Effect of stress on strain rate at 75°C

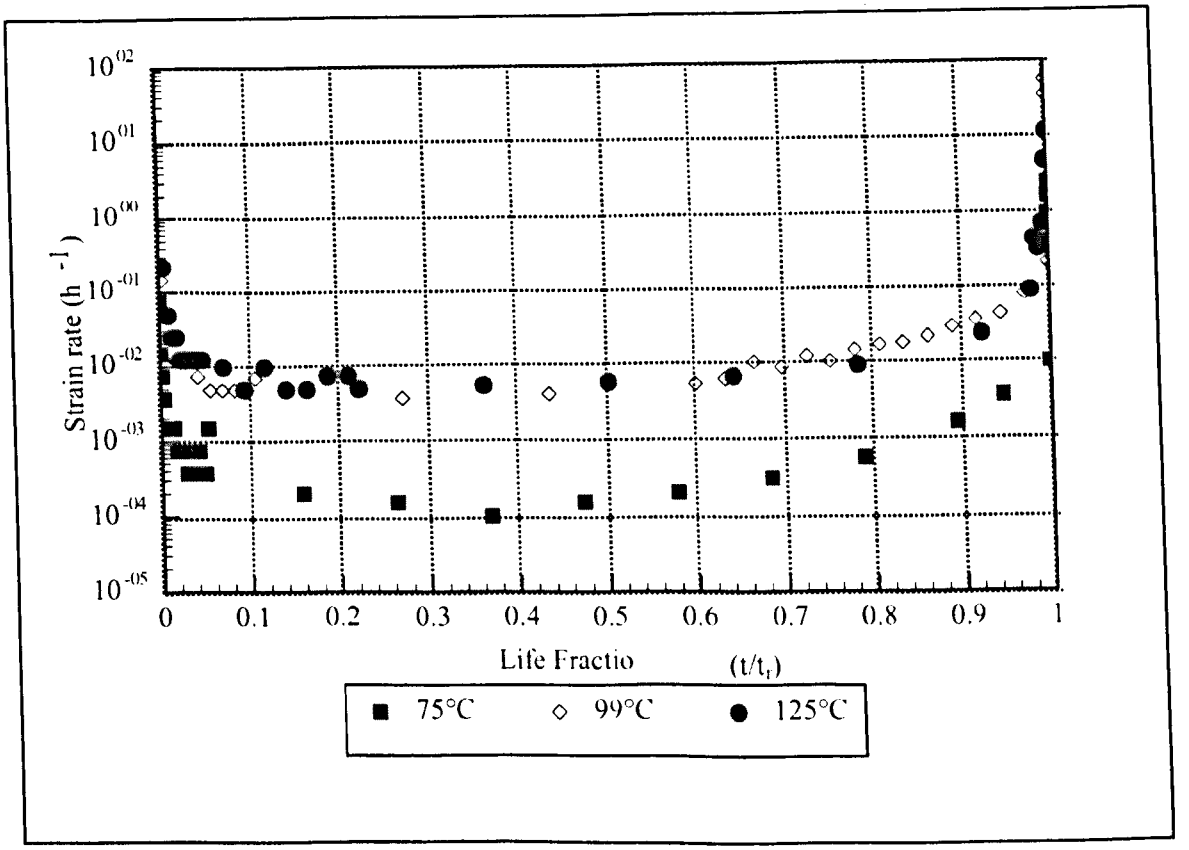


Figure 5.9 Effect of temperature on strain rate at 20MPa

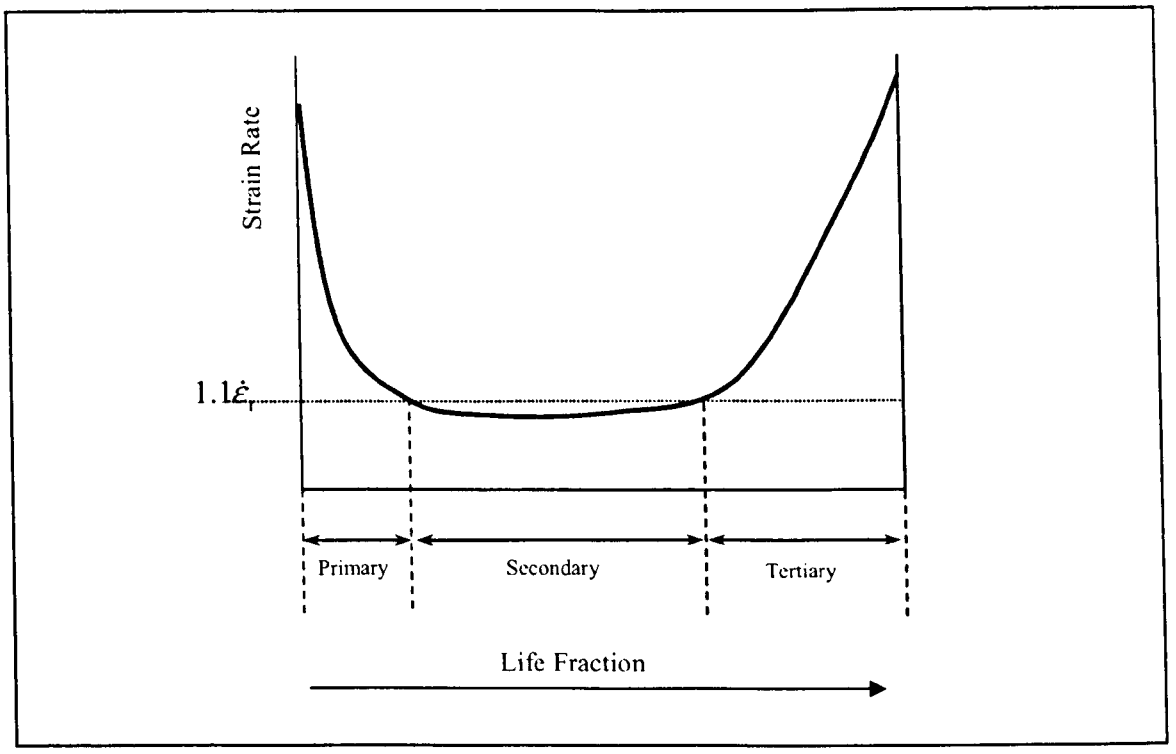


Figure 5.10 Demonstration of the procedure for estimating creep proportions

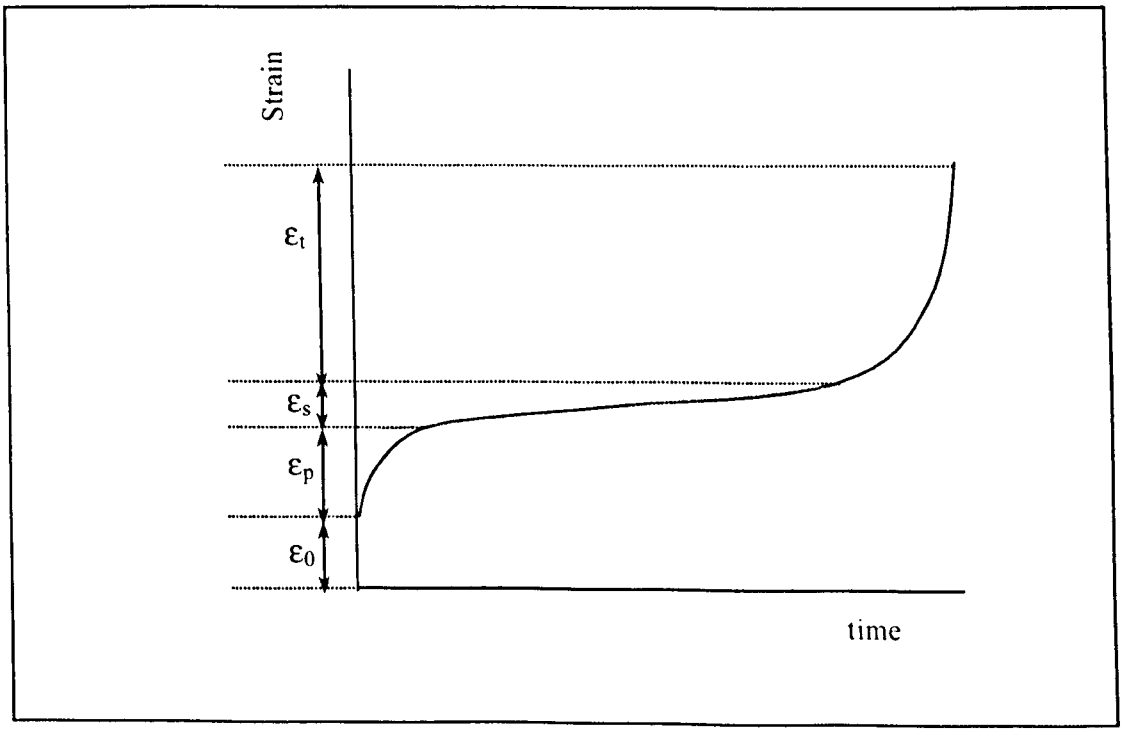


Figure 5.11 Determination of individual strains occurring in each regime

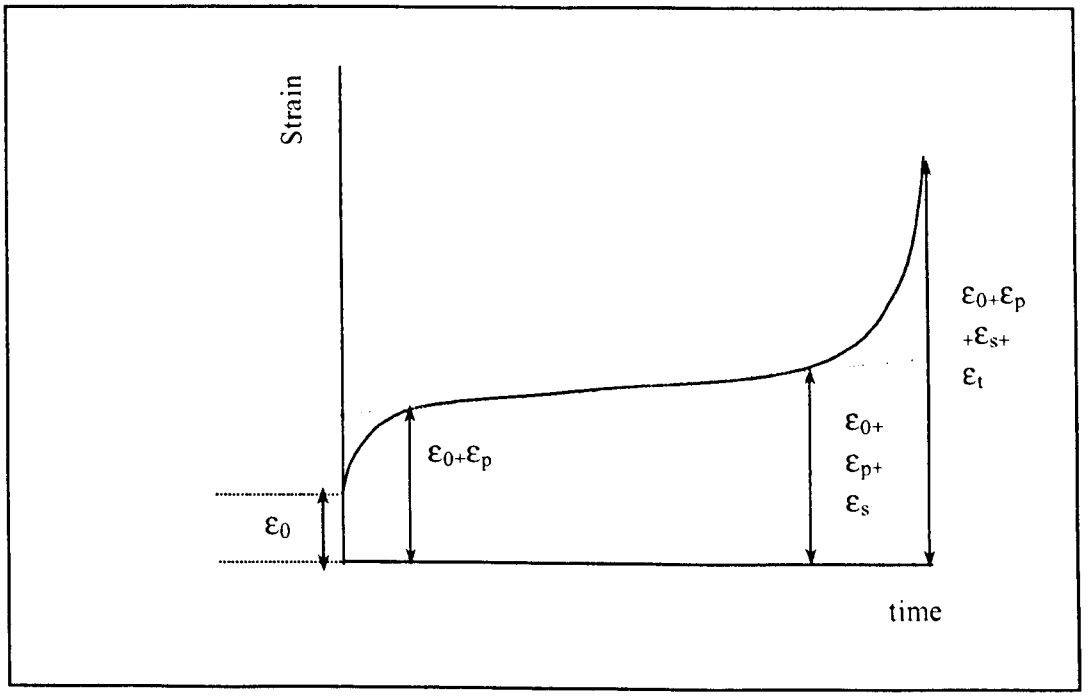


Figure 5.12 Determination of accumulative strains occurring during creep lifetime (by inspection)

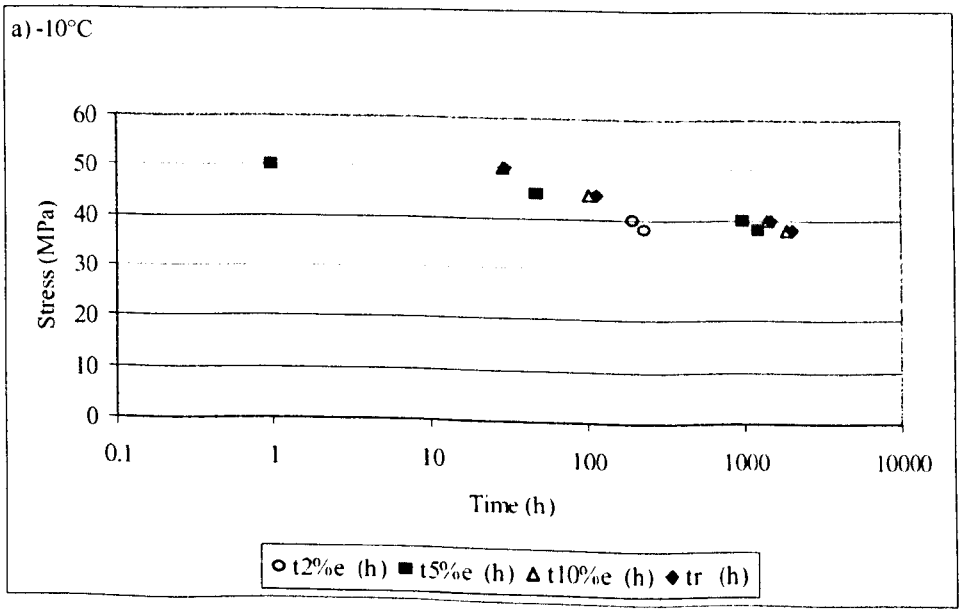

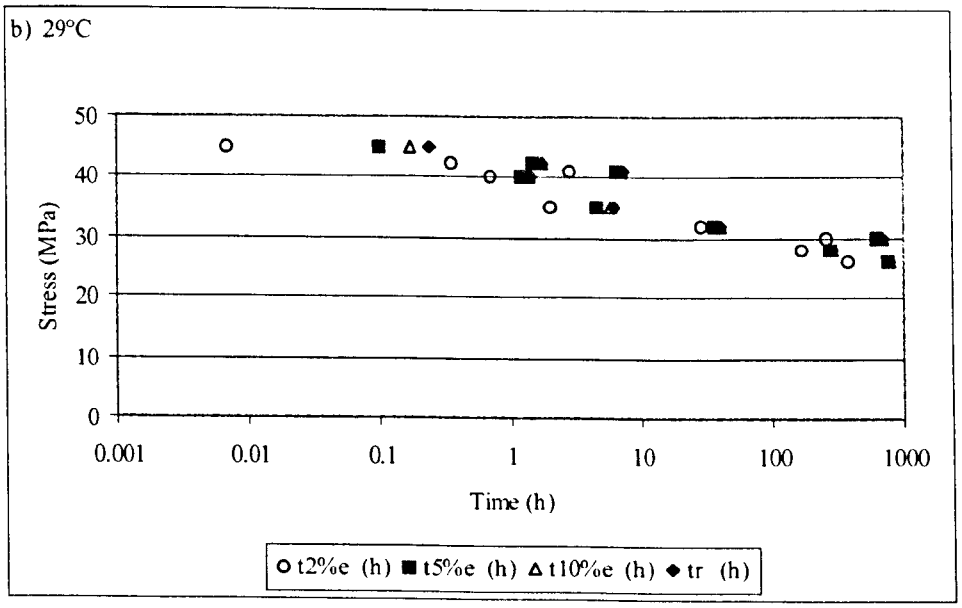
b) 29°C
Stress (MPa)
50
40
30
20
10
0
0.001
0.01
0.1
1
10
100
1000
Time (h)
t2%e (h)
t5%e (h)
t10%e (h)
tr (h)

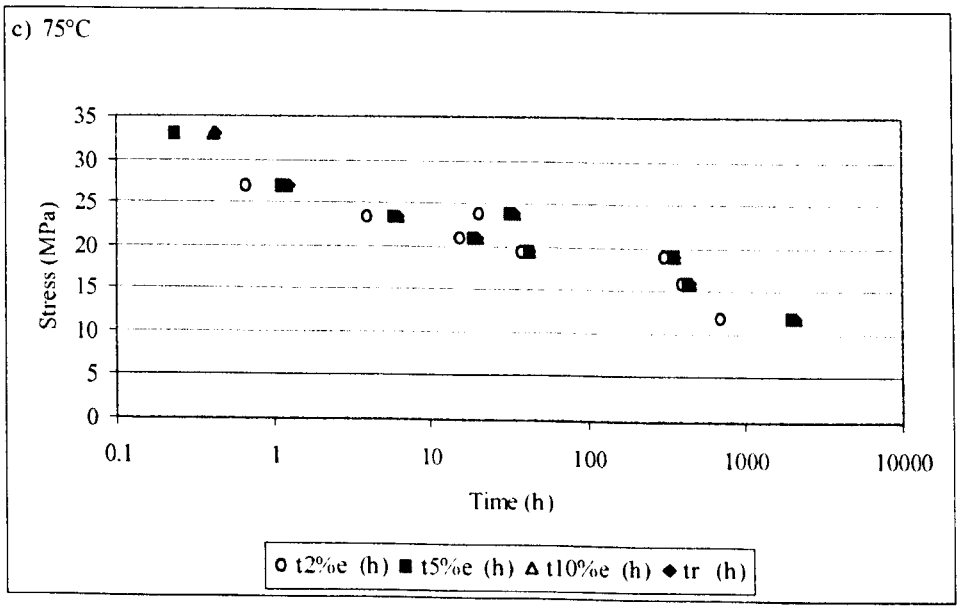
c) 75°C
Stress (MPa)
35
30
25
20
15
10
5
0
0.1
1
10
100
1000
10000
Time (h)
t2%e (h)
t5%e (h)
t10%e (h)
tr (h)

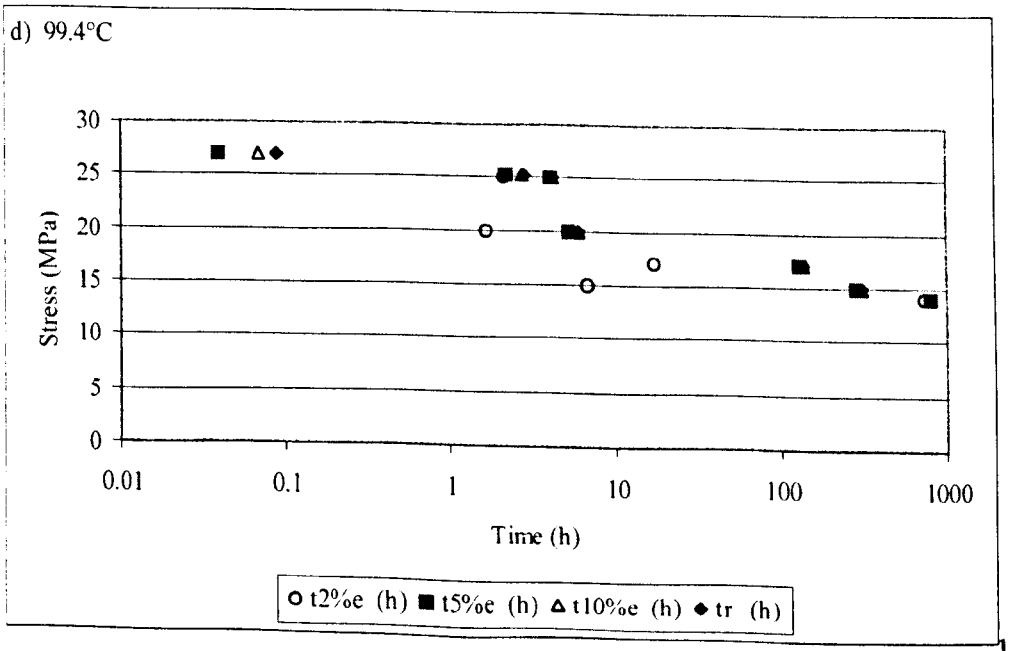
d) 99.4°C
Stress (MPa)
30
25
20
15
10
5
0
0.01
0.1
1
10
100
1000
Time (h)
t2%e (h)
t5%e (h)
t10%e (h)
tr (h)

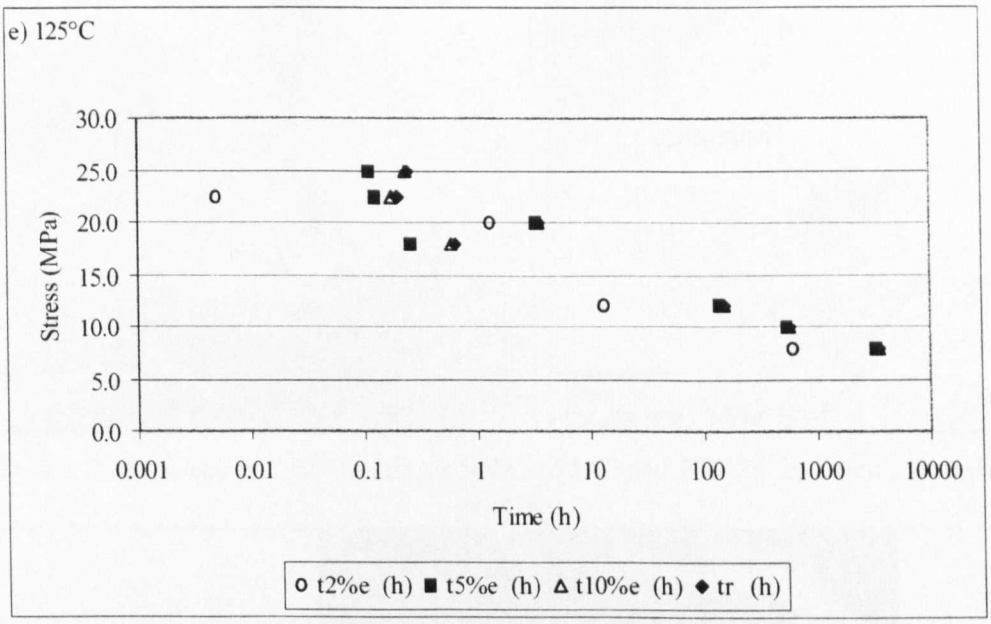


Figures 5.13a to e Failure criterion plots for bulk SnAgCu at a) –10C b) room temperature, c) 75°C, d) 99.4°C and e)125°C


Figure 5.14 Damage accumulation near the fracture surface in a necked sample tested at 75°C for over 800 hours

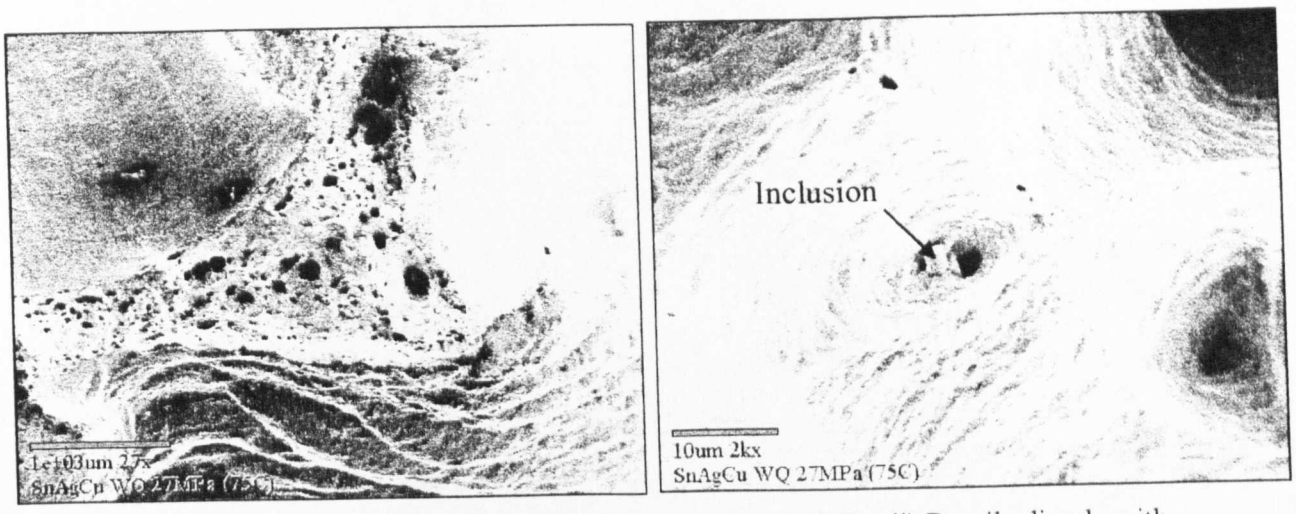


Figure 5.15 a i and ii i) Ductile fracture at 75°C and 27MPa ii) Ductile dimple with inclusion

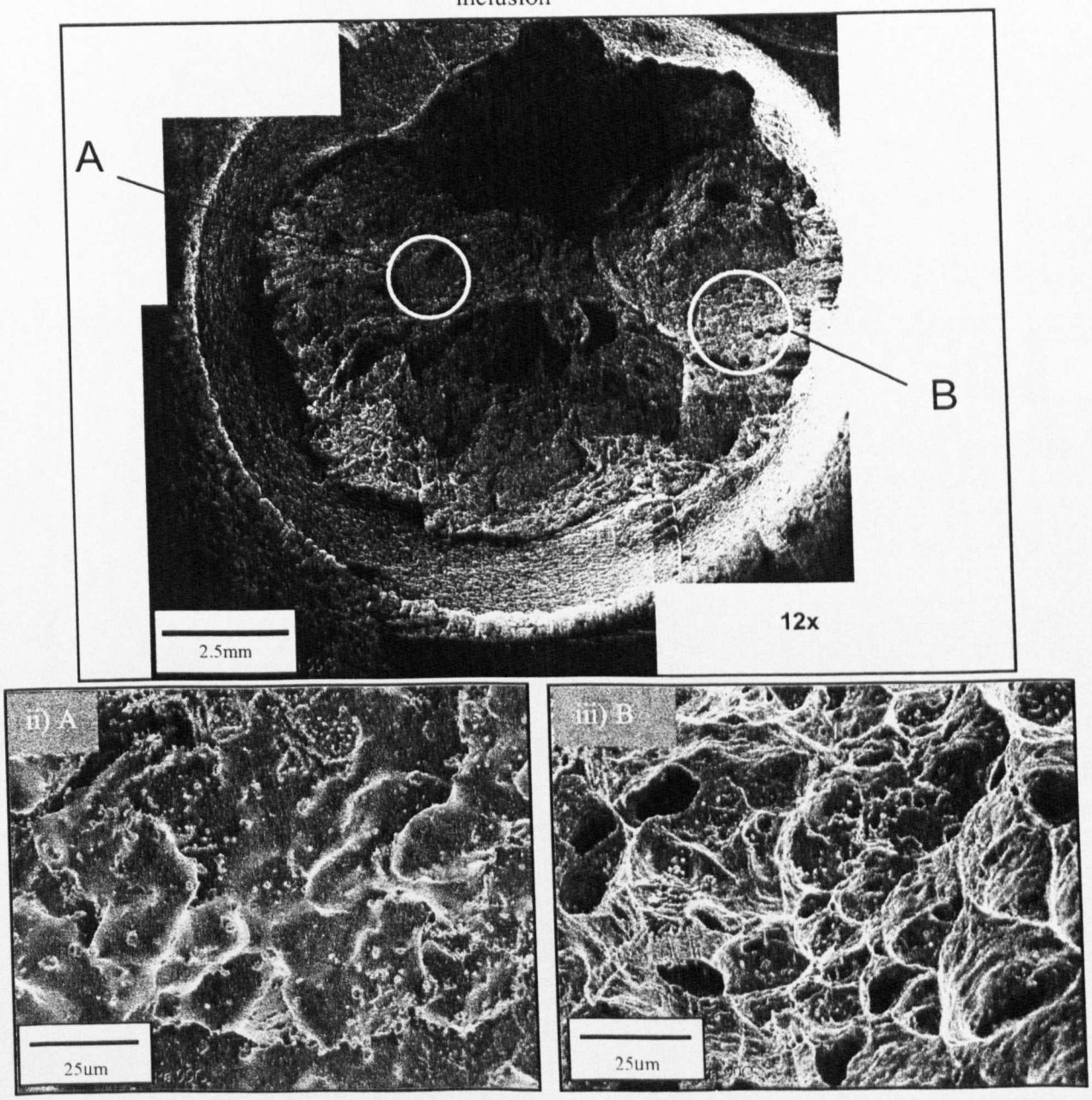


Figure 5.15b i,ii,iii i) Mixed-mode fracture at 99°C and 15MPa ii) colony separation iii) ductile characteristics

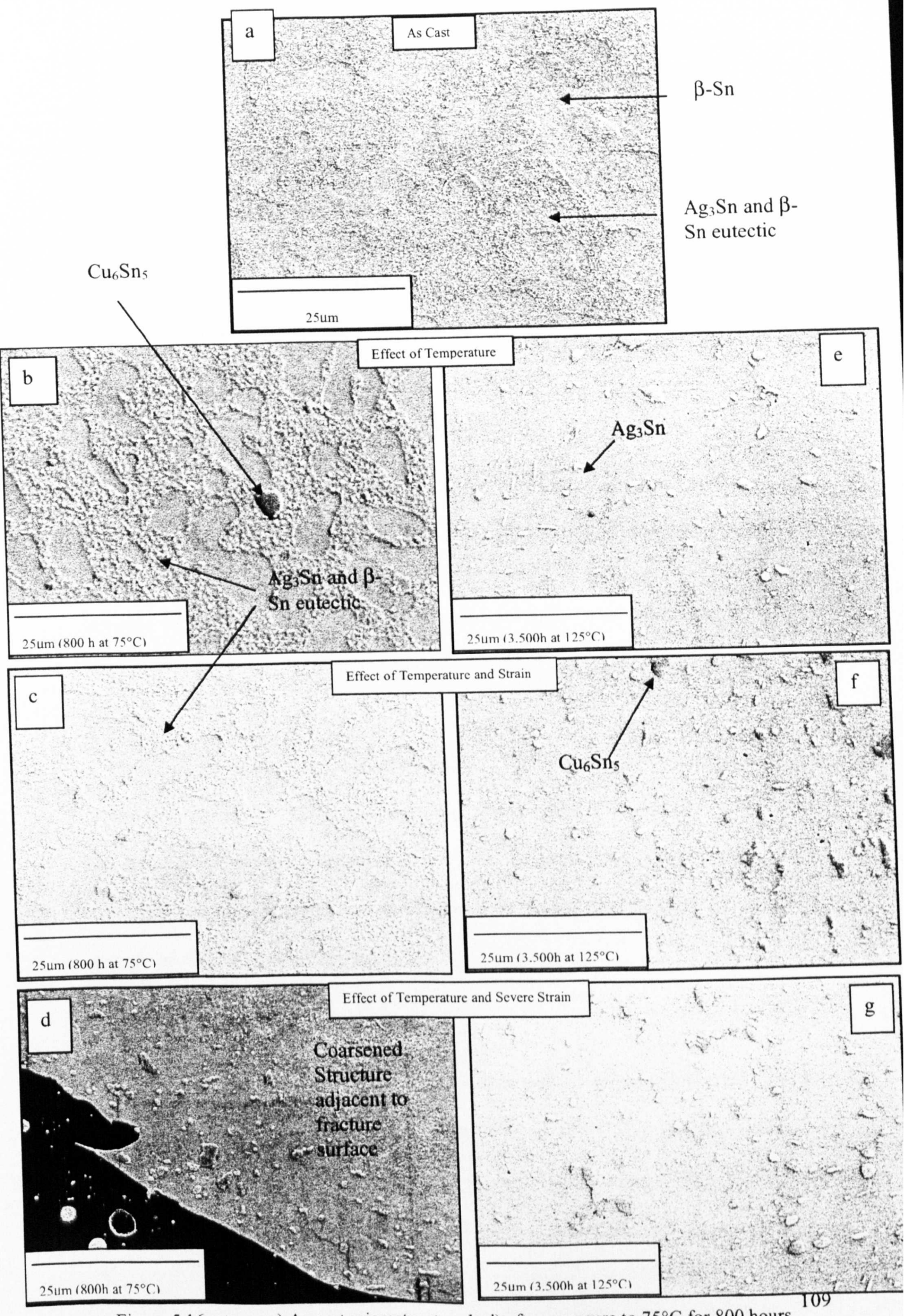




Figure 5.16 a to g a) As cast microstructure b-d) after exposure to 75°C for 800 hours e-f) after exposure to 125°C for 3,500 hours

## 5.2 Sn-3.8Ag-0.7Cu in Model 'Pin in Ring' Joints

### *5.2.1 Individual Creep Test Analysis*

Figure 5.17 shows shear strain versus time for a 'pin in ring' (copper/SnAgCu) joint tested at 75°C (348K, $T_h$=0.71) with an initial shear stress of 6.4MPa. The sample possesses a creep life greater than 1100 hours and exhibits the conventional creep curve shape for a metal, showing evidence of each creep regime (primary, secondary and tertiary). Large strains are evident both on loading and in tertiary creep. Note that the instantaneous strain may not be solely due to displacement in the solder, there may also be slipping at the gripping mechanism or some displacement of the copper/loading assembly (see section 4.2.4). This has been investigated, however, as yet the results are inconclusive (appendix 4.7). Therefore, for the purpose of model joint analysis, instantaneous strain was subtracted from the measured strain values, resulting in the curve shifting down the 'y' axis and only the creep strain being presented.

When shear strain rate is plotted against lifetime, a bathtub shape curve is produced, figure 5.18. As for bulk data, this plot is used to determine the proportions of each creep regime (section 5.2.7). Tables of joint data, shear strain (minus instantaneous strain) versus time and shear strain rate versus time plots are presented for all model joint tests in appendix 5.6.

### *5.2.2 Time to Rupture*

Figures 5.19a and b show shear stress versus time to rupture plots (semi-log and log scales) for temperatures ranging from 29°C to 125°C. By increasing stress or temperature, the resulting creep life of the model joints is reduced. From figure 5.19a it appears that the lines converge at lower applied shear stress values. Assuming no

bi-linearity of the data, creep strengths (in MPa) at 10, 100 and 1,000 hours-life at each temperature are shown in table 5.12. At 29°C and 75°C, creep strengths at 1,000 hours are approximately sixty percent of those at 100 hours and forty-five percent of those at 10 hours.

| **Temperature °C** | **Creep strength (MPa) at 10 hrs** | **Creep strength (MPa) at 100 hrs** | **Creep strength (MPa) at 1,000 hrs** |
|---|---|---|---|
| 29 | 21.8 | 15 | 8.9 |
| 75 | 15.7 | 11.4 | 7.5 |
| 125 | 2.9 | 2.5 | 2.1 |

Table 5.12 Creep strengths at 10, 100 and 1,000 hours-life.

Creep life increases and the strain to failure appears to decrease, with decreasing applied shear stress. Ratios of creep lives are shown in table 5.13.

| **Temperature °C** | **Initial Applied Stress** */Creep Life Ratio* | | |
|---|---|---|---|
| 29 | **10.6MPa** *120* | **15.9MPa** *40* | **21.2MPa** *1* |
| 75 | **6.4MPa** *450* | **10.6MPa** *50* | **18MPa** *1* |

Table 5.13 Effect of stress on creep life at each test temperature

Trends for each of the lines in the stress versus time to rupture plot were calculated using Excel computer software, figure 5.19b. Table 5.14 shows the gradients and intercepts obtained using the following equation:

$$\tau = C.\, t_r^{m} \qquad (5.10)$$

Where $t$ = shear stress
$C$ = constant
$t_r$ = time to rupture

which, by taking logarithms expands to:

$$\text{Log } \tau = m \log t_r + \log C \qquad (5.11)$$

| Temperature °C | Gradient | Intercept |
|---|---|---|
| 29 | 0.1471 | 27.55 |
| 75 | 0.1453 | 20.29 |
| 125 | 0.0840 | 3.39 |

Table 5.14 Constants obtained from stress vs. time to rupture trend lines

The gradients decrease with increasing temperature. Therefore, testing at higher temperatures is more stress dependant than that at lower temperatures, although there is little difference between 29 and 75°C. Creep strength at one hour is identified by the intercept value. There is no clear bi-linearity of the data when plotted on the log-log scale. However, when plotted on the semi-log scale there appears to be a slight downward turn of the 75°C data at low stress values (<10MPa). More testing would be required to confirm this observation. Figure 5.19a (semi-log plot) shows that there may be two changes of dominant creep mechanism throughout the 29°C temperature regime. The line appears to have a steep gradient at both high and low stress values but is shallower between 20 to 15MPa. Another test is required at approximately 50 hours to determine whether this is correct. Unfortunately due to equipment failure and time restrictions this test has yet to be completed.

### *5.2.3 Creep Ductility*

Figures 5.20a and b show strain to failure as both a function of 'stress' and of 'time to rupture'. No trends are apparent for either plot. The minimum shear ductility was approximately fifty per cent. Note that failure ductility in the model joint testing does not take into account any instantaneous strain due to the gripping/slipping problems previously mentioned.

The strain to failure was very difficult to measure accurately in model joints in comparison to the bulk materials. For bulk specimens, the ends of the failed specimen can be placed together to estimate the extension, this in turn can be

compared with the strain versus time measurement on the chart recorder. Such a method cannot be utilised for the model joint and measurements are taken purely from the chart recorder. Failure is defined as the time when the pin pulls through the ring. The shear strain measurement (on a x-t chart recorder) is continuous near failure, however, as the model joint fails suddenly it is difficult to measure the precise strain at failure (see appendix 5.7).

### *5.2.4 Monkman-Grant Relationship*

Figure 5.21 shows the linear trend of the model creep joint data in agreement with the Monkman-Grant relationship (equation 5.5), where $\dot{\varepsilon}_{min}$ is replaced with minimum shear strain rate, $\dot{\gamma}_{min}$. Table 5.15 shows the 'best fit' relationship at each test temperature, obtained as before in the bulk samples, using excel software. However, the sigmoidal trend seen at 29°C in figure 5.19a (time to rupture) is also observed here, i.e. the dominant creep mechanism may change depending on initial applied stress. However, for the purpose of the trend calculation this is not taken into account and the trend is established for all data at 29°C (an average).

| Temperature °C | Equation | Gradient |
|---|---|---|
| All | $\dot{\gamma}_{min} . t_r^{0.99} = 5.7 \times 10^{-2}$ | 0.99 |
| 29 | $\dot{\gamma}_{min} . t_r^{1.07} = 6.8 \times 10^{-2}$ | 1.07 |
| 75 | $\dot{\gamma}_{min} . t_r^{0.93} = 3.6 \times 10^{-2}$ | 0.93 |
| 125 | $\dot{\gamma}_{min} . t_r^{0.92} = 8.9 \times 10^{-2}$ | 0.92 |

Table 5.15 Constants obtained from the Monkman-Grant relationship

### *5.2.5 Minimum Creep Rate – Stress Relationships*

Figure 5.22 shows minimum shear creep rate as a function of applied stress over a range of temperatures (29 to 125°C). Power law relationships in accordance with Norton's Law, are observed for each test temperature. However, trends have not been

established at 125°C due to the limited number of data available at present, further testing is currently underway.

At high initial shear stresses (>12MPa), at 29°C and 75°C, gradients (or creep exponents) of 10 and 13 are obtained (table 5.16), these are similar to those obtained for the bulk material. However, creep exponents in the bulk material decreased with increasing temperature, the opposite appears to occur in the joint specimens. This is difficult to substantiate at present, as only two test temperatures have been utilised, one other temperature is currently under investigation. However, at both 29°C and 75°C there is a change in gradient at stress levels less than 12MPa. At lower shear stresses the gradient becomes shallower (n = 3) indicating a change in dominant creep mechanism at longer lifetimes. These shallower gradients are similar for both test temperatures and would suggest that a similar creep mechanism is operating at lower stresses at both 29°C and 75°C.

At 20MPa there is approximately an order of magnitude difference between minimum shear strain rates at 75°C and 29°C, this difference decreases as the stress decreases.

| **Temperature °C** | **Constant $A_1$** | **Creep Exponent n** |
|---|---|---|
| *High Shear Stress (>12MPa)* | | |
| 29 | $1 \times 10^{-16}$ | 10 |
| 75 | $5 \times 10^{-19}$ | 13 |
| *Low Shear Stress (<12MPa)* | | |
| 29 | $4 \times 10^{-8}$ | 3 |
| 75 | $4 \times 10^{-7}$ | 3 |
| *All Shear Stresses (average of all data)* | | |
| 29 | $4 \times 10^{-12}$ | 7 |
| 75 | $4 \times 10^{-10}$ | 6 |

Table 5.16 Calculation of creep exponent from Norton's Law

Additional evaluation was performed due to the transition occurring between high and low stress data when using the power law relationship. The Garofalo 'sinh' relationship ( $\dot{\varepsilon}_{min} = A\sinh(\alpha\sigma)$ ) [40] which represents combination creep, removed the bi-linearity observed in the Norton's Law plot and provided a better description of the 'pin in ring' data. To determine a value of '$\alpha$' in the 'sinh' relationship a Zener-Holloman plot was used. Firstly, creep activation energy was determined from an Arrhenius plot (described in section 5.2.6). Then, Z was plotted versus stress on a log-log scale where $Z = \dot{\varepsilon}_{min} \exp\left(\frac{Q}{RT}\right)$. Curved relationships were produced (at both 29°C and 75°C) rather than a straight line (figure 5.23) thus indicating that the 'sinh' relationship should be examined. If a straight-line relationship was obtained, either the power law (as for bulk data) or exponential law would be the best descriptor of the data. The value of '$\alpha$' in the sinh relationship is estimated from the Zener-Holloman plot and is the reciprocal of the stress at the point of inflection. By plotting 'Z' versus 'sinh$\alpha\sigma$', alpha was 'optimised' by using the $R^2$ method in 'Excel' computer software so that $R^2$ equals a value close to one. Figure 5.24 illustrates the 'sinh' relationship for the model joint data at 29°C and 75°C, where both are consistent with the relationship. Table 5.17 below illustrates the similarity between the gradients when compared using this relationship, showing very little difference between the two test temperatures. Testing is still required at additional test temperatures. This analysis was not performed for the bulk material and therefore a comparison between bulk and joint can not be performed.

| Temperature °C | Constant | Gradient |
|---|---|---|
| 29 | $5 \times 10^{-4}$ | 4.2 |
| 75 | $7 \times 10^{-5}$ | 4.6 |

Table 5.17 Constants obtained from the sinh$\alpha\sigma$ relationship

### 5.2.6 *Determination of Activation Energy*

Using the same method utilised for the bulk specimens, values of minimum shear strain rate were obtained from Norton's Law at three values of initial applied shear stress (using the value of 'n' above the transition) 15, 20 and 35MPa. Apparent activation values were determined by plotting logarithmic (ln) minimum shear strain rates against the inverse of the product of the gas constant, R (8.314 $JK^{-1}mol^{-1}$), and absolute temperature, T (K), figure 5.25.

Table 5.18 shows the apparent activation energies and constants obtained at each stress level. The low values of activation energy may correspond to that of short circuit diffusion in tin (e.g. pipe diffusion), as discussed in chapter two. Although at a high stress of 35MPa activation is sufficiently high to correspond to self-diffusion in tin.

| Stress (MPa) | Activation Energy (kJ/mol) | ln $A_2$ | $A_2$ |
|---|---|---|---|
| 15 | 48 | 10.09 | $2.4 \times 10^{4}$ |
| 20 | 64 | 19.33 | $2.5 \times 10^{8}$ |
| 35 | 94 | 37.32 | $1.6 \times 10^{16}$ |

Table 5.18 Apparent activation energy and constants for model joints

True activation energy for creep in model joints was determined using the method previously described for the bulk material. It should be noted that only an equation for the temperature dependence of the Young's modulus of tin (not shear modulus) was available, therefore the relevant shear quantities were converted into tensile data. Using values obtained in the high stress regime (>12MPa) and selected a normalised stress of ($\sigma/E \times 10^{-4}$) = 10 and 12, values for true activation energy of 45 and 49 $kJmol^{-1}$ were obtained. Values for the true activation energy for creep are similar to apparent activation energy values (in the high shear stress regime) at 15MPa –

20MPa, possibly representative of circuit diffusion. In the low stress regime (<12MPa) and selected a normalised stress of ($\sigma$/E x $10^{-4}$) = 3 and 4, values for true activation energy of 15 and 38 kJmol$^{-1}$ were obtained. Similarly, apparent activation energies (in shear) in the low stress regime are also low at approximately 20kJmol$^{-1}$. As a matter of comparison, apparent activation energy values were also calculated for the converted data (to tensile) and similar values were produced. At present the author is not entirely satisfied with these results, as tests have only been performed at two temperatures and is unable to clarify or make conclusions from this data.

### *5.2.7 Factors Affecting Strain Rate*

*Effect of Stress*

Shear strain rate versus life fraction graphs were used to illustrate the effect of stress on strain rate. Three graphs were drawn (one for each test temperature) where selected shear stress values (high, medium and low) represent the testing extremes. Figure 5.26 demonstrates the effect of stress at 75°C, graphs for the additional test temperatures can be found in appendix 5.8. Minimum shear strain rate is effected by initial applied shear stress, table 5.19. It is difficult to directly compare bulk and joint ratios as different 'time to rupture' ranges were utilised.

| **Temperature °C** | **Initial Applied Stress** */Strain Rate Ratio* | | |
|---|---|---|---|
| 29 | **10.6MPa** *1* | **15.9MPa** *2* | **21.2MPa** *19* |
| 75 | **6.4MPa** *1* | **10.6MPa** *4* | **18MPa** *260* |

Table 5.19 Effect of stress on strain rate at each test temperature

*Effect of Temperature*

Figures 5.27a and b illustrate the effect of temperature when shear stress is held constant at 10.6MPa and 15.9MPa. No such data are available at 125°C due to the low failure strengths at this temperature. At 10.6MPa, temperature does not appear to have a marked effect and the ratio between the minimum shear strain rates at 29°C and 75°C was 1:2. As expected, at higher stresses temperature has more of an effect, for example at 15.9MPa, the minimum shear strain rate ratio between 29°C and 75°C is 1:10.

*Using Strain Rates to Determine Creep Regime*

Many constitutive equations used in computational methods of life prediction rely on steady state creep behaviour; therefore it is beneficial to determine the proportion of life spent in each regime. The method first described in section 5.1.7, (where steady state creep is arbitrarily defined as the time spent below $1.1\dot{\gamma}_{min}$ on shear strain rate versus life fraction plots), was used to determine the proportions of creep life occupied by each creep regime, table 5.20.

| Temperature °C | Stress MPa | Primary % | Secondary % | Tertiary % |
|---|---|---|---|---|
| 29 | 9.6 | 17 | 44 | 39 |
| 29 | 10.6 | 8 | 40 | 52 |
| 29 | 15.9 | 25 | 35 | 40 |
| 29 | 21.2 | 44 | 37 | 19 |
| 29 | 29.7 | 24 | 37 | 39 |
| 29 | 31.8 | 25 | 34 | 41 |
| 75 | 6.4 | 13 | 30 | 57 |
| 75 | 8.5 | 21 | 39 | 40 |
| 75 | 10.6 | 18 | 42 | 40 |
| 75 | 15.9 | 45 | 29 | 26 |
| 75 | 18 | 26 | 41 | 33 |
| 75 | 20.2 | 36 | 37 | 27 |
| 125 | 2.1 | 10 | 30 | 60 |
| 125 | 3.2 | 14 | 38 | 48 |

Table 5.20 Proportions of life occupied by each creep regime (model joints)

Table 5.20 shows that no definite correlation exists between the extent of each creep regime with applied stress and temperature. In the majority of cases secondary creep occupies approximately forty percent of creep life, with the greater part of the remaining life in tertiary creep. Occasionally, creep life is evenly divided between the regimes; this appears to occur at higher shear stresses.

### *5.2.8 Creep Strain*

*Extent of Creep Strain Occurring in Each Regime*

The proportions of each regime with respect to shear strain rate were determined in section 5.2.7. This section now determines how much strain is occurring in each regime. Creep strains were obtained both separately and accumulatively using the method first described in section 5.1.8. Tables illustrating both types of analysis performed on all data can be found in appendix 5.9. Determination of the proportion of creep strain occurring in each regime is shown in table 5.21.

| **Temperature °C** | **Stress MPa** | **% $\gamma_o$** (=$\gamma_o/\gamma_f$ x 100) | **%$\gamma_p$** (=$\gamma_p/\gamma_f$ x 100) | **%$\gamma_s$** (=$\gamma_s/\gamma_f$ x 100) | **%$\gamma_t$** (=$\gamma_t/\gamma_f$ x 100) |
|---|---|---|---|---|---|
| 29 | 9.6 | 14 | 2 | 1 | 82 |
| 29 | 10.6 | 6 | 1 | 1 | 91 |
| 29 | 15.9 | 18 | 8 | 3 | 72 |
| 29 | 21.2 | 47 | 2 | 1 | 49 |
| 29 | 29.7 | 17 | 1 | 2 | 79 |
| 29 | 31.8 | 14 | 15 | 3 | 68 |
| 75 | 6.4 | 14 | 3 | 3 | 80 |
| 75 | 8.5 | 4 | 3 | 2 | 90 |
| 75 | 10.6 | 21 | 5 | 2 | 71 |
| 75 | 15.9 | 16 | 6 | 3 | 76 |
| 75 | 18 | 24 | 2 | 2 | 71 |
| 75 | 20.2 | 20 | 2 | 2 | 76 |
| 125 | 2.1 | 5 | 3 | 5 | 86 |
| 125 | 3.2 | 21 | 19 | 16 | 44 |

Table 5.21 Proportion of creep strain occurring in each creep regime

The table illustrates that, in general, only a very small percentage of creep strain occurs during primary and secondary creep. The majority (up to ninety percent) of creep strain occurs in tertiary creep. The highest shear stresses used at 29°C and 125°C produced a larger proportion of primary creep. In the instance of table 5.21, '% $\gamma_0$' includes the gripping/slipping of the copper in the gripping mechanism in addition to elastic strain occurring on loading. A similar table has been compiled omitting the instantaneous strain value, appendix 5.10, to correspond to other analysis, such as ductility plots. By excluding instantaneous strain from the analysis it was observed that, on average, six percent of shear strain occurs in primary creep, four percent in secondary and approximately ninety percent in tertiary creep. In general, there does not appear to be any correlation of any type of shear creep strain with stress and temperature.

*Using Creep Strain During Creep Life to Determine Failure Definitions*

Analysis was performed to determine the time taken to achieve 2%, 5% and 10% shear strain for model joints. However, it was discovered that the results were inconclusive, as the shear strains occurring on loading and were so large, possibly due to the gripping/slipping of the sample on loading. Therefore, analysis was performed using only creep strain (omitting instantaneous strain), table 5.22. The shear strain was also converted into tensile strain (using $\gamma = \sqrt{3}\varepsilon$), as shear strains are larger than tensile strains and so that the results could be compared with those obtained for the bulk material (see discussion).

| Temperature (°C) | Stress (MPa) | $t_{2\%}$ (h) | $t_{5\%}$ (h) | $t_{10\%}$ (h) | $t_r$ (h) | % life 2% strain | % life 5%strain | % life 10% strain |
|---|---|---|---|---|---|---|---|---|
| 29 | 9.6 | | 426.9 | 715.4 | 767.4 | 0 | 56 | 93 |
| 29 | 10.6 | 138.1 | 295.2 | 430.1 | 441.27 | 31 | 67 | 97 |
| 29 | 15.9 | | 2.6 | 125.2 | 154.73 | 0 | 2 | 81 |
| 29 | 21.2 | 0.4 | 3.65 | 3.75 | 3.75 | 11 | 97 | 100 |
| 29 | 29.7 | 0.07 | 0.3 | 0.45 | 0.58 | 12 | 52 | 78 |
| 29 | 31.8 | | | | 0.42 | 0 | 0 | 0 |
| 75 | 6.4 | 17.1 | 406 | 823 | 1134.5 | 2 | 36 | 73 |
| 75 | 8.5 | 31.4 | 317.1 | 525.7 | 555.7 | 6 | 57 | 95 |
| 75 | 10.6 | | 3.3 | 122 | 132.53 | 0 | 2 | 92 |
| 75 | 15.9 | 0.11 | 6 | 10.57 | 10.83 | 1 | 55 | 98 |
| 75 | 18 | 0.06 | 1.53 | 2.44 | 2.55 | 2 | 60 | 96 |
| 75 | 20.2 | 0.02 | 0.32 | 0.52 | 0.53 | 4 | 60 | 98 |
| 125 | 2.1 | | 83.3 | 186.7 | 300.9 | 0 | 28 | 62 |
| 125 | 3.2 | | 0.31 | 1.36 | 2 | 0 | 16 | 68 |

Table 5.22 Failure criterion for SnAgCu in model joint form (converting shear strain into tensile strain)

Figures 5.28a-c show the time at each failure criterion (time at 2, 5 and 10% strain) for each test temperature. The pin in ring joint specimens produce a wider scatter of data in comparison to that obtained for the bulk specimens. The narrow band of data for bulk specimens suggests that very little strain is occurring until tertiary creep, close to the time to rupture. Larger strains are achieved in model joints and as a result data are more widely distributed. In some cases strains occurring during the creep test exceed 2% on loading even after the instantaneous strain has been subtracted, figure 5.28c.

### *5.2.9 Microstructural Evaluation of Model Joints.*

Microstructural evaluation was performed on the 'as cast' structure to demonstrate the quality of the joints, where particular attention was paid to defects and intermetallic compounds throughout the bulk and at the interface. Analysis was also carried out at both temperatures, at each stress extreme, to determine any differences which may suggest an explanation of the mechanism change.

Figure 5.29 shows an 'as cast' model joint, possessing an intermetallic layer of approximately 2μm and a fine networked structure of sub-micron $Ag_3Sn$ surrounding β-Sn globules. Some $Cu_6Sn_5$ particles are seen to have broken away from the IMC layer and floated into the bulk during the soldering procedure, these being approximately 3 to 4μm. After exposure to 75°C for over 1,000 hours the microstructure shows signs of coarsening similar to that seen in the bulk material, figure 5.30. As all the solder within the joint is subjected to strain there is no area that can be examined to identify the microstructural changes occurring solely due to the effect of temperature. Therefore, the changes observed occur under the influence of both strain and temperature. In the mid-section away from the intermetallic layer, coarsening of $Ag_3Sn$ and $Cu_6Sn_5$ is observed. $Cu_6Sn_5$ (to 3μm) coarsens more rapidly than $Ag_3Sn$ (1μm), the networked eutectic region is no longer evident. At the fracture surface (pin-side) where the material has been severely strained there is no evidence of the finely dispersed $Ag_3Sn$ structure observed in the 'as cast' condition. The large (approximately 7μm) particles of $Cu_6Sn_5$ appear to be those initially formed during the soldering procedure, which separated from the main layer, floated into the bulk and have coarsened. There is no evidence of particles as large or in such quantities away from the IMC layer. It may be suggested that these form during the creep test through the diffusion of copper from the pin or ring. If this were the case the IMC would also be expected to grow during testing, however, there is no evidence from microstructural examination to support this.

When compared to the 'as cast' structure, testing at room temperature (29°C) produced no significant changes to microstructure, figure 5.31. Coarsening was only evident at the highly strained fracture surface. Some accumulation of damage, such as the coalescence of voids, is also evident in this region. As yet, there is no

suggestion of the mechanism change at lower stresses. The microstructure for a short-term test at 75°C resembled that seen for the room temperature tests.

Fractography was performed to determine the mode and location of failure, however, as the samples were tested in shear the fracture surface became 'smeared' and difficult to interpret, figure 5.32. Energy dispersion spectroscopy performed on the fracture surface determined the elements present and suggested the location of failure. Generally, the majority of the failure surface was comprised of Sn although there were some areas of $Cu_6Sn_5$. This suggests that failure commonly occurred above the IMC layer and occasionally moved to the solder/IMC interface. Figure 5.33 shows the cracking formed in a SnAgCu model joint tested in a screw driven Instron machine as part of preliminary testing. Here, the crack is seen to occur largely within the bulk solder, however the crack occasionally runs along the IMC/solder interface, where the $Cu_6Sn_5$ grains are large, therefore, exposing them. This is also thought to occur in creep testing and is suggested by fractography, nevertheless, interrupted creep tests are still required to provide microstructural evidence of coarsening and crack propagation prior to failure. Occasionally, cracks are seen to dissect the larger $Cu_6Sn_5$ grains in the interfacial layer. It may be suggested that these cracks may be formed during the water quenching procedure due to thermal shock, although there is little evidence to support this from the microstructural evaluation of the 'as cast' specimens.

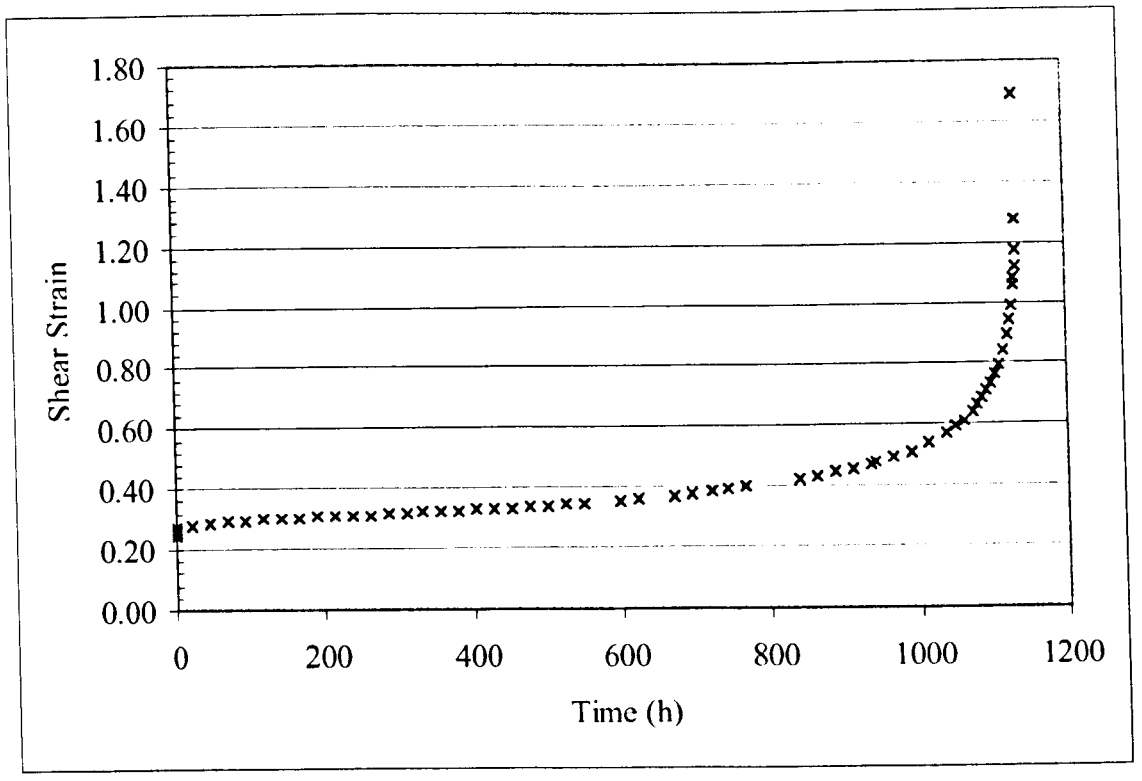


Figure 5.17 Shear strain vs time for SnAgCu/Cu model joint at 75°C and 6.4MPa

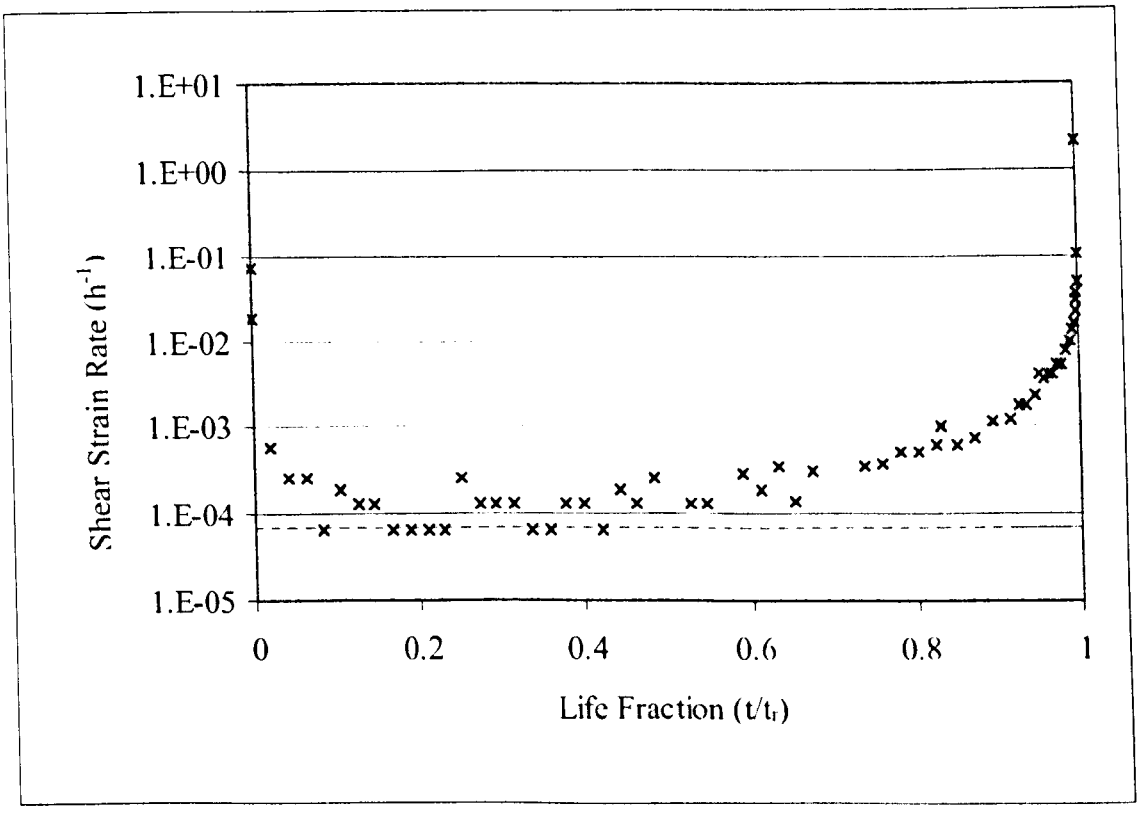


Figure 5.18 Shear strain rate vs life fraction for SnAgCu/Cu model joint at 75°C and 6.4MPa

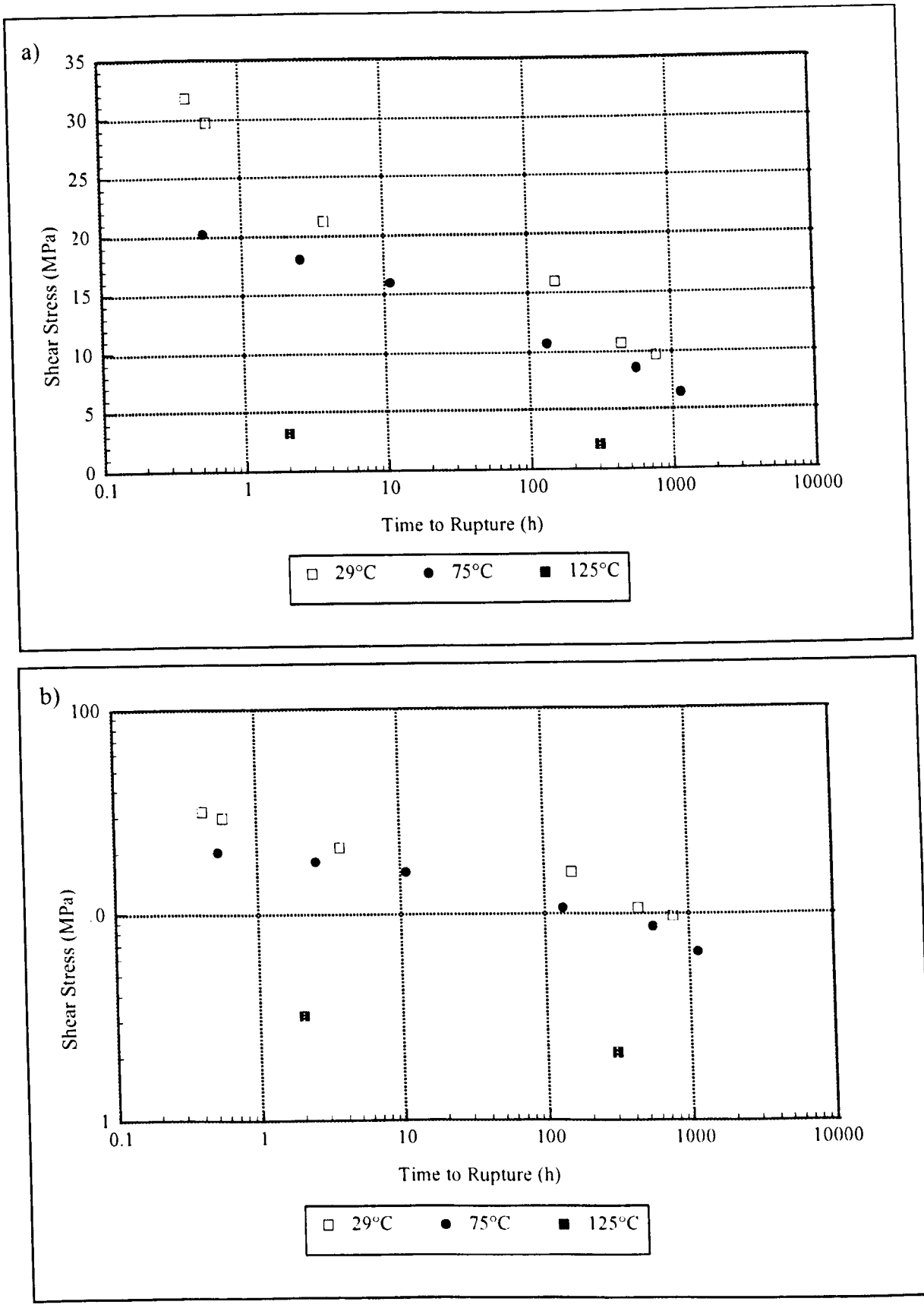


Figure 5.19 a & b Shear stress vs time to rupture a) semi-log scale b) log-log scale

(see Appendix 5.2b for trend lines)

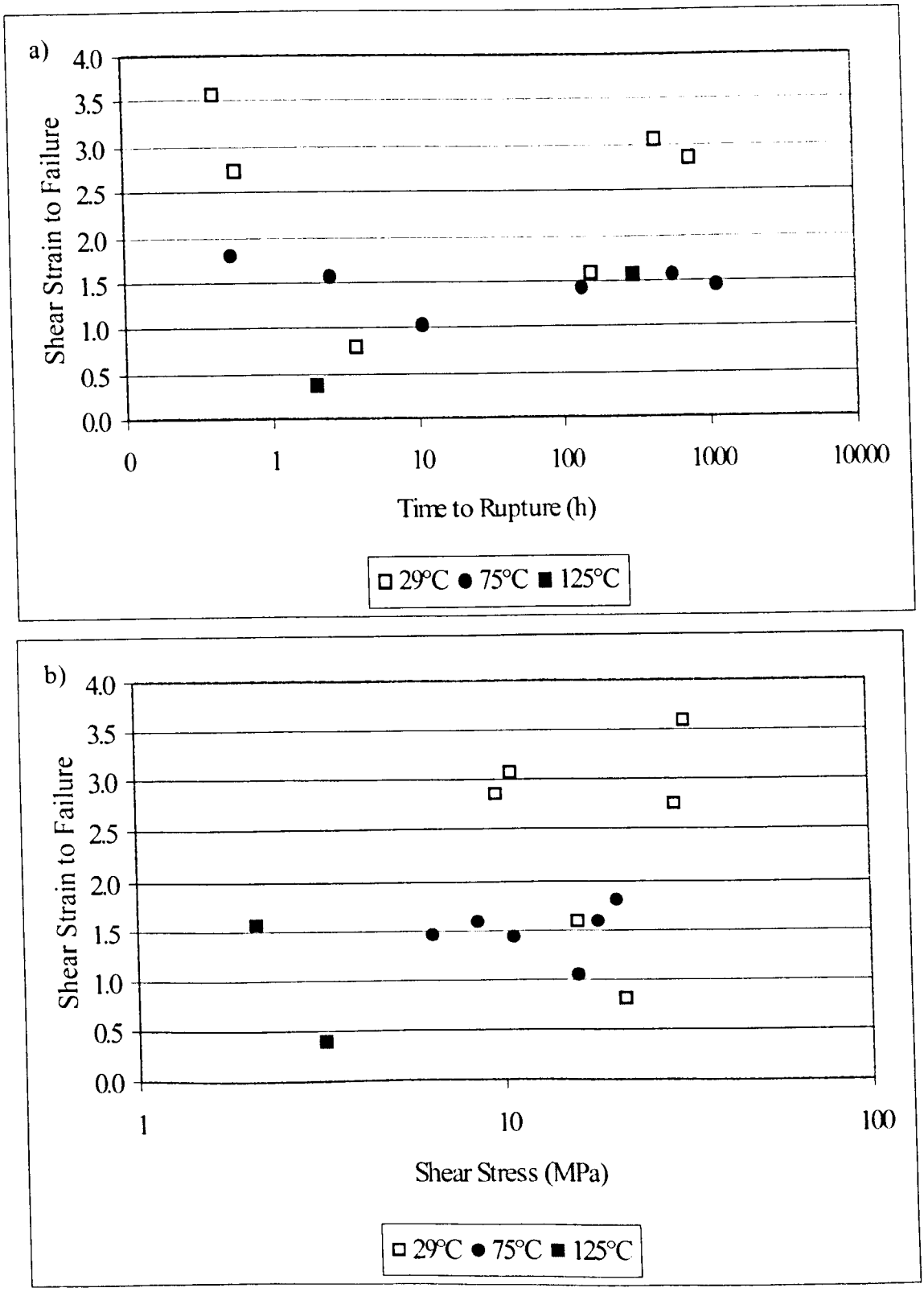


Figure 5.20 a & b Ductility of SnAgCu joints in creep a) vs. time to rupture b) vs. shear stress

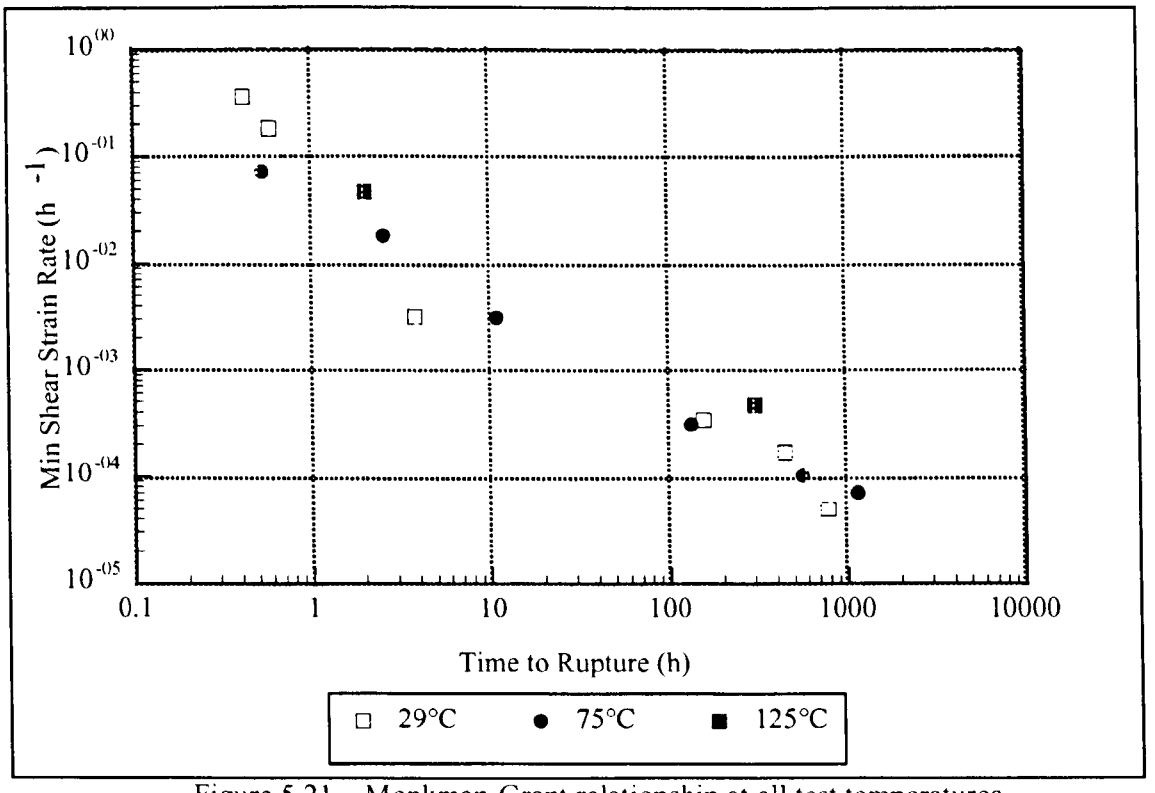


Figure 5.21 Monkman-Grant relationship at all test temperatures

(see Appendix 5.2b for trend lines)

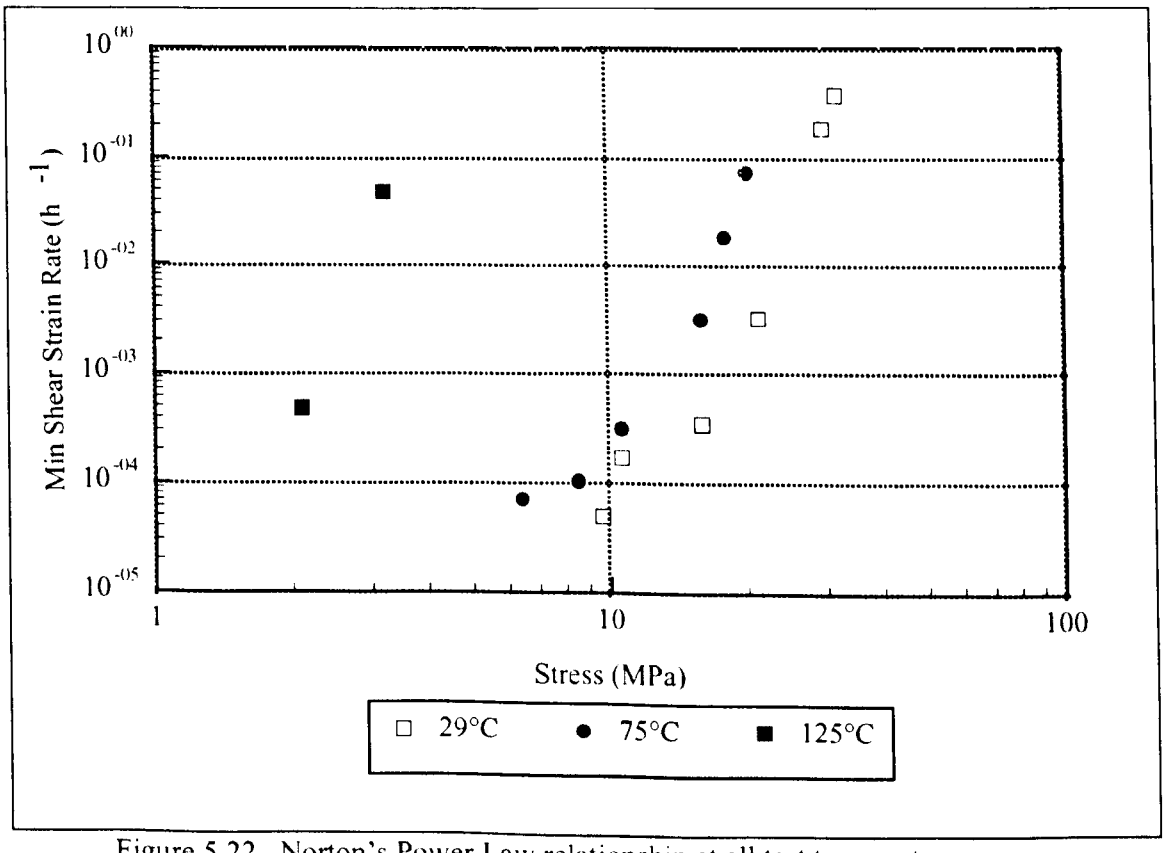


Figure 5.22 Norton's Power Law relationship at all test temperatures

(see Appendix 5.2b for trend lines)

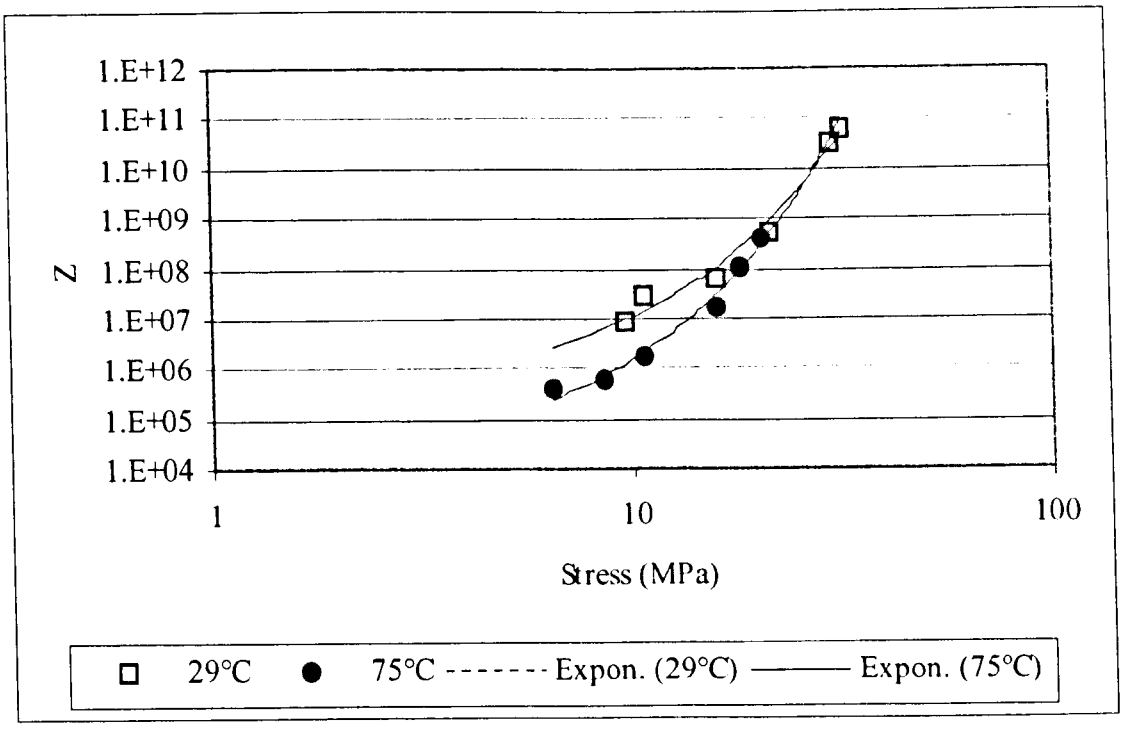


Figure 5.23 Zener-Holloman plot to determine alpha

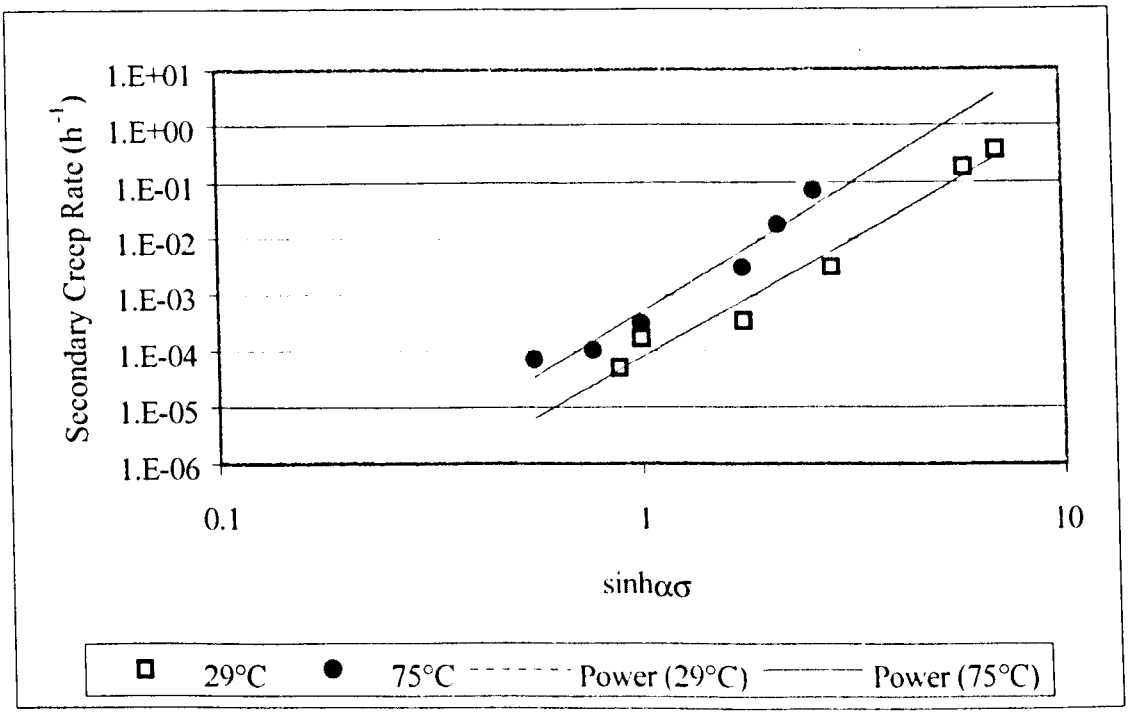


Figure 5.24 'Sinh' relationship using value of alpha determined from figure 5.23

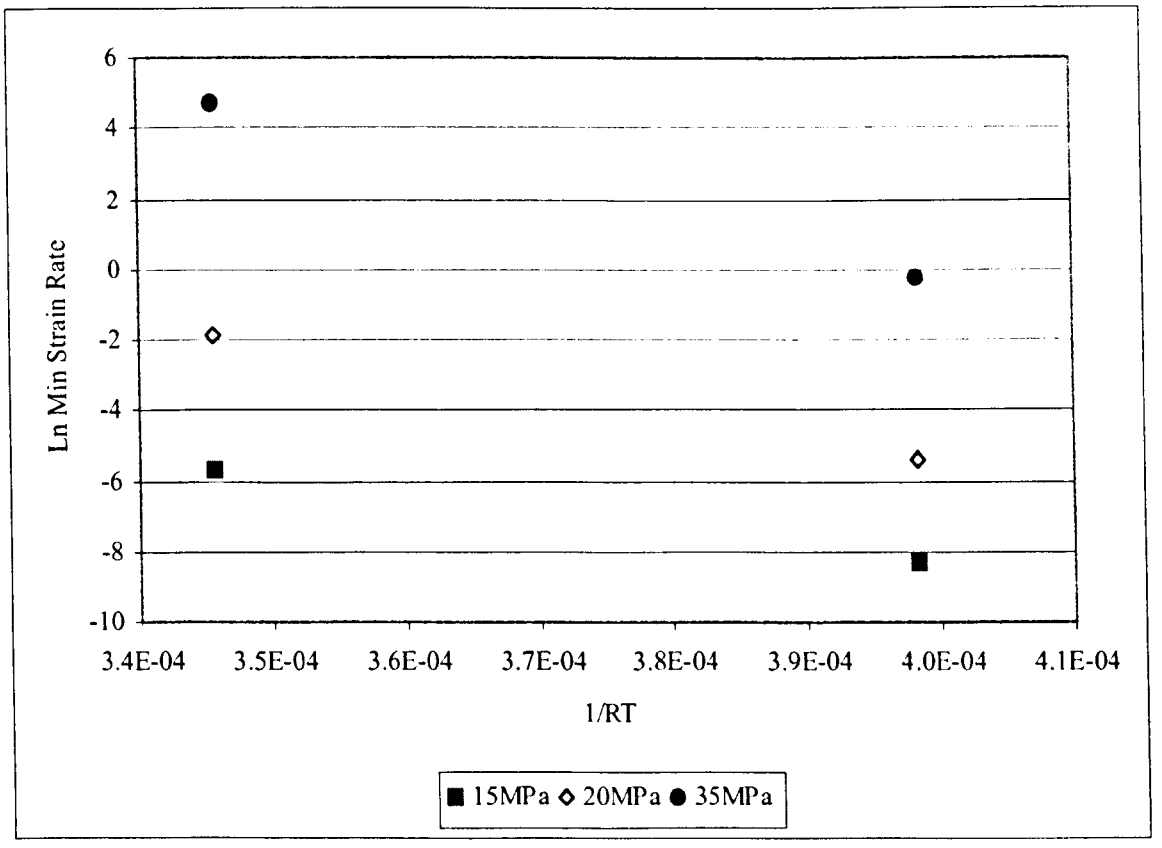


Figure 5.25 Determination of apparent activation energy for creep at high stress

(See Appendix 5.2b for trend lines)

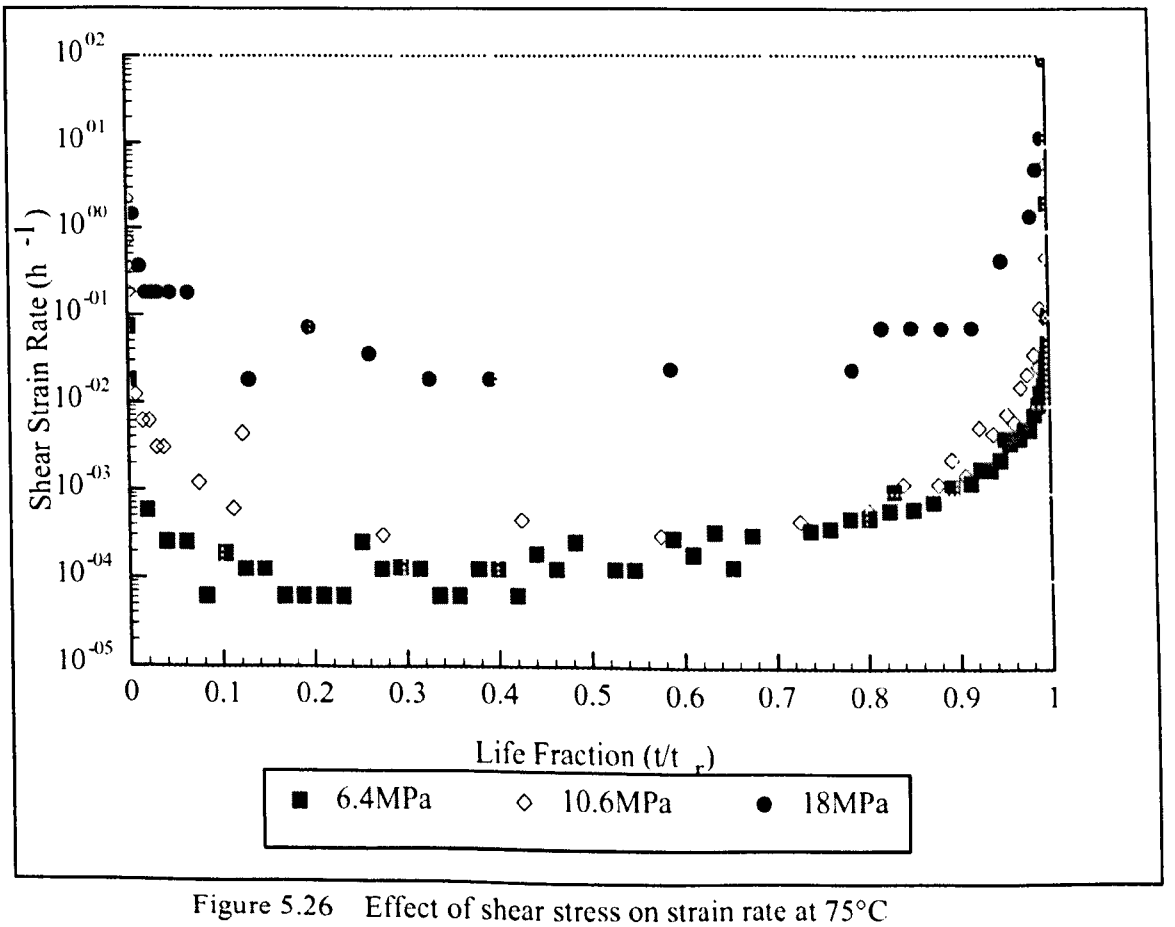


Figure 5.26 Effect of shear stress on strain rate at 75°C

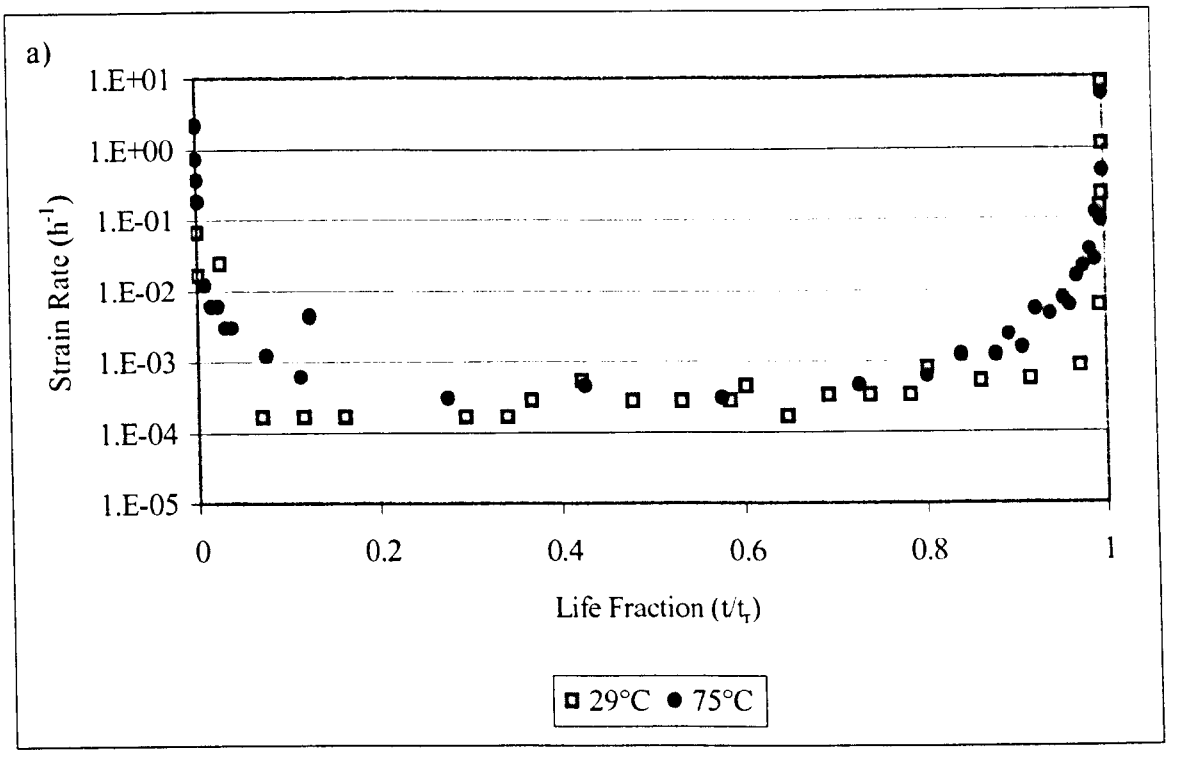


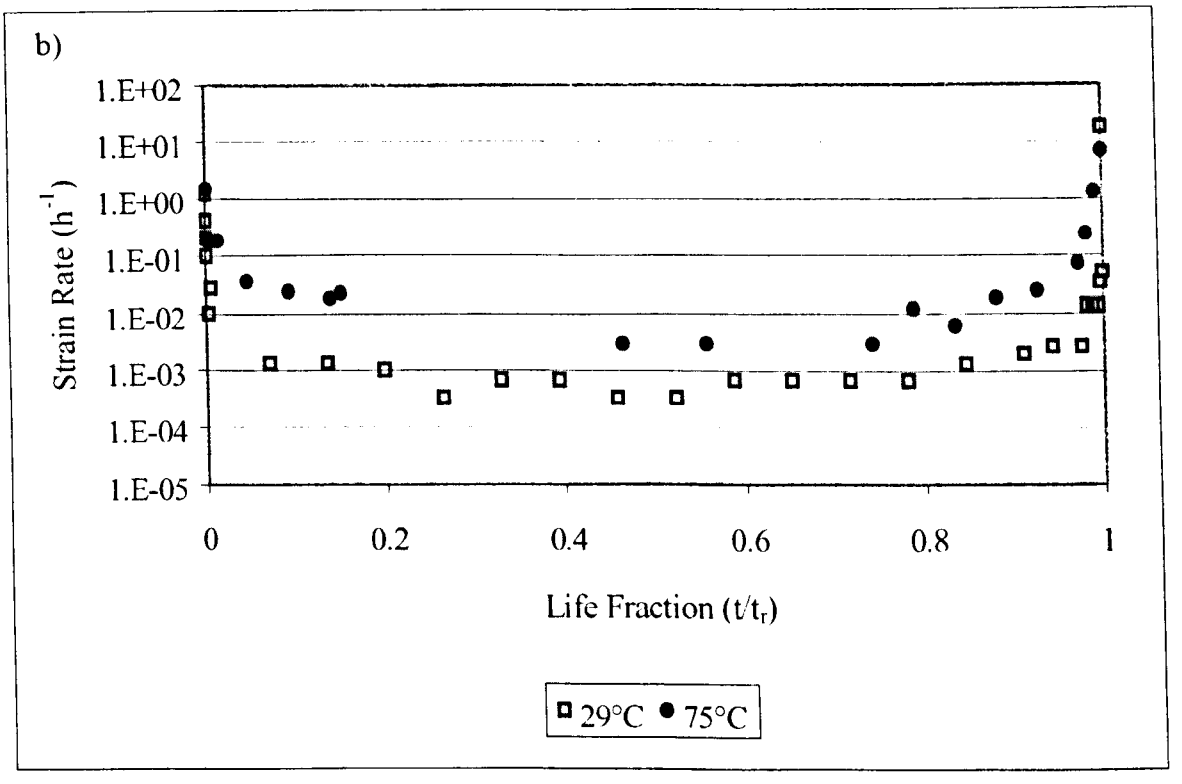


Figure 5.27 a & b Effect of temperature on strain rate at a)10.6MPa b) 15.9MPa

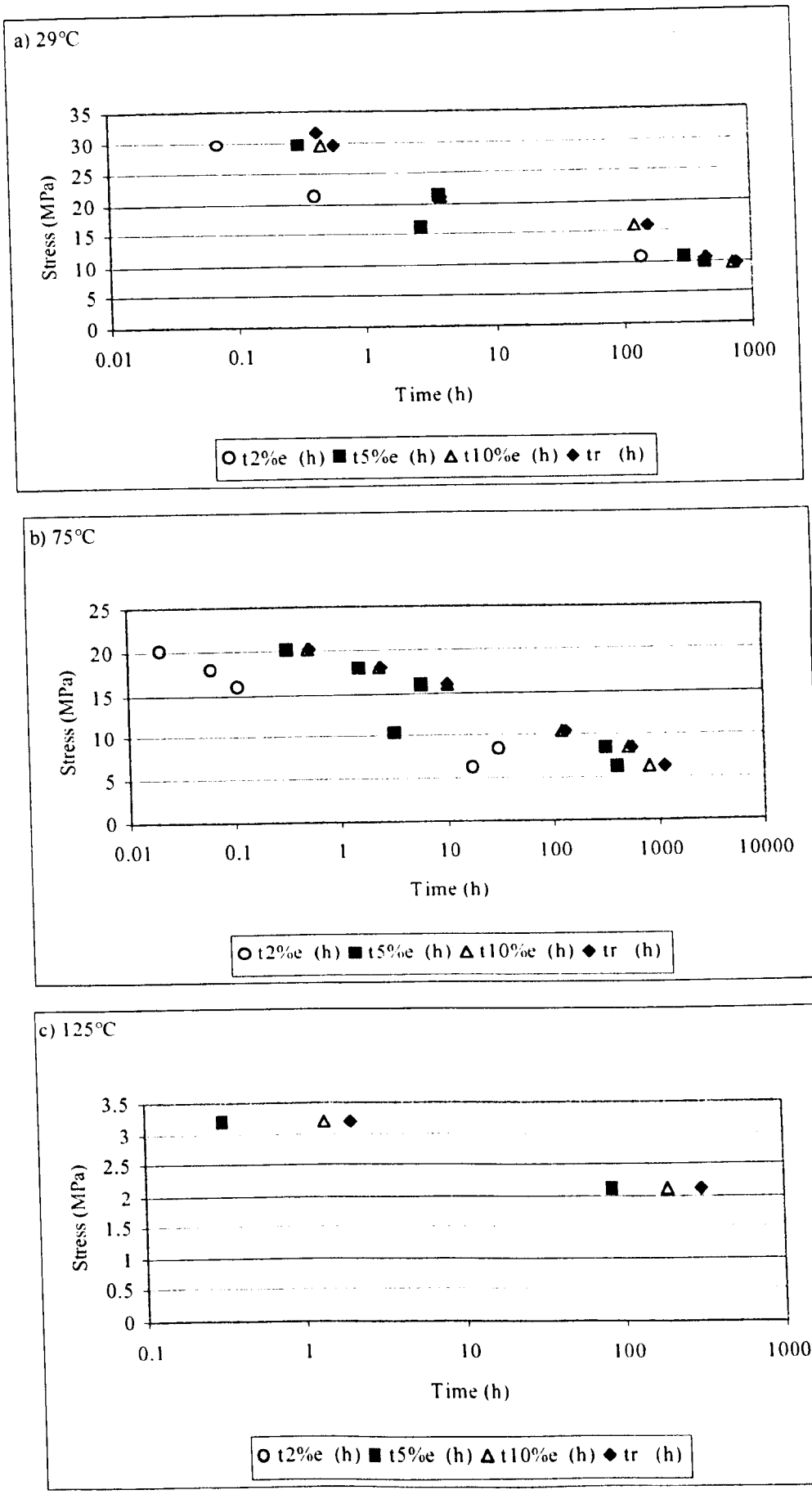


Figure 5.28 a-c Failure criterion plots for model joints at a) room temperature, b) 75°C and c) 125°C

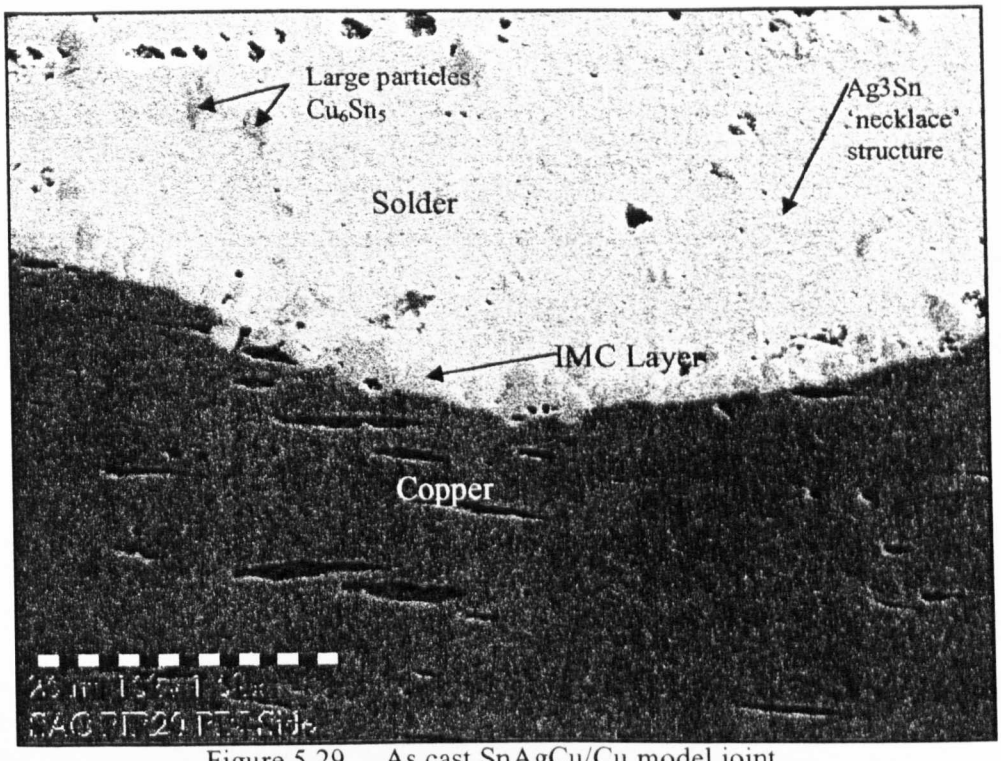


Figure 5.29 As cast SnAgCu/Cu model joint

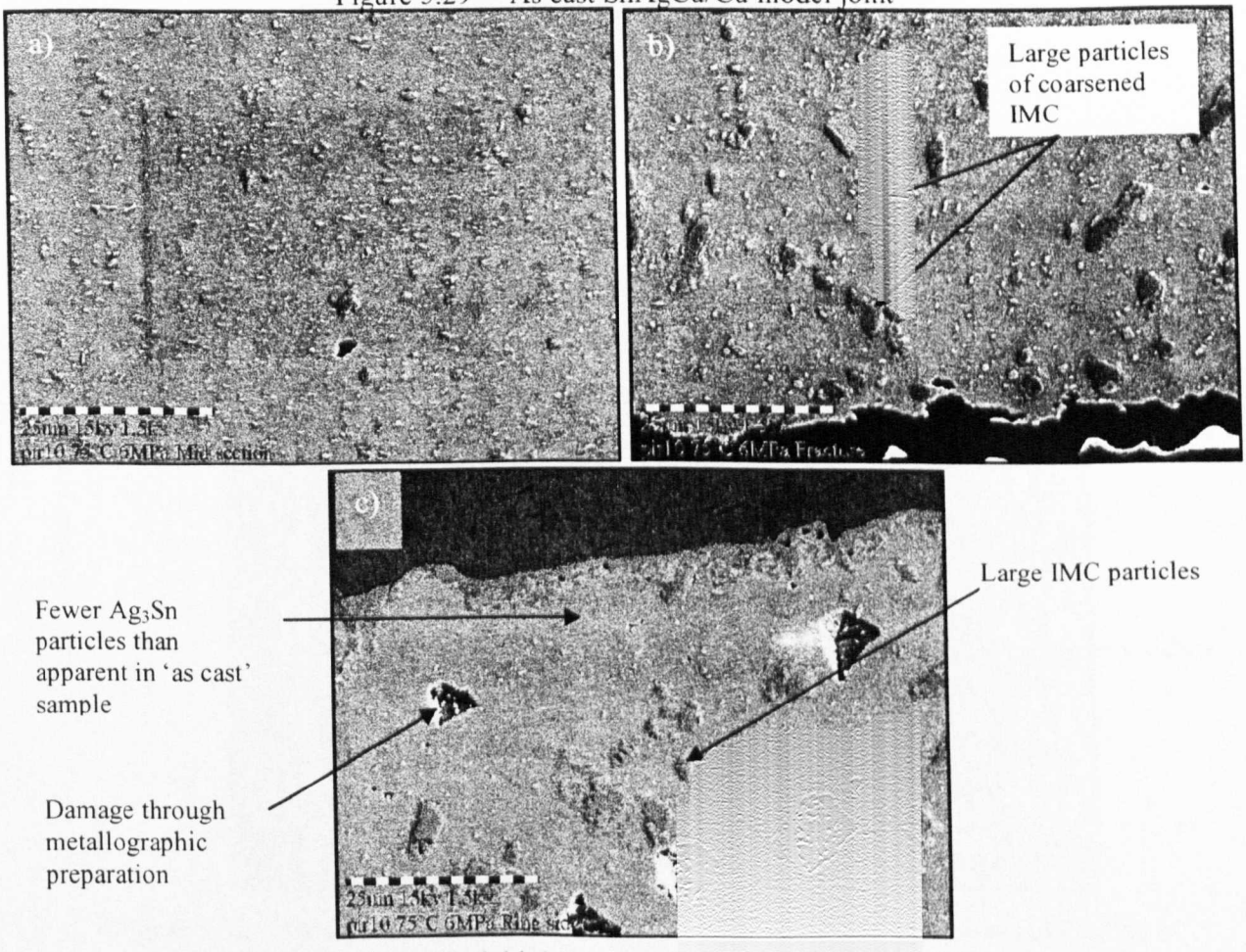


Figure 5.30a-c Model joint exposed to 75°C for over 1000 hours
a) mid section b) fracture surface (pin side) c) ring/solder interface

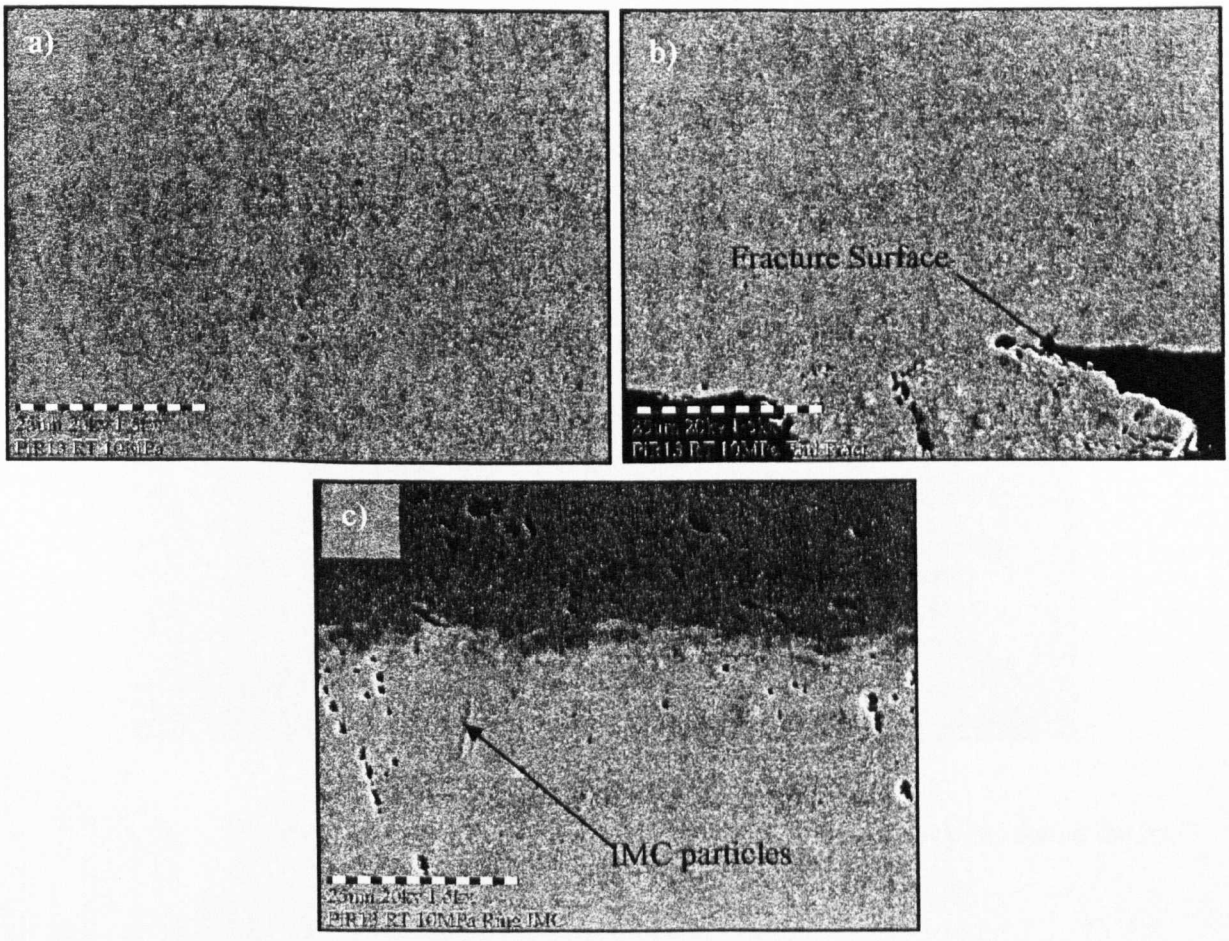


Figure 5.31 a-c Model joint exposed to 29°C for over 400 hours
a) mid section b) fracture surface (pin side) c) ring/solder interface

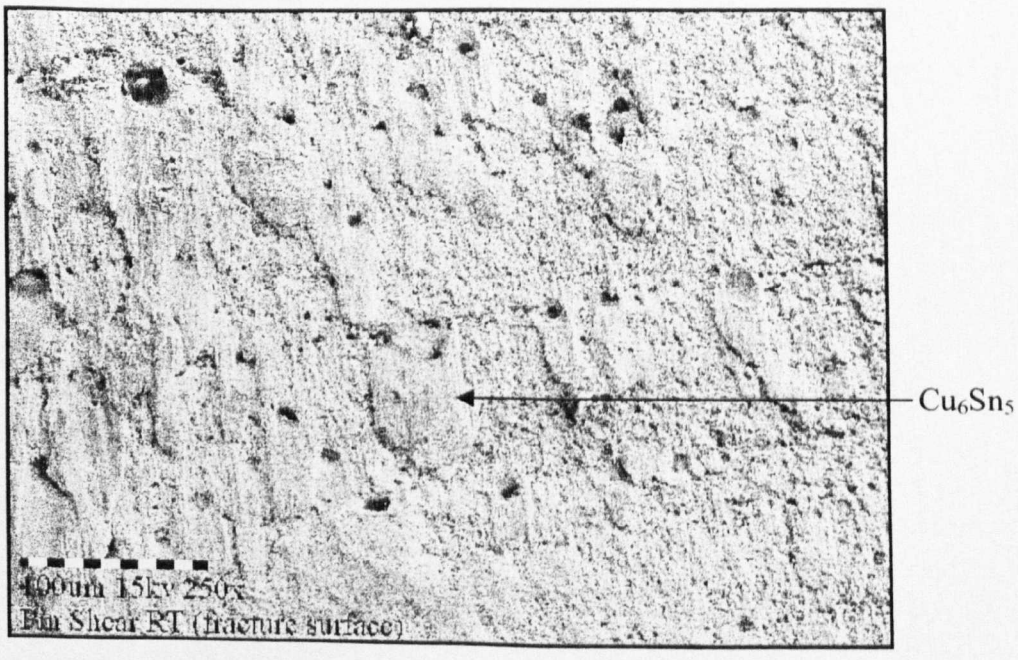


Figure 5.32 Model joint sheared fracture surface (pin side), showing areas of $Cu_6Sn_5$ and matrix material as identified by EDX

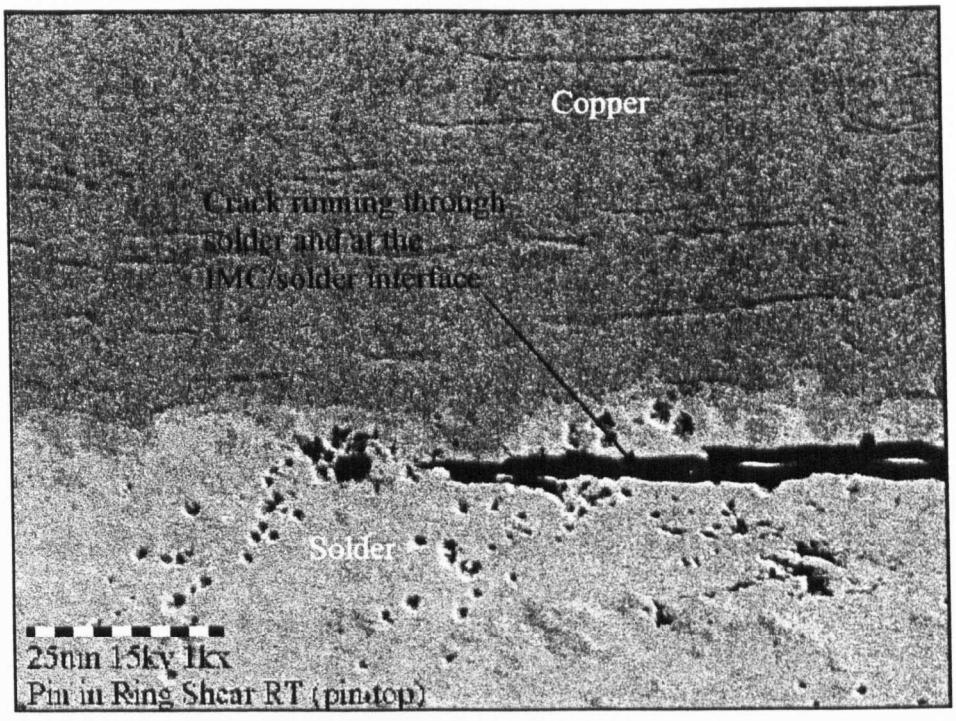


Figure 5.33 Failure from preliminary testing illustrating that the crack can run in the tin matrix and at the IMC/solder interface

# CHAPTER SIX

## 6 DISCUSSION

Chapter five presented the results obtained for each of the bulk and joint testing regimes, these are now discussed with possible mechanisms of creep suggested. Microstructural evaluation is used to substantiate the quantitative findings. Once examined separately, the behaviour of SnAgCu in bulk and joint form is compared, both quantitatively and in terms of microstructural findings, with the aim of establishing a correlation between both sets of data.

A comparison is also made between the behaviour of SnAgCu in bulk form and that of other lead-free and lead-containing alloys at 75°C and at $T_h$ = 0.76. Two members of the Solder Research Group performed the testing, on different alloys, in the same laboratory enabling a direct comparison between the data sets.

### 6.1 Bulk Sn-3.8Ag-0.7Cu Solder Alloy

This section discusses the findings obtained from the creep testing of SnAgCu in bulk form. The shape of the creep curves typical for SnAgCu are examined in addition to the 'constants' obtained during testing.

The creep curves observed during bulk tin-silver-copper testing follow the conventional strain-time pattern exhibiting primary, secondary and tertiary creep. Although not substantiated through microstructural evidence, due to the difficulty in producing specimens for transmission electron microscopy, it is believed that each creep process is due to those processes described in chapter two i.e. the movement of dislocations throughout the structure. However, microstructural examination provides some evidence relating to the relationship of creep resistance with temperature and stress. This is discussed in the following section.

### *6.1.1 Creep Constants*

The value of creep exponent 'n', in accordance with Norton's law, $\dot{\varepsilon}_{min} = A_2\sigma^n$, decreases with increasing temperature. However, values of 'n' greater than ten were observed at all temperatures. The high values of 'n' and subsequently high creep resistance suggest that SnAgCu is strengthened in creep by dispersion hardening. This implies that dislocation motion is hindered by small particles of intermetallic compound dispersed within the tin-based matrix. Thus supporting the suggestion that dislocation motion (climb and slip) plays a significant role in the creep process. Therefore, any microstructural obstruction to dislocation motion is assumed to be an indicator of creep resistance. Dispersion hardened alloys do exhibit a stronger stress dependence of creep rate than pure metals, possessing 'n' values between 10 to 40.

The 'as cast' micrograph of 'water quenched' bulk SnAgCu (figure 5.16a) illustrates the fine dispersion of intermetallic particles of $Ag_3Sn$ and $Cu_6Sn_5$ within the tin-based matrix. It is these intermetallic particles which are thought to provide the creep resistance to this alloy.

The number of vacancies increases due to higher temperatures, this allows diffusion to occur more readily and may explain the decrease in 'n' with increasing temperature. However, it is also evident from microstructural evaluation, figure 5.16a-g, that microstructural coarsening occurs when the solder is exposed to elevated temperatures and strain. The coarsening of intermetallic compounds would provide less resistance to dislocation motion, allowing creep deformation to occur more readily. Also present is the inherent resistance of the microstructure to creep, which is often termed friction or 'internal stress', $\sigma_o$. During a test or in service, the 'effective' stress producing the creep deformation is the applied stress minus the friction/internal stress i.e. $\sigma_{applied} - \sigma_o = \sigma_{effective}$. Therefore, as the internal/friction

stress is reduced by external factors such as temperature, the effective stress is increased lowering the creep resistance i.e. creep exponent (in Norton's Law) is reduced.

The values of creep exponent 'n' in this research are in a similar range to those observed in the published literature [65,66,68 and 36]. However, it should be noted that there is a wide variation of 'constants', which have been determined over a range of conditions and are therefore difficult to directly compare. In the 'higher' stress region, high values of 'n' were obtained which show some similarities to the data obtained during this research. At lower applied stress values, a change in creep exponent 'n' and therefore dominant creep mechanism has been suggested [64, 73]. Although this trend has not been confirmed during this research, a scatter of data is apparent at lower applied stresses suggesting that further work is required in this area.

Clech [71] reviewed the most recent data on the bulk ternary alloy (including slight variations on the alloy, such as Castin, which includes a small addition of antimony). The data obtained during this research was then compared to that from the review by plotting all data onto one graph, figure 6.1a and b. Here, figure 6.1a illustrates how data obtained for this research relates to that from other authors, where data from other sources are represented by the black data points. Figure 6.1b shows each data set as a different colour, where estimated isotherms have been drawn. These figures show that the data obtained for this research (with the exception of 99.4°C data set) relate well to that obtained from different sources, falling into comparable isotherms with similar gradients. However, there does appear to be some discrepancy with the data obtained from Schubert, it does not fall into the isotherms suggested by the addition of the authors' data. This is especially noticeable

for the Schubert room temperature data and may be explained by the fact that Schubert uses different sized specimens (cross section of $9mm^2$) compared to those used at the Open University ($100mm^2$). Also, the microstructure of the Schubert specimens was very different to that observed during this work i.e. elongated rod-like $Ag_3Sn$ IMCs in comparison to a very finely dispersed $Ag_3Sn$ structure. Again emphasising the importance of testing 'standards' and the difficulty in directly comparing data from different sources.

Generally, from a review of the published literature [45,63,70 and 36], it is suggested that the activation energy for creep in SnAgCu relates to the activation energy for 'short circuit diffusion controlled dislocation climb'. However, the values obtained during this work indicate a higher value of activation energy, greater than 100kJ/mol. It was suggested within the literature [68] that creep activation energy in a tin-based solder alloy is dependent on the size and distribution of intermetallic particles within the microstructure. Finely dispersed intermetallics throughout the microstructure tend to produce a higher creep activation energy than a microstructure consisting of rod-like particles. Microstructural examination of the bulk solder specimens confirms the presence of a fine distribution of particles, reinforcing the suggestion that creep activation energy is dependent upon microstructure.

It has been suggested that at temperatures above $T_h = 0.5$, activation energy is assumed not to vary with stress and closely approaches the activation energy for self-diffusion [101]. All testing during this research was performed above $T_h = 0.5$ and the activation energy value obtained at 20MPa (mid stress) of 120kJ/mol is similar to that of the self-diffusion of tin. However, apparent activation energy values determined at other applied stress values varied between 97kJ/mol to 136kJ/mol, showing an increase with decreasing stress, this is also been seen to occur in tin-lead

[102]. However, even though this slight increase in apparent creep activation energy has been observed, the values obtained remain in the range described for the self-diffusion of tin.

## 6.2 Sn-3.8Ag-0.7Cu in Model Joints

### *6.2.1 Description of a Typical Creep Curve for Model Joints*

The creep curve for the model joints follows a similar shape to that observed for the bulk material. However, figure 5.17 illustrates that both instantaneous strain on loading and strain to failure are large in comparison to those observed in the bulk testing. It should be remembered that the strains reported in this instance are in shear and are therefore larger than tensile strains.

Given the moduli of both copper, aluminium (loading apparatus) and the solder, all displacement was initially assumed to occur in the solder. However, instantaneous strains reported in this instance were larger than those expected to occur in the solder alone, (see appendix 4.5). Therefore, the large displacement on loading may be due to displacement occurring in the loading equipment, slipping of the copper in the gripping fixture or deformation occurring when the grips 'bite' into the copper pin.

Work was performed to determine the extent of displacement on loading. Here, solid copper specimens were attached to the rig in the same way as a joint sample and loaded using four different applied loads representative of those used in an actual creep test. This was repeated at all test temperatures utilised in the joint testing regime. Both plastic and elastic deformation was measured and by plotting the calculated stress and strain values, an elastic modulus for copper was established. However, values obtained were approximately one hundred times lower than the stated modulus at room temperature. This is indicative of excessive deformation

occurring elsewhere. Further investigation was performed and given the lower modulus of aluminium; some elastic displacement is thought to be occurring in the aluminium mounting apparatus during loading. Plastic deformation was seen to occur in the copper 'pin' where the gripping mechanism 'bites' into the copper. Also some slippage may occur during the application of the load. Although this test method provided an indication of the deformation occurring within the copper and loading apparatus, given the relative moduli for each of the materials in the assembly it was difficult to determine how each material would behave together. Therefore the test method was not necessarily representative of what actually occurs during each creep test. Given this uncertainty of the determination of plastic deformation and any other deformation occurring within the loading apparatus, instantaneous strain was omitted from the joint results and only creep strain examined.

### *6.2.2 Creep Constants*

Creep exponents 'n' (Norton's law) were determined at 29°C, 75°C and 125°C. At 29 and 75°C and high applied shear stresses the creep exponent 'n' is greater than 10, again suggesting that creep is controlled by dispersion hardening. However, these results indicate that 'n' increases with increasing temperature. The creep exponent has yet to be determined at 125°C as only two data points are currently available. At both 29 and 75°C, a change of dominant creep mechanism at low stress occurs in shear and is indicated by a change in 'n', to a value of three.

Creep exponent in the bulk samples reduces with increasing temperature therefore the reduction in creep exponent 'n' with decreasing temperature in joints was unexpected. On examination of the literature relating to joints, Hua *et al* [73] also demonstrated a decrease in 'n' with increasing temperature. This would suggest an anomaly in the joint data collated for this research. However, at present the author is

unable to express whether the trend observed during this research is unique or a conflict due to the lack of data currently available. An error in the calculated joint values of 'n' may have arisen as values of creep exponent at higher stress levels (>12MPa) were established using an average of all the data rather than 'splitting' the data into apparent trends, especially at 29°C, as these trends have yet to be confirmed. It can only be suggested that additional experimental work be performed to confirm the mechanism changes occurring at 29°C and at other test temperatures. The author believes that three test temperatures are not sufficient on which to base these observations but 'pin in ring' experimental work has been restricted due to time and equipment limitations and the unpredictable nature of creep testing. Recently due to equipment failure and the requirement to repeat some of the pin in ring testing, it has become apparent that joint creep tests aren't necessarily as repeatable as bulk testing. Although manufacture was performed using the same procedure for each batch of samples, it was difficult to confirm whether the differences in creep lives were the result of microstructural differences, as the only way to determine microstructure was through destructive analysis (sectioning).

Values of creep activation energy obtained for the model joints have been determined using data produced at two test temperatures. Again, the author is not entirely satisfied with this. However, testing at a third test temperature is currently underway. The values obtained (to date) are approximately half those observed in the bulk material (approximately 60kJ/mol) which suggests that short circuit diffusion, such as pipe diffusion may be the dominant creep mechanism in model joints. From the creep activation energy calculations performed to date on bulk and joint behaviour, a different creep mechanism is suggested for each configuration. However, this hasn't yet been confirmed due to the lack of data currently available

for the model joints. On examination of the literature (see chapter two), values of activation energy are seen to range between 60-120kJ/mol for both the joint and the bulk data sets, therefore the author is unsure which is correct. A possible explanation for the difference in creep activation energy between the two data sets obtained for this work may involve the differences in size, shape and distribution of intermetallic compounds in each sample type. Bulk solder tends to have $Ag_3Sn$ and $Cu_6Sn_5$ finely dispersed within a tin-based matrix whereas the 'pin in ring' samples tend to have larger $Ag_3Sn$ particles forming a 'necklace' arrangement around the grain boundaries and a large concentration of $Cu_6Sn_5$ at and close to the intermetallic layer. This is examined further in the following section. The effect of the intermetallic layer and its relative thickness on creep has still to be determined (see section on further work).

In addition to bulk SnAgCu data, Clech [71] also examined data obtained from the testing of tin-silver used in model joints. The review confirmed the author's findings regarding the difficulty of comparison of different data by highlighting the substantial range of joint dimensions used. Joint thicknesses ranged from 0.1mm to 0.43mm and joint length from 0.2mm to 16mm. By plotting the ternary joint data onto the same graph as the tin-silver data, it was discovered that that a similar relationship to that first seen between bulk SnAg and SnAgCu is observed. Although, a wide scatter is observed for all data, a general trend was suggested. The ternary alloy exhibits lower strain rates than that of the binary alloy tested under similar conditions. The change in gradient at low stress observed in the ternary alloy is not evident in the binary alloy. However, it appears that little work has been performed in this 'low stress' regime and both the author and Clech believe that more work is required. Clech also states that a correlation between joint and bulk test results was

not evident. However, during a comparison of bulk and joint behaviour in the ternary alloy, section 6.3, there does appear to be some similarities at high stress.

Hua *et al.* [73] suggest a higher creep activation energy for joints than that determined during this work. The value obtained corresponded to that determined for the bulk specimens in this work. It should be noted that only an examination of the creep activation energy in joint specimens was performed by Hua *et al.* Song *et al.* [74] suggest a creep activation energy for soldered joints in the region of 80kJ/mol determined using the conventional Dorn equation, this value being similar to that obtained during this research for joint specimens. These contradictions in creep activation energies in the literature reiterates the authors' uncertainty in the model joint behaviour to date.

## 6.3 Comparison of Joint and Bulk Behaviour

This section compares the behaviour of SnAgCu when used in joint and bulk specimens. By converting stresses and strains obtained for joints from shear into tension both sets of quantitative data can be directly compared.

Both quantitative and qualitative data were compared to determine whether the differences/similarities in behaviour were reflected in the relative microstructures. Also, any correlation between bulk and joint behaviour was investigated.

### *6.3.1 Time to Rupture*

Generally, when applied shear stress values were converted into tensile stresses (at 29°C and 75°C) and plotted versus time to rupture, bulk and joint behaviour are similar. However, more scatter in data is apparent at room temperature. Log-log and semi-log plots were utilised to show any relationship between joint and bulk behaviour, figures 6.2a and b. Model joint behaviour deviated slightly from bulk

behaviour at lower stress values (<12MPa). Data collated at 125°C were also plotted in these figures even though there is a lack of data at present. Preliminary observations indicate substantially lower creep strengths in the joint than in the bulk sample at this temperature (125°C) e.g. at 100 hours the bulk creep strength is approximately three times greater than the joint strength. The relationship $\log \sigma = m.\log t_r + \log C$ ($\sigma = Ct_r^m$) was used to determine gradients and intercepts for each configuration. Table 6.1 shows constants obtained from logarithmic stress versus time to rupture plots of joint and bulk samples.

| | Gradient | Intercept |
|---|---|---|
| 29°C Bulk | 0.0644 | 41.99 |
| 29°C Model Joints | 0.1471 | 47.72 |
| 75°C Bulk | 0.1005 | 29.56 |
| 75°C Model Joints | 0.1453 | 35.14 |
| 125°C Bulk | 0.1073 | 19.94 |
| 125°C Model Joints | 0.0840 | 5.87 |

Table 6.1 Constants obtained from stress vs time to rupture plot (converting into tensile stress).

In general, joints tested at 29 and 75°C have steeper gradients than the bulk material which would imply that in bulk form the material is more stress sensitive and possesses higher creep exponent 'n' (according to Norton's Law) values than when it is used within a joint. This suggests that small changes in stress will produce bigger changes in time to rupture in the bulk material than in joint form. The joint trend appears to cross the bulk data so that at short lifetimes (high applied stress) model joints have slightly higher creep strengths than the bulk material, but at longer, more realistic lifetimes have lower strengths. This trend is reflected in the Norton's law plot where at low applied stress values a change in gradient occurs suggesting a change in dominant creep mechanism and creep strain rates are higher than those seen in the bulk material see section 6.3.4.

### 6.3.2 *Creep Ductility*

Creep ductility data for joint specimens were not entirely satisfactory due to the large displacements occurring on loading. However, by omitting instantaneous strain and converting shear strain into tensile strain (in the case of model joints) a comparison between bulk and joint creep ductility data was made. Even though instantaneous strain (typically less than 1%) is included as part of the total strain (typically 15 to 30%) in the bulk material, overall ductilities of the joint specimens are still consistently higher than in the bulk specimen. In model joints (and omitting instantaneous strain) creep ductility is generally around 100%, whereas ductility in bulk form is generally less than 40%, figure 6.3. There doesn't appear to be any significant trend between ductility and applied stress (after data has been converted into tensile form).

The large differences between bulk and joint strains to failure occur as bulk samples are tested in tension and joints in shear, therefore resulting in greater deformation. An error in strain to failure measurement in joints (previously mentioned in chapter five) should also be noted as this may add to the overall ductility value. Therefore, it would be beneficial to establish a more accurate method of measuring strain at failure. A sample generally fails rapidly after tertiary creep has been reached. If this is unexpected and the time scale (on the chart recorder) has not been altered to compensate for the rate of deformation a sharp increase in the strain-time curve occurs making it difficult to determine the exact strain at failure.

### 6.3.3 *Monkman-Grant Relationship*

For the purpose of comparison, strain rates obtained for the joint specimens have been converted into tensile strain rates. A linear trend is observed for all data, including that obtained at 125°C, indicating a correlation between bulk and joint

behaviour up until approximately sixty hours, figure 6.4. At longer lives more scatter occurs with the joint data falling above that of the bulk. This scatter in joint data is reflected in both the time to rupture and the Norton's Law plots at both 29°C and 75°C, where a change in dominant creep mechanism is suggested. Table 6.2 presents the equations determined for the Monkman-Grant trend line, using the relationship, $\dot{\varepsilon}_{\min} t_r = C$ (which by taking logarithms expands to $Log\dot{\varepsilon}_{\min} = m \log t_r + \log C$). However, it should be noted that the trends do not take into account any change in slope i.e. are an average of all data.

| Temperature | Bulk | Joint |
|---|---|---|
| 29°C | $\dot{\varepsilon}_{\min} t_r^{1.23} = 2.4\times10^{-2}$ | $\dot{\varepsilon}_{\min} t_r^{1.02} = 4.3\times10^{-2}$ |
| 75°C | $\dot{\varepsilon}_{\min} t_r^{1.34} = 3.1\times10^{-2}$ | $\dot{\varepsilon}_{\min} t_r^{0.95} = 2.4\times10^{-2}$ |
| 125°C | $\dot{\varepsilon}_{\min} t_r^{1.12} = 2.1\times10^{-2}$ | $\dot{\varepsilon}_{\min} t_r^{0.92} = 5.1\times10^{-2}$ |

Combined data: $\dot{\varepsilon}_{\min} t_r^{1.13} = 2.7\times10^{-2}$

(grey shading represents only 2 results to date as of 29th August 02, other testing is currently underway)

Table 6.2 Constants obtained from the Monkman-Grant relationship

### *6.3.4 Minimum Creep Rate – Stress Relationships*

Although the 'sinh' relationship best describes the behaviour of SnAgCu, at 29 and 75°C, in joint form due to the inflection of the data at lower stresses (Zener–Holloman plot), the power law (Norton's Law) best describes the bulk behaviour. Therefore, for the purpose of comparing bulk with joint behaviour the power law relationship has been utilised.

At 29°C and at higher stresses, joint behaviour appears to be similar to that of bulk behaviour. However, this similarity ends at around 12MPa where there is a change in slope of the joint trend, figure 6.5a. Here, strain rates in the joint specimens are an order of magnitude faster than specimens experiencing similar applied stresses in the bulk samples. A similar relationship is also observed at 75°C,

figure 6.5b. This potentially sigmoidal behaviour has also been observed in bulk SnPb solders and is reported in the published literature [7]. It has also been reported for 'model lead-free joints' at low stresses [73].

The author believes that a similar trend may possibly be exhibited by the bulk SnAgCu solders but at much lower stress levels. There are indications of a similar change in slope in the bulk specimens (i.e. a large scatter in data at low stresses) but more experimental work at lower stress levels is required to substantiate these claims. Unfortunately, the work required is very time consuming (lifetimes greater than 10,000 hours) and given the available resources would have been impractical during this research programme.

Figure 6.5c illustrates both bulk and joint behaviour at 125°C to date. Preliminary results indicate that joint data obtained at 125°C do not correlate with the bulk 125°C data and bear no similarity to the trends observed at 29 and 75°C. Further work is currently underway at 125° to substantiate these findings.

### *6.3.5 Microstructural Evaluation*

When comparing joint and bulk specimens, changes in microstructure occurring during the soldering process and also during testing should be taken into account. Not only do changes occur at the solder/copper interfaces but also different microstructures may be apparent throughout the 'bulk' of the material. The following section examines and compares the microstructures observed in bulk and joint samples.

It was thought that it would be possible for copper, from the pin or ring, to diffuse into the solder during manufacture and testing at high temperatures. Therefore to establish the quantity of copper throughout the joint, in comparison to the bulk material, energy dispersion spectroscopy (using a Noran–Vantage X-ray

microanalyser) was performed on the bulk (as cast) material, an 'as cast' model joint and a joint tested at 75°C for 1,000 hours. It was determined that the only additional copper in the joint was that making up the intermetallic layer i.e. the copper did not diffuse any further than approximately 3μm into the joint. The quantity of copper found in the mid-section of the joint is comparable to that in the bulk material. The size of the intermetallics are small (generally submicron) and finely distributed in the microstructure, therefore it was difficult to obtain precise readings of the composition of individual intermetallic compounds either by line or spot scanning. Therefore, an average reading was established at each scan point giving proportions of tin, silver and copper respectively, figures 6.6 a and b.

After exposure to 75°C for approximately 1,000 hours the overall quantity of copper is not seen to increase, however, there are areas of concentrated copper and of silver. This increase was seen to coincide with a drop in tin. When examined with the associated micrograph it is determined that these were areas of large coarsened IMC particles, figures 6.6 a and b.

Generally for both bulk and joint samples, the 'as cast' structures and those tested at high stress showed a resemblance to each other. The main difference being that $Ag_3Sn$ in the joint specimen appear to be distributed around the β-Sn grains in a 'necklace' arrangement, whereas in the bulk it is more evenly distributed as a eutectic structure. Microstructural evaluation was also performed on bulk and joint samples tested at 75°C at low stress levels (<12MPa) to determine microstructural differences which may contribute to the higher strain rates observed at low stress in the joint specimens, figure 6.7. At these lower stress levels (with lifetimes of approximately 1,000 hours) the difference between microstructures is quite considerable. Although there is a difference of 300 hours between the two samples

(bulk and joint) tested at 75°C, it is thought that such a significant change in microstructure would not occur in this time frame. The intermetallic compounds within the joint structure have coarsened dramatically (from submicron to between 1 to 2μm) in comparison to that of the bulk, thus offering less resistance to dislocation motion resulting in a higher creep rate than in the bulk specimen. This suggests that in comparison to the bulk material, joint microstructures are less stable thus contributing to deformation. As previously mentioned, the change in slope (and microstructure) in the joint specimens is an area requiring further examination. It would also be beneficial to perform interrupted tests to determine the change in microstructure throughout the duration of a creep test and the location/mechanisms of failure. This would involve destructive testing, as the samples would require sectioning at each stage of the examination. Experimental work involving model joints is very important in the determination of how bulk properties relate to actual joints, however, to date work on model joints manufactured with lead-free solders is limited. Therefore, a more extensive research programme is required and this is discussed in the section on further work.

### *6.3.6 Conclusions*

From the analysis performed, it was concluded that at high initial applied stress values bulk and joint behaviour is comparable, however, this similarity diminishes at lower stress levels (less than 12MPa) for alloys tested at 75°C and 29°C. At present, there is insufficient data at 125°C to comment. In the model joint, the dominant creep mechanism appears to change in this area causing a shift away from the bulk behaviour. Nevertheless, a similar type of behaviour (i.e. a change in dominant creep mechanism) is suggested in the bulk material but at much lower stress levels than in the joint. Creep activation energy values, obtained during this research, suggest that

self-diffusion is the dominant creep mechanism in the bulk material, whereas short-circuit diffusion is indicated in the joint material. The similarity of creep resistance but difference in activation energy between bulk and joint samples is not completely understood at present. Therefore, additional work is required at various temperatures for model joint specimens to establish a more reliable value of activation energy.

## 6.4 Comparison of SnAgCu with Other Solder Alloys at 75°C

This section compares the behaviour of the bulk ternary alloy with other alternative lead-free alloys (Sn0.5Cu, Sn3.5Ag) and the conventional lead-containing alloy (Sn37Pb) at 75°C. All the samples were tested under similar conditions in the same laboratory, which enabled a direct comparison to be made between data. Testing of most alloys has been performed by the Solder Research Group at temperatures ranging from −10°C to 125°C [102]. However, for this direct comparison a test temperature of 75°C was selected.

For the purpose of this project, observations were focussed upon the behaviour of the ternary lead-free alloy in relation to the other alloys. Any proposed creep mechanisms, activation energies and microstructures for the other alloys (SnPb, SnCu and SnAg) may be found elsewhere [7][8].

### *6.4.1 Time to Rupture*

Figures 6.8 a and b show both log-log and semi-log scale plots of stress versus time to rupture for all alloys at 75°C. Figure 6.8a illustrates that all alloys seem to follow a linear trend (according to the '$\log \sigma = m.\log t_r + \log C$' relationship) with the exception of tin-lead which appears to deviate from the trend at high and low applied stress levels (producing a shallower gradient at high and low stress levels). This behaviour of tin-lead is better illustrated and is more indicative of a mechanism

change when minimum strain rate is plotted against stress (according to Norton's Law, figure 6.9).

| Alloy | Gradient m | Intercept C |
|---|---|---|
| SnAgCu | 0.0972 | 28.41 |
| SnAg | 0.0835 | 19.49 |
| SnCu | 0.1834 | 14.05 |
| SnPb (All data) | 0.2921 | 13.80 |

Table 6.3 Stress versus time to rupture relationships at 75°C

Table 6.3 indicates that the gradients for the silver-containing alloys are much lower than SnCu and SnPb, suggesting that they are more stress sensitive than SnCu and SnPb. The intercept value provides an indication of creep strength at 1 hour and table 6.4 illustrates the creep strength of each alloy at 100 and 1,000 hours-life.

| Alloy | Creep Strength (MPa) at 100 h - life | Creep Strength (MPa) at 1,000 h - life |
|---|---|---|
| SnAgCu | 18.2 | 14.5 |
| SnAg | 13.3 | 10.9 |
| SnCu | 6.0 | 4.0 |
| SnPb (All data) | 3.6 | 1.8 |

Table 6.4 Creep strength at 100 and 1,000 hours life at 75°C

Of the four alloys examined at 75°C, the silver-containing solders have emerged as the most creep resistant, with the ternary alloy performing better than the binary alloy. This is substantiated by figure 6.8 where the ternary alloy 'sits' above the binary alloy and at 12MPa is 100 times more creep resistant than tin-silver. The increased creep resistance of the silver-containing alloys may be attributed to the fine dispersion of intermetallic compound within the β-tin matrix. This is in comparison to the relatively coarse microstructure observed in Sn-Pb or the dilute Sn-Cu alloy.

Figures 6.10 a to d illustrate the 'as cast' microstructures of the three lead-free alloys, SnAgCu, SnCu and SnAg, in the water quenched condition. Figures 6.10 a and b show the ternary alloy after different etching procedures, HCl vapour to enhance the grains and ammonium persulphate to highlight the intermetallic particles. Figures 6.10 c and d show SnCu and SnAg etch using HCl vapour where both grains and IMC particles are visible. Although Sn-0.5Cu possesses a fine dispersion of intermetallic compound, the volume of dispersoids is much less than the silver-containing alloys, therefore offering less creep resistance, figure 6.10c. The ternary alloy is thought to be superior to the binary alloy due to the increased proportion of silver (3.8% in the ternary to 3.5% in the binary). The 0.7% Cu, which forms $Cu_6Sn_5$ in the ternary alloy is also thought to aid creep resistance. By visual inspection, SnAgCu possesses a higher percentage of dispersoids within the matrix in comparison to the binary alloy, further inhibiting the movement of dislocations through the material. There is also a more uniform distribution of intermetallics in the ternary alloy than in the binary solder, resulting in smaller precipitate-free β-Sn globules. This supports the suggestion that dispersion strengthening in SnAgCu will be more effective than that of Sn-Ag, resulting in superior creep strength. This increase in resistance is also reflected in the higher creep exponent values obtained from the Norton's Law plot see figure 6.9 and table 6.5.

### *6.4.2 Strain to Failure*

A plot of failure ductility against stress shows a wide scatter of data with no obvious trend, figure 6.11. Failure ductility ranges between 0.1 to 0.6 (10 to 60%), the higher strains to failure were achieved by SnPb and SnCu. The silver-containing alloys both have lower failure strains falling below 40%, with the majority falling below 30% i.e. they are less ductile. In summary the greater creep resistance

exhibited by the silver-containing alloys has been obtained at the expense of creep ductility. However, it should be noted that strains to failure generally exceed 10% and wouldn't be an issue to the engineer.

### *6.4.3 Minimum Creep Rate – Stress Relationships*

Creep exponents and constants according to the power law relationship ($\dot{\varepsilon}_{min} = A\sigma^n$) were obtained by plotting minimum strain rate versus stress on a logarithmic scale, figure 6.9 and table 6.5. The constants for SnPb have been established from a single line describing all the data, in reality the data is split into two regions (high and low stress) and there is a transition in creep exponent from 3 (below 10MPa) to 7. A change in slope was not particularly evident for the other alloys in this particular testing regime.

| Alloy | Gradient (n) | Constant (A) |
|---|---|---|
| SnAgCu | 14 | $5 \times 10^{-23}$ |
| SnAg | 12 | $1 \times 10^{-18}$ |
| SnCu | 5 | $1 \times 10^{-8}$ |
| (All data) SnPb | 5 | $3 \times 10^{-7}$ |

Table 6.5 Constants obtained from Norton's Law for solders tested at 75°C

The change in exponent suggests a difference in dominant creep mechanism. Both SnAgCu and SnAg have high values of creep exponent (>10) suggesting dispersion hardening, although the ternary alloy has a slightly higher value (as discussed in section 6.4.1).

### *6.4.4 Monkman-Grant Relationship*

The data from all alloys agree with the Monkman-Grant relationship ($\dot{\varepsilon}_{min} t_r = C$). However, some scatter of data is evident around the 1,000-hour life mark, in particularly for the tin-lead alloy, figure 6.12. The scatter and possible change in

slope for this alloy is also apparent in the Norton's law and stress versus time to rupture plots. Again, this suggests a change of dominant creep mechanism at lower applied stresses. Best-fit relationships were established (using the equation $Log\dot{\varepsilon}_{min} = m.\log t_r + LogC$) for all data (treated as one data set) and for each individual alloy, see table 6.6. The change in slope of the SnPb data was not taken into account for this trend line and an average was taken.

| Alloy | Equation |
|---|---|
| All | $\dot{\varepsilon}_{min} t_r^{1.09} = 1.6\times10^{-2}$ |
| SnAgCu | $\dot{\varepsilon}_{min} t_r^{1.18} = 1.7\times10^{-2}$ |
| SnAg | $\dot{\varepsilon}_{min} t_r^{1.15} = 1.6\times10^{-2}$ |
| SnCu | $\dot{\varepsilon}_{min} t_r^{0.97} = 8.9\times10^{-2}$ |
| (All data) SnPb | $\dot{\varepsilon}_{min} t_r^{1.06} = 2.9\times10^{-2}$ |

Table 6.6 Constants for Monkman-Grant Relationship

### *6.4.5 Failure Definitions*

Table 6.7 illustrates the time to achieve 2%, 5%, 10% strain, time to rupture and percentage of life elapsed at each creep phase for all alloys at 75°C. The strains observed during the creep of the silver-containing alloys are very small and generally by the time 5% strain is achieved more than 90% of the life has elapsed. In most cases, tertiary creep has been reached and failure occurs rapidly i.e. fast strain rates. There is a large scatter in the tin-copper data. The tin-lead alloy possesses a greater ductility than the lead-free solder alloys. In some instances when Sn-Pb has achieved 10% strain only 70% of lifetime has elapsed. The values of 'lifetime elapsed' at 10% strain are higher for SnCu than for SnPb although they both possess similar strains to failure. This can be explained by the fact that in general SnCu and SnPb exhibit different creep curve shapes. Generally, in SnCu, the majority of strain occurs during a relatively short period of tertiary creep in comparison to that of tin-lead, see figure

6.13. There doesn't appear to be any correlation between applied stress and percentage of life elapsed at each failure criterion.

| Sample | Stress (MPa) | $t_{2\%\varepsilon}$ (h) | $t_{5\%\varepsilon}$ (h) | $t_{10\%\varepsilon}$ (h) | $t_r$ (h) | %life 2%strain | %life 5%strain | %life 10%strain |
|---|---|---|---|---|---|---|---|---|
| SnPb | 2.63 | 383.33 | 633.00 | 833.30 | 1055.50 | 36% | 60% | 79% |
| SnPb | 2.63 | 391.00 | 722.70 | 900.00 | 950.00 | 41% | 76% | 95% |
| SnPb | 3.04 | 208.33 | 270.50 | 278.70 | 285.60 | 73% | 95% | 98% |
| SnPb | 4.07 | 20.00 | 39.30 | 70.00 | 89.30 | 22% | 44% | 78% |
| SnPb | 5.07 | 18.90 | 32.10 | 45.90 | 54.80 | 34% | 59% | 84% |
| SnPb | 8.12 | 0.65 | 3.60 | 6.60 | 9.50 | 7% | 38% | 69% |
| SnPb | 15.10 | 0.01 | 0.10 | 0.24 | 0.36 | 3% | 28% | 68% |
| SnCu | 3.00 | 292.00 | 3208.30 | 7270.80 | 7791.60 | 4% | 41% | 93% |
| SnCu | 4.01 | 110.80 | 186.50 | 218.75 | 257.00 | 43% | 73% | 85% |
| SnCu | 6.00 | 80.00 | 90.90 | 93.00 | 93.00 | 86% | 98% | 100% |
| SnCu | 8.00 | 26.10 | 31.60 | 32.50 | 35.23 | 74% | 90% | 92% |
| SnCu | 10.00 | 4.00 | 8.50 | 8.91 | 9.32 | 43% | 91% | 96% |
| SnCu | 12.75 | 0.77 | 1.28 | 1.72 | 1.77 | 44% | 72% | 97% |
| SnCu | 15.10 | 0.36 | 0.55 | 0.60 | 0.62 | 58% | 89% | 98% |
| SnAg | 11.00 | 172.70 | 800.00 | 854.50 | 868.20 | 20% | 92% | 98% |
| SnAg | 12.00 | 153.00 | 194.60 | 206.80 | 209.50 | 73% | 93% | 99% |
| SnAg | 13.00 | 91.25 | 110.63 | 123.10 | 123.10 | 74% | 90% | 100% |
| SnAg | 14.00 | 9.44 | 13.44 | 15.92 | 16.16 | 58% | 83% | 99% |
| SnAg | 15.00 | 10.36 | 12.93 | 13.49 | 13.57 | 76% | 95% | 99% |
| SnAg | 15.50 | 4.10 | 9.35 | 10.24 | 10.65 | 38% | 88% | 96% |
| SnAg | 16.00 | 5.29 | 16.63 | 17.98 | 18.58 | 28% | 90% | 97% |
| SnAg | 20.00 | 0.17 | 0.82 | 1.03 | 1.07 | 16% | 77% | 97% |
| SnAg | 23.00 | 0.15 | 0.29 | 0.30 | 0.30 | 51% | 98% | 100% |
| SnAgCu | 12.00 | 714.30 | 1988.00 | 2121.00 | 2121.00 | 34% | 94% | 100% |
| SnAgCu | 16.00 | 400.00 | 435.00 | 443.00 | 443.36 | 90% | 98% | 100% |
| SnAgCu | 19.00 | 309.60 | 355.53 | 355.53 | 355.53 | 87% | 100% | 100% |
| SnAgCu | 19.50 | 38.45 | 42.90 | 43.30 | 43.31 | 89% | 99% | 100% |
| SnAgCu | 21.00 | 15.73 | 19.15 | 20.25 | 20.25 | 78% | 95% | 100% |
| SnAgCu | 23.50 | 4.00 | 5.93 | 6.33 | 6.40 | 63% | 93% | 99% |
| SnAgCu | 24.00 | 20.77 | 32.70 | 34.30 | 34.30 | 61% | 95% | 100% |
| SnAgCu | 27.00 | 0.67 | 1.12 | 1.24 | 1.25 | 54% | 90% | 99% |
| SnAgCu | 33.00 | - | 0.24 | 0.42 | 0.43 | | 56% | 99% |

Table 6.7 Alternative failure definitions for alloys tested at 75°C (including instantaneous strain)

### *6.4.6 Extent of Steady State Creep*

The extent of steady state creep was determined by defining secondary creep as the time spent below $1.1\dot{\varepsilon}_{min}$. For all the alloys secondary creep accounts for approximately 30% of life. There is no apparent correlation between applied stress and percentage of steady state creep within the range of stresses examined. A graph of extent of steady state creep and stress confirms the large scatter of data and lack of correlation, figure 6.14.

## 6.5 Direct Comparison of SnAgCu and Other Solders at $T_h = 0.76$

Section 6.4 demonstrated that silver-containing alloys possess a superior creep resistance over the other alloys when compared at the same temperature (75°C). This may be attributed to the higher melting points of these alloys. This section examines whether the silver-containing alloys retain their superiority when alloys are tested at the same homologous temperature, $T_h$ =0.76 (SnAgCu = 99.4°C, SnAg = 102°C, SnCu = 107°C and SnPb = 75°C).

### *6.5.1 Time to Rupture*

The trends observed at $T_h = 0.76$ were similar to those achieved at 75°C, figure 6.15 a and b. SnPb and SnCu behave similarly to each other and the silver-containing alloys retain their superior creep resistance even at these elevated temperatures. The ternary alloy still possesses a greater creep resistance than Sn3.5Ag.

Table 6.8 presents the constants obtained from best-fit lines according to the $\log\sigma = m.\log t_r + \log C$ relationship, for each data set. An average has been taken of the tin-lead data so the change in slope is not described. For the silver-containing alloys, creep strength at 1,000 hours is approximately 83% that at 100 hours. For SnCu and SnPb, creep strength at 1,000 hours is approximately 60% of that at 100 hours, table 6.9. Table 6.10 illustrates the creep life ratios obtained, through data extrapolation, for each of the four alloys tested. It confirms the superiority of the ternary alloy to the others at a homologous temperature of 0.76.

| Alloy | Gradient | Intercept |
|---|---|---|
| SnAgCu | -0.0795 | 24.61 |
| SnAg | -0.0777 | 15.17 |
| SnCu | -0.1186 | 8.06 |
| SnPb | -0.2351 | 11.95 |

Table 6.8 Constants obtained for stress versus time to rupture relationship

| Alloy | Strength (MPa) 100 hours-life | Strength (MPa) 1,000 hours-life |
|---|---|---|
| SnAgCu | 17.1 | 14.2 |
| SnAg | 10.6 | 8.9 |
| SnCu | 4.7 | 3.6 |
| SnPb | 4.0 | 2.4 |

Table 6.9 Creep strength at $T_h = 0.76$

| SnCu | SnPb | SnAg | SnAgCu |
|---|---|---|---|
| 1 | 15 * | 2000 | 100,000 ** |

* note that the ratios were established by using visual inspection and accounts for the bi-linearity of the SnPb data.

** data for SnAgCu was extrapolated to obtain this ratio.

Table 6.10 Creep life ratios at 10MPa

### *6.5.2 Strain to Failure*

In general, strain to failure at the same homologous temperature increases with increasing stress i.e. decreases with increasing time to rupture although this cannot be quantified due to a wide scatter of data, figure 6.16. This is a similar trend to that seen at 75°C, however, there is a large scatter of data in figure 6.11 making the trend unclear. The silver-containing alloys continue to be less ductile than SnCu and SnPb. Overall ductility ranges between 10-60%. The silver-containing alloys generally possess a ductility of less than 30%, a value not changed with the increase in test temperature. However, these strains to failure are not low enough to cause concern in engineering applications.

### *6.5.3 Minimum Creep Rate – Stress Relationships*

With the exception of tin-lead, which exhibits a change in slope at low stress, Norton's power law relationship best describes the stress versus minimum strain rate plot at $T_h$=0.76. There is a questionable scatter of the ternary alloy data at 99.4°C (shape of data results in three possible changes in slope) however, this has already

been discussed in the bulk analysis. The silver-containing alloys possess steeper gradients than SnCu and SnPb, figure 6.17 i.e. the value of creep exponent 'n' is higher, indicating a greater creep resistance (as illustrated by the time to rupture plot, figure 6.15). The high value of 'n' suggests that a dispersion hardening mechanism is continuing to occur in the silver-containing alloys at the higher temperatures. Both SnCu and SnPb show a change in gradient at lower stress levels (longer creep lives) indicating a change in creep mechanism. Table 6.11 shows the trend calculated for all the data for each alloy and therefore doesn't take into account any bi-linearity.

| Alloy | Constant $A_1$ | Creep Exponent n |
|---|---|---|
| SnAgCu | $1 \times 10^{-20}$ | 13 |
| SnAg | $1 \times 10^{-19}$ | 14 |
| SnCu | $5 \times 10^{-9}$ | 8 |
| SnPb | $3 \times 10^{-7}$ | 5 |

Table 6.11 Constants obtained from Norton's Law

### *6.5.4 Monkman-Grant Relationship*

By plotting minimum strain rate versus time to rupture on a logarithmic scale, a linear trend is produced (figure 6.18); however, there is a large amount of scatter especially at longer lifetimes (lower stress values). Quantitative relationships according to '$Log\dot{\varepsilon}_{min} = m.\log t_r + LogC$' have been calculated for all the data (collectively and singularly), table 6.12.

| Alloy | Equation |
|---|---|
| All | $\dot{\varepsilon}_{min} t_r^{1.16} = 3.2\times10^{-2}$ |
| SnAgCu | $\dot{\varepsilon}_{min} t_r^{1.17} = 3.5\times10^{-2}$ |
| SnAg | $\dot{\varepsilon}_{min} t_r^{1.42} = 2.9\times10^{-2}$ |
| SnCu | $\dot{\varepsilon}_{min} t_r^{0.96} = 4.6\times10^{-2}$ |
| SnPb | $\dot{\varepsilon}_{min} t_r^{1.06} = 2.9\times10^{-2}$ |

Table 6.12 Constants obtained from Monkman-Grant relationship at $T_h$=0.76

### *6.5.5 Conclusions*

By comparing the behaviour of alloys at both 75°C and $T_h$ = 0.76 it becomes apparent that the silver-containing alloys are superior, and this superiority is retained when tested at similar homologous temperatures. This work suggests that this due to the quantity and distribution of intermetallic particles resulting in dispersion strengthening. However, the ductility of silver-containing alloys is lower than that of SnCu and SnPb, although not low enough to be a concern during engineering applications.

Even though the ternary alloy is superior to the other most popular lead-free alloys and tin-lead in bulk form, work is now necessary to determine whether this superiority is retained when the alloy is used in joint form (model and actual).

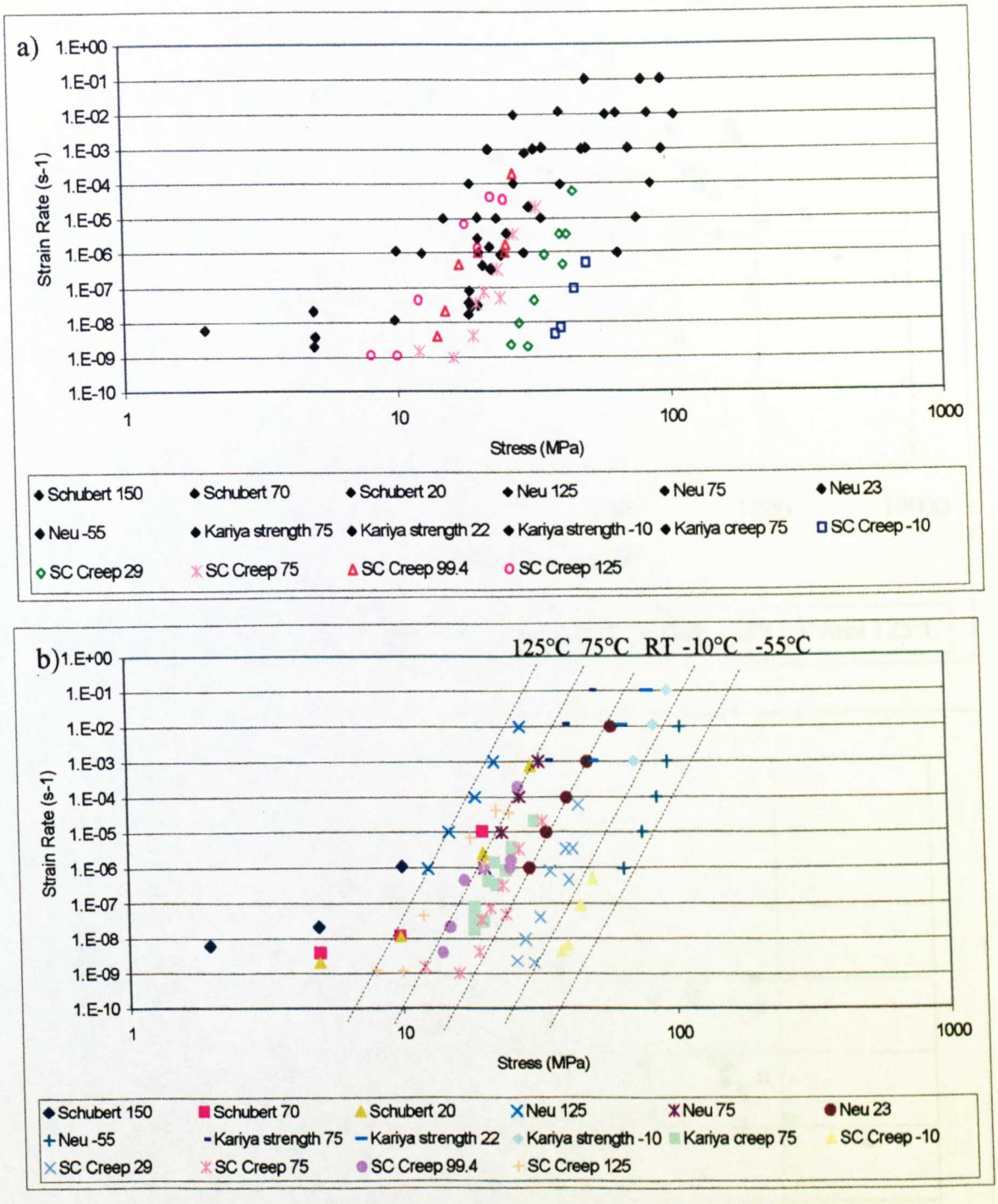


Figure 6.1 Comparison of research data with that from a review by Clech, a) Open University data highlighted in colour b) all data identified individually (References: Schubert [103], Neu [104], Kariya, [36], SC: Authors data)

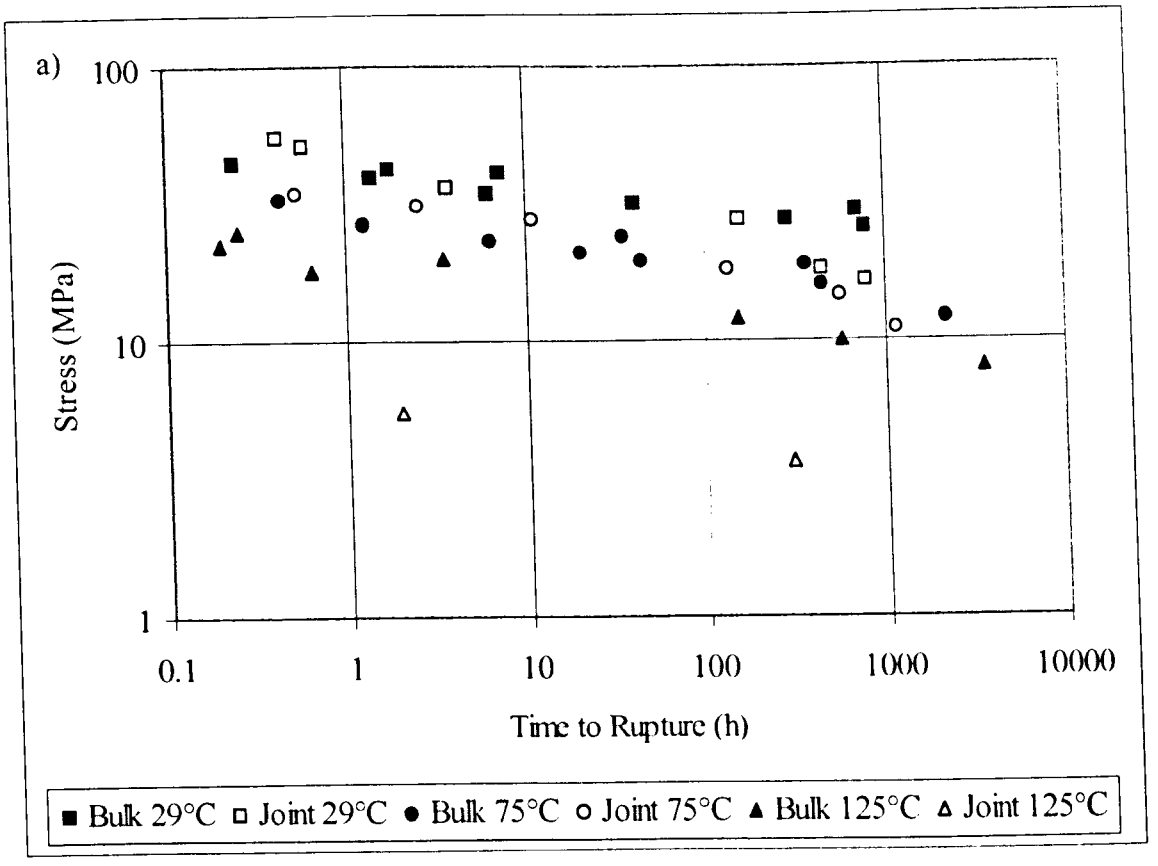


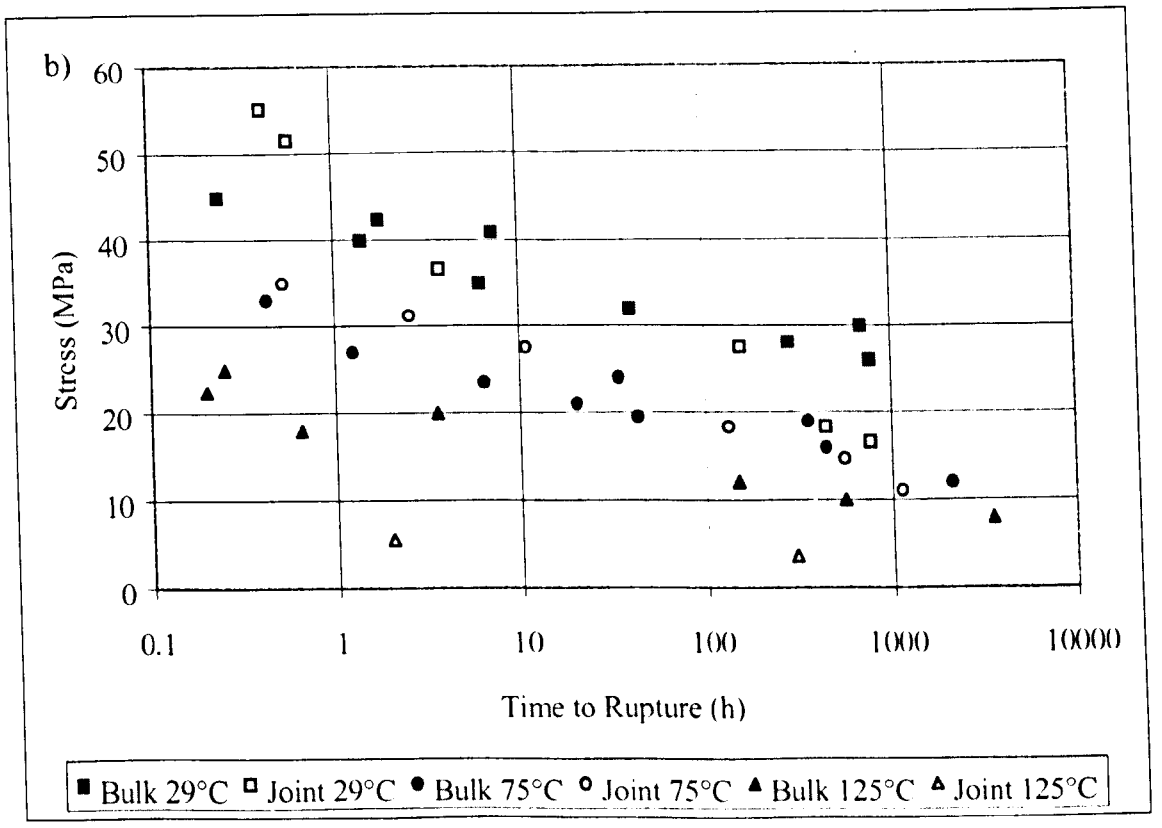


Figure 6.2a and b Variation of time to rupture with stress for bulk and model joint samples a) log-log scale and b) semi-log scale (after conversion to tensile stress)

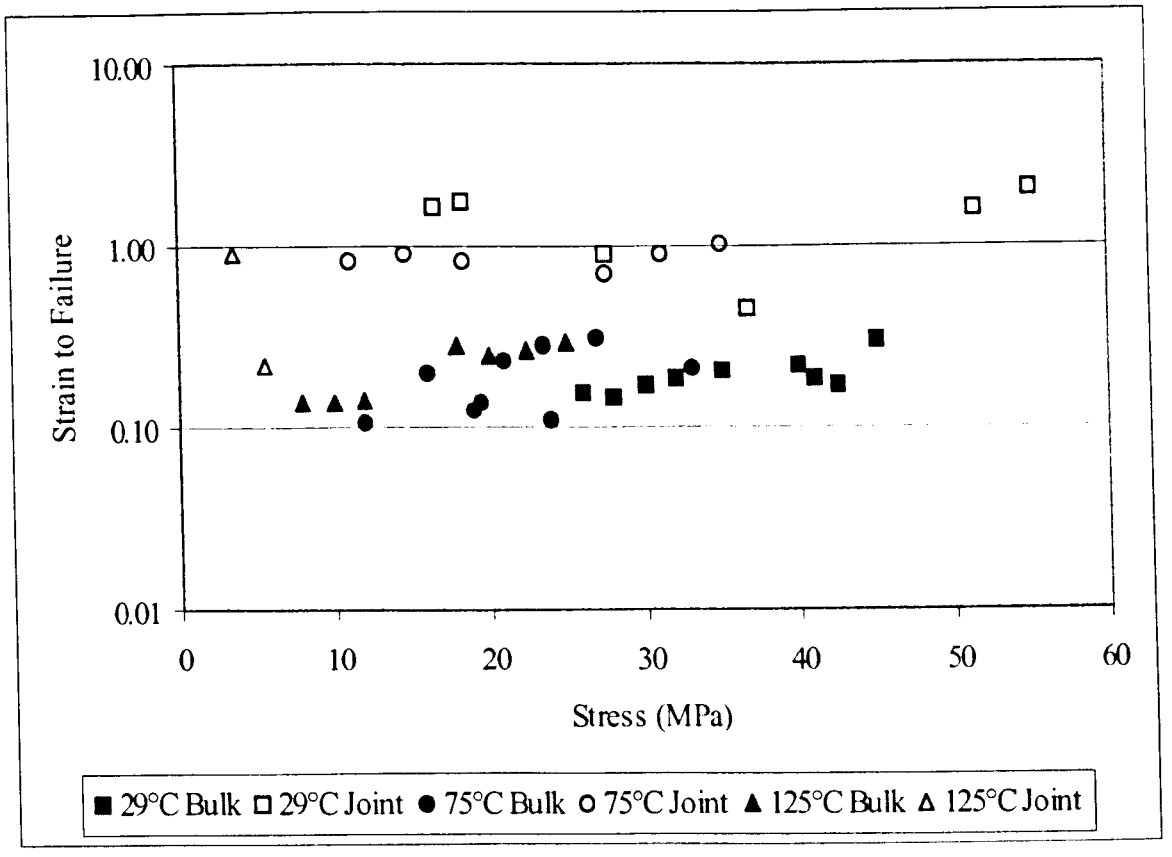


Figure 6.3 Comparison of failure ductility between bulk and joint specimens (conversion of shear data into tensile strain to failure and tensile stress)

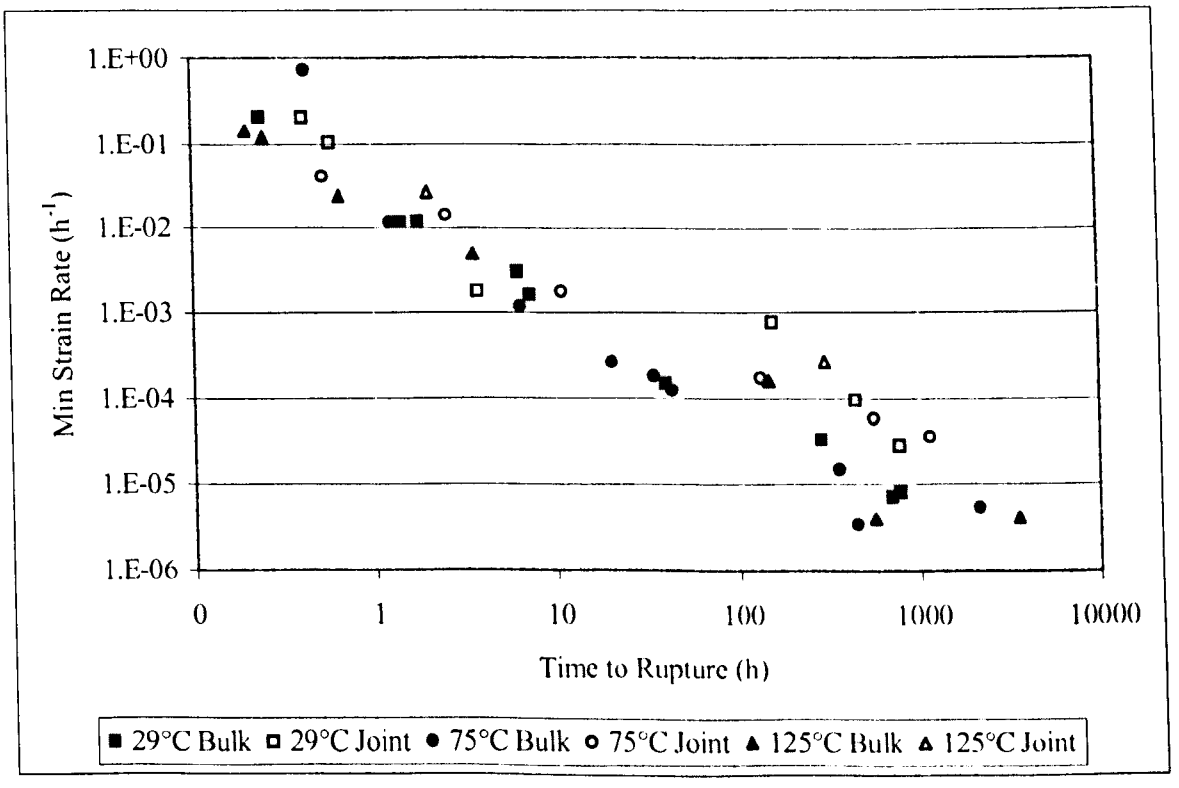


Figure 6.4 Monkman-Grant relationship for bulk and model joint samples (after conversion of shear strain rate to tensile strain rate)

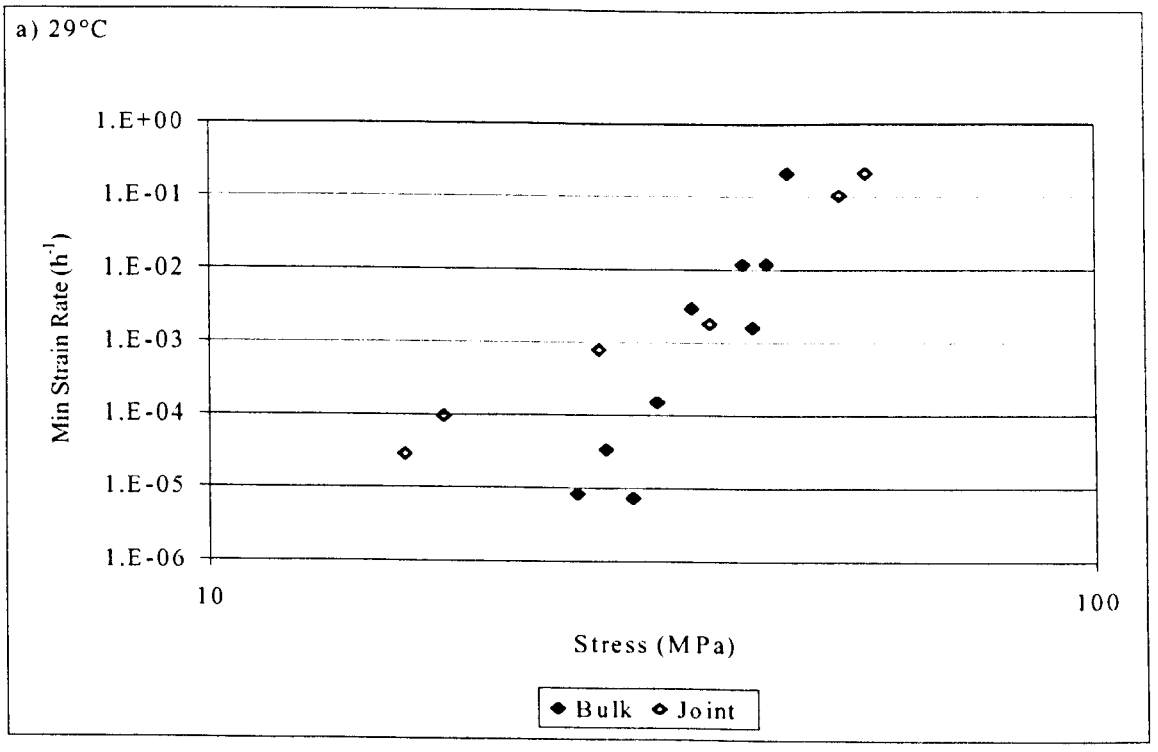
a) 29°C
1.E+00
1.E-01
1.E-02
1.E-03
1.E-04
1.E-05
1.E-06
Min Strain Rate (h-1)
10
100
Stress (MPa)
Bulk
Joint

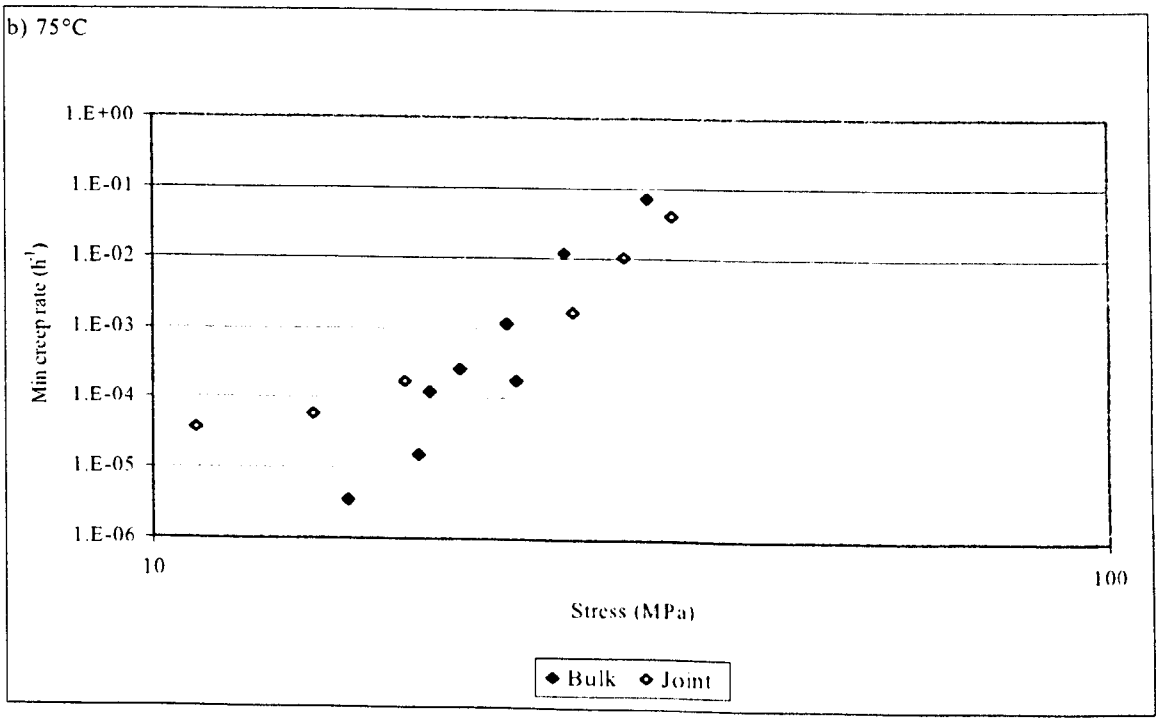
b) 75°C
1.E+00
1.E-01
1.E-02
1.E-03
1.E-04
1.E-05
1.E-06
Min creep rate (h-1)
10
100
Stress (MPa)
Bulk
Joint

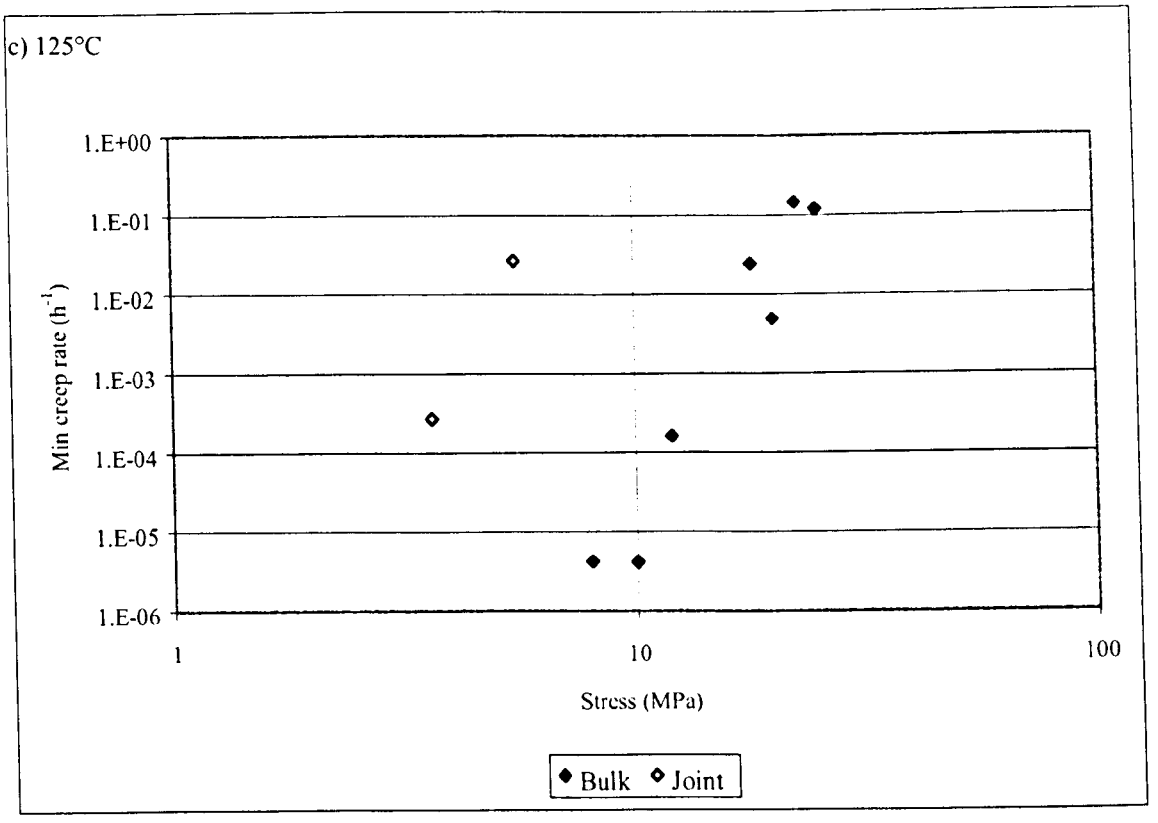


Figure 6.5 Norton's law relationship for bulk and model joint samples at a) 29°C, b) 75°C and c) 125°C
(after conversion of shear strain rate and stress to tensile strain rate and stress)

*(Count scales are different in each plot)*

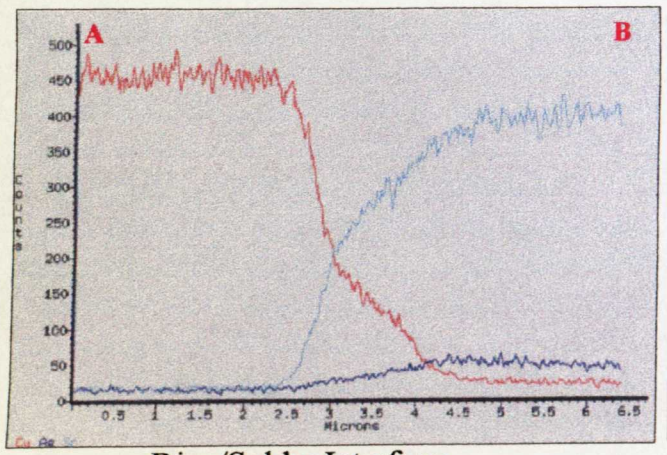


Ring/Solder Interface

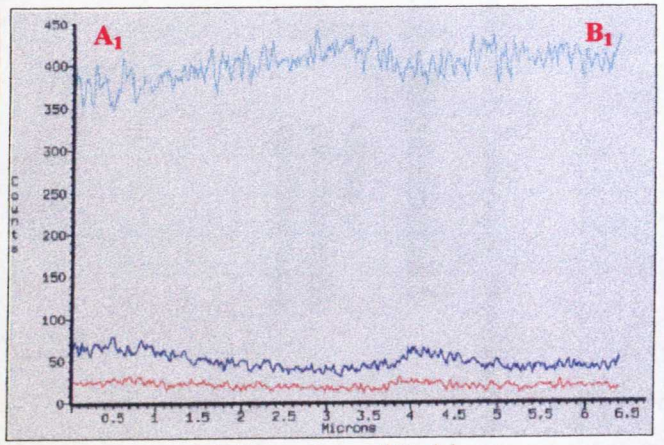


Mid-section of Solder

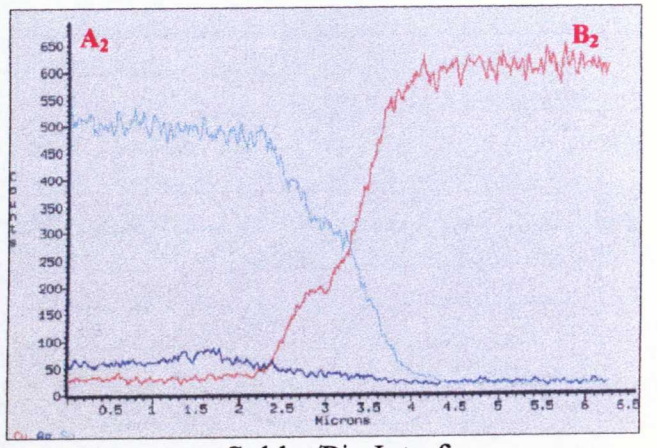


Solder/Pin Interface

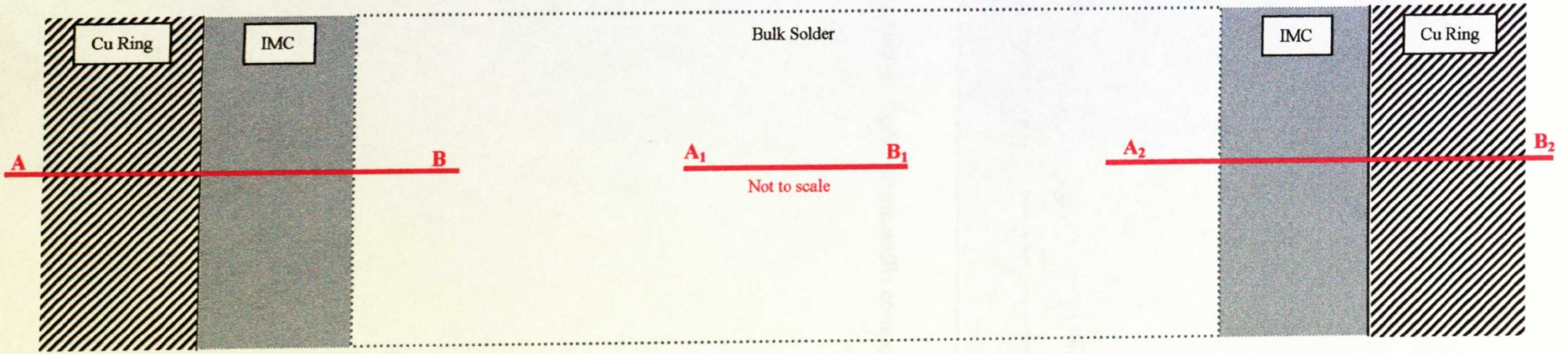


Figure 6.6a Analysis by EDX

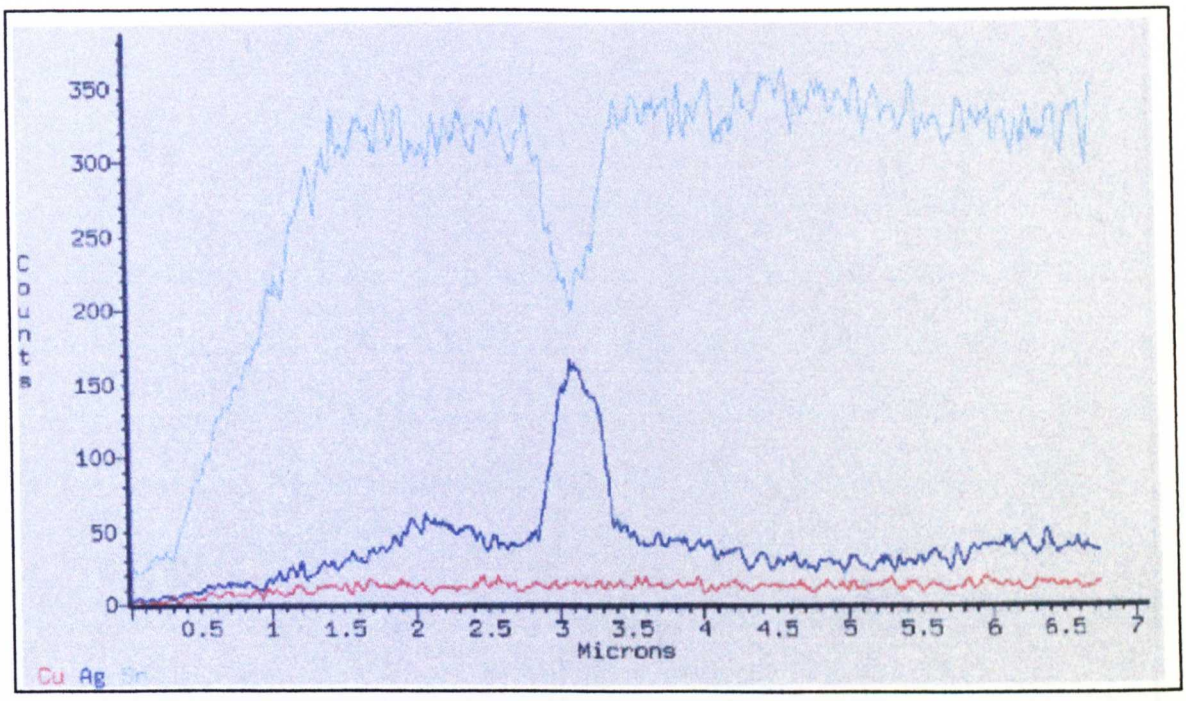


Figure 6.6b Increase in silver content suggesting area of $Ag_3Sn$ intermetallic compound

**Key for figures 6.6a and b**

Cu = red trace
Ag = dark blue trace
Sn = light blue trace

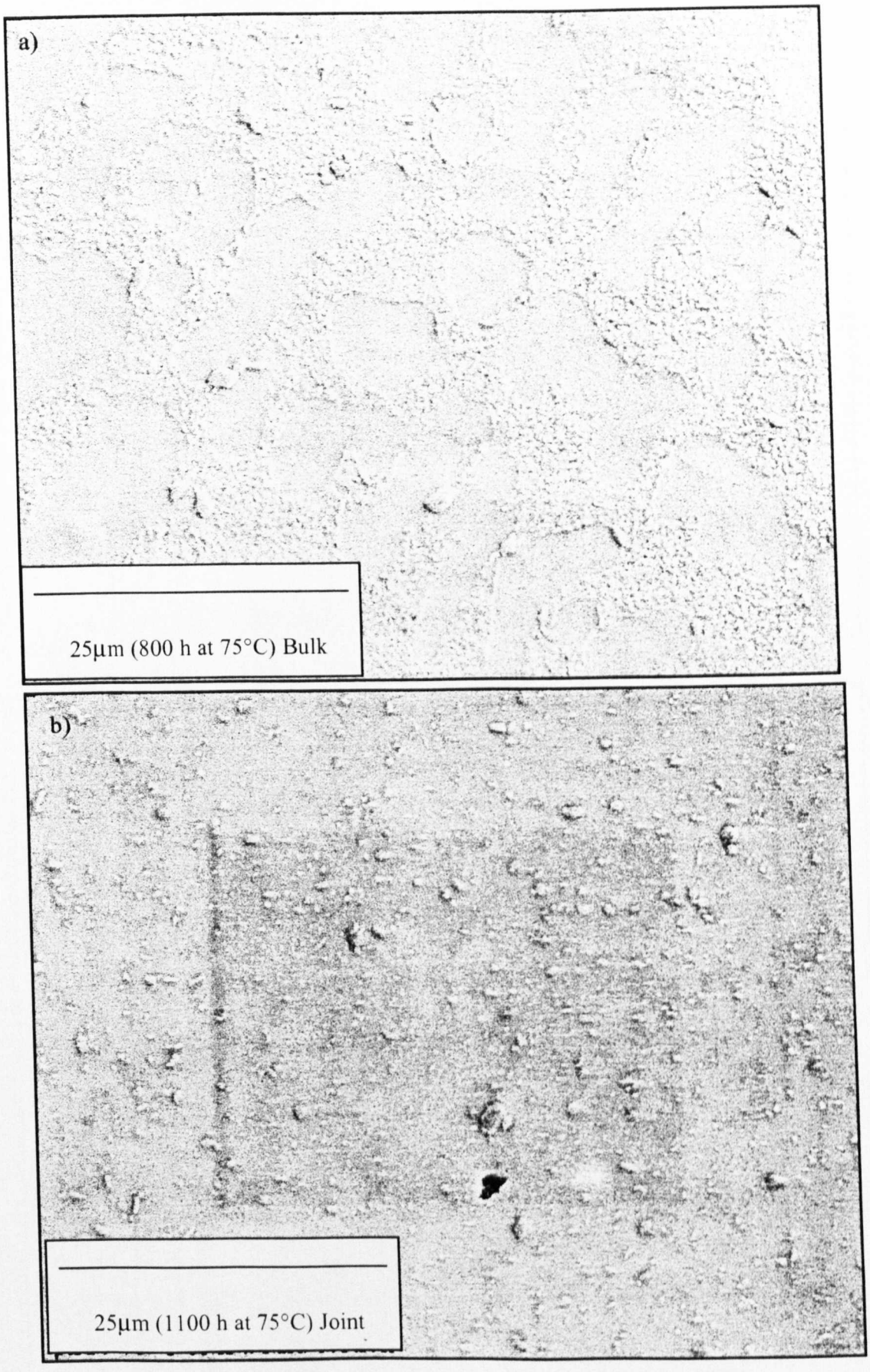


Figure 6.7 Comparison of a) bulk and b) joint microstructures after exposure to 75°C for extended periods of time

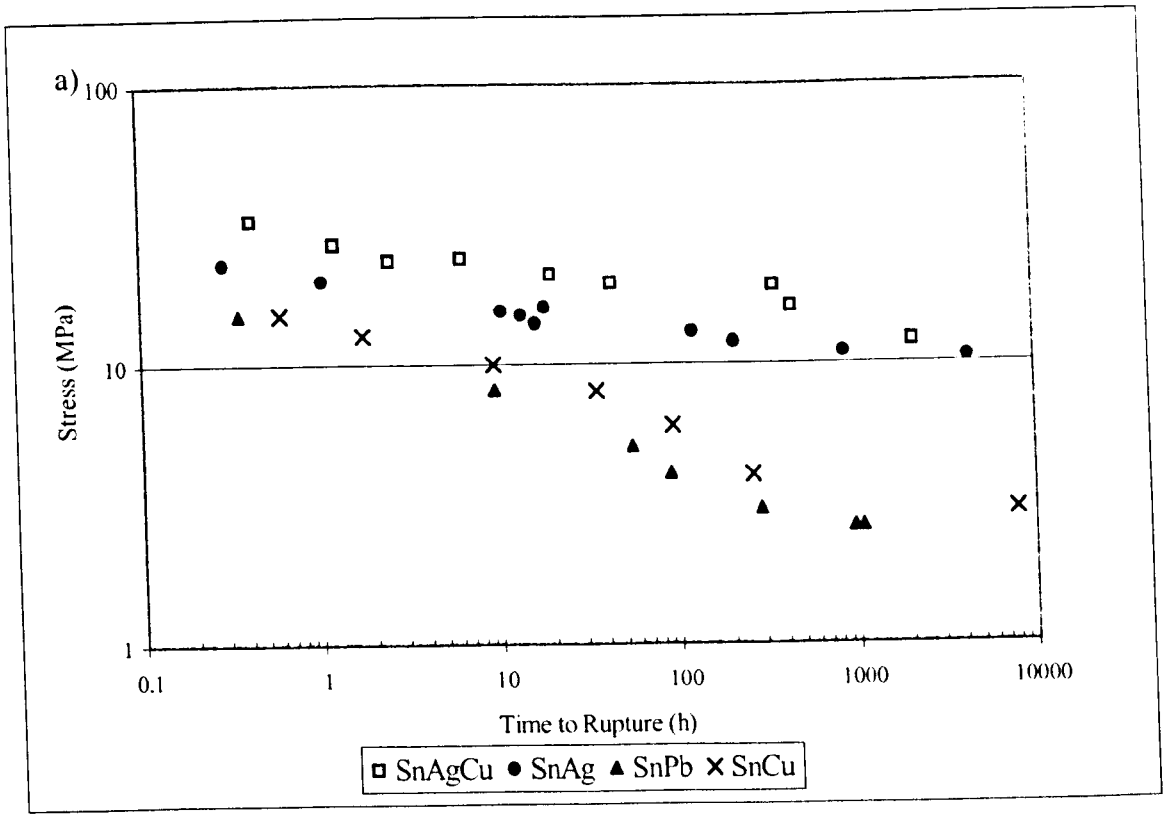


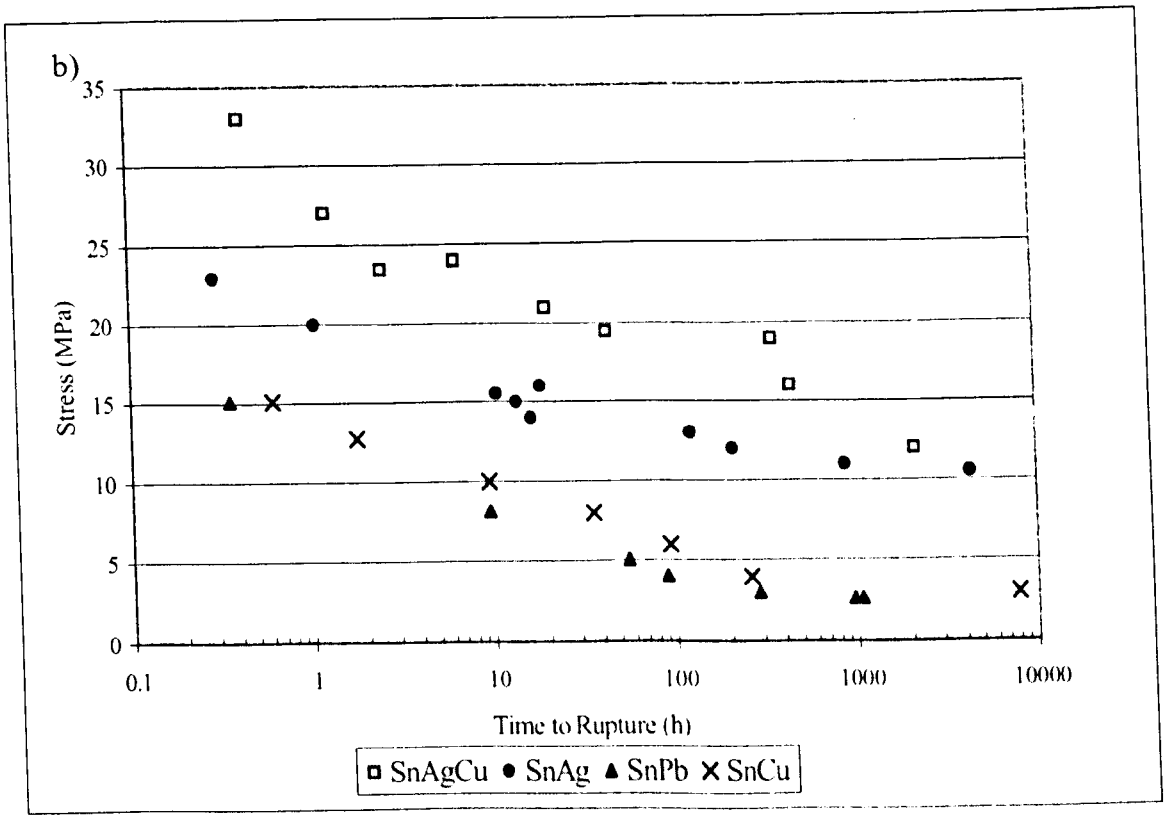


Figure 6.8 Time to rupture of solder alloys tested at 75°C

a) log – log plot b) semi – log plot

(See Appendix 6.1 for trend lines)

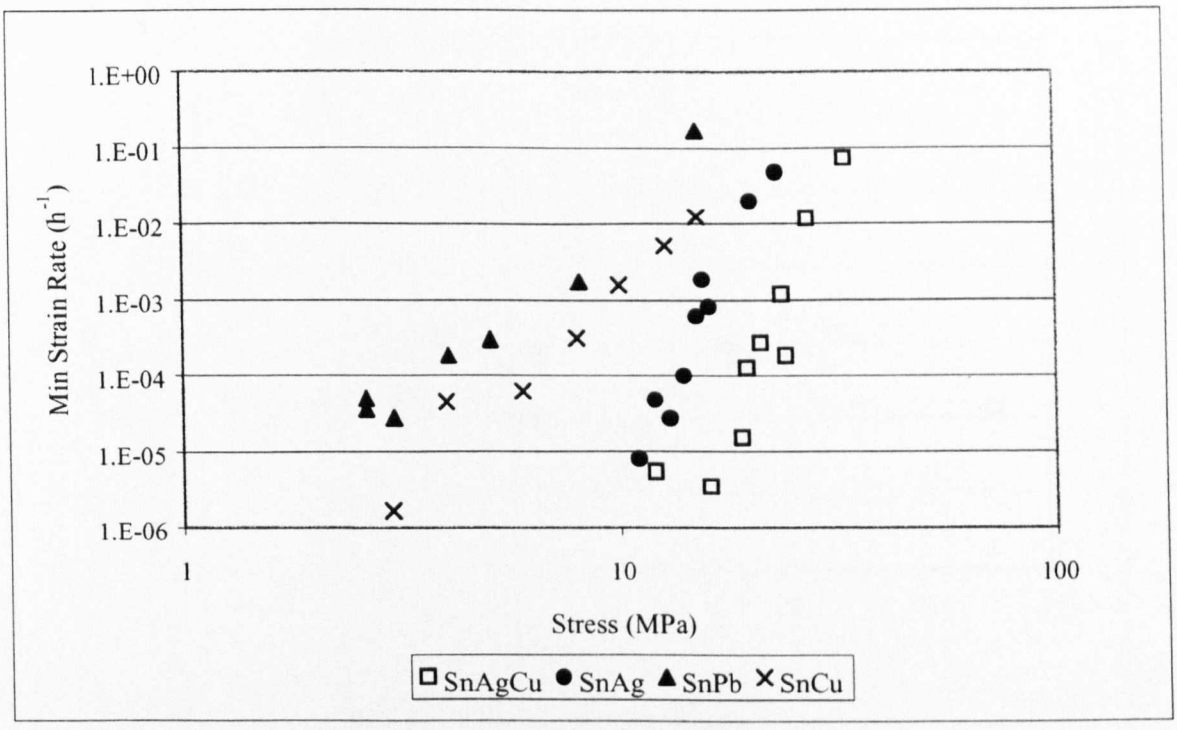


Figure 6.9 Minimum strain rate vs. stress plot at 75°C (See Appendix 6.1 for trend lines)

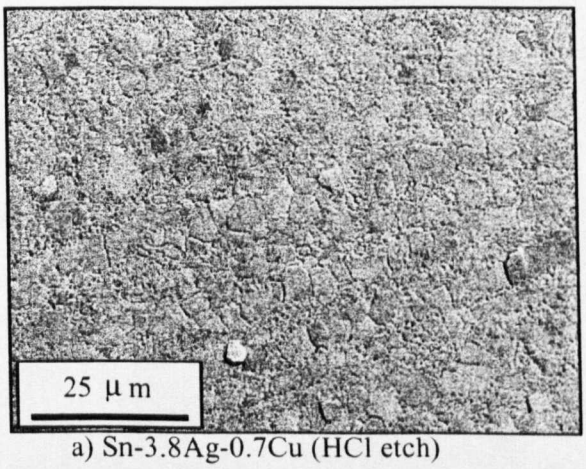


a) Sn-3.8Ag-0.7Cu (HCl etch)

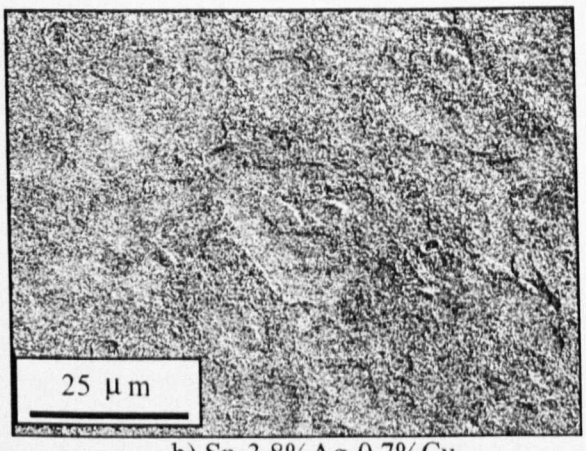


b) Sn-3.8%Ag-0.7%Cu

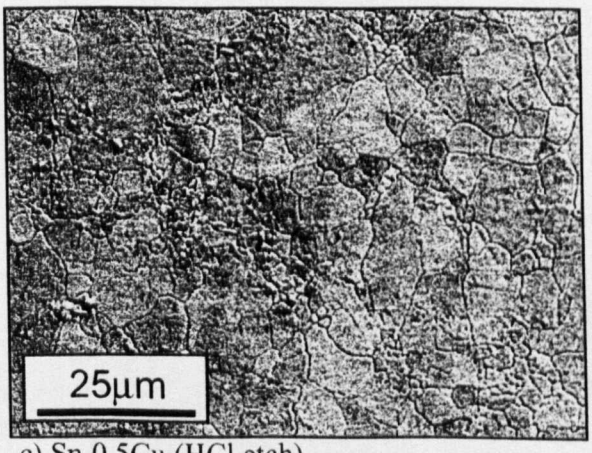


c) Sn-0.5Cu (HCl etch)

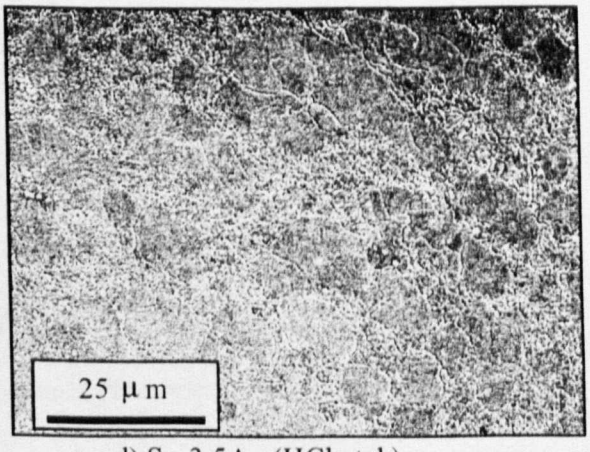


d) Sn-3.5Ag (HCl etch)

Figure 6.10 a to d 'As cast' microstructures of water quenched a) Sn3.8Ag0.7Cu (HCl etch), b) Sn3.8Ag0.7Cu (ammonium persuphate etch), c) Sn0.5Cu (HCl etch) and d) Sn3.5Ag (HCl etch)

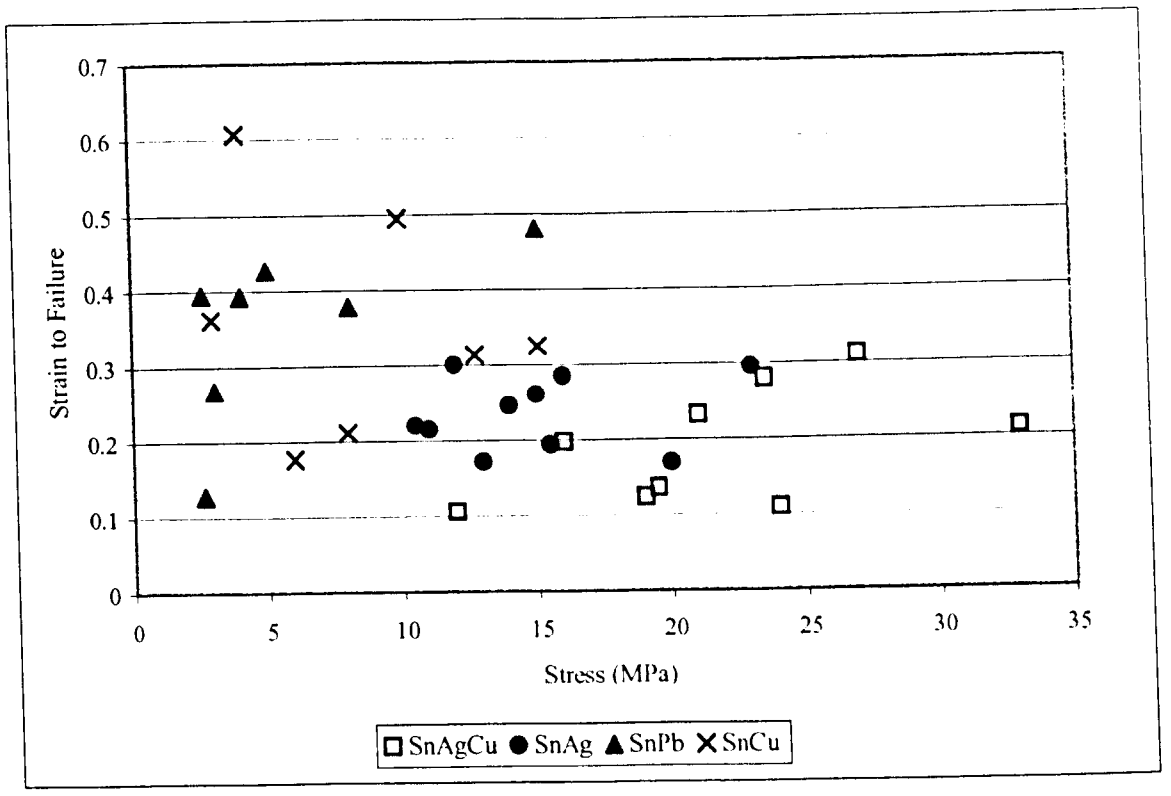


Figure 6.11 Strain to failure vs. stress plot at 75°C

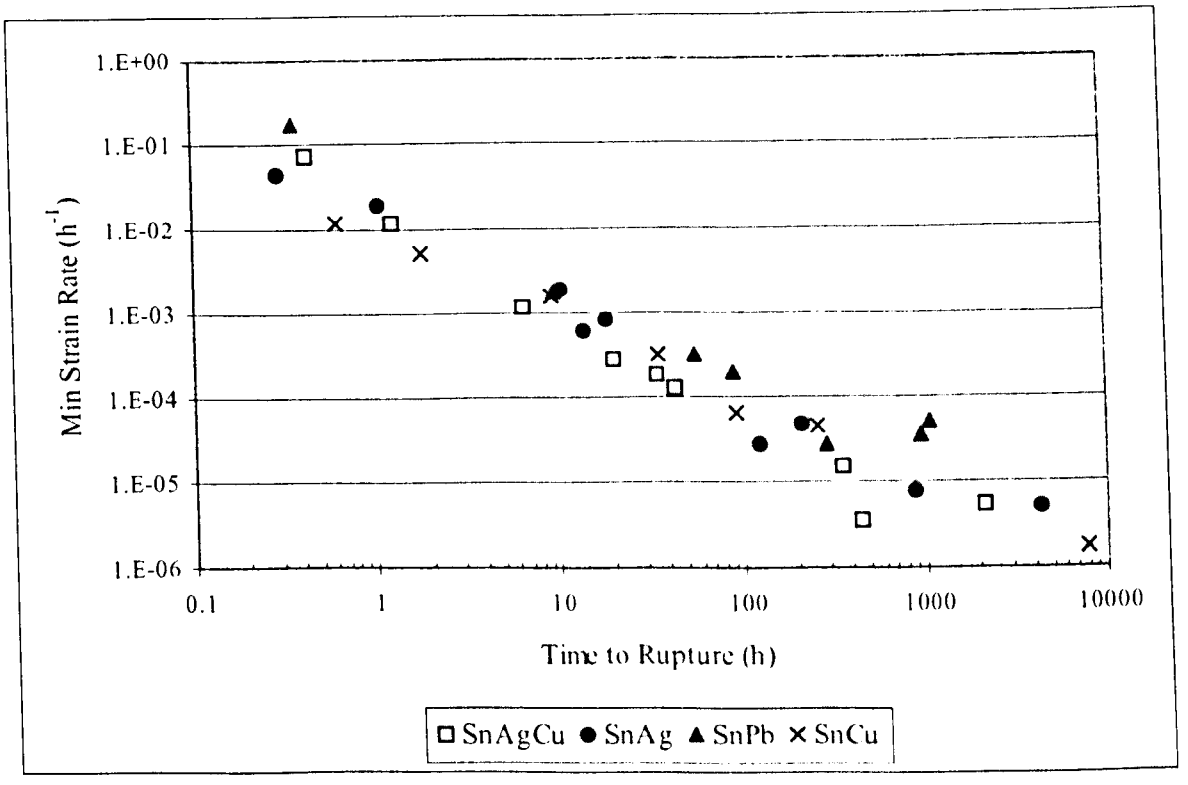


Figure 6.12 Monkman-Grant relationship at 75°C

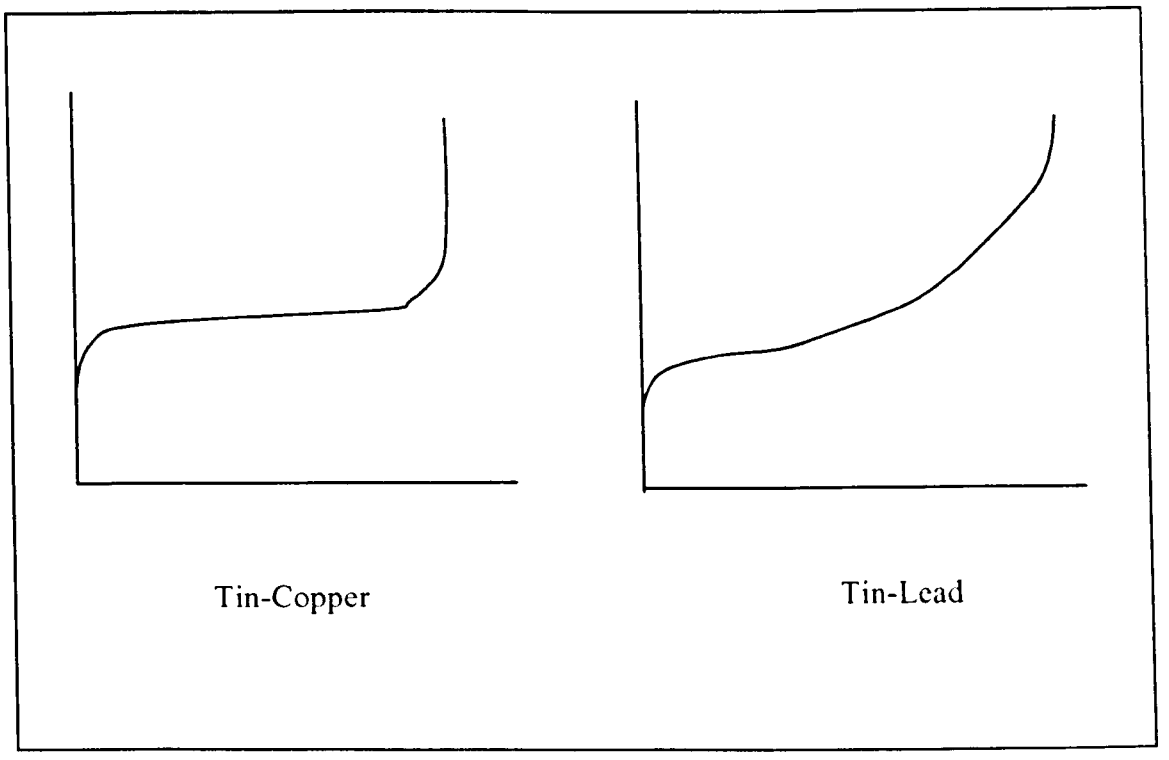


Figure 6.13 Difference in typical creep curve shape between SnCu and SnPb

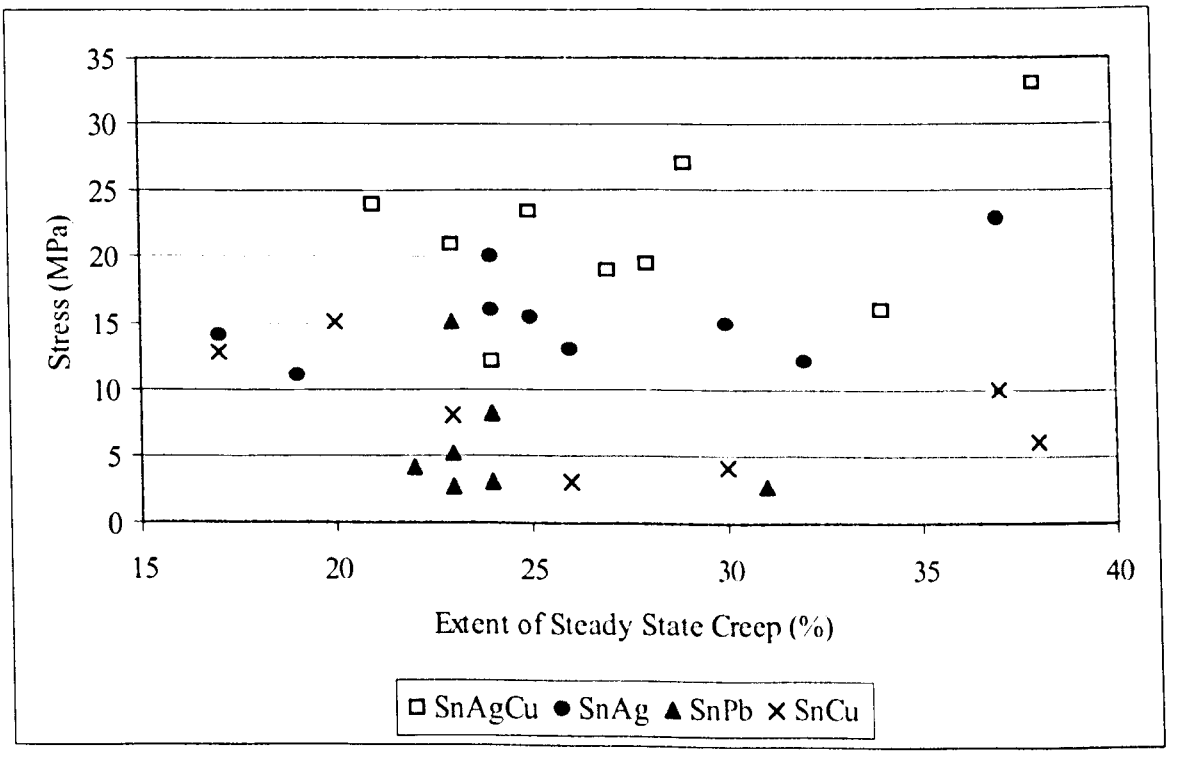


Figure 6.14 Extent of steady-state creep with relation to stress at 75°C

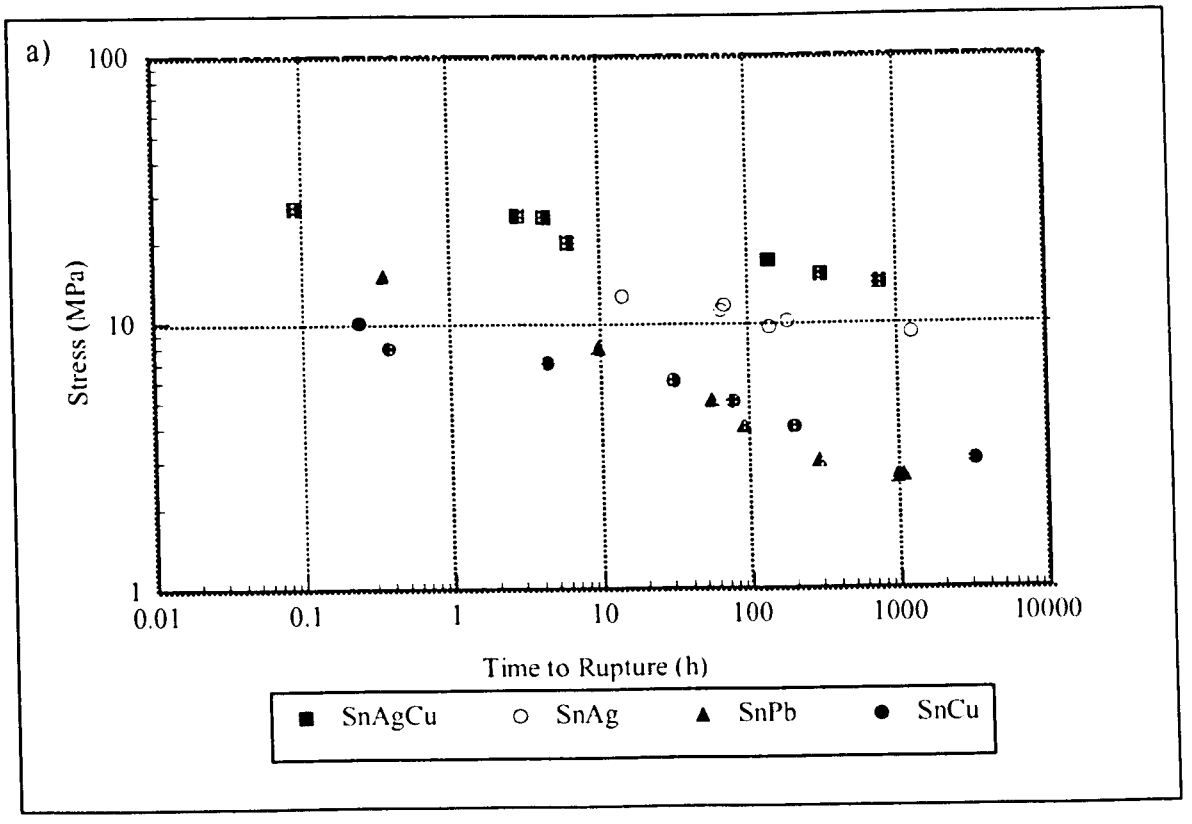


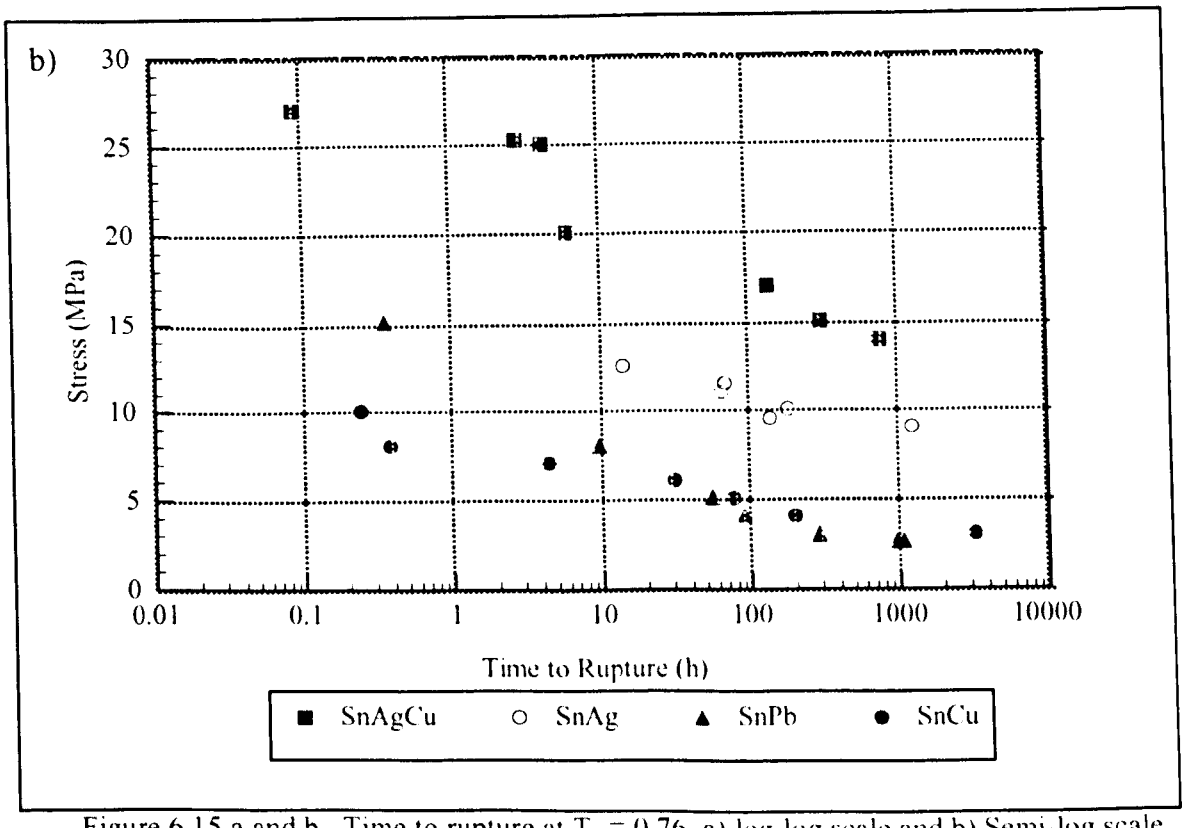


Figure 6.15 a and b Time to rupture at $T_h = 0.76$ a) log-log scale and b) Semi-log scale

(See Appendix 6.1 for trend lines)

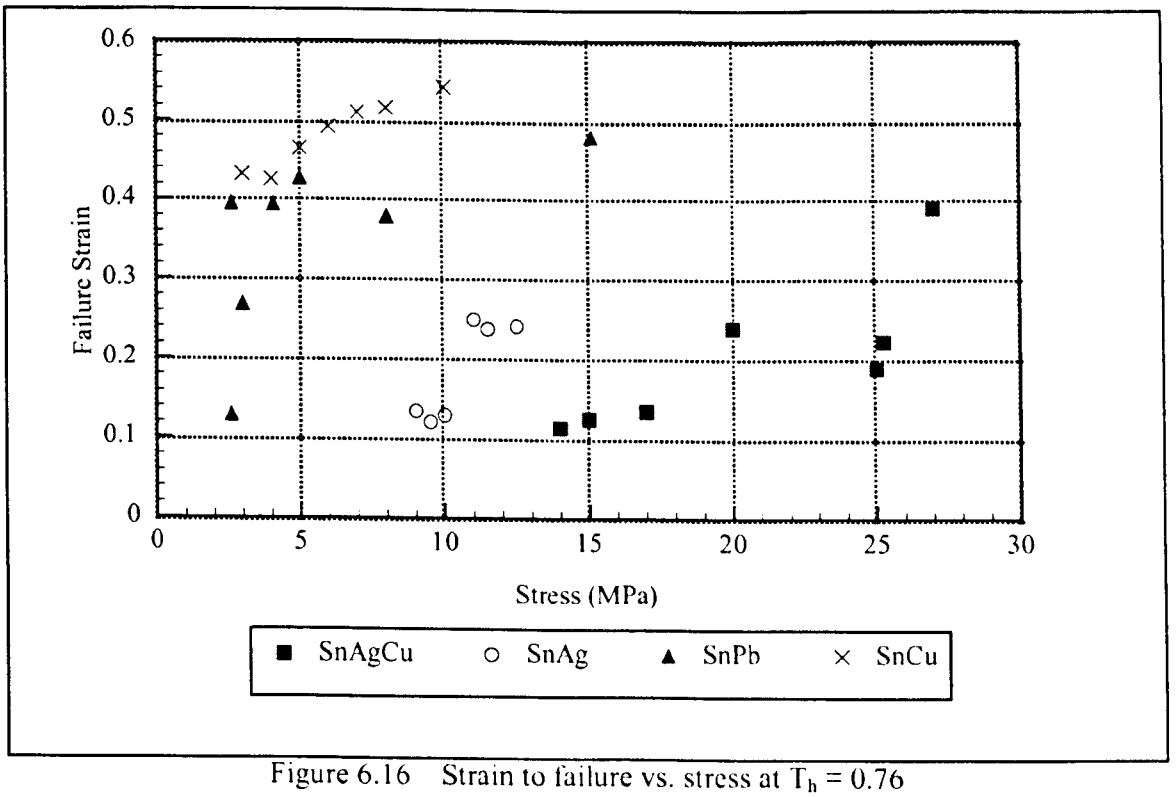


Figure 6.16 Strain to failure vs. stress at $T_h = 0.76$

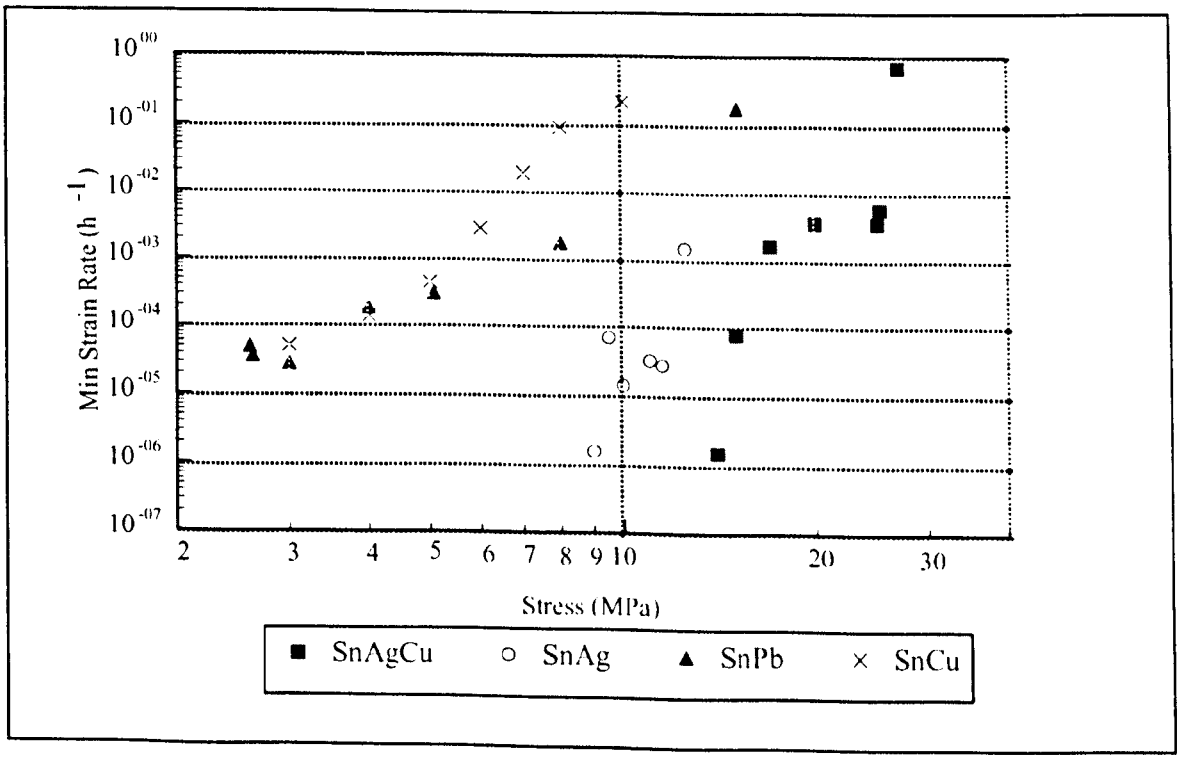


Figure 6.17 Norton's Law plot at $T_h = 0.76$

(See Appendix 6.1 for trend lines)

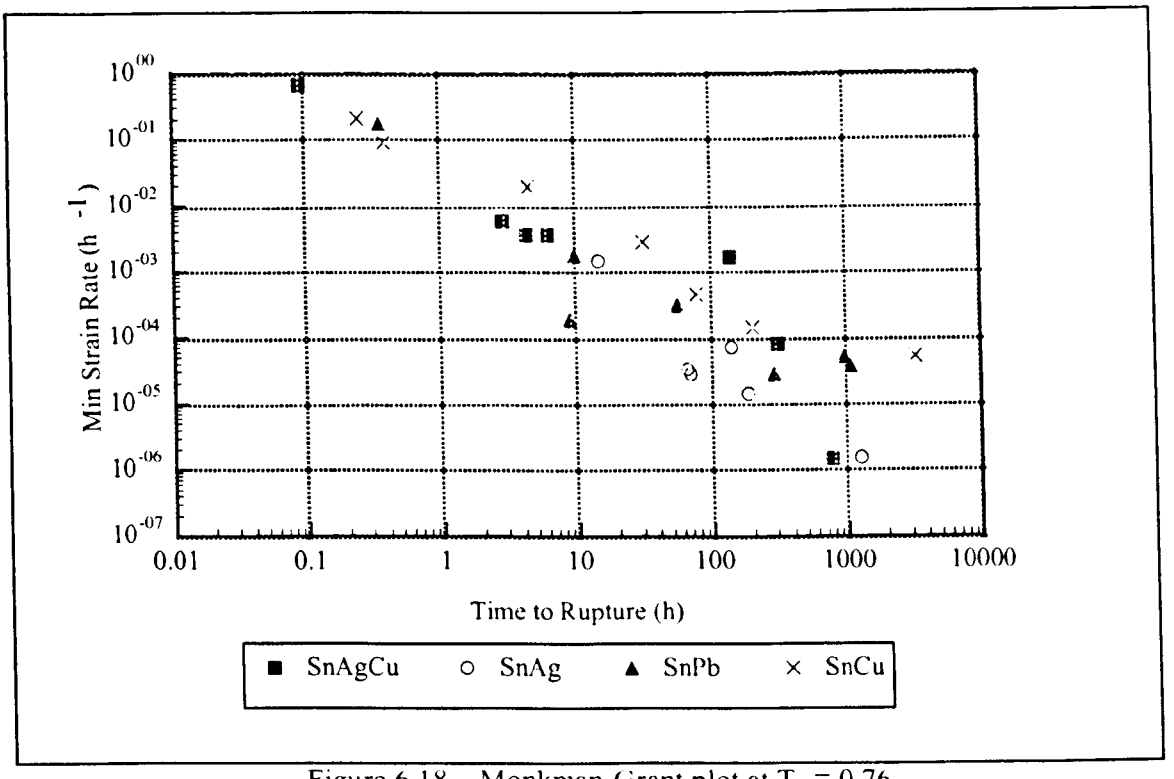


Figure 6.18 Monkman-Grant plot at $T_h = 0.76$

# CHAPTER SEVEN

## 7 CONCLUSIONS AND FURTHER WORK

The creep behaviour of Sn-3.8wt%Ag-0.7wt%Cu, in both bulk and model joint form, has been examined during this study. The data from both types of configuration have been discussed separately and then compared with each other. This was to determine whether there was any correlation between the behaviour observed in each case. The data obtained have also been compared with other potential lead-replacement alloys to determine relative performance when used in bulk form. This chapter summarises the key findings of this research and presents the author's recommendations for further work.

### 7.1 Conclusions

#### *7.1.1 Bulk Sn-3.8Ag-0.7Cu Alloy*

In terms of creep mechanism, a high creep exponent 'n' (according to the $\dot{\varepsilon}_{min} = A\sigma^n$ relationship) obtained for the bulk material at all test temperatures indicated a mechanism consistent with a dispersion hardened alloy. Microstructural examination of the 'as cast' structure confirmed a fine distribution of $Ag_3Sn$ and $Cu_6Sn_5$ particles within a β-Sn-based matrix. These fine intermetallic particles inhibit the motion of dislocations, increasing creep resistance. Although remaining high (above 10), the creep exponent decreased with increasing temperature, explained by the coarsening of the microstructure, the increase in applied energy, facilitating diffusional recovery mechanisms, and the drop in 'friction stress' (due to external factors e.g. temperature) resulting in a greater 'effective' stress.

The scatter in bulk data at low stress levels suggests a change in dominant creep mechanism, which is generally indicated by a change in slope in the Norton's power law plot. However, further 'long-term' work is required to substantiate this suggestion.

The high values of creep activation energy obtained for the bulk material correlates well with the creep activation energy of self-diffusion in tin, 120 kJ/mol.

Ductility (strain to failure) of the bulk ternary alloy remained low under all test conditions, generally between 10 to 30%. Although this is not low enough to cause concern when the alloy is used in engineering applications.

Failure occurred in a ductile manner at high stresses and exhibited mixed-mode characteristics (i.e. both ductile and brittle features were apparent) at lower stresses.

When using strain as a failure definition it was determined that the majority of strain occurred in tertiary creep. In some cases, over 90% of life had elapsed by the time 5% strain had been achieved. Generally, tertiary creep dominated creep life in the bulk specimens with secondary creep occupying approximately 20 to 40% of life. Commonly up to 90% of the total strain to failure in the bulk material occurred during tertiary creep. This observation questions the validity of the life prediction methodologies that are based upon secondary creep.

### *7.1.2 Sn-3.8Ag-0.7Cu in Pin in Ring Model Joints*

A high creep exponent 'n' (according to the $\dot{\varepsilon}_{min} = A\sigma^n$ relationship) was also obtained for the model joint specimens at all test temperatures. Microstructural evaluation suggested dispersion hardening as the dominant creep mechanism. A fine network of $Ag_3Sn$ and $Cu_6Sn_5$ particles within a β-Sn-based matrix was evident, with an approximately 2μm thick intermetallic layer of $Cu_6Sn_5$ at the solder/copper

interfaces. The effect of the interfacial intermetallic layer is not completely understood and would be a focus of further work. The two most comprehensive test temperatures (29°C and 75°C) exhibit a change in dominant creep mechanism at low applied stress levels (indicated by a change in creep exponent around 12MPa from greater than ten to three). At present there is no definite explanation for this change. However, microstructural evaluation does suggest extensive coarsening after a long exposure to heat and strain. To substantiate this hypothesis interrupted tests would be necessary to determine the mechanisms and location of the structural change.

The value of apparent creep activation energy obtained for the alloy when used in model joint form correlates to that seen for the short circuit diffusion of tin, 60 kJ/mol. However, given the similarity of high stress behaviour, the difference between creep activation energy in the bulk (120kJ/mol) and the model joint is not understood at present. Further work is required for the model joint samples, as at present an estimated value of creep activation energy was made from only two test temperatures due to equipment and time limitations.

In model joints strains to failure were high as they were tested in shear. Yet, the values were still substantially higher than expected and further work was performed to determine how much instantaneous strain was occurring solely in the solder. However, the results were inconclusive and for the purpose of analysis instantaneous strain was omitted from the strain readings i.e. only creep strain was considered.

It was difficult to determine the actual location and nature of failure as fractography revealed an 'smeared' shear fracture surface. However, in conjunction with energy dispersion spectroscopy, microscopy confirmed that failure occurred both in the solder above the intermetallic layer and occasionally shifted to the $Cu_6Sn_5$ IMC/solder interface when the grains were large.

Generally, secondary creep in the model joints occupied approximately 30 to 40% and tertiary 30 to 60% of the entire creep life. By disregarding instantaneous strain a similar trend to that observed in the bulk samples took place in the model joints, where up to 90% of the total strain to failure occurred during tertiary creep.

### *7.1.3 Comparison Between Joint and Bulk Behaviour*

For the purpose of comparison the shear stress and strain values obtained during joint testing were converted into tension. At high stress levels bulk and joint behaviour is comparable, however at stress levels below 12MPa model joint behaviour deviates away from that of the bulk. At low stresses, the material tested in the bulk form possesses lower strain rates than that observed in the joints. This is illustrated by a transition in 'n' (according to the $\dot{\varepsilon}_{min} = A\sigma^n$ relationship) at low applied stress levels for model joints; from greater than 10 at high stress to approximately 3 below 12MPa. This transition is not seen in the bulk material, although due to a scatter of data at low stress, there is some suggestion that a transition may occur only at much lower stresses.

Sn-3.8Ag-0.7Cu proved to be more stress sensitive in bulk form than when used in model joint form, i.e. for comparative test conditions the creep exponent 'n' (from Norton's Law) is higher in the bulk material than it is in the model joint.

Although creep is controlled by dislocation motion, according to creep activation energy values determined from this research, the diffusion mechanisms in bulk (self-diffusion) and joint samples (short circuit diffusion) appear to be different. As discussed in the previous section, more work is required to verify the activation energy of solder used in model joints.

### *7.1.4 Comparison of Bulk SnAgCu with Other Solder Alloys*

As previously mentioned it is difficult to directly compare data from different sources as generally results have been obtained under differing conditions. Therefore for the purpose of this research the bulk results obtained for SnAgCu were compared with results collated for other alloys tested under identical conditions (i.e. using the same manufacturing procedures and testing equipment). It was shown that the silver-containing alloys possessed a superior creep resistance to SnCu and SnPb, with the ternary alloy outperforming the binary alloy. This superiority was maintained when all the alloys were tested at the same homologous temperature.

The ductility of the silver-containing alloys was lower than that of the alternative alloys, although not low enough to cause concern when used in engineering applications.

The superiority of the silver-containing alloys was attributed to the fine dispersion of intermetallics within the tin-based matrix. In comparison to the binary alloy the ternary alloy has a more uniform distribution and a larger quantity of $Ag_3Sn$ and $Cu_6Sn_5$ finely dispersed within the microstructure thus aiding creep resistance.

### *7.1.5 General Conclusions*

- Sn-3.8Ag-0.7Cu possesses a superior creep resistance to the other possible lead-free alternative alloys and to the conventional tin-lead alloy.
- This superiority is retained when alloys were tested at the same homologous temperature.
- The superiority is attributed to the fine dispersion of $Ag_3Sn$ and $Cu_6Sn_5$ particles i.e. dispersion hardening (resulting in a high value of creep exponent both in bulk and joint form).

- At high stress levels, bulk and joint behaviour is comparable. At lower stress levels bulk behaviour becomes superior to the joint due to a transition in creep exponent (change in creep mechanism).
- In the bulk form, creep activation energy suggests that creep is controlled by self-diffusion.
- In the model joint form creep activation energy suggests that creep is controlled by short circuit-diffusion.
- Ductility of the bulk ternary alloy is low, although not low enough to cause concern.
- Ductility values in model joints are higher than those obtained in the bulk form due to loading in shear.
- Generally, in terms of creep resistance, the Sn-3.8Ag-0.7Cu alloy would be a suitable alternative (for electronics manufacturing) to the conventional Sn-37Pb alloy currently in use.

## 7.2 Recommended Further Work

This research programme has determined the creep performance of a popular lead-free replacement alloy both in bulk and model joint form and has identified possible similarities between bulk and joint behaviour. A comparison has also been made between the behaviour of SnAgCu (in bulk form) with other solder alloys. However, it would be beneficial to perform additional work, as listed below, to clarify and/or confirm some of the conclusions obtained.

- Bulk creep testing at all test temperatures for low stress levels i.e. providing lifetimes in excess of 10,000 hours, is necessary to determine whether a low stress transition, similar to that observed in the joint configuration, is also apparent in the bulk material.
- Microstructural evaluation of interrupted tests for bulk and model joint samples is necessary to evaluate the accumulation of damage during a creep test. It would be beneficial to perform three interrupted tests under each specified condition, i.e. at 75%, 50% and 25% of lifetime based on original strain versus time plots. Separate tests are necessary, as examination would be destructive i.e. samples would require sectioning. At present, failure in the model joint is observed to cross between the solder and the solder/IMC interface, interrupted testing would allow the determination of the precise location and initiation of failure in the model joint.
- Additional testing of SnAgCu model joints at various temperatures, e.g. –10°C, 99.4°C and 125°C, and extensive testing at lower stress levels would provide a more accurate estimation of activation energy and therefore, more comprehensive understanding of the effect of stress and temperature on model joint behaviour.
- The creep testing of SnAgCu model joints manufactured with varying solder joint thicknesses, using the same testing regime, is necessary to determine the effect

of solder width on intermetallic thickness and in turn creep behaviour. This type of testing is reliant on the determination of a suitable manufacturing technique. Smaller gap widths (0.1mm and 0.5mm) were manufactured using the technique devised for this research with limited success.

- The creep testing of model joints having undergone varying heat treatments is necessary to determine the growth rates of intermetallic compounds (in particular at the solder/substrate interfacial IMC layer) and their effect on the creep strength of model joints.
- The creep testing of model joints manufactured with Sn37Pb, using the same testing regime previously used for SnAgCu, is necessary as a matter of comparison of the lead-free and lead-containing alloys.
- The creep testing of model joints manufactured with Sn-3.5Ag and Sn-0.5Cu, using the same testing regime previously used for SnAgCu, is necessary as a matter of comparison of the alternative lead-free alloys.
- Finite Element Analysis (FEA) performed using data collected through mechanical testing would be interesting to evaluate the capabilities and reliability of computer packages with regards to actual solder data. Preliminary studies performed in this area have, to date, proved to be inconclusive.
- Supposing 'infinite' time, it would be ideal to perform a number of tests at each of the conditions evaluated in this programme to determine the repeatability of creep testing of solder alloys. Given the small number of 'repeat tests' performed during testing, the limited repeatability established may be a possible source of error when investigating computer-modelling packages.
- Finally, assuming that a reliable correlation between bulk and model joint behaviour had been established, it would be beneficial to perform creep testing on

actual joints under similar conditions to enable further correlation between the three configurations of solder. However, this would require specialist equipment.

The programme of work outlined above would allow the creep behaviour of Sn-3.8Ag-0.7Cu lead-free solder alloy in three relevant configurations to be examined directly and in detail. A database of bulk, model joint and actual joint data would allow relationships to be drawn between the configurations. When combined with other information collated within the Open University research facility, such as fatigue, monotonic and computer modelling data, it would be an extremely valuable information source to research scientists and industrial engineers alike.

## REFERENCES


1. Humpston, G. and Jacobson, D. .M., Principles of Soldering and Brazing. 1993: ASM International.
2. Thwaites, C.J. "Soldering Technology - A Decade of Developments". *International Metals Reviews*, Vol. 29, No. 2, 1984, pp. 45-74.
3. Vianco, P.T. and Frear, D.R., "Issues in the Replacement of Lead-bearing Solders". *Journal of Materials*, July 1993, pp. 14-19.
4. Public-Law (99-339) Safe Drinking Water Act Amendments, 1986: United States of America.
5. Fukuda, A., *Nikkei Electronics*, Vol. 91, 1995, pp. 635.
6. Napp, D., "Lead free interconnect materials for the electronics industry", *SAMPE Journa*l, Vol. 32 No. 59, 1996, pp. 59-65.
7. Plumbridge, W.J., Gagg, C.R. and Peters, S., "The Creep of Lead-free Solders at 75°C". in 2001 TMS Annual Meeting and Exhibition Lead-free Solder Materials and Soldering Technologies. 2001. New Orleans, Louisiana.
8. Plumbridge, W.J., The Solder Programme at the Open University Materials Engineering Department - An Update, The Open University. 2001, pp 1-11.
9. Jacobson, D.M. and Harrison, M.R., "Brite/Euram III, Project Number BE95-1994". *GEC Journal of Research*, Vol. 12, No. 2. 1997.
10. Suetsugu, K. Lead-free Solders - Matsushita, Personal communication. 1998.
11. Hester, L., "Administration promotes rule on lead emissions information", in *EPA Environmental news*. 2001: Washington DC, USA.
12. European Legislation concerning "Waste End of Life Electronic and Electrical Equipment", 2000.

13. Ministry of International Trade and Industry web site: http://www.miti.go.jp [accessed 2000].

14. IPC dedicated Pb-Free web site: http//www.leadfree.org [accessed 2001].

15. Harris, P.G. and Whitmore, M.A., "Alternative Solders for Electronics Assemblies Part 1: Materials Selection". in BAB Autumn Conference. 1992. Coventry.

16. Hwang, J.S. and Hoenigsmann, H.J., "New Lead-free Solders for Electronics Packaging and Assembly". in Surface Mount International Conference '97. 1997. San Jose CA.

17. Hwang, J.S., "Promising Lead-free Solder Alloys". *Surface Mount Technology*, October 1999, pp. 18-20.

18. McCormack, M. and Jin, S., "Progress in the Design of the New Lead-free Solder Alloys". *Journal of Minerals, Metals and Materials*, July, 1993, pp. 36-40.

19. Sigelko, J.D. and Subramanian, K.N., "Overview of Lead-free Solders". *Advanced Material & Processes*, March 2000.

20. Richards, B.P., Levoguer, C.L., Hunt, C.P., Nimmo, K., Peters, S. and Cusack, P., "Lead Free Soldering - An Analysis of the Current Status of Lead-free Soldering". 1999: DTI.

21. Vincent, J.H., "Alternative Solders for Electronics Assemblies Part 2: UK Progress and Preliminary Trials". in BAB Autumn Conference. 1992. Coventry.

22. Vincent, J.H. and Humpston, G., "Lead-free Solders for Electronic Assembly". *GEC Journal of Research*, Vol. 11, No. 2. 1994.

23. Harrison, M.R. and Vincent, J.H., "IDEALS - Improved Design Life and Environmentally Aware Manufacturing of Electronics Assemblies by Lead-free Soldering", 1999.

24. Ashby M.F. and Jones, D.R.H., "Engineering Materials 1: An Introduction to their Properties and Applications". 1993: Pergamon.

25. Schmidt, C.G., Simon, W., Kanazawa, C.H. and Erlich, D.C., *IEEE Transactions on Components, Packing and Manufacturing Technology*, Vol. 18, 1995, pp. 611.

26. NCMS (National Centre for Manufacturing Sciences) Report "0401RE96", "Lead-free solder alternatives" 1997.

27. Nimmo, K., "Review of Current Issues in Lead-free Soldering". in Surface Mount International Conference '97. 1997. San Jose, CA.

28. Plumbridge, W.J., Kariya, Y. and Gagg, C. "Tin Pest in Solder Alloys". *Soldering and Surface Mount Technology*, Vol. 13, 2001, pp. 39-40.

29. Suganuma, K., Ueshima, M., Ohnaka, I., Yasuda, H., Zhu, J. and Matsuda, T., "Lift-off Phenomenon in Wave Soldering". *Acta Materialia*,Vol. 48, 2000. pp. 4475-4481.

30. Vincent, J., Personal communication relating to the IDEALS programme, 1999.

31. Warwick, M. "Implementing Lead-free Soldering - European Consortium Research". SMTA, *Journal of Surface Mount Technology*, Vol. 12, No. 4, 1999, pp 1-12.

32. Anderson, I., Yost, F.G., Smith, J.F., Miller, C.M., and Terpstra, R.L., "Pb-free Sn-Ag-Cu Ternary Eutectic Solder", 1996, Iowa State University, Research Foundation Inc. Sandia Corporation: United States. pp. 9.

33. Anderson, I. and Karsjen, S., "Ames Laboratory Signs International Licensing Agreement on Lead-free Solder", Press Release 1997.

34. Karsjen, S., "Lead-free Solder Goes International: Lab Signs Second Licensing Agreement on Lead-free Solder", Press Release. 1998.

35. Kariya, Y., "Effect of Third Element on the Mechanical Reliability of Sn-3.5mass%Ag Lead-free Solder for Micro-joining and Anti-Fatigue Damage Design in the Development of New Lead-free Solder", in Technology. 1999, Shibura Institute of Technology, Shibura. pp. 168.

36. Kariya, Y. and Plumbridge, W.J. "Mechanical Properties of Sn-3.0mass%Ag-0.5mass%Cu Alloy". Proceedings, Seventh Symposium on Microjoining and Assembly Technology in Electronics, MATE 2001, February 2001, Yokohama, Japan, pp 383-388.

37. Gedney, R., "NEMI Group Recommends Tin/Silver/Copper Alloy as Industry Standard for Lead-free Solder Reflow in Board Assemblies", www.lead-free.org [accessed 2000].

38. Evans, R.W. and Wilshire, B., Creep of Metals and Alloys. 1985: IOM Communications. p.320

39. Cottrell, A.H., Theory of Dislocation. 1964: Blackie and Son Ltd. p. 91.

40. Garofalo, F., Fundamentals of Creep and Creep Rupture in Metals. 1966: Macmillan Series in Materials Science.

41. Frost, H.J. and Ashby, M.F., .Deformation-mechanism Maps. 1982: Pergamon. p. 165.

42. Monkman, F.C. and Grant, N.J. "An Empirical Relationship Between Rupture Life and Minimum Creep Rate in Creep Rupture Test". *Proceedings American Society for Testing and Materials*, 1956 pp. 593-620.

43. Kizilyalli, M., Corish, J. and Metsellaar, R., "Definitions of Terms for Diffusion in the Solid State". *Pure Applied Chemistry*, Vol. 71 No. 7, 1999, pp. 1307-1325.

44. Choi, S., Lee, J.G., Guo, F., Bieler, T.R., Subramanian, K.N. and Lucas, J.P., "Creep Properties of Sn-Ag Solder Joints Containing Intermetallic Particles". *Journal of Materials*, June, 2001, pp. 22-26.

45. McCabe, R.J. and Fine, M.E., "The Creep Properties of Precipitation-Strengthened Tin-Based Alloys". *Journal of Materials*, Vol. 52, No. 6, 2000, pp. 33-35.

46. Hertzberg, R.W., Deformation and Fracture Mechanics of Engineering Materials, 3rd Ed. New York. Wiley and Sons, 1989. ISBN 0-471-61722-9.

47. Plumbridge, W.J., "Review - Solders in Electronics". *Journal of Materials Science*, Vol. 31, 1996, pp. 2501-2514.

48. Newey, C. and Weaver, G., Materials Principles and Practice. Materials in Action. Vol. 1. 1990: Butterworth Scientific. pp. 405.

49. Nabarro, F.R.N., Report of a Conference on Strength of Solids. in The Physical Society of London. 1948.

50. C. Herring, *Journal of Applied Physics*, Vol. 21, 1950, pp. 437

51. Courtney, T.H., Mechanical Behaviour of Materials. Materials Science Series. 1990: McGraw-Hill International Editions.

52. Nabarro, F.R.N., and de Villiers, H.L., The Physics of Creep. 1995: Taylor and Francis.

53. Coble, R.L., "Model for Boundary Diffusion-controlled Creep in Polycrystalline Materials", *Journal of Applied Physics*, Vol. 34, No 6, 1963, pp. 1679-1682.

54. Smallman, R.E. and Bishop, R.J., Metals and Materials - Science, Processes, Applications. 1995: Butterworth Heinemann.

55. Rachinger, W.A. *Journal. International Metals*, Vol. 81, 1952, pp. 33.

56. Lifshitz, I.M., "Structure of the Energy Spectrum of Impurity Bands in Disordered Solid Solutions", *Soviet Physics. JETP*, Vol. 17, 1963. pp. 1159-1170.

57. Evans, B.W. and Wilshire, B., Introduction to Creep. 1993: The Institute of Materials.

58. Gagg, C.R. and Williams, N., "Microstructural Effects Caused by Machining", Personal communication, 2000.

59. Gagg, C.R., Personal communication including data from [7], 2002.

60. Stephens, J.J. and Frear, D.R., "Time-Dependent Deformation Behaviour of Near-Eutectic 60Sn-40Pb Solder". *Metallurgical and Materials Transactions A*, Vol. 30A May, 1999, pp. 1301-1313.

61. Tribula, D., and Morris Jr, J.W., "Creep in Shear of Experimental Solder Joints". *Journal of Electronic Packaging*, Vol. 112 June, 1990, pp. 87-93.

62. Mathew, M.D., Movva, S. and Murty, K., "Deformation Mechanisms in Tin and Tin-Based Electronic Solder Alloys". *Key Engineering Materials*, Vol. 171-174, 2000. pp. 655-662.

63. Guo, F., Lucas, J.P., and Subramanian, K., "Creep Behaviour in Cu and Ag Particle Reinforced Composite and Eutectic Sn-3.5Ag and Sn-4Ag-0.5Cu Non-Composite Solder Joints". *Journal of Materials Science:Materials in Electronics*, Vol. 12, 2001, pp.27-35.

64. Grivas, D., Murty, K.L., and Morris, J.W., "Deformation of Pb/Sn Eutectic Alloys at Relatively High Strain Rates", *Acta Metallurgica*, Vol. 27, 1979, pp. 731-737.

65. Mavoori, H., Chin, J., Vaynman, S., Moran, B., Keer, L. and Fine, M., "Creep, Stress Relaxation and Plastic Deformation in Sn-Ag and Sn-Zn", *Journal of Electronic Materials*, Vol. 26, No. 7, 1997, pp. 783-790.

66. Mavoori, H., Vaynman, S., Chin, J., Moran, B., Keer, L., and Fine, M., "Mechanical Behaviour of Eutectic SnAg and SnZn Solders". *Materials Research Society Symposium Proceedings*, Vol. 390, 1995, pp. 161-175.

67. Hwang, J.S. and Vargas, R.M., "Solder Joint Reliability - Can Solders Creep?" *Soldering and Surface Mount Technology*, Vol. 5, June, 1990.

68. Igoshev, V.I., and Kleiman, J.I., "Creep Phenomena in Lead-free Solders". *Journal of Electronic Materials*, Vol. 29, No. 2, 2000, pp. 244-251.

69. Igoshev, V.I., Kleiman, J.I., Shangguan, D., Lock, C., Wong, S. and Wiseman, M., "Microstructural Changes in Sn-3.5Ag Solder Alloy During Creep". *Journal of Electronic Materials*, Vol. 27, No. 12, 1998, pp. 1367-1371.

70. Kariya, Y. and Atsumi, K., "Creep Properties of Sn3.5Ag-xBi and Sn-3.5Ag-xCu Solder Alloys", to be published.

71. Clech, J.-P., "Review and Analysis of Lead-free Solder Material Properties", August 20, 2002, EPSI Inc. p. 70.

72. Darveaux, R. and Banerji, K., "Constitutive Relations for Tin-based Solder Joints".*IEEE Transactions on Components, Hybrids and Manufacturing Technology*, Vol. 15, No. 6, December 1992, pp. 1013 - 1024.

73. Hua, F., Garner, C.M., Song, H.G., and Morris Jr, J.W., "Creep Behaviour of Pb-free Solders", in proceedings, ASME, Pittsburgh, September, 2001

74. Song, H.G., Morris, J.W., and Hua, F., "The Creep Properties of Lead-free Solder Joints". *Journal of Materials*, Vol. 54, No. 6, 2002, pp. 30-32.

75. Wiese, S., Feustel, F. and Meusel, E., "Characterisation of Constitutive Behaviour of SnAg, SnAgCu and SnPb Solder in Flip Chip Joints". *Sensors and Actuators A*, Vol. 3289, 2002, pp. 1-6.

76. Klein Wassink, R.J., Soldering in Electronics. 1984: Electrochemical Publications.

77. Harris, P.G. and Chagger, K.S. "The Role of Intermetallic Compounds in Lead-free Soldering". *Soldering and Surface Mount Technology*, Vol. 10, No. 3, 1998, pp. 38-52.

78. Hampshire, W.B., Solders - Electronic Materials Handbook, Vol. 1 - Packaging. 1989: ASM International.

79. Tu, P.L., Chan, Y.C. and Lai, J.K.L., "Effect of Intermetallic Compounds on the Thermal Fatigue of Surface Mount Solder Joints". *IEEE Transactions on Components, Packaging, and Manufacturing Technology, Part B*, Vo. 20, No. 1, 1997.

80. Frear, D.R. and Vianco, P.T., "Intermetallic Growth and Mechanical Behaviour of Low and High Melting Temperature Solder Alloys". *Metallurgical and Materials Transactions A*, Vol. 25, 1994, pp. 1509-1523.

81. Dirnfeld, S.F. and Ramon, J.J., "Microstructure Investigation of Copper-Tin Intermetallics and the Influence of Layer Thickness on Shear Strength". *Supplement to the Welding Journal*, October, 1990.

82. Dummer, G.W.A and Winton, R.C., An Elementary Guide to Reliability. 3rd Edition ed. 1986: Pergamon Press Ltd. 47.

83. Grossman, G., Weber, L. and Heiduschke, K., "Metallurgical Considerations for Accelerated Testing of Soft Solder Joints". in IEE/CPMT International Electronics Manufacturing Technology Symposium. 1996.

84. Thwaites, C.J. and Duckett, R., "Effects of Soldered Joint Geometry on their Mechanical Strength". *Revue de la Soudre*, Vol.4, 1976, pp 1-6.

85. Unal, O., Barnard, D.J. and Anderson, I.E., "A Shear Test Method to Measure the Shear Strength of Metallic Materials and Solder Joints using Small Specimens". *Scripta Metallurgica and Materialia*, Vol. 40, No. 3, 1999.

86. Ramon, J.J. and Dirnfeld, S.F., "A Practical Way to Measure the Strength of Small Soldered Joints". *Welding Journal,* Vol. 67, No. 10, 1988. pp. 19-21.

87. Foley, J.C., Gickler, A., Leprevost, F.H. and Brown, D., "Analysis of Ring and Plug Shear Strengths for Comparison of Lead-free Solders". *Journal of Electronic Materials*, Vol. 29, No. 10, 2000, pp. 1258-1263.

88. Stone, K.R., Duckett, R., Muckett, S. and Warwick, M.E., "Mechanical Properties of Solders and Solder Joints", ITRI report No. 636, Uxbridge 1983.

89. Gillot, F., "Fatigue Behaviour in Electronics Solder Joints", Swedish Institute for Metals Research, Stockholm. 1997, pp. 46.

90. Rynemark, M., Nylen, M. and Hutchinson, B., "On the Fatigue of Solder Subjected to Isothermal Cyclic Shear". *Scripta Metallurgica and Materialia*, Vol. 28, 1993, pp. 349-352.

91. Vianco, P.T. and Rejent, J.A., "Properties of Ternary Sn-Ag-Bi Solder Alloys: Part II-Wettability and Mechanical Properties Analyses". *Journal of Electronic Materials*, Vol. 28, No. 10, 1999, pp. 1138-1143.

92. Rod, O. and Nylen, M., "Influence of the Microstructure on the Fatigue Properties of Solder Joint", Swedish Institute for Metals Research, Stockholm, 1999, p. 73.

93. Tomlinson, W.J. and Collier, I., "The Mechanical Properties and Microstructures of Copper and Brass Joints Soldered with Eutectic Tin-Bismuth Solder". *Journal of Materials Science*, Vol. 22, No. 5, 1987.

94. Hampshire, W.B., "The Search for Lead-free Solders". in Surface Mount International Conference. 1992. San Jose, CA.

95. Anderson, I.E., Bloomer, T.E., Terpstra, R.L., Foley, J.C., Cook, B.A. and Harringa, J., "Development of Eutectic and Near Eutectic Tin-silver-copper Solder Alloys for Lead-free Assemblies". in IPC Works '99: An International Summit on Lead-free Electronics Assemblies. 1999. Minneapolis, MN.

96. Anderson, I.E., Bloomer, T.E., Terpstra, R.L., Foley, J.C., Cook B.A. and Harringa, J., "Development of Eutectic and Near Eutectic Tin-silver-copper Solder Alloys for Lead-free Joining Applications". in IPC Works '99: An International Summit on Lead-free Electronics Assemblies. 1999.

97. Shawki, G.S.A. and El-Shabbagh, A.A.S., "Shear Strength of Brazed and Soldered Joints". *Welding Research Supplement*, 1975.

98. Unknown, Multicore Ecosol TSC Product Information (MSL Ref: 733 9/99), 2001, Multicore: Hemel Hempstead.

99. Unknown, Alpha Product Information Vaculoy Bar Solder TEchnical Bulletin, 2001, Alpha Metals: Croydon.

100. Plumbridge, W.J. and Gagg. C., "The Effect of Ageing on the Creep of a Eutectic Lead-tin Alloy". in BABS Autumn Conference. Solihull, October 1996, p 1-7.

101. Bernasconi, G.and Piatti, G., "Creep of Engineering Materials and Structures". in Proceedings of the Joint Research Centre of the Commission of The EC. 1978. Italy: Applied Science Publishers Ltd, London.

102. Gagg, C., Personal communication, 2002.

103. Schubert, A., Walter, H., Dudek, R., Michel, B., Lefranc, G., Otto, J. and Mitic, G., "Thermo-mechanical Properties and Creep deformation of Lead-containing and Lead-free Solders", Proceedings, 2001 International Symposium on Advanced Packaging Materials, pp. 129-134.

104. Neu, R.W., Scott, D. T. and Woodmansee, M. W., "Thermomenchanical Behaviour of 96Sn-4Ag and Castin Alloy", *ASME Transactions, Journal of Electronic Packaging*, Vol 123, No. 3, September 2001, pp. 238-246.

105. Siewert, T., Liu, S., Smith, D.R., Madeni, J.C., "Properties of Lead-free Solders Database for Solder Properties, Release 4.0. A database for Solder Properties with Emphasis on New Lead-free Solders" National Institute of Standards and Technology and Colorado School of Mines, Colorado 11 February 2002.

106. Smithells Metals Reference Book 7$^{th}$ Edition Butterworth-Heinemann Ltd, Oxford 1992 ISBN 0-7506-1020-4.

## APPENDICES

Appendix 1.1: The wave soldering process and illustration of printing onto a PCB

Appendix 4.1: Plate 4.1:Photograph of specimens used in the SRG programme

Appendix 4.1: Plate 4.2: Photograph of the Open University creep facility

Appendix 4.2: Temperature control capabilities of a creep furnace

Appendix 4.3: Heating profile for model joint manufacture

Appendix 4.4: Photograph of a pin in ring model joint specimen

Appendix 4.5: Calculation of shear stress values for model joint creep testing

Appendix 4.6: Detailed illustration of mounting configuration for joint creep testing

Appendix 4.7: Investigation of large instantaneous strain occurring on loading of model joints

Appendix 5.1: Bulk solder testing log, strain vs time and strain rate versus life fraction plots for all bulk tests

Appendix 5.2: Calculation of errors and the utilisation of error bars

Appendix 5.2b: Trend lines for figures using a 'best fit' plot

Appendix 5.3: Effect of stress on strain rate (bulk) at –10, 29, 94.4 and 125°C

Appendix 5.4: Tables of separate measurements of creep strain occurring in each regime and accumulative measurements of creep strain occurring in each regime

Appendix 5.5: Percentage of creep life in each regime as determined by creep strain (omitting instantaneous strain)

Appendix 5.6: Model joint testing log, strain vs time and strain rate versus life fraction plots for all bulk tests

Appendix 5.7: Chart recorder plot of shear strain vs time (to illustrate the difficulty in measuring strain at failure)

Appendix 5.8: Effect of stress on strain rate (model joint) at 29, and 125°C

Appendix 5.9: Tables of separate measurements of creep strain occurring in each regime and accumulative measurements of creep strain occurring in each regime (model joint)

Appendix 5.10: Percentage of creep life in each regime as determined by creep strain (omitting instantaneous strain)

Appendix 6.1: Trend lines for figures using a 'best fit' plot.

**Appendix 1.1**

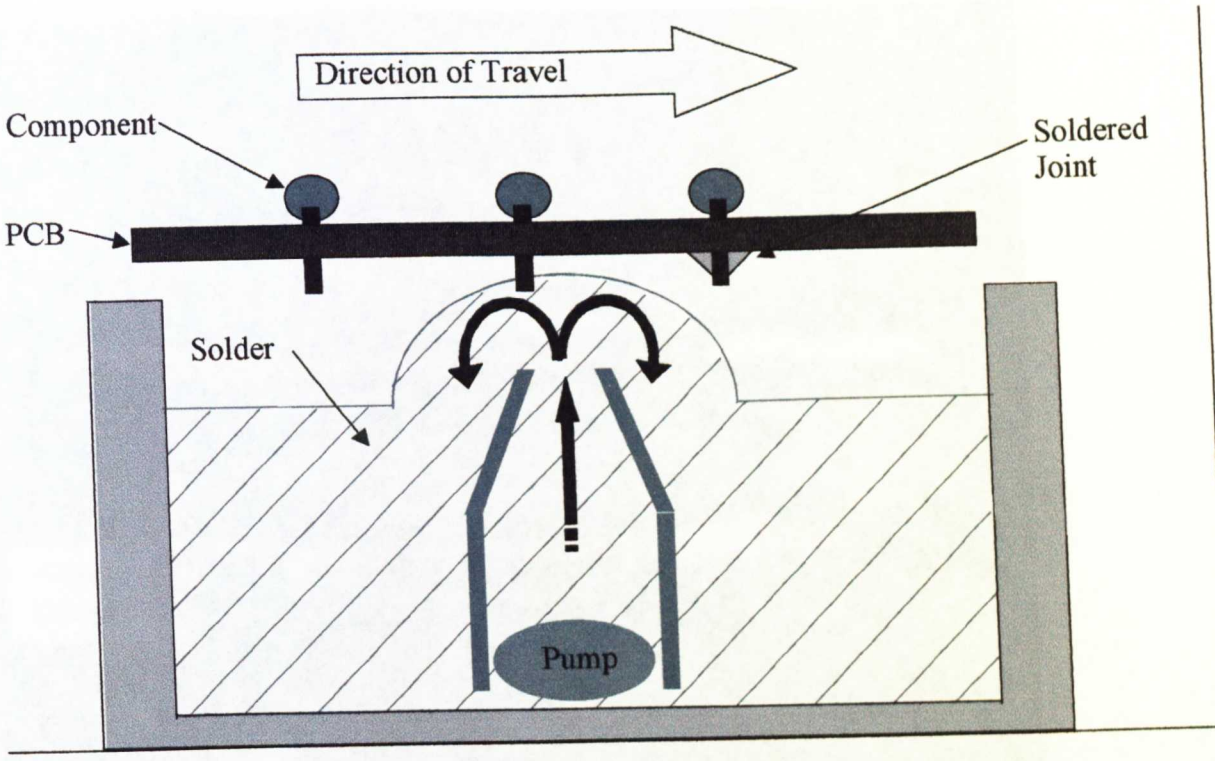


*The wave soldering process*

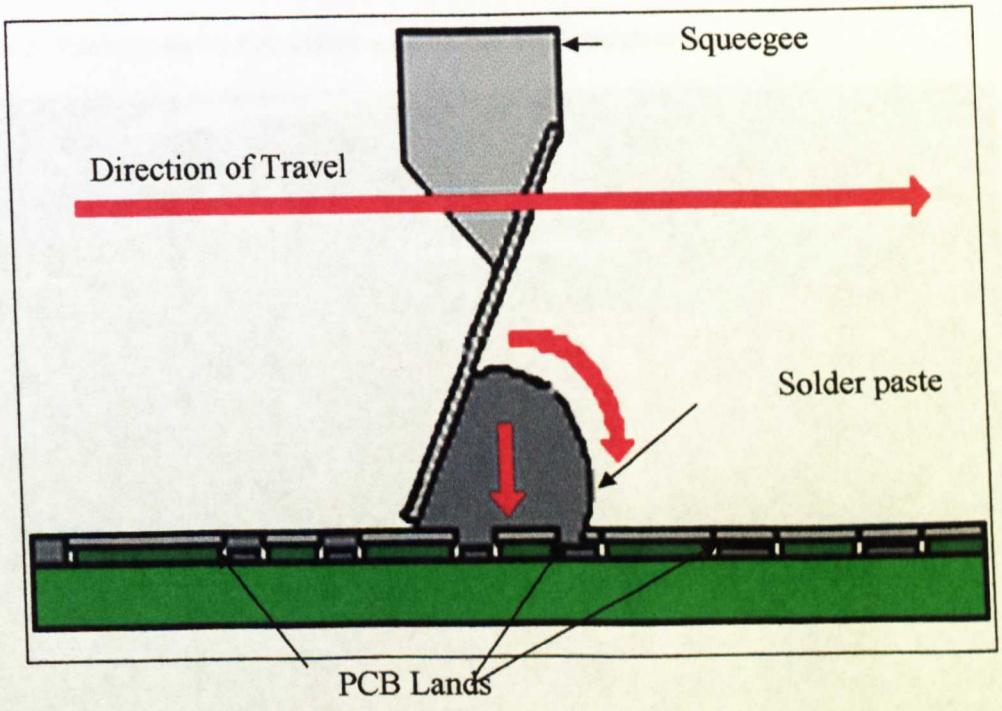


*Illustration of screen printing onto a PCB (SMT).*

*(source: www.smtinfocus.com)*

**Appendix 4.1**

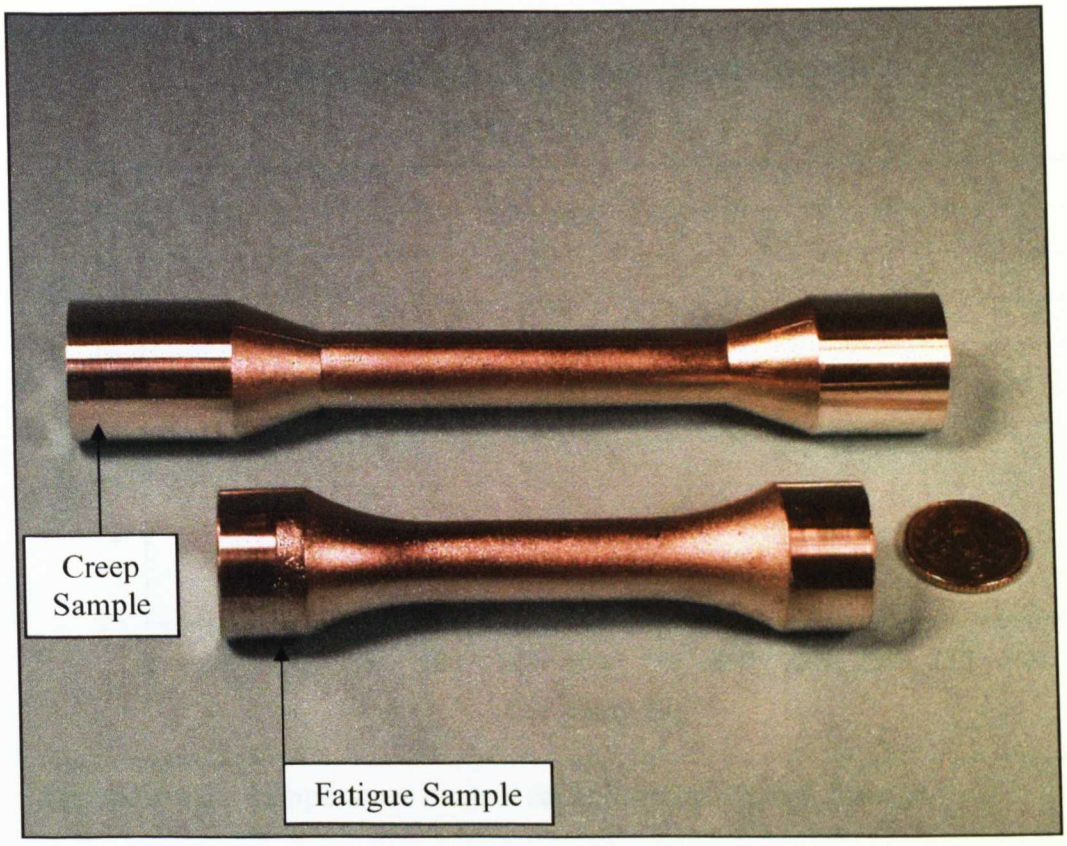


Plate 4.1: Photograph of specimens used in the SRG programme

Plate 4.2: Photograph of the Open University Creep Facility

**Appendix 4.2 and 4.3**

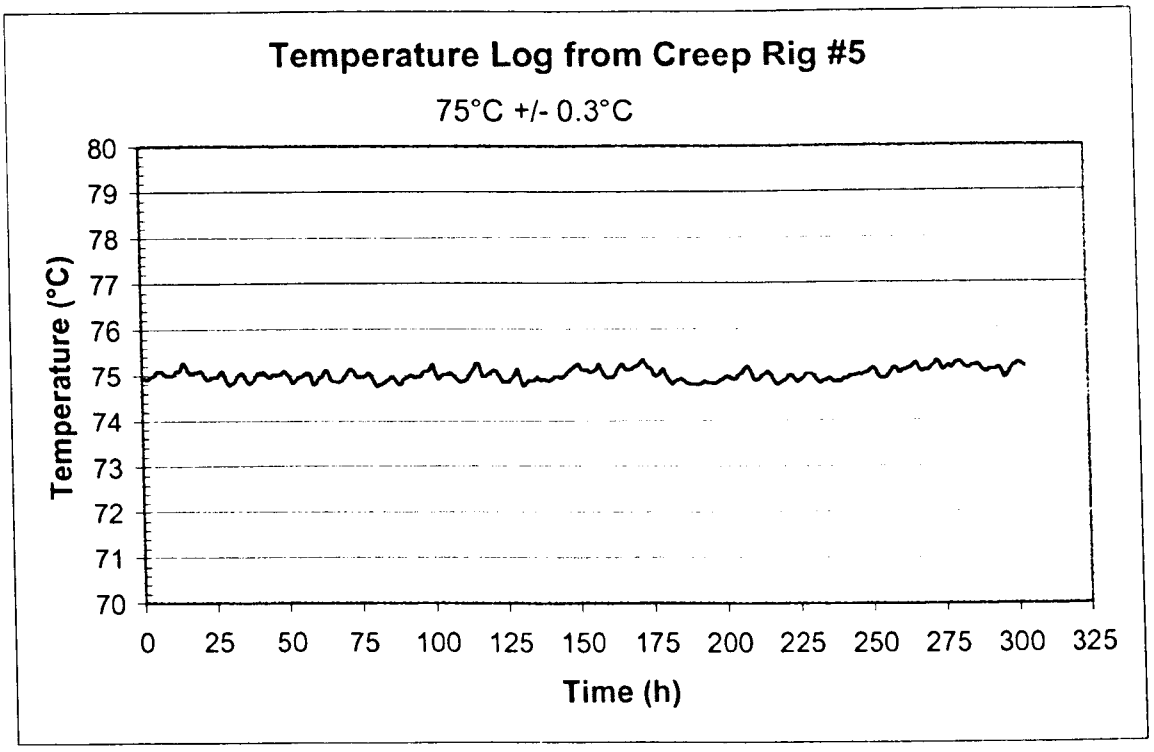


Appendix 4.2 Temperature control capabilities of a creep furnace

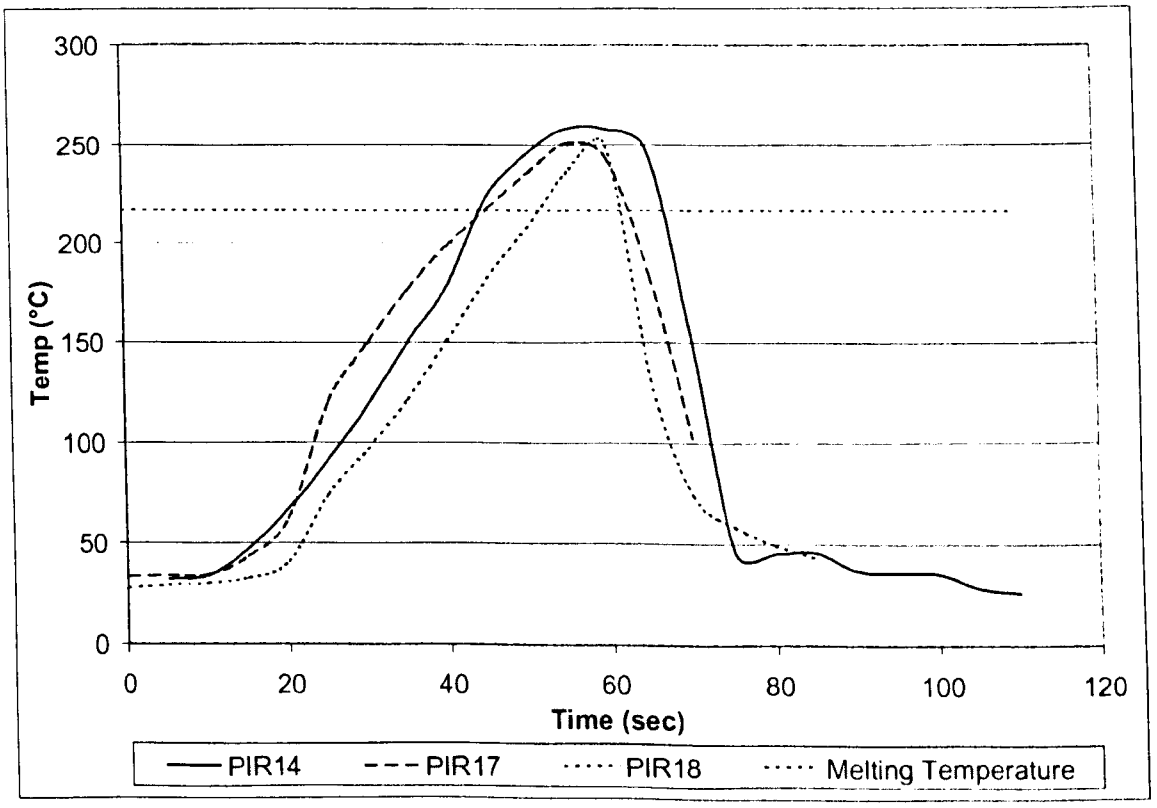


Appendix 4.3 Heating profile for model joint manufacture

**Appendix 4.4**

Photograph of pin in ring model joint specimen

**Appendix 4.5**

*Calculation of Shear Stress Values for Creep Testing*

| | | |
|---|---|---|
| $R_p$ | = | radius of pin (3mm) |
| h | = | height of solder (5mm) |
| t | = | solder layer thickness (1mm) |
| $R_s$ | = | radius of pin + solder thickness (4mm) |
| $A_p$ | = | area of pin |
| $A_s$ | = | area of pin + solder |

Area of solder = $h \times 2\pi r$ ($h \times 2\pi R_p$ or $h \times 2\pi R_s$)

$$\frac{A_p}{A_s} = \frac{h.2\pi R_p}{h.2\pi(R_p + t)} = \frac{R_p}{R_p + t}$$

$$\frac{A_s}{A_p} = \frac{R_p + t}{R_p} = 1 + \frac{t}{R_p}$$

The larger the radius of the pin the less difference in $\tau_p$ and $\tau_s$ i.e. the shear stress, $\tau$, at the pin/solder interface is greater than at the ring/solder interface and failure will preferentially occur at the former location (the pin/solder interface), as proven in experimental work.

If, h = 5mm, $R_p$ = 3mm, t = 1mm, and $R_s$ = 4mm
Area at pin/solder interface = $5 \times 2\pi 3 = 94.2mm^2$

$\tau = F/A$
$\tau = F/94.2mm^2$

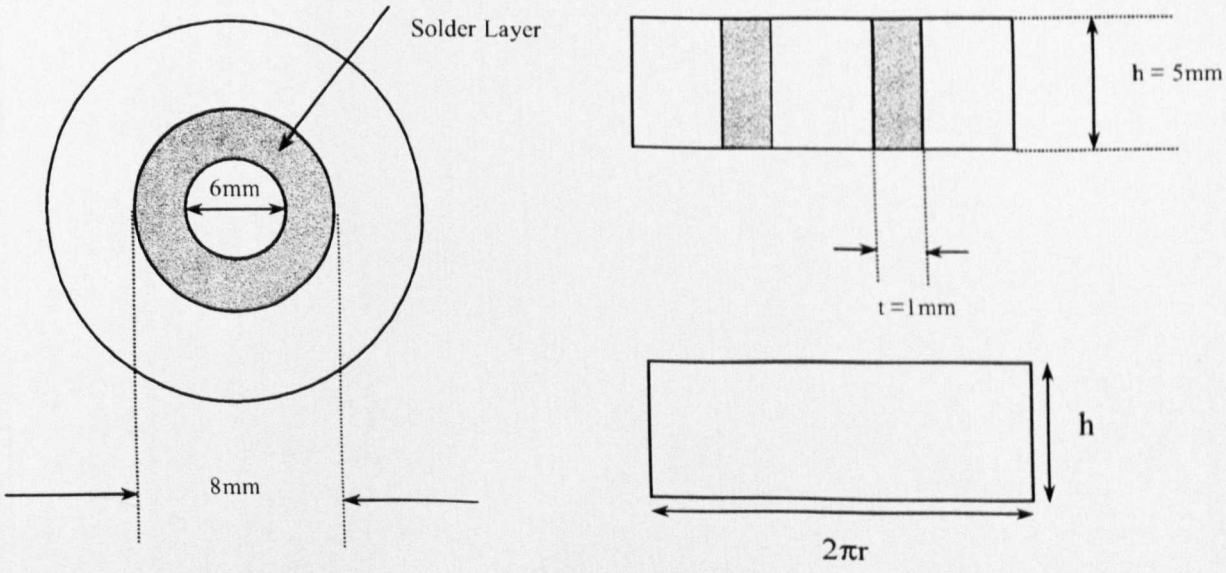

APPENDIX 4.6 : DETAILED ILLUSTRATION OF MOUNTING CONFIGURATION FOR JOINT CREEP TESTING.

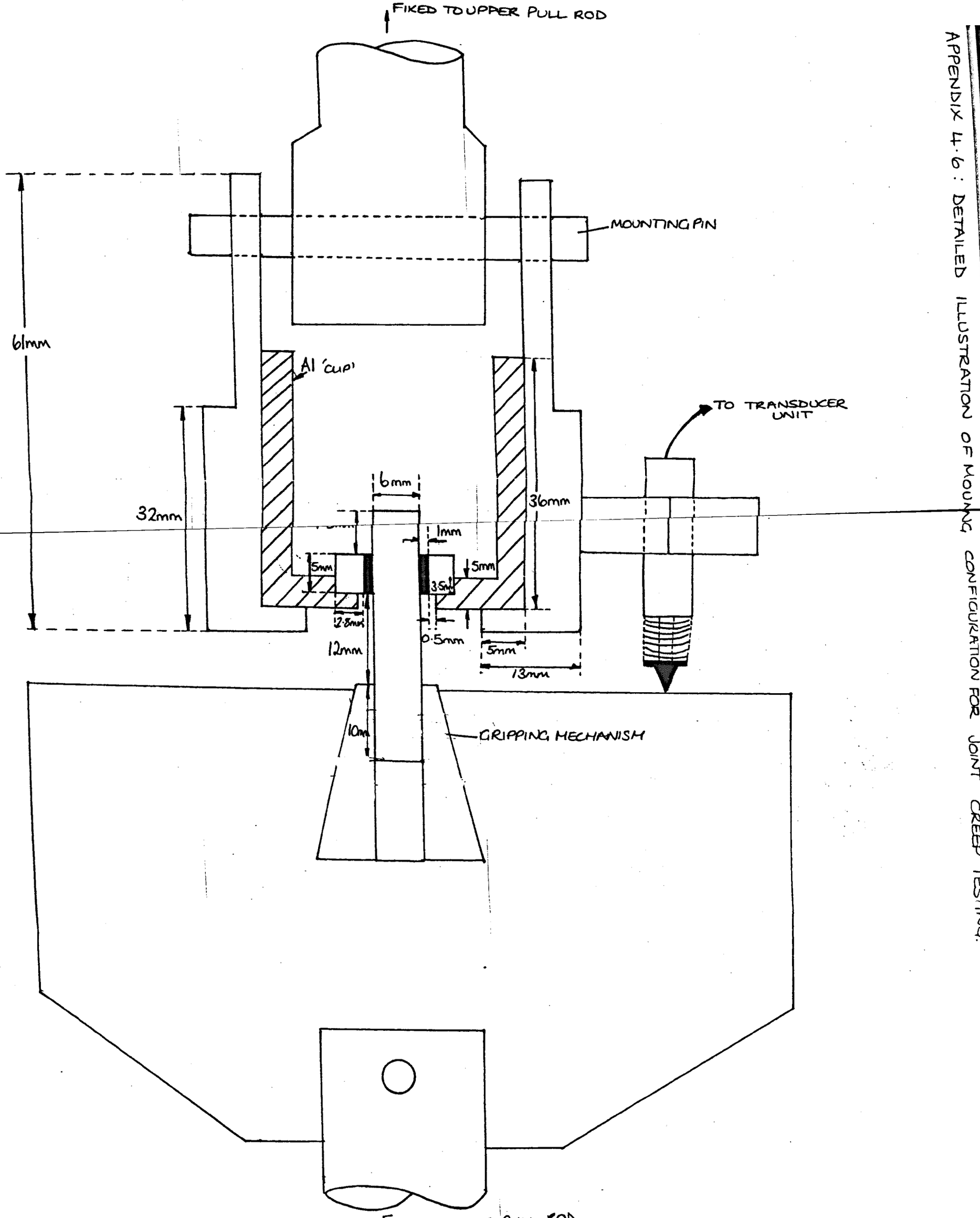

**Appendix 4.7**

*'Investigation of 'large' instantaneous strains occurring on loading of model joints'*

Originally, it was assumed that due to the moduli of the materials used in both the 'pin in ring joint' and loading apparatus (table 1) any displacement would occur in the solder. However, on examination of strain versus time data obtained from model joint testing, it was determined that an unusually large strain occurred on the application of load (instantaneous strain). To investigate the extent of displacement occurring simply within the solder, a solid copper replica of the sample was manufactured and tested in the same manner as a 'pin in ring' sample. It was expected that to obtain the representative displacement of solder, the displacement observed in the copper should be subtracted from the 'original' instantaneous strain.

| Material | Elastic Modulus (RT) GPa |
|---|---|
| SnAgCu Solder | 50.86[105] |
| Copper | 130[106] |
| Aluminium (loading apparatus) | 70[106] |

Table 1 Elastic moduli of materials used in model joint creep tests

Four samples were examined at each test temperature (29 and 75°C), at loads of 500, 1000, 2000 and 3000 Newtons. For the purpose of analysis, it was assumed that the maximum stress would be in shear and occur in the same region as that determined in the 'pin in ring' joints. Therefore, by dividing by a cross sectional area of 94.2mm$^2$ (appendix 4.5) values for shear stress were determined (5.3, 10.6, 21.2, 31.8MPa) and were representative of actual test conditions. In total, each individual sample was loaded six times. Although the first load was most representative of the

actual testing procedure, additional loads were useful in determining any elastic deformation.

Figure 1 represents the initial displacement ($d_i$) and plastic displacement ($d_p$) at each test temperature (after the first load). Some plastic deformation is evident where the gripping mechanism 'bites' into the copper pin area, this would occur on loading. Some of the measured plastic deformation may also be caused by the slipping of this grips also on loading. Deformation increased linearly with increasing applied stress. An increase in temperature also caused an increase in displacement. Subsequent loading produced very little differences between '$d_i$ and $d_p$', i.e. little to no plastic deformation, and the subsequent displacements were termed '$d_s$'. Therefore, it was assumed that '$d_s$' represented elastic deformation occurring during subsequent loading. By subtracting '$d_p$ from $d_i$' (obtained from the initial load) a representative value for the elastic deformation on loading could be determined and should be similar in value to '$d_s$'. To investigate this assumption '$d_i$-$d_p$' and '$d_s$' were plotted versus stress for each temperature, figure 2 a and b.

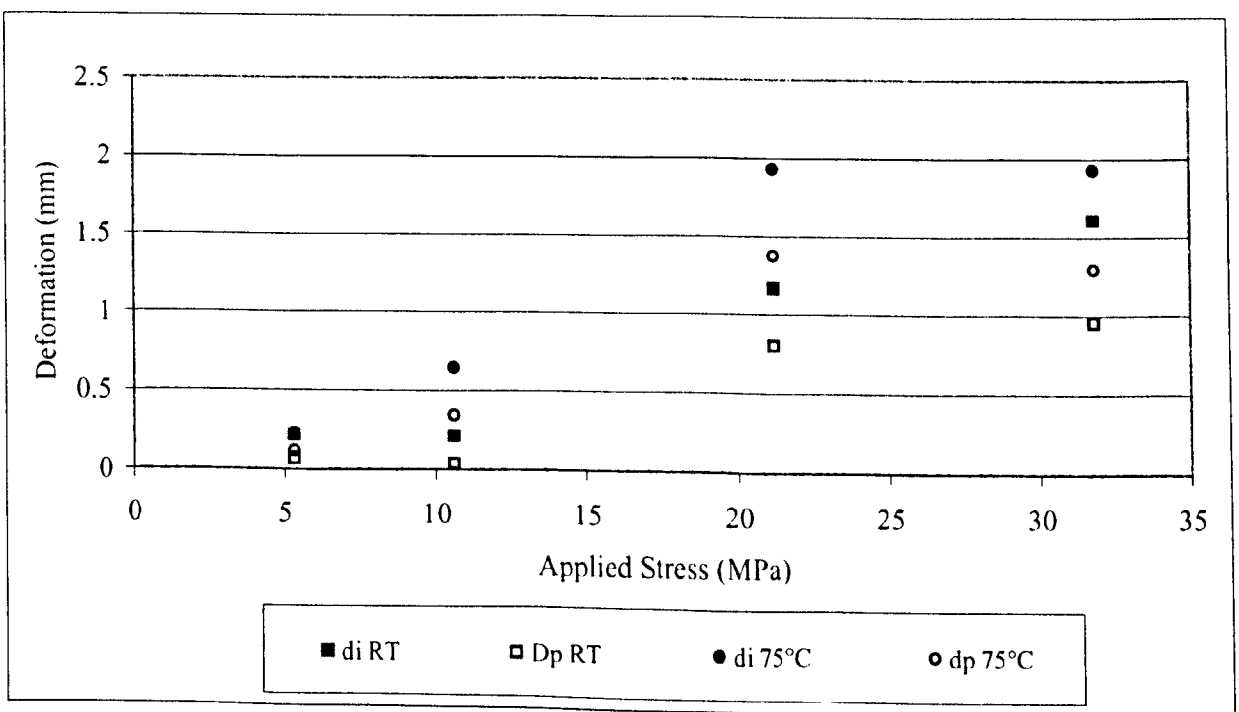


Figure 1 Displacement occurring on the application and removal of the initial load

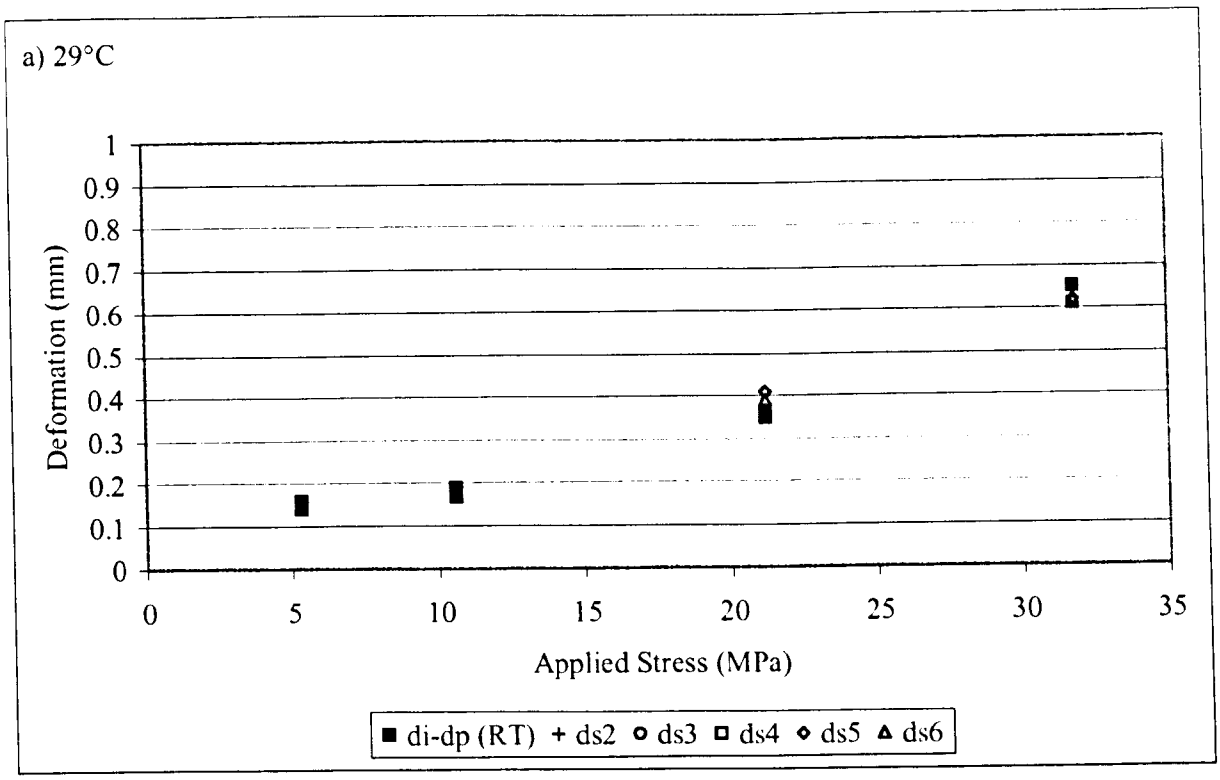


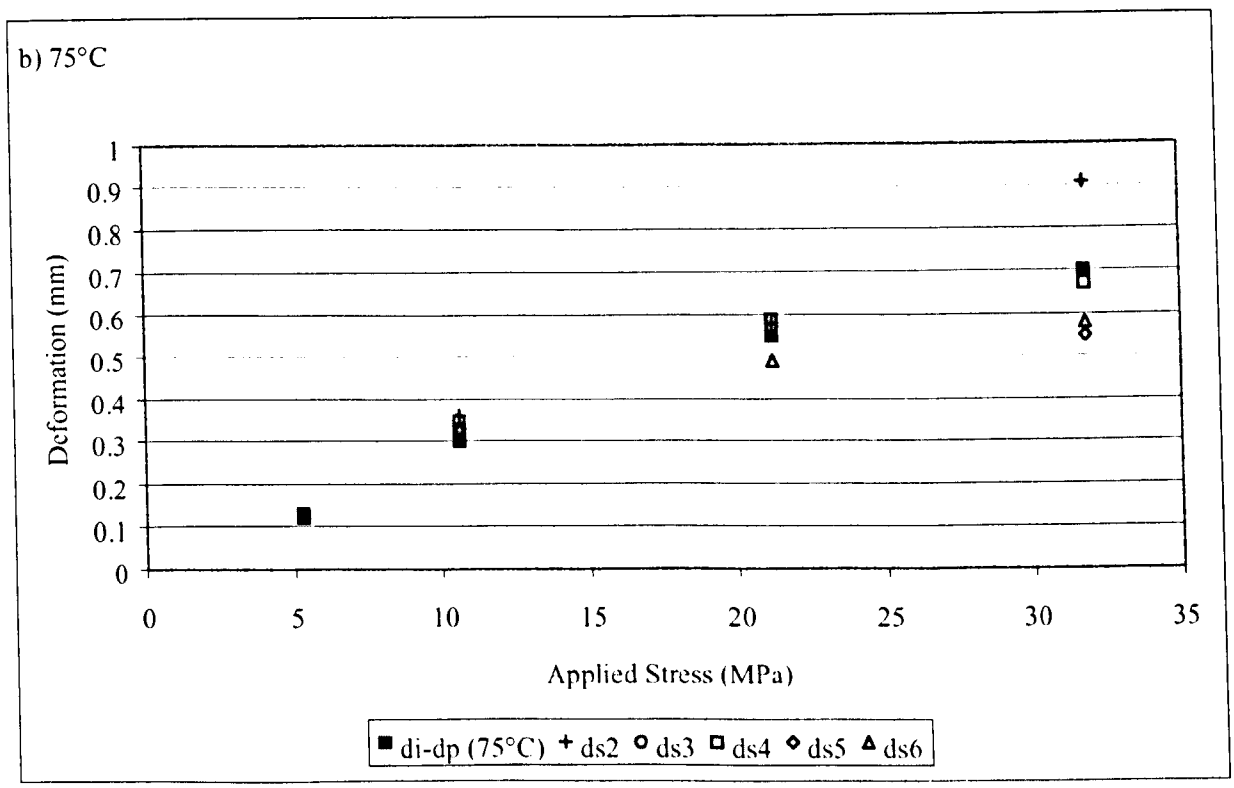


Figure 2 a and b Comparison of elastic displacements occurring during the testing of pure copper a) at 29°C and b) at 75°C

Although this assumption proved to be legitimate at low applied stress, figure 2 illustrates that the scatter in elastic displacements increases with increasing stress and temperature i.e. during these tests the greatest scatter occurred at 31.8MPa and 75°C.

By using the data collated, the elastic modulus of copper was calculated to confirm results. It was assumed that the copper replica was a solid cylinder (radius of 3mm and a height of 12mm) and was loaded in tension. From these dimensions and the known loads, stress and strain were calculated see table 2 and figure 3.

| | | Elastic Deformation (mm) | | Strain (orig l 12mm) | |
|---|---|---|---|---|---|
| Actual Load (N) (25:1 ratio) | Stress (X-sect area: 28.3mm$^2$ )MPa | $d_i$-$d_p$ (RT) | $d_i$-$d_p$ (75°C) | $d_i$-$d_p$ (RT) | $d_i$-$d_p$ (75°C) |
| 500 | 17.68 | 0.14 | | 0.01167 | |
| 1000 | 35.37 | 0.17 | | 0.01417 | |
| 2000 | 70.74 | 0.36 | | 0.03000 | |
| 3000 | 106.10 | 0.65 | | 0.05417 | |
| 500 | 17.68 | | 0.12 | | 0.01000 |
| 1000 | 35.37 | | 0.3 | | 0.02500 |
| 2000 | 70.74 | | 0.55 | | 0.04583 |
| 3000 | 106.10 | | 0.7 | | 0.05833 |

Table 2 Calculation of stress and strain values used in the determination of the elastic modulus of copper

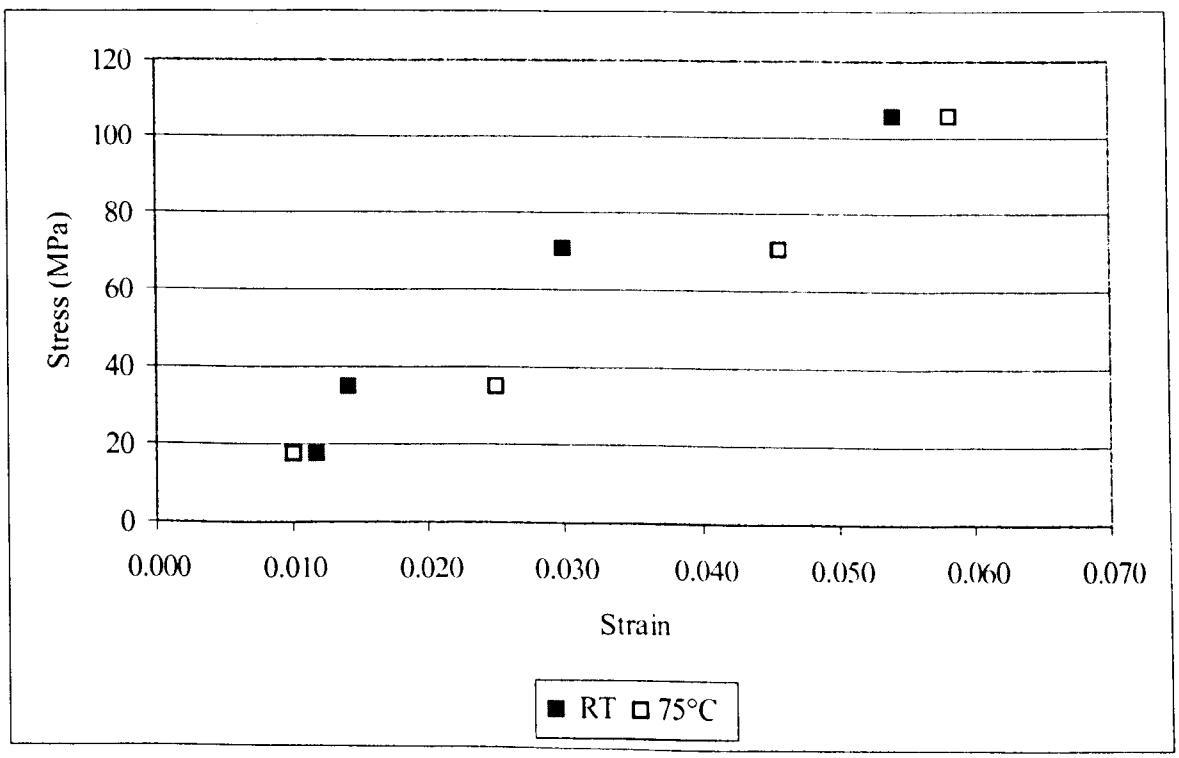


Figure 3 Determination of elastic modulus at room temperature and 75°C

Values for elastic modulus were established from the gradients of the trend lines produced in figure 3. These ranged from 1.80 GPa at 75°C to 1.97GPa at room temperature. These values are approximately one hundred times less the value of elastic modulus previously stated, which suggested that deformation might also occur elsewhere in the loading mechanism, e.g. in the aluminium. Using the elastic modulus previously stated for copper, an estimation of the additional displacement could be established (assuming that there was no deflection in the 'ring' part of the copper replica) see formula below. Displacements of up to 0.7mm (at high stress) were estimated and were assumed to occur in the aluminium or elsewhere within the loading mechanism. The aluminium part was visually examined for signs of deformation after testing, but no conclusions could be made.

Due to this uncertainty concerning the measurement of displacements caused on loading, for the purpose of pin in ring evaluation all instantaneous strain was omitted i.e. only creep strain was analysed.

| | | |
|---|---|---|
| $\sigma$ | = | Stress |
| $\varepsilon$ | = | Strain |
| E | = | Elastic modulus (130GPa) |
| L | = | Load |
| A | = | Area |
| D | = | Displacement |
| $D_0$ | = | Original length (12mm) |
| $D_{exp}$ | = | Experimental displacement |
| $D_{Cu}$ | = | Copper displacement |
| $D_{add}$ | = | Additional displacement |

$E = \sigma/\varepsilon$ $\quad \sigma = L/A$ $\quad \varepsilon = D/D_0$

$\varepsilon = D_{Cu}/12$

$\varepsilon = \sigma/E = L/(A.E)$ $\quad \therefore L/(A.E) = D_{Cu}/12$ $\quad \therefore D_{Cu} = 12.(L/(A.E))$

$\therefore \mathbf{D_{add} = D_{exp} - D_{Cu}}$

Appendix 5.1

## BULK SOLDER TESTING LOG

| Temperature °C | Stress MPa | Time to Rupture (h) | Strain to Failure | Minimum Strain Rate ($h^{-1}$) |
|---|---|---|---|---|
| -10 | 50 | 29.5 | 0.178 | 0.0018 |
| -10 | 45 | 115.2 | 0.188 | 0.00032 |
| -10 | 40 | 1148.5 | 0.195 | 0.00002437 |
| -10 | 38 | 2027.67 | 0.213 | 0.00001642 |
| 29 | 45 | 0.24 | 0.301 | 0.21053 |
| 29 | 42.5 | 1.78 | 0.173 | 0.012195 |
| 29 | 41 | 7.29 | 0.188 | 0.001626 |
| 29 | 40 | 1.42 | 0.223 | 0.011905 |
| 29 | 35 | 6.21 | 0.209 | 0.003012 |
| 29 | 32 | 40.01 | 0.190 | 0.00015060 |
| 29 | 30 | 694.25 | 0.169 | 0.00000735 |
| 29 | 28 | 284.02 | 0.147 | 0.00003401 |
| 29 | 26 | 775.56 | 0.154 | 0.00000828 |
| 75 | 33 | 0.43 | 0.212 | 0.0731707 |
| 75 | 27 | 1.25 | 0.310 | 0.01190480 |
| 75 | 24 | 34.33 | 0.110 | 0.00018380 |
| 75 | 23.5 | 6.43 | 0.280 | 0.00119050 |
| 75 | 21 | 20.25 | 0.233 | 0.00026880 |
| 75 | 19.5 | 43.31 | 0.136 | 0.00012630 |
| 75 | 19 | 355.53 | 0.125 | 0.00001530 |
| 75 | 16 | 443.36 | 0.198 | 0.00000351 |
| 75 | 12 | 2121 | 0.107 | 0.00000550 |
| 99.4 | 27 | 0.09 | 0.390 | 0.6829 |
| 99.4 | 25.25 | 2.82 | 0.222 | 0.005854 |
| 99.4 | 25 | 4.22 | 0.188 | 0.003658 |
| 99.4 | 20 | 6.07 | 0.238 | 0.0036646 |
| 99.4 | 17 | 136.13 | 0.134 | 0.001659 |
| 99.4 | 15 | 306.95 | 0.124 | 0.00007817 |
| 99.4 | 14 | 758.42 | 0.113 | 0.000001478 |
| 125 | 25 | 0.25 | 0.29 | 0.1204819 |
| 125 | 22.5 | 0.20 | 0.263 | 0.1445783 |
| 125 | 20 | 3.57 | 0.251 | 0.004878 |
| 125 | 18 | 0.65 | 0.285 | 0.0243902 |
| 125 | 12 | 147.77 | 0.142 | 0.0001626 |
| 125 | 10 | 558.8 | 0.138 | 0.00000412 |
| 125 | 8 | 3528.03 | 0.137 | 0.00000423 |

Data at –10°C

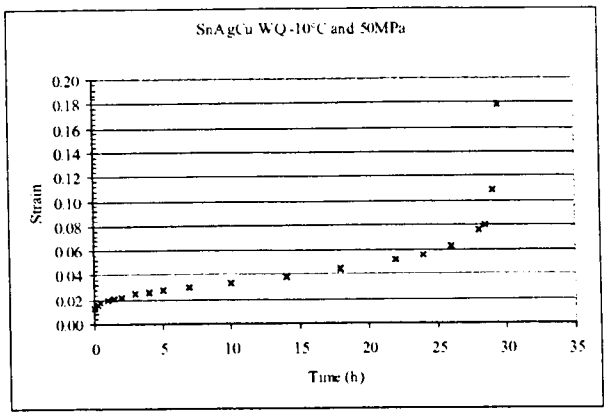
SnAgCu WQ -10°C and 50MPa
Strain
Time (h)

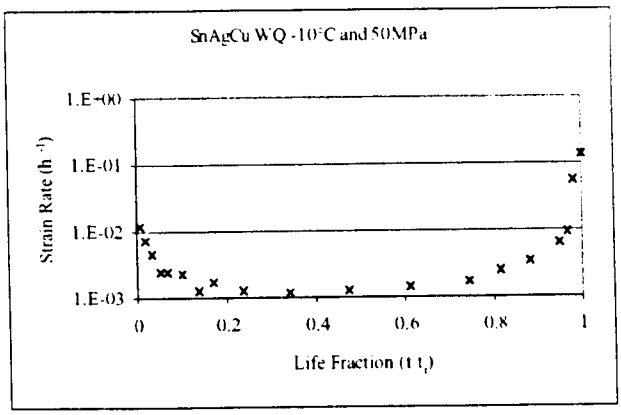
SnAgCu WQ -10°C and 50MPa
Strain Rate (h⁻¹)
Life Fraction (t/t_f)

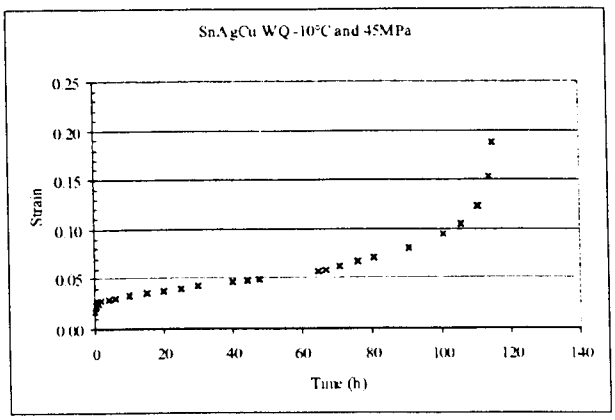
SnAgCu WQ -10°C and 45MPa
Strain
Time (h)

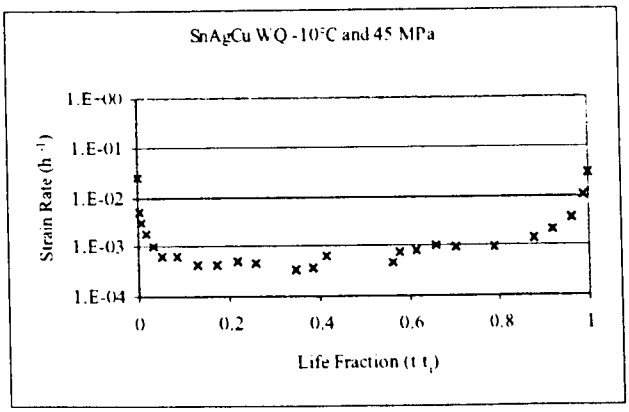
SnAgCu WQ -10°C and 45 MPa
Strain Rate (h⁻¹)
Life Fraction (t/t_f)

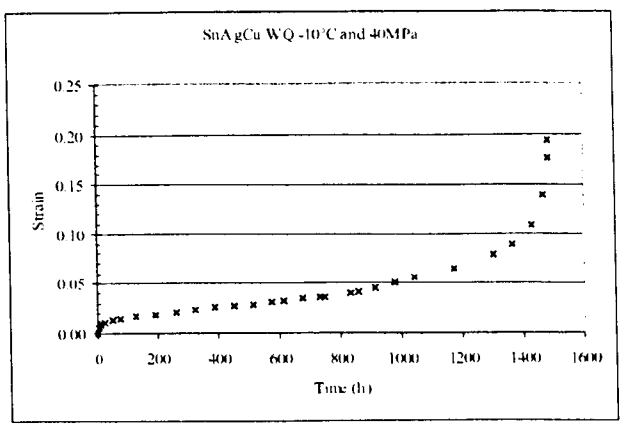
SnAgCu WQ -10°C and 40MPa
Strain
Time (h)

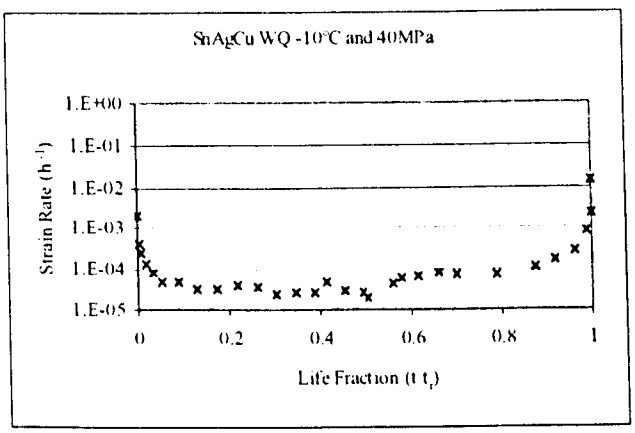
SnAgCu WQ -10°C and 40MPa
Strain Rate (h⁻¹)
Life Fraction (t/t_f)

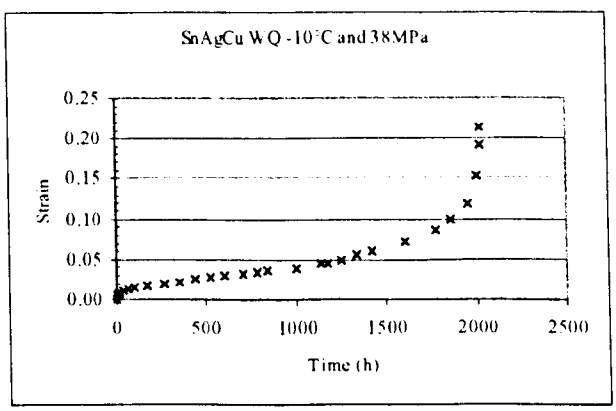
SnAgCu WQ -10°C and 38MPa
Strain
Time (h)

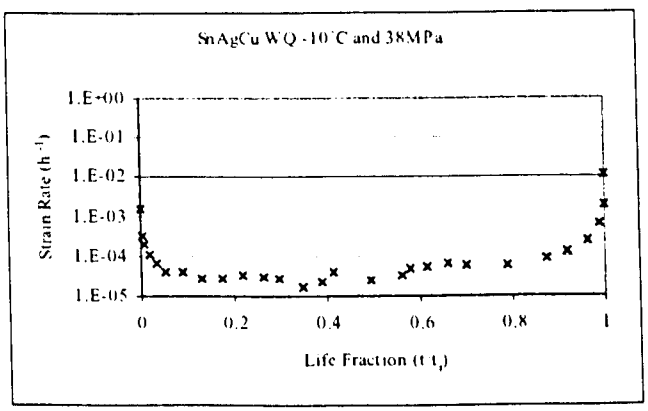
SnAgCu WQ -10°C and 38MPa
Strain Rate (h⁻¹)
Life Fraction (t/t_f)

Data at 29°C

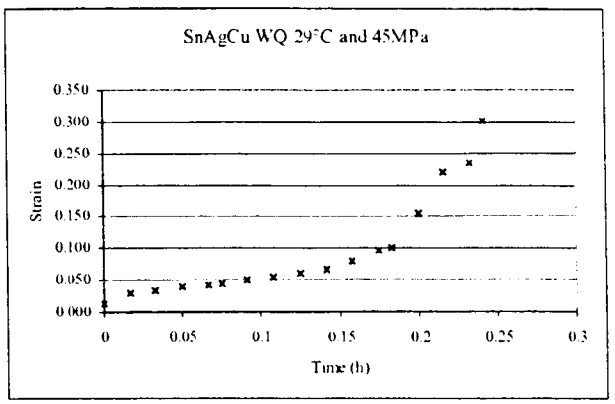
SnAgCu WQ 29°C and 45MPa
Strain
Time (h)

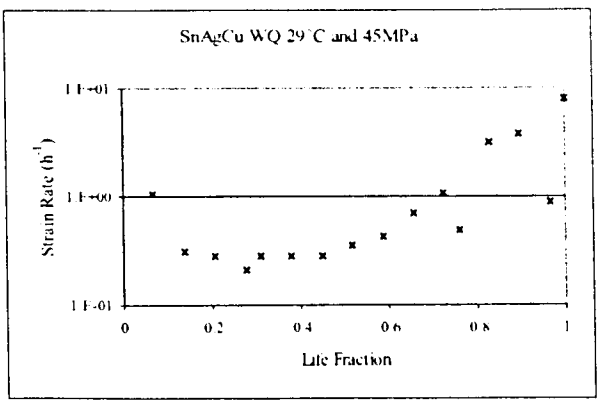
SnAgCu WQ 29°C and 45MPa
Strain Rate (h-1)
Life Fraction

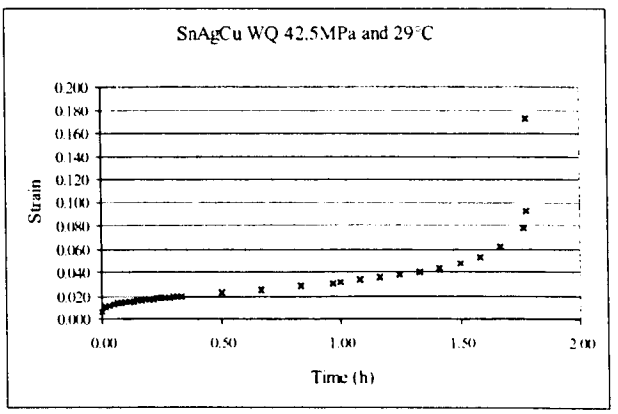
SnAgCu WQ 42.5MPa and 29°C
Strain
Time (h)

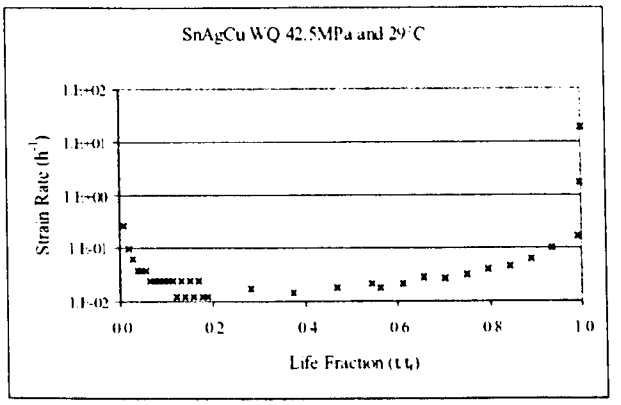
SnAgCu WQ 42.5MPa and 29°C
Strain Rate (h-1)
Life Fraction (tt)

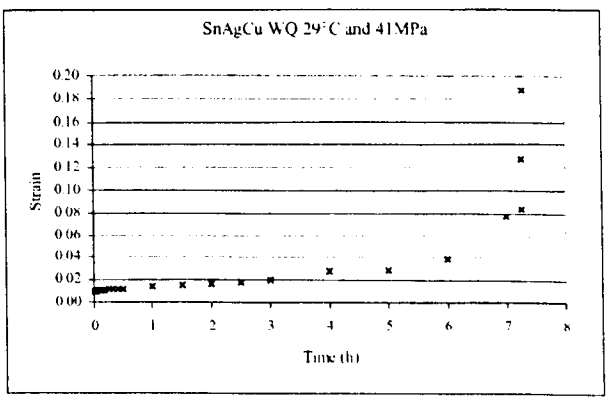
SnAgCu WQ 29°C and 41MPa
Strain
Time (h)

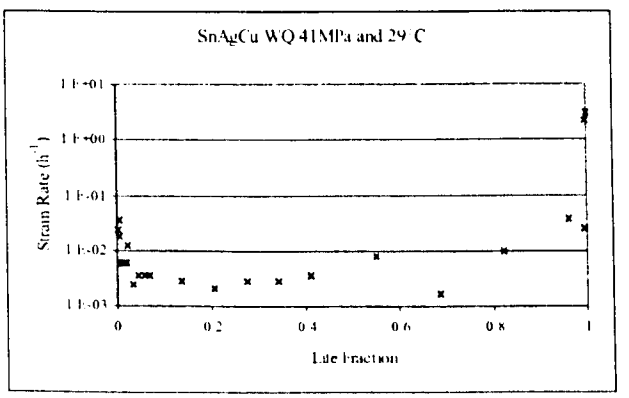
SnAgCu WQ 41MPa and 29°C
Strain Rate (h-1)
Life Fraction

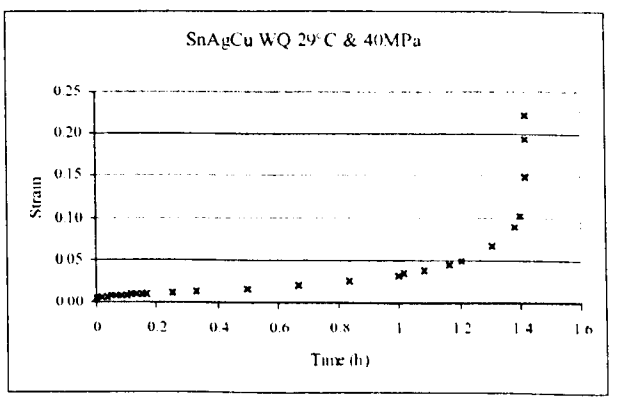
SnAgCu WQ 29°C & 40MPa
Strain
Time (h)

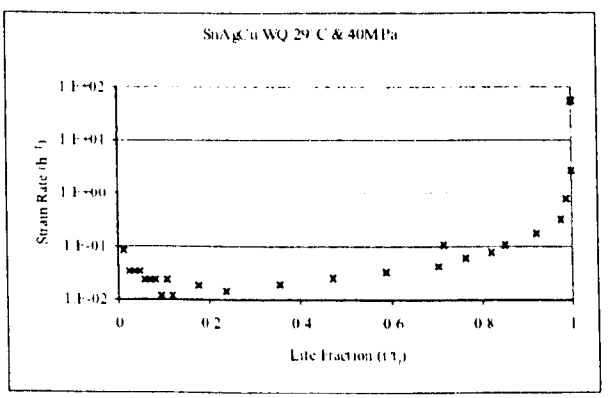
SnAgCu WQ 29°C & 40MPa
Life Fraction (tt)

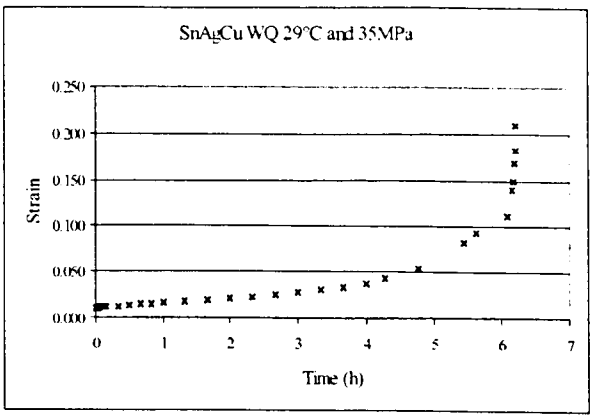
SnAgCu WQ 29°C and 35MPa
Strain
Time (h)

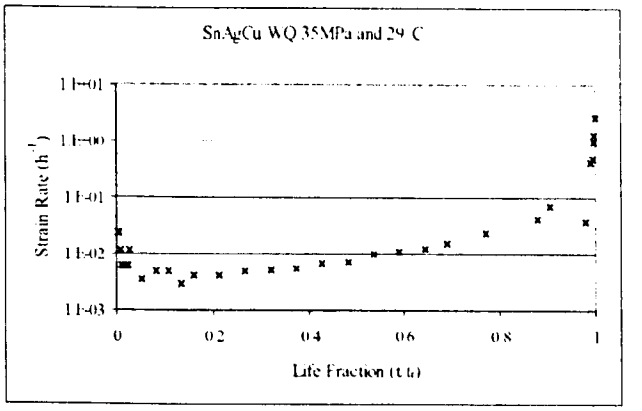
SnAgCu WQ 35MPa and 29°C
Strain Rate (h⁻¹)
Life Fraction (t/tf)

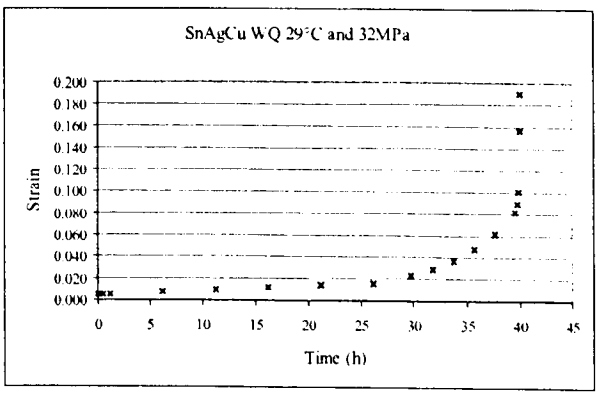
SnAgCu WQ 29°C and 32MPa
Strain
Time (h)

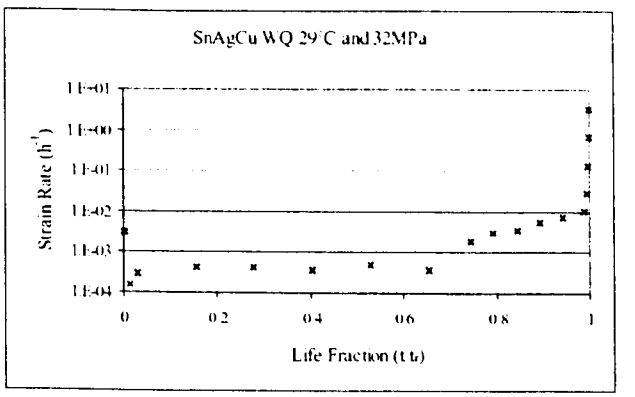
SnAgCu WQ 29°C and 32MPa
Strain Rate (h⁻¹)
Life Fraction (t/tf)

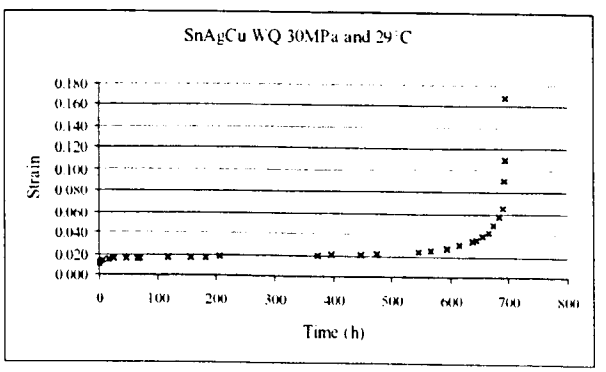
SnAgCu WQ 30MPa and 29°C
Strain
Time (h)

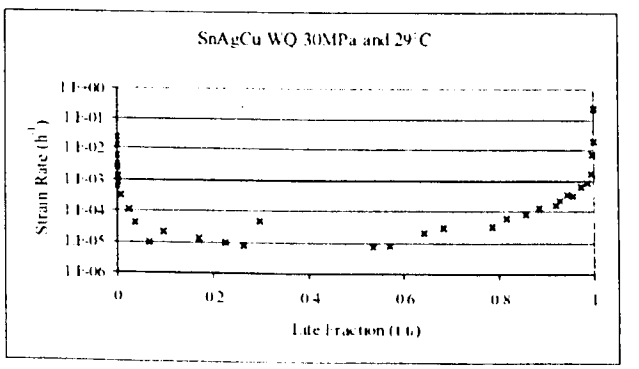
SnAgCu WQ 30MPa and 29°C
Strain Rate (h⁻¹)
Life Fraction (t/tf)

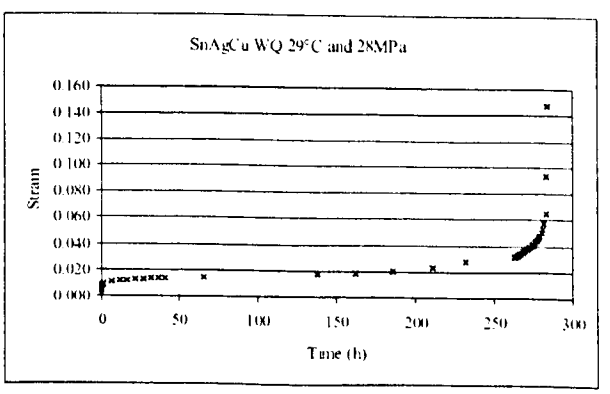
SnAgCu WQ 29°C and 28MPa
Strain
Time (h)

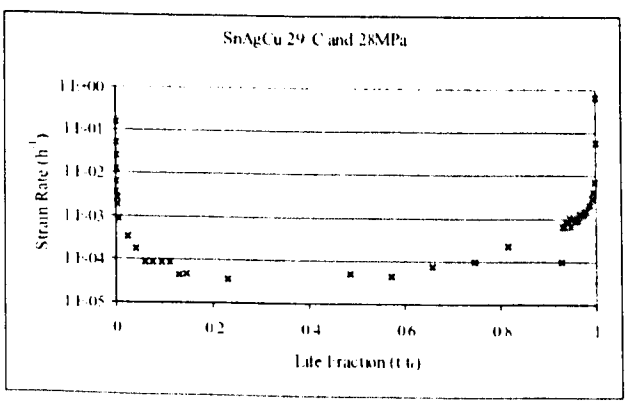
SnAgCu 29°C and 28MPa
Strain Rate (h⁻¹)
Life Fraction (t/tf)

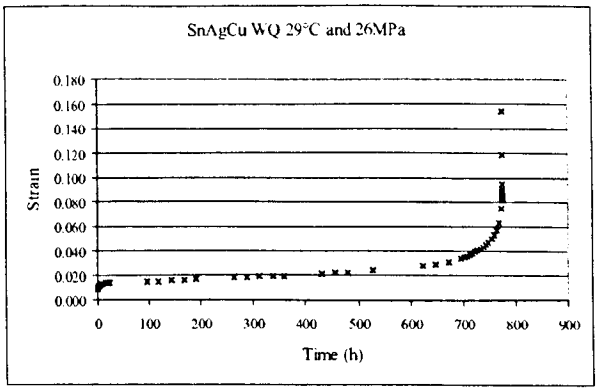
SnAgCu WQ 29°C and 26MPa
Strain
0.180
0.160
0.140
0.120
0.100
0.080
0.060
0.040
0.020
0.000
0
100
200
300
400
500
600
700
800
900
Time (h)

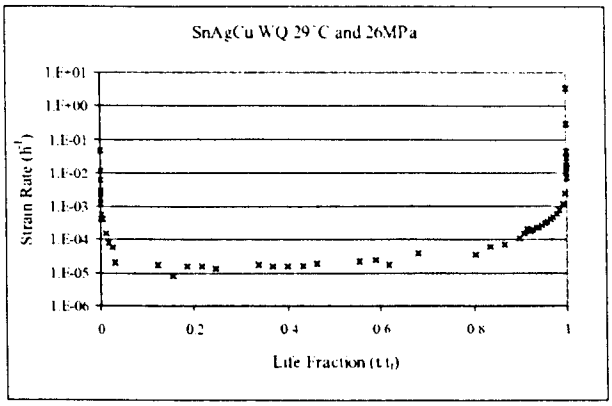
SnAgCu WQ 29°C and 26MPa
Strain Rate (h-1)
1E+01
1E+00
1E-01
1E-02
1E-03
1E-04
1E-05
1E-06
0
0.2
0.4
0.6
0.8
1
Life Fraction (t/tf)

Data at 75°C

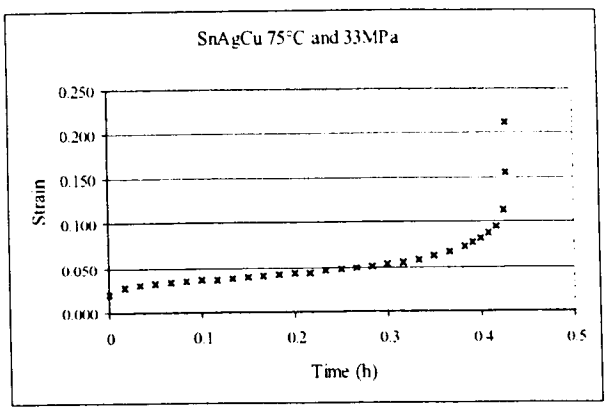
SnAgCu 75°C and 33MPa
Strain
Time (h)

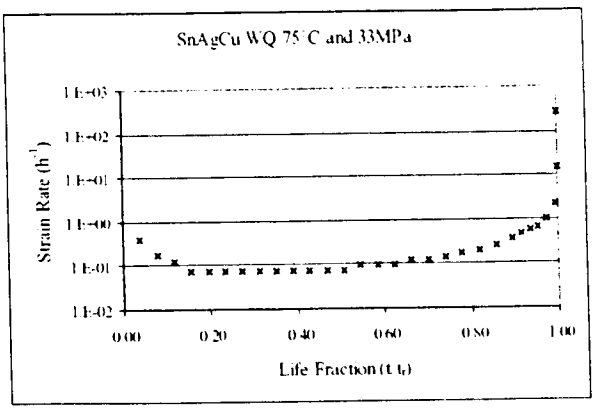
SnAgCu WQ 75°C and 33MPa
Strain Rate (h-1)
Life Fraction (t/tf)

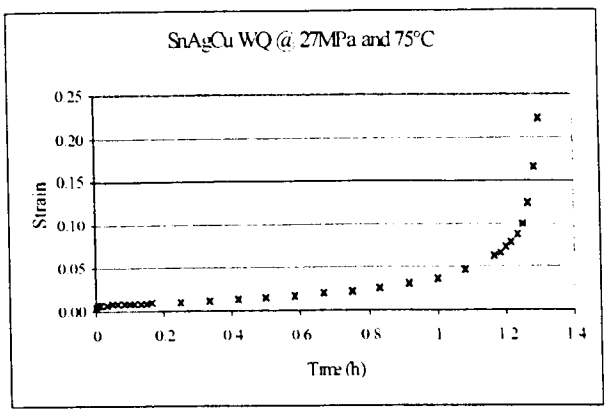
SnAgCu WQ @ 27MPa and 75°C
Strain
Time (h)

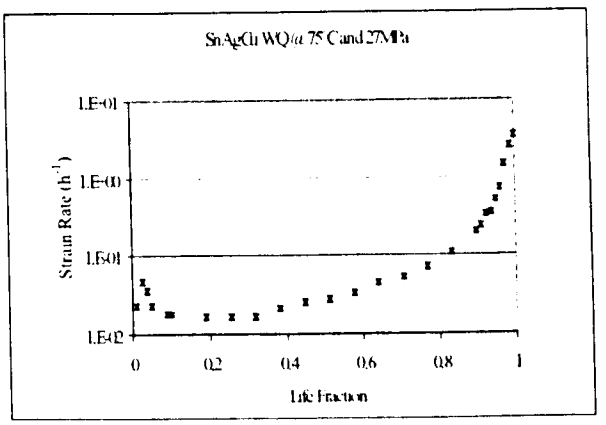
SnAgCu WQ@ 75 C and 27MPa
Strain Rate (h-1)
Life Fraction

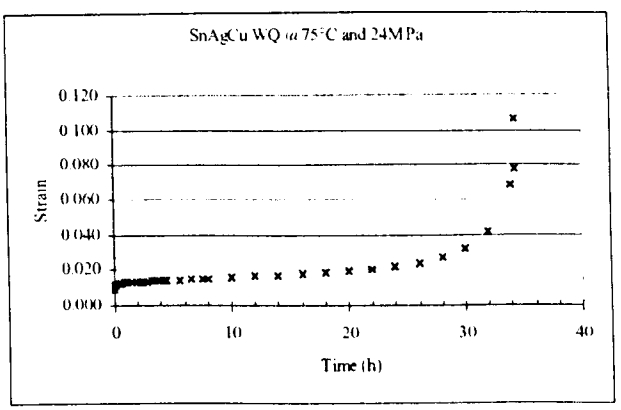
SnAgCu WQ @ 75°C and 24MPa
Strain
Time (h)

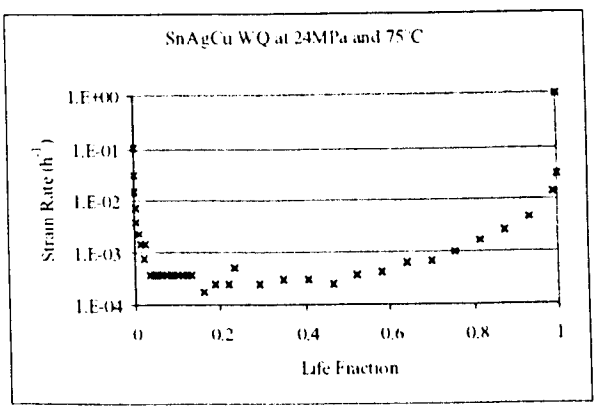
SnAgCu WQ at 24MPa and 75°C
Strain Rate (h-1)
Life Fraction

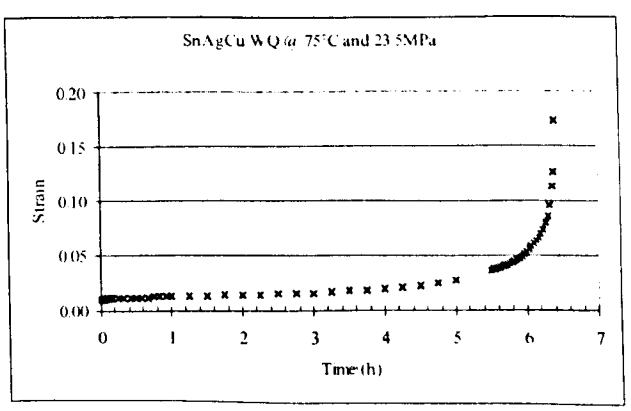
SnAgCu WQ @ 75°C and 23.5MPa
Strain
Time (h)

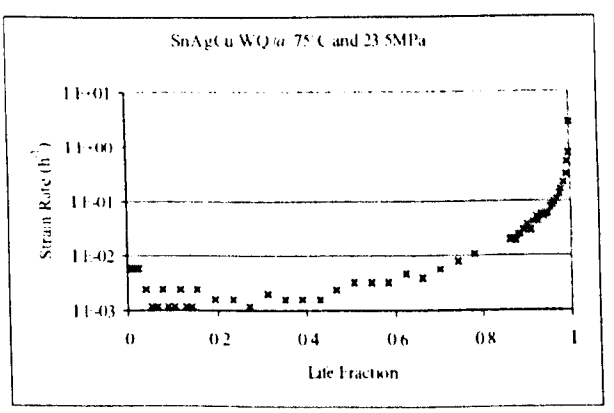
SnAgCu WQ @ 75°C and 23.5MPa
Strain Rate (h-1)
Life Fraction

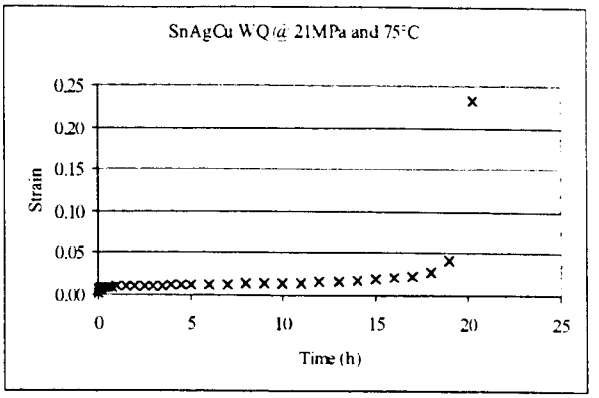
SnAgCu WQ @ 21MPa and 75°C
Strain
Time (h)

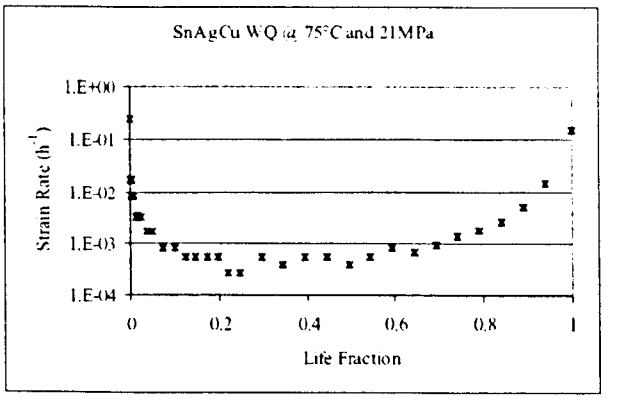
SnAgCu WQ @ 75°C and 21MPa
Strain Rate (h⁻¹)
Life Fraction

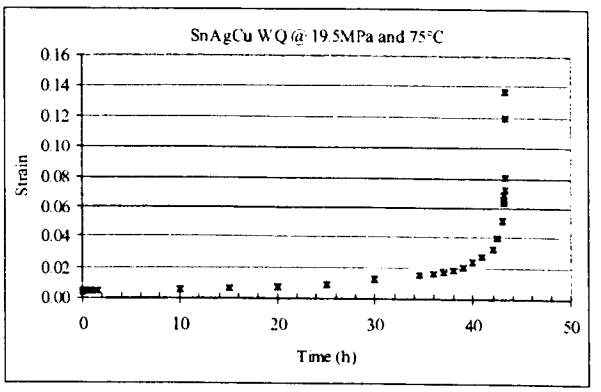
SnAgCu WQ @ 19.5MPa and 75°C
Strain
Time (h)

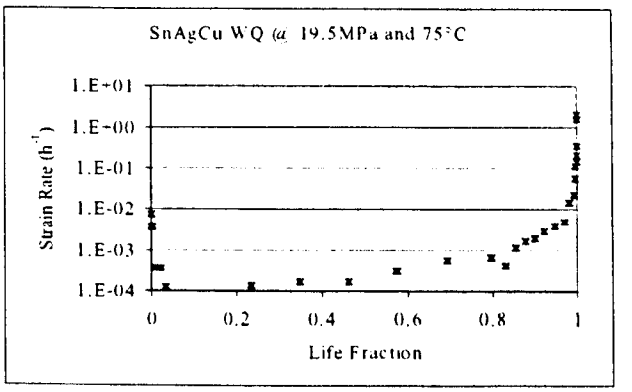
SnAgCu WQ @ 19.5MPa and 75°C
Strain Rate (h⁻¹)
Life Fraction

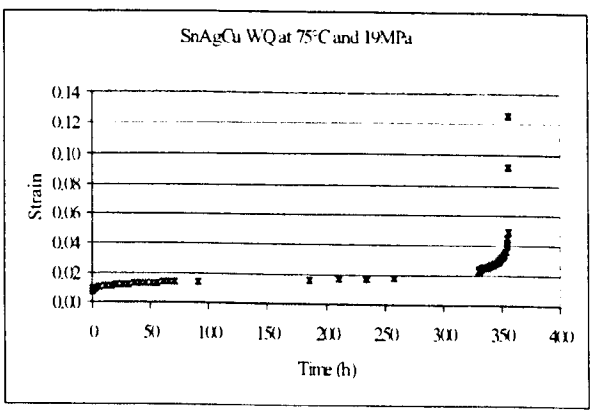
SnAgCu WQ at 75°C and 19MPa
Strain
Time (h)

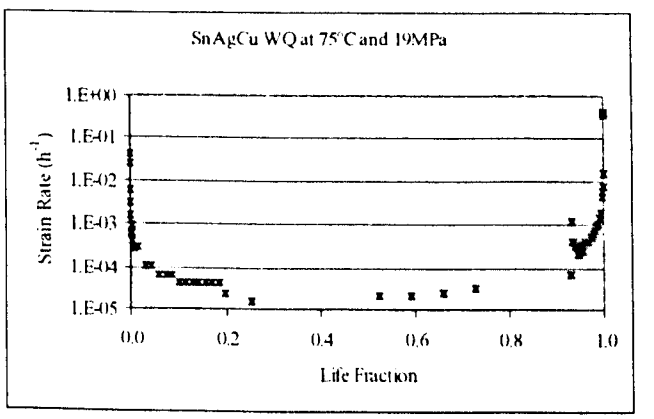
SnAgCu WQ at 75°C and 19MPa
Strain Rate (h⁻¹)
Life Fraction

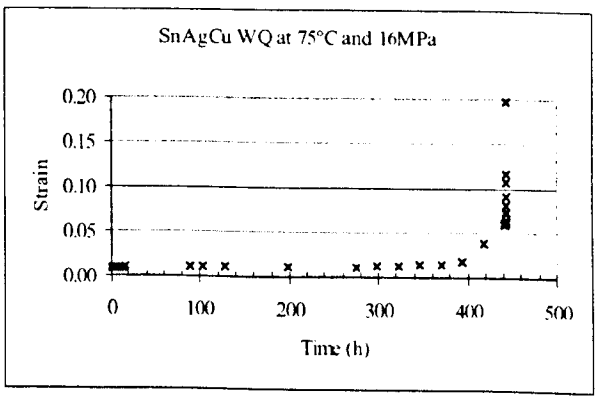
SnAgCu WQ at 75°C and 16MPa
Strain
Time (h)

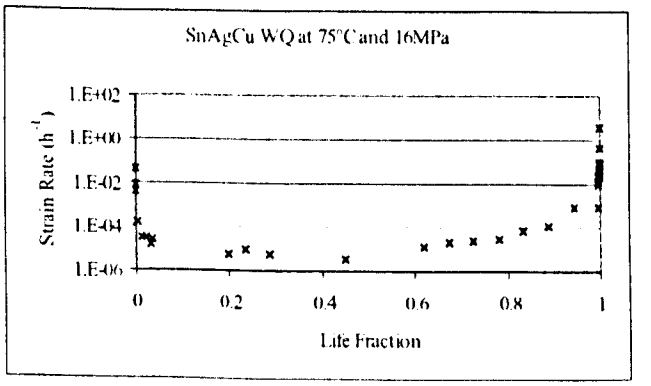
SnAgCu WQ at 75°C and 16MPa
Strain Rate (h⁻¹)
Life Fraction

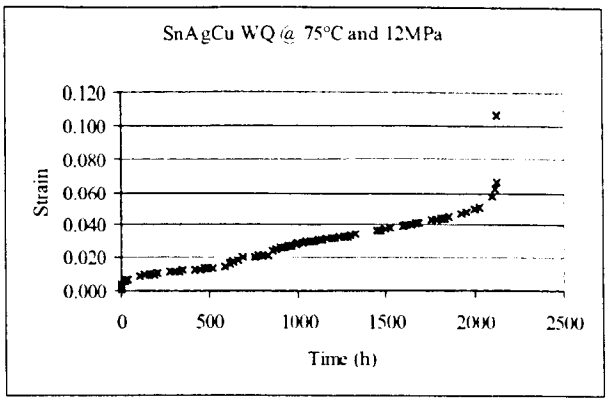
SnAgCu WQ @ 75°C and 12MPa
Strain
0.120
0.100
0.080
0.060
0.040
0.020
0.000
0
500
1000
1500
2000
2500
Time (h)

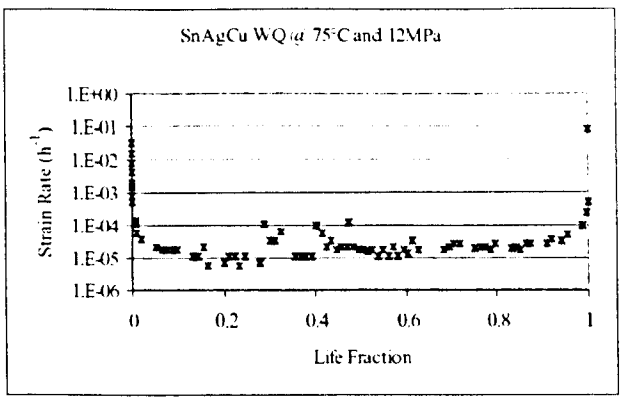
SnAgCu WQ @ 75°C and 12MPa
Strain Rate (h-1)
1.E+00
1.E-01
1.E-02
1.E-03
1.E-04
1.E-05
1.E-06
0
0.2
0.4
0.6
0.8
1
Life Fraction

Data at 99.4°C

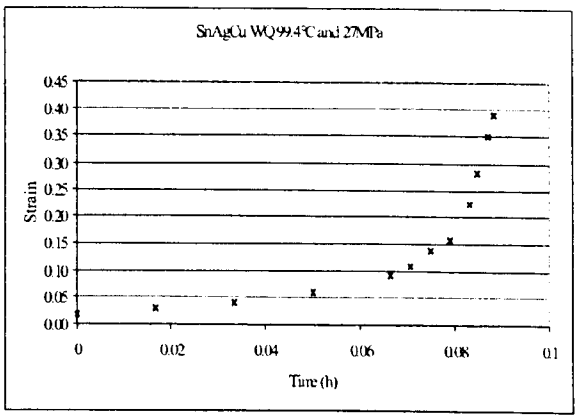
SnAgCu WQ99.4°C and 27MPa
Strain
Time (h)

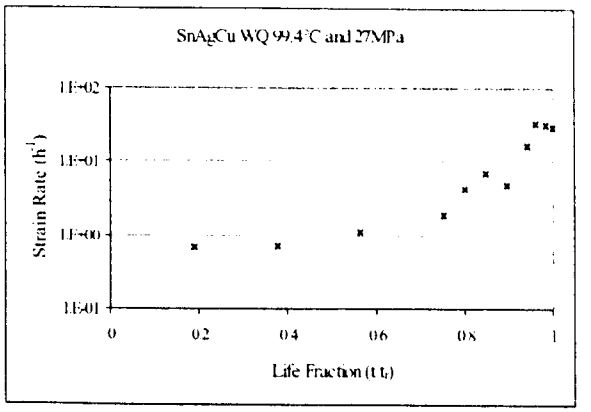
SnAgCu WQ 99.4°C and 27MPa
Strain Rate (h-1)
Life Fraction (t tf)

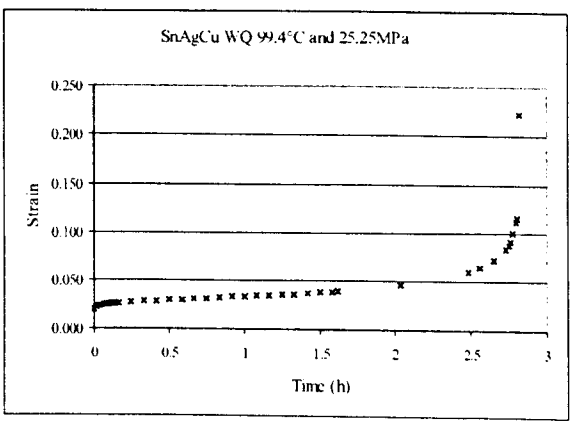
SnAgCu WQ 99.4°C and 25.25MPa
Strain
Time (h)

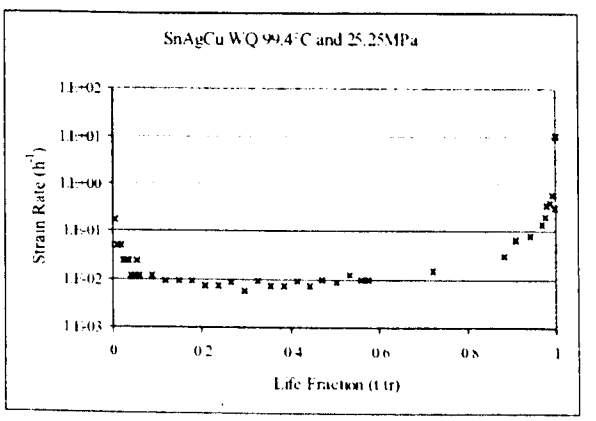
SnAgCu WQ 99.4°C and 25.25MPa
Strain Rate (h-1)
Life Fraction (t tr)

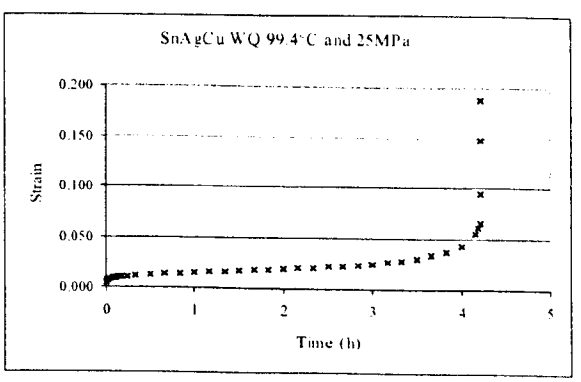
SnAgCu WQ 99.4°C and 25MPa
Strain
Time (h)

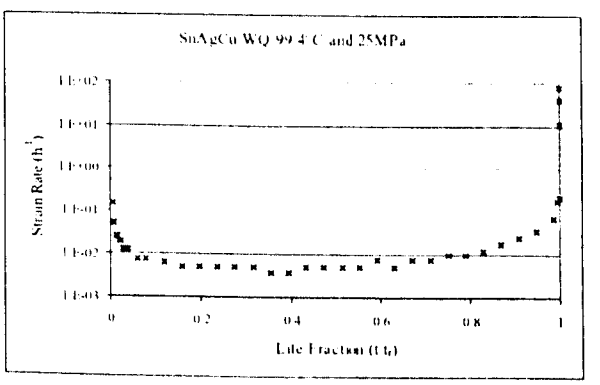
SnAgCu WQ 99.4°C and 25MPa
Strain Rate (h-1)
Life Fraction (t tf)

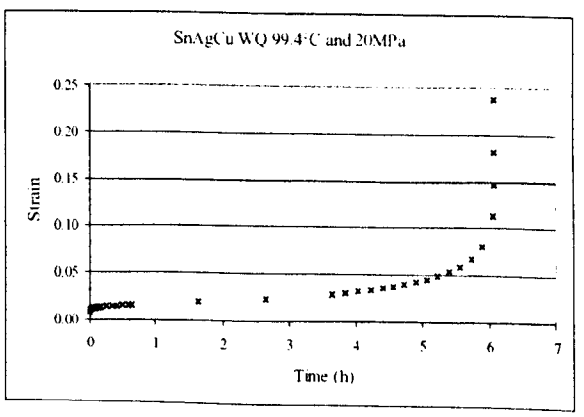
SnAgCu WQ 99.4°C and 20MPa
Strain
Time (h)

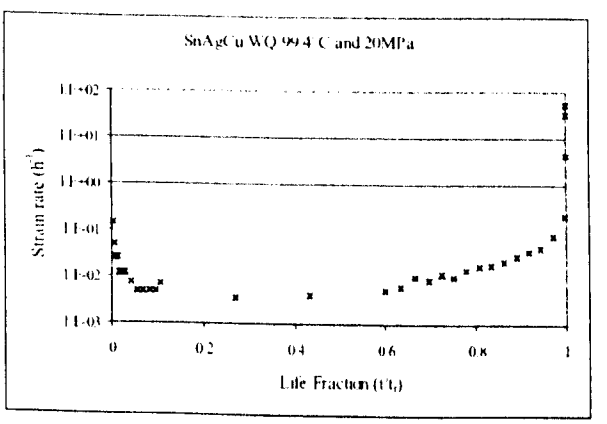
SnAgCu WQ 99.4°C and 20MPa
Strain rate (h-1)
Life Fraction (t tf)

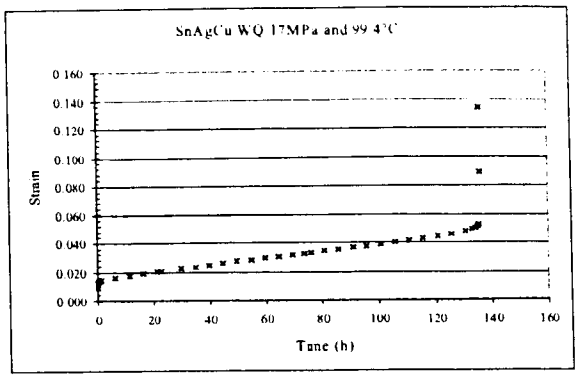
SnAgCu WQ 17MPa and 99.4°C
Strain
Time (h)

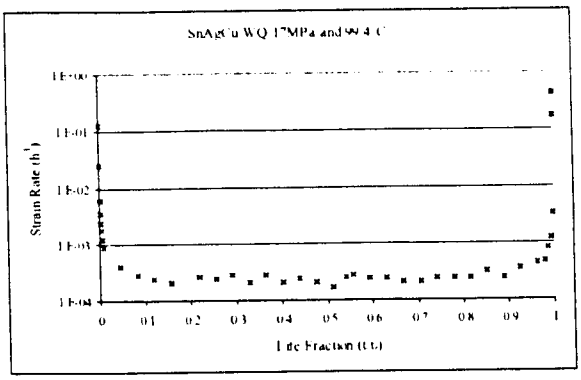
SnAgCu WQ 17MPa and 99.4°C
Strain Rate (h-1)
Life Fraction (LF)

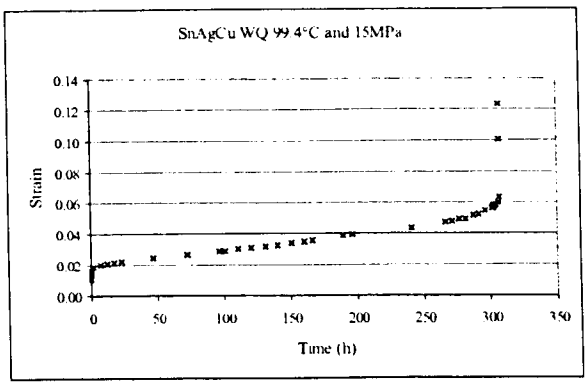
SnAgCu WQ 99.4°C and 15MPa
Strain
Time (h)

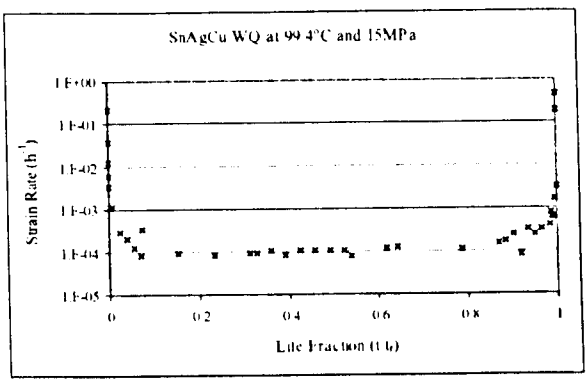
SnAgCu WQ at 99.4°C and 15MPa
Strain Rate (h-1)
Life Fraction (LF)

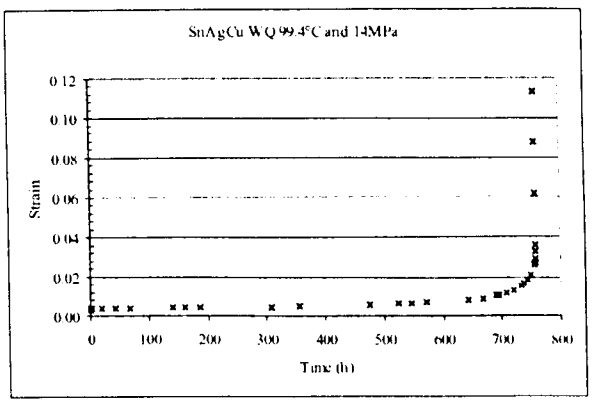
SnAgCu WQ 99.4°C and 14MPa
Strain
Time (h)

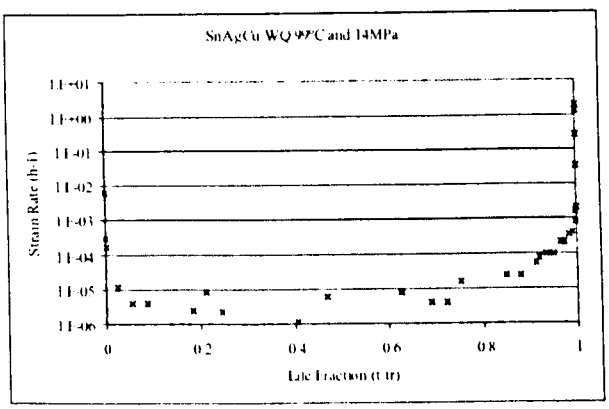
SnAgCu WQ 99°C and 14MPa
Strain Rate (h-1)
Life Fraction (LF)

Data at 125°C

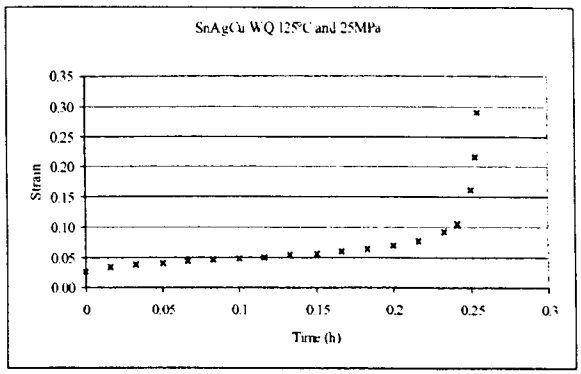
SnAgCu WQ 125°C and 25MPa
Strain
Time (h)

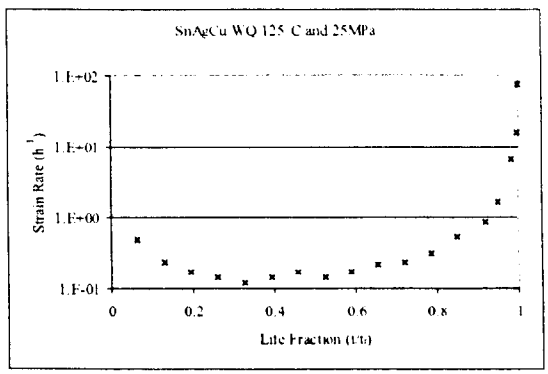
SnAgCu WQ 125°C and 25MPa
Strain Rate (h-1)
Life Fraction (t/tf)

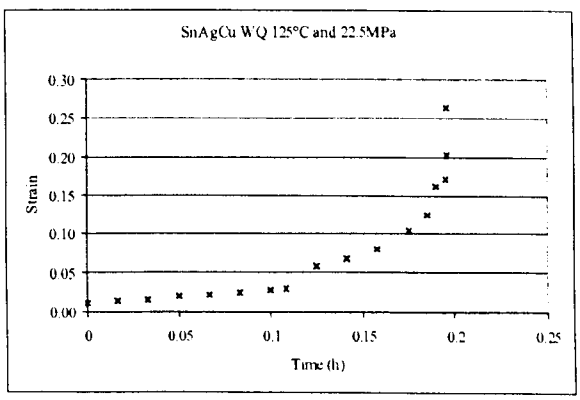
SnAgCu WQ 125°C and 22.5MPa
Strain
Time (h)

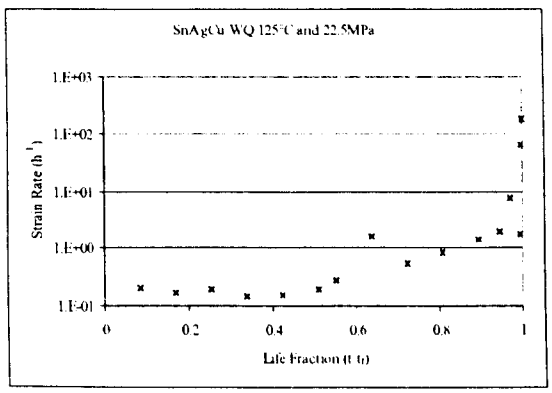
SnAgCu WQ 125°C and 22.5MPa
Strain Rate (h-1)
Life Fraction (t/tf)

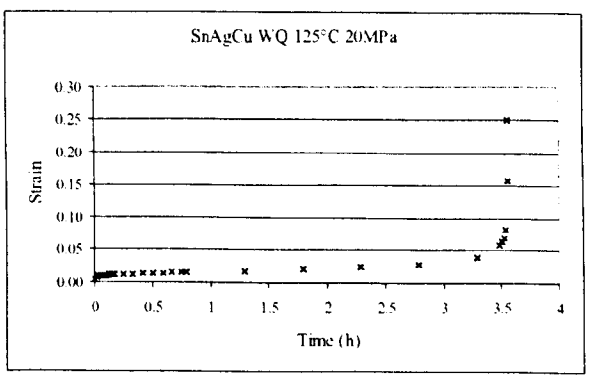
SnAgCu WQ 125°C 20MPa
Strain
Time (h)

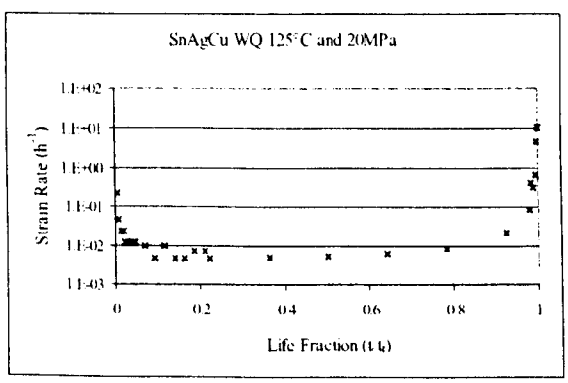
SnAgCu WQ 125°C and 20MPa
Strain Rate (h-1)
Life Fraction (t/tf)

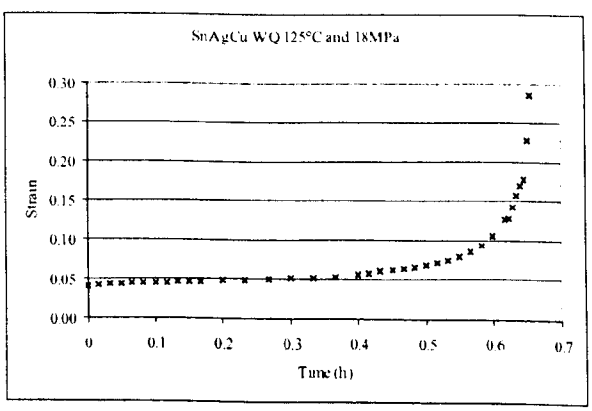
SnAgCu WQ 125°C and 18MPa
Strain
Time (h)

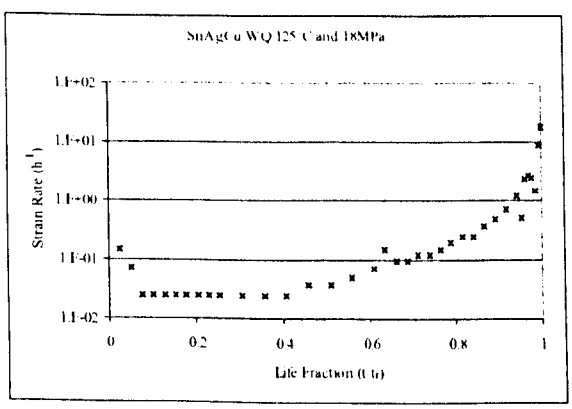
SnAgCu WQ 125°C and 18MPa
Strain Rate (h-1)
Life Fraction (t/tf)

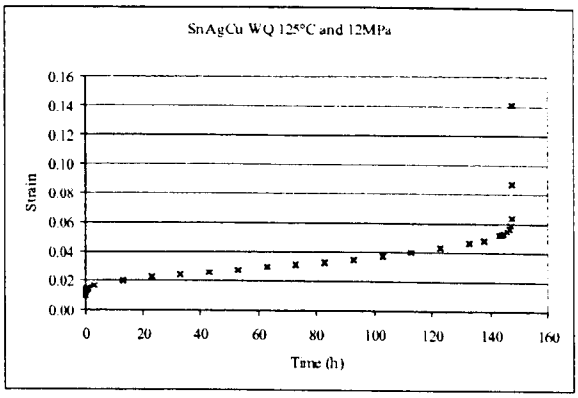
SnAgCu WQ 125°C and 12MPa
Strain
Time (h)

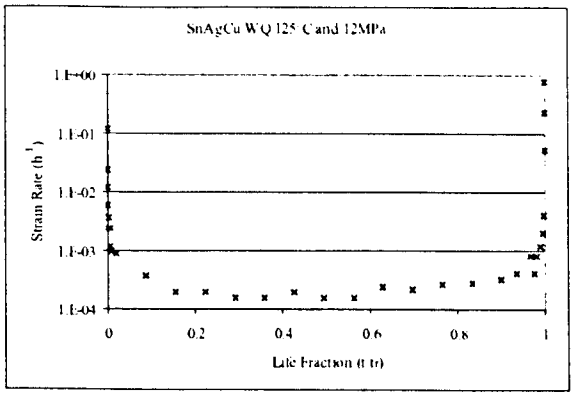
SnAgCu WQ 125°C and 12MPa
Strain Rate (h-1)
Life Fraction (t/tr)

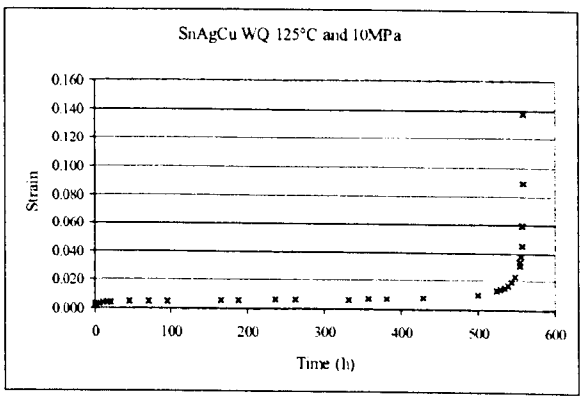
SnAgCu WQ 125°C and 10MPa
Strain
Time (h)

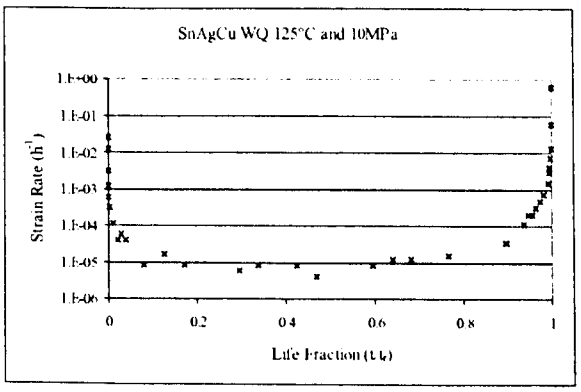
SnAgCu WQ 125°C and 10MPa
Strain Rate (h-1)
Life Fraction (t/tr)

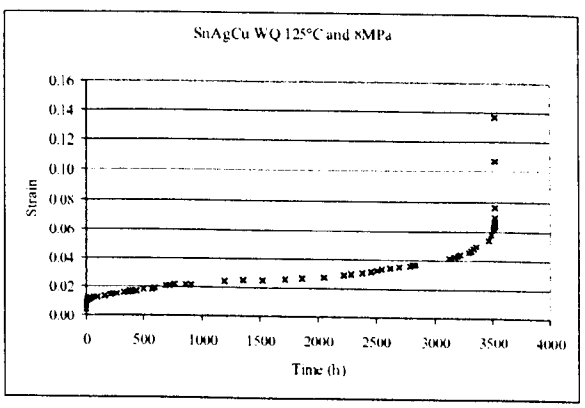
SnAgCu WQ 125°C and 8MPa
Strain
Time (h)

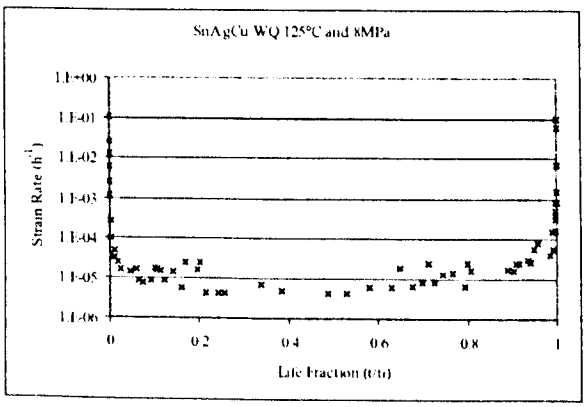
SnAgCu WQ 125°C and 8MPa
Strain Rate (h-1)
Life Fraction (t/tr)

## Appendix 5.2 Calculation of error and the utilisation of error bars

Trends and errors for each 'Time to Rupture' dataset for bulk solder

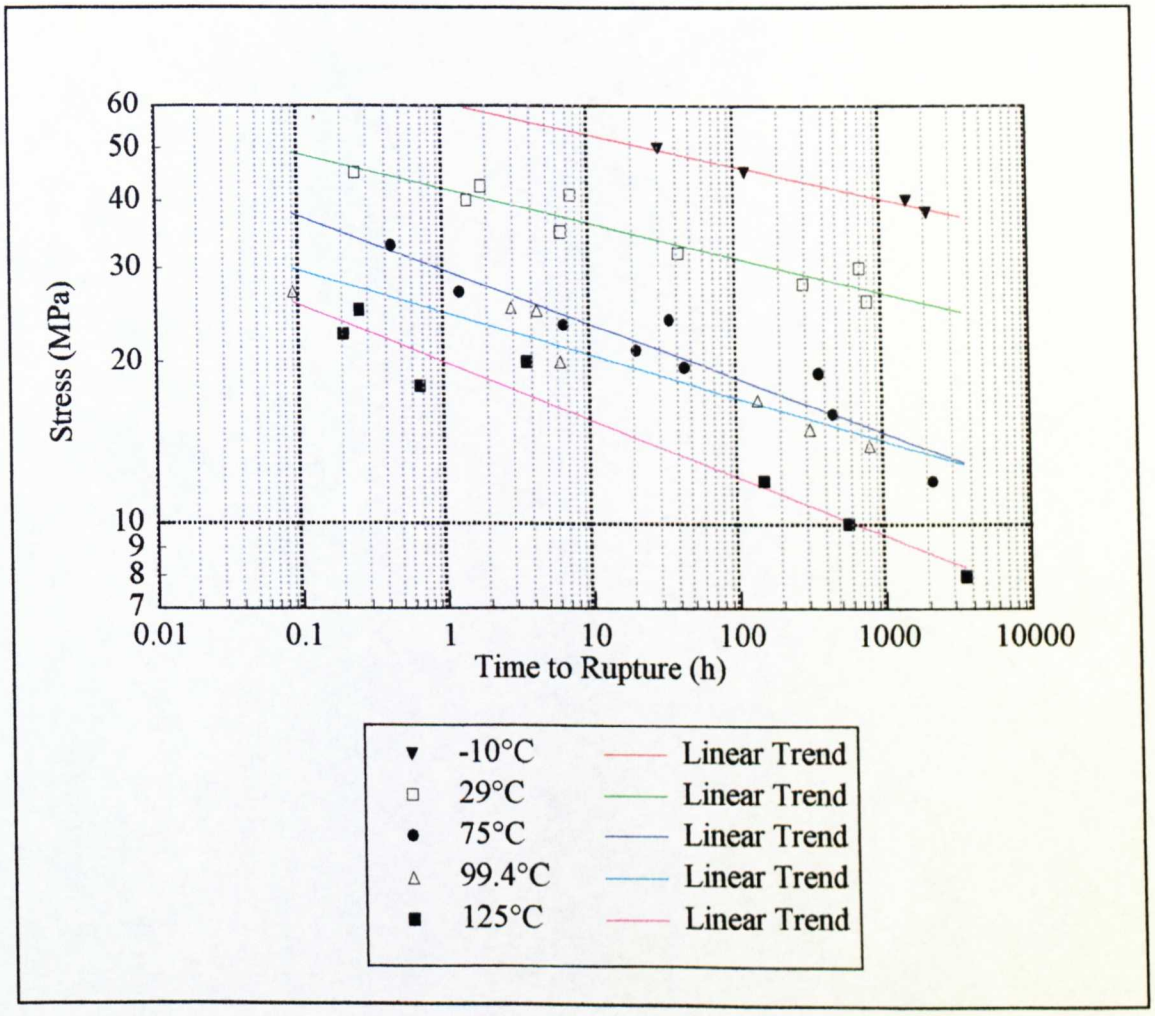


**-10 degrees**

| *Parameter* | *Value* |
|---|---|
| a | 1.7828 |
| b | -0.0596592 |

| $X_{in}$ | $Y_{in}$ | $Y_{out}$ | *Error* |
|---|---|---|---|
| 29.5 | 50 | 49.5582 | 0.441827 |
| 115.2 | 45 | 45.6898 | -0.68978 |
| 1485 | 40 | 39.2266 | 0.773374 |
| 2027.67 | 38 | 38.5044 | -0.504439 |

**29 degrees**

| *Parameter* | *Value* |
|---|---|
| a | 1.6231 |
| b | -0.0643939 |

| $X_{in}$ | $Y_{in}$ | $Y_{out}$ | *Error* |
|---|---|---|---|
| 0.242 | 45 | 46.0027 | -1.00266 |
| 1.418 | 40 | 41.0523 | -1.05229 |
| 1.779 | 42.5 | 40.4571 | 2.04291 |
| 6.21 | 35 | 37.3279 | -2.32795 |
| 7.29 | 41 | 36.9445 | 4.05548 |
| 40.01 | 32 | 33.1081 | -1.10812 |
| 284.02 | 28 | 29.1826 | -1.18258 |
| 694.25 | 30 | 27.5504 | 2.44959 |
| 775.56 | 26 | 27.3546 | -1.35462 |

**75 degrees**

| *Parameter* | *Value* |
|---|---|
| a | 1.47068 |
| b | -0.100494 |

| $X_{in}$ | $Y_{in}$ | $Y_{out}$ | *Error* |
|---|---|---|---|
| 0.428 | 33 | 32.1896 | 0.810423 |
| 1.25 | 27 | 28.9027 | -1.90272 |
| 6.43 | 23.5 | 24.5164 | -1.01642 |
| 20.25 | 21 | 21.8469 | -0.846886 |
| 34.33 | 24 | 20.7182 | 3.28183 |
| 43.31 | 19.5 | 20.24 | -0.73998 |
| 355.53 | 19 | 16.3806 | 2.61941 |
| 443.36 | 16 | 16.0212 | -0.0211665 |
| 2121 | 12 | 13.6893 | -1.68926 |

**99 degrees**

| *Parameter* | *Value* |
|---|---|
| a | 1.3921 |
| b | -0.0792283 |

| $X_{in}$ | $Y_{in}$ | $Y_{out}$ | *Error* |
|---|---|---|---|
| 0.0885 | 27 | 29.8907 | -2.89066 |
| 2.82 | 25.25 | 22.7212 | 2.5288 |
| 4.221 | 25 | 22.0066 | 2.99339 |
| 6.07 | 20 | 21.3822 | -1.38223 |
| 136.13 | 17 | 16.7122 | 0.287777 |
| 306.95 | 15 | 15.6696 | -0.66959 |
| 788.416 | 14 | 14.5412 | -0.541151 |

**125 degrees**

| *Parameter* | *Value* |
|---|---|
| a | 1.29953 |
| b | -0.107328 |

| $X_{in}$ | $Y_{in}$ | $Y_{out}$ | *Error* |
|---|---|---|---|
| 0.196 | 22.5 | 23.7408 | -1.24078 |
| 0.254 | 25 | 23.0894 | 1.91063 |
| 0.653 | 18 | 20.8641 | -2.86407 |
| 3.567 | 20 | 17.3883 | 2.61174 |
| 147.77 | 12 | 11.6594 | 0.340613 |
| 558.8 | 10 | 10.1082 | -0.108235 |
| 3528.03 | 8 | 8.29436 | -0.294362 |

Trends and errors for each 'Norton's Law' dataset for bulk solder

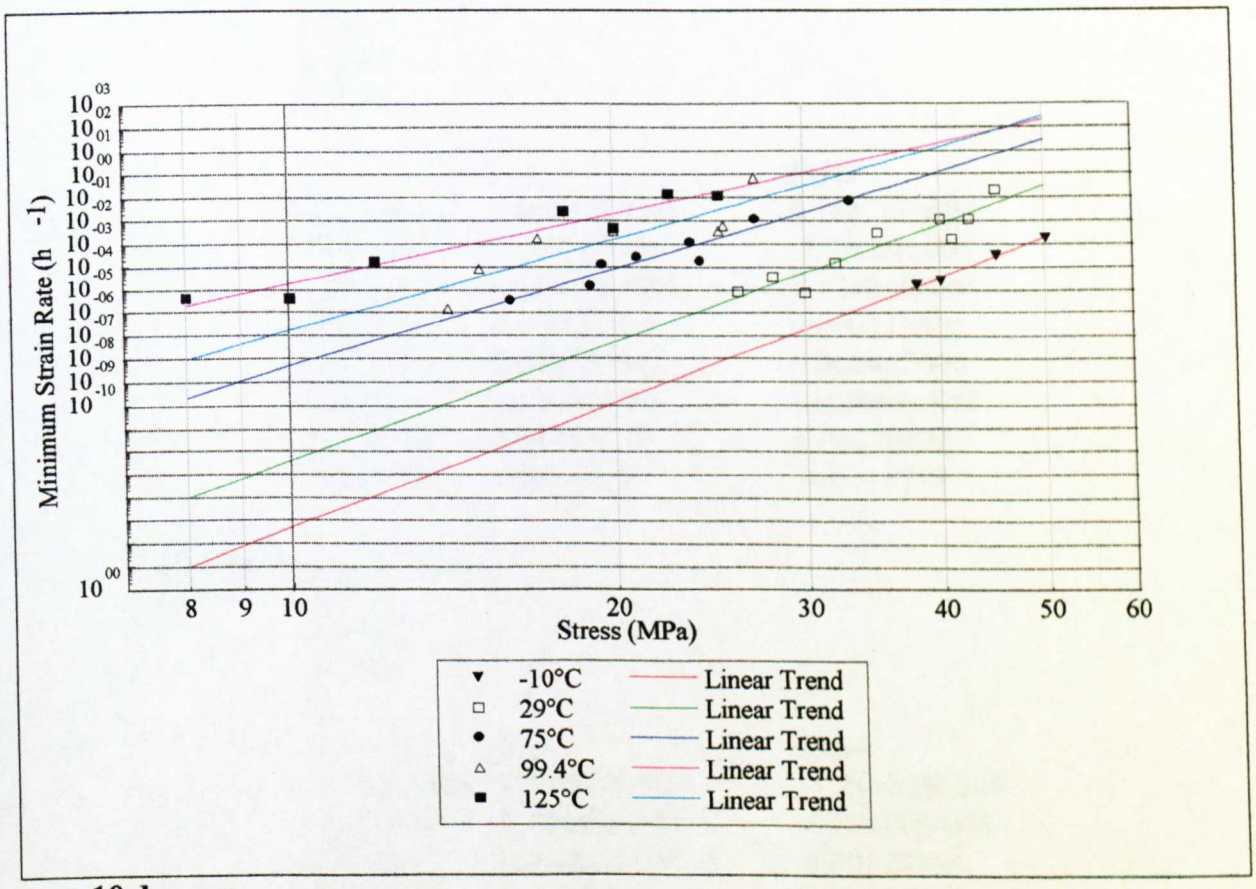


**-10 degrees**

| *Parameter* | *Value* |
|---|---|
| a | -33.252 |
| b | 17.963 |

| $X_{in}$ | $Y_{in}$ | $Y_{out}$ | *Error* |
|---|---|---|---|
| 40 | 2.437E-005 | 3.35574E-005 | -9.18741E-006 |
| 38 | 1.642E-005 | 1.33548E-005 | 3.0652E-006 |
| 45 | 0.00032 | 0.000278382 | 4.16177E-005 |
| 50 | 0.0018 | 0.0018475 | -4.74968E-005 |

**29 degrees**

| *Parameter* | *Value* |
|---|---|
| a | -29.3949 |
| b | 17.0129 |

| $X_{in}$ | $Y_{in}$ | $Y_{out}$ | *Error* |
|---|---|---|---|
| 26 | 8.28E-006 | 4.76363E-006 | 3.51637E-006 |
| 28 | 3.401E-005 | 1.68071E-005 | 1.72029E-005 |
| 30 | 7.35001E-006 | 5.4357E-005 | -4.7007E-005 |
| 32 | 0.0001506 | 0.000162969 | -1.23693E-005 |
| 35 | 0.003012 | 0.000748541 | 0.00226346 |
| 40 | 0.011905 | 0.00725819 | 0.0046468 |
| 41 | 0.001626 | 0.0110477 | -0.00942171 |
| 42.5 | 0.012195 | 0.0203592 | -0.00816418 |
| 45 | 0.21053 | 0.0538371 | 0.156693 |

**75 degrees**

| *Parameter* | *Value* |
|---|---|
| a | -22.2699 |
| b | 13.9584 |

| $X_{in}$ | $Y_{in}$ | $Y_{out}$ | *Error* |
|---|---|---|---|
| 16 | 3.51E-006 | 3.44842E-006 | 6.15824E-008 |
| 19 | 1.53E-005 | 3.7965E-005 | -2.2665E-005 |
| 19.5 | 0.0001263 | 5.45567E-005 | 7.17433E-005 |
| 21 | 0.0002688 | 0.000153495 | 0.000115305 |
| 23.5 | 0.0011905 | 0.000737802 | 0.000452696 |
| 24 | 0.000183 | 0.000989844 | -0.000806844 |
| 27 | 0.0119048 | 0.00512357 | 0.00678124 |
| 33 | 0.0731707 | 0.0843425 | -0.0111718 |

**99 degrees**

| *Parameter* | *Value* |
|---|---|
| a | -19.907 |
| b | 13.1378 |

| $X_{in}$ | $Y_{in}$ | $Y_{out}$ | *Error* |
|---|---|---|---|
| 14 | 1.4784E-006 | 1.41466E-005 | -1.26682E-005 |
| 15 | 7.817E-005 | 3.50189E-005 | 4.31511E-005 |
| 17 | 0.001659 | 0.000181319 | 0.00147768 |
| 20 | 0.00366458 | 0.00153365 | 0.00213093 |
| 25 | 0.003658 | 0.0287683 | -0.0251103 |
| 25.25 | 0.005854 | 0.0327859 | -0.0269319 |
| 27 | 0.682898 | 0.0790732 | 0.603825 |

**125 degrees**

| *Parameter* | *Value* |
|---|---|
| a | -14.7874 |
| b | 10.0474 |

| $X_{in}$ | $Y_{in}$ | $Y_{out}$ | *Error* |
|---|---|---|---|
| 8 | 4.23443E-006 | 1.93373E-006 | 2.3007E-006 |
| 10 | 4.11502E-006 | 1.8201E-005 | 1.40859E-005 |
| 12 | 0.0001626 | 0.000113675 | 4.89253E-005 |
| 18 | 0.0243902 | 0.00668239 | 0.0177078 |
| 20 | 0.004878 | 0.0192609 | -0.0143829 |
| 22.5 | 0.144578 | 0.062897 | 0.0816811 |
| 25 | 0.120482 | 0.181291 | -0.060809 |

Discussion of errors for the time to rupture and Norton's Law plots (bulk solder)

As mentioned in the main text, due to the nature of creep testing it is difficult to graphically incorporate error bars. This is because only a very limited number of tests can be carried out, sometimes only single tests, due to the long lifetimes of samples and time constraints. Therefore, with only one data point available at a given stress and temperature, it is impossible to calculate errors between results. The errors for the datasets above have been calculated from a 'best-fit' trend computation from the Harvard XL software. Here, from each given dataset a best fit trend-line, shown on each graph, was calculated thus generating the parameter values 'a' and 'b'. The $X_{in}$ and $Y_{in}$ values are data obtained from actual creep tests, the $Y_{out}$ value is that calculated using the trend parameters and the $X_{in}$ value. In this case the error is the difference between the actual Y values obtained from testing and the calculated Y value i.e. the distance from the trend-line. Error bars in this instance have not been shown.

Sources of error were referred to within the main text highlighting areas such as temperature and microstructural changes. Appendix 4.2 illustrates the temperature fluctuation on the surface of a sample held at 75°C, where the temperature was constant to plus or minus 0.3°C. Errors may also be introduced during the calculation

of steady state creep rate, generally this is the minimum creep rate reached during a test. However, as can be seen from the graphs in appendix 5.1 and 5.6 (graphs obtained from individual tests) there is variation in the strain rate values during steady state creep, figure 1a. By estimating the duration of steady state creep and isolating the relevant data, a best fit line can be taken, figure 1b.

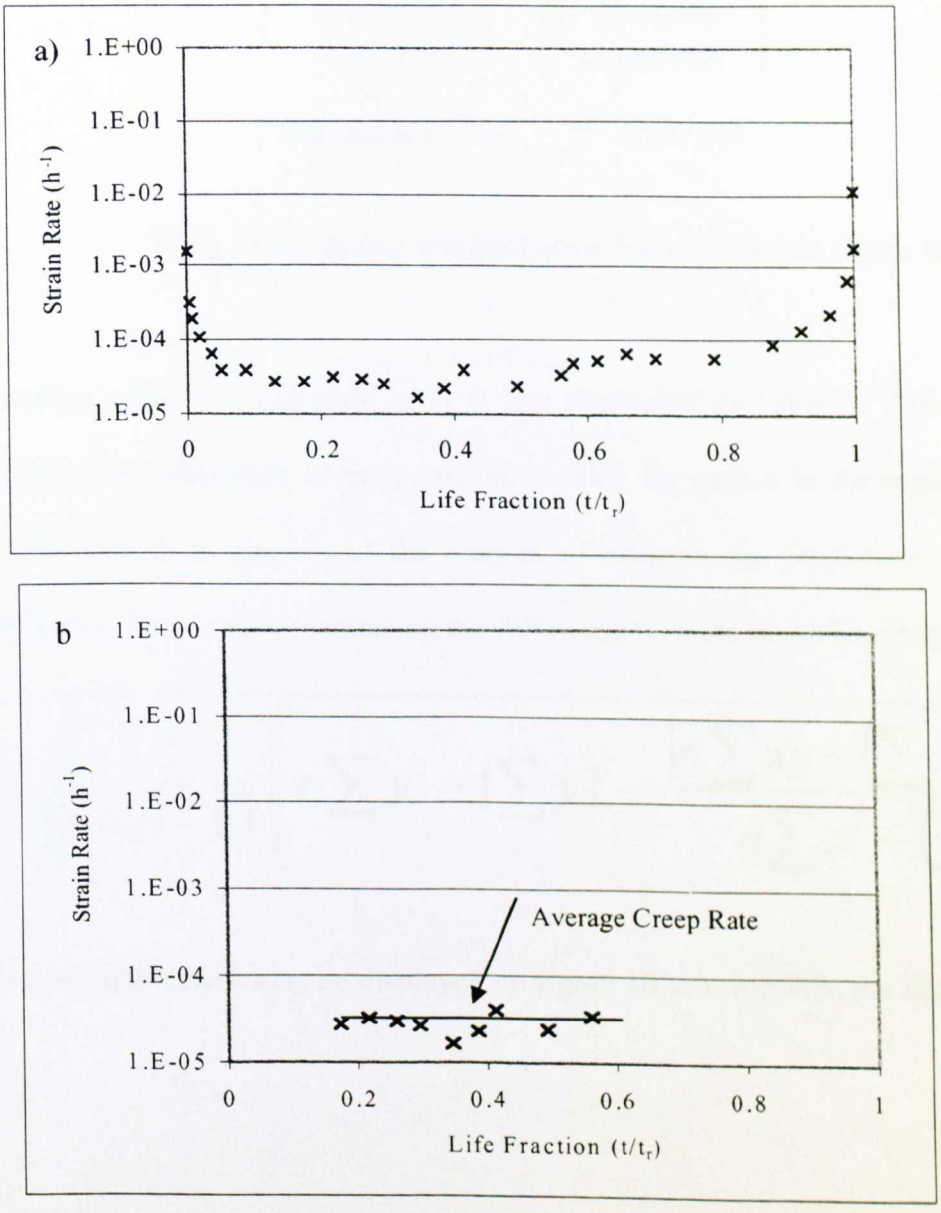


Figure 1a) Strain rate vs life fraction for SnAgCu tested at –10°C and 38MPa
b) As figure 1a showing only steady state creep and average creep rate.

| Life Fraction $t/t_r$ | Strain Rate $h^{-1}$ |
|---|---|
| 0.173450315 | 2.71E-05 |
| 0.216812894 | 3.2E-05 |
| 0.260175472 | 2.97E-05 |
| 0.296177386 | 2.63E-05 |
| 0.34690063 | 1.64E-05 |
| 0.385926951 | 2.29E-05 |
| 0.413679001 | 3.99E-05 |
| 0.493423486 | 2.39E-05 |
| 0.561111769 | 3.45E-05 |
| **Standard Error** | 0.135247 |

Table 1 Calculating standard error from the data in figure 1b.

Another method to calculate error is that illustrated in Table 1. This shows the standard error calculation of the predicted y-value for each x in the regression. The standard error is a measure of the amount of error in the prediction of y for an individual x. This is calculated using the following formula on an Excel spreadsheet:

$$s_{y.x} = \sqrt{\left[\frac{1}{n(n-2)}\right]\left[n\sum y^2 - \left(\sum y\right)^2 - \frac{\left[n\sum xy - \left(\sum x\right)\left(\sum y\right)\right]^2}{n\sum x^2 - \left(\sum x\right)^2}\right]}$$

This standard error may be displayed on figure 1b as error bars, see figure 2.

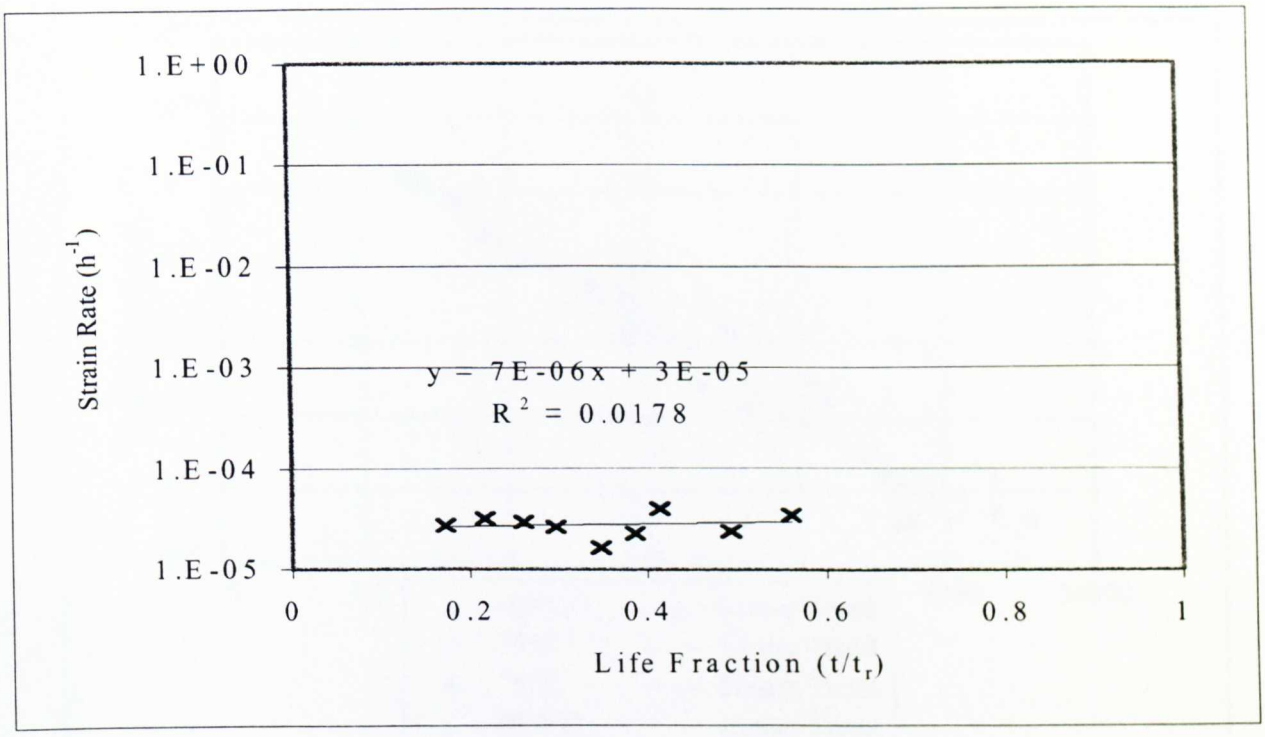


Figure 2 Data from figure 1b illustrating error bars.

This appendix illustrates that error bars may be used but due to the nature of creep testing where limited numbers of tests were carried out, error calculation and the utilisation of error bars were not performed for all sets of data. For the purpose of consistency throughout the thesis the minimum strain rate value achieved was utilised. This was because it was not always obvious where steady state creep become tertiary creep, therefore which data to use in the calculations was unclear. It would also be useful to estimate and combine the errors introduced by the various parameters of testing (such as stress and temperature), however this would be difficult to quantify and has not been investigated further for this research.

**Appendix 5.2b: Trend lines for figures using a 'best fit' plot.**

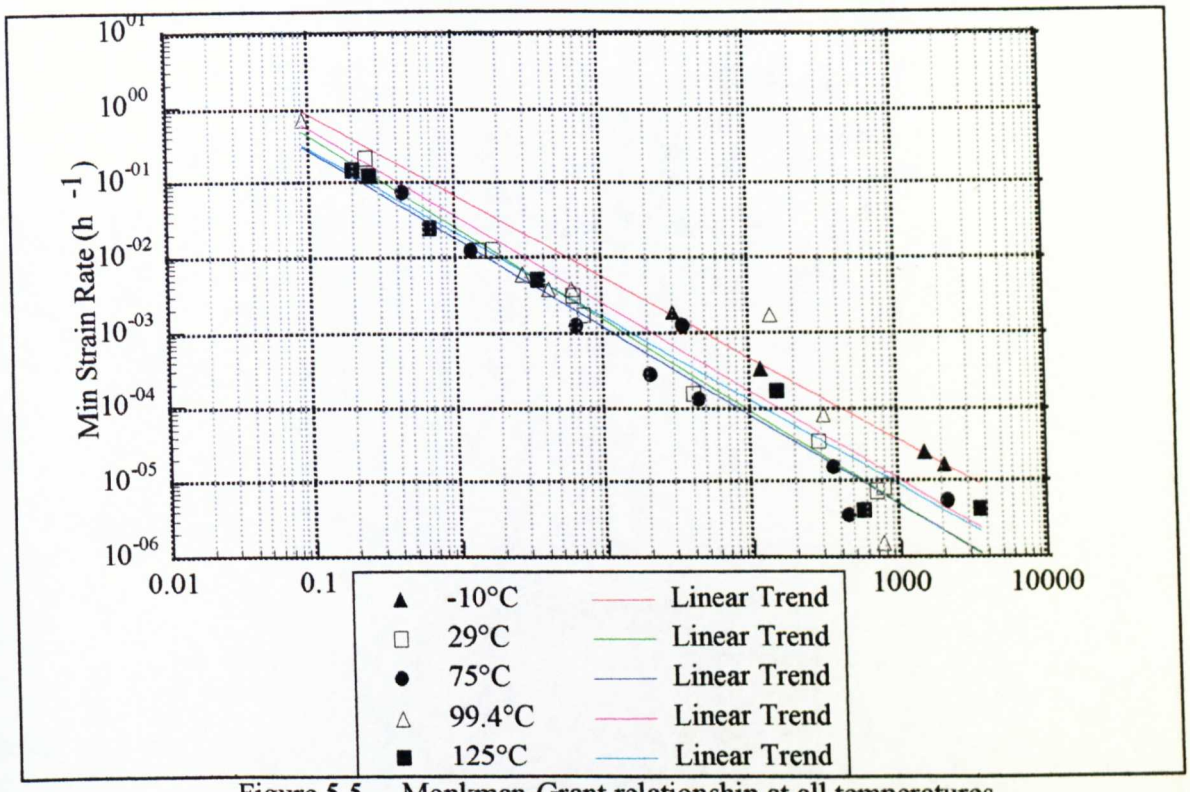


Figure 5.5 Monkman-Grant relationship at all temperatures

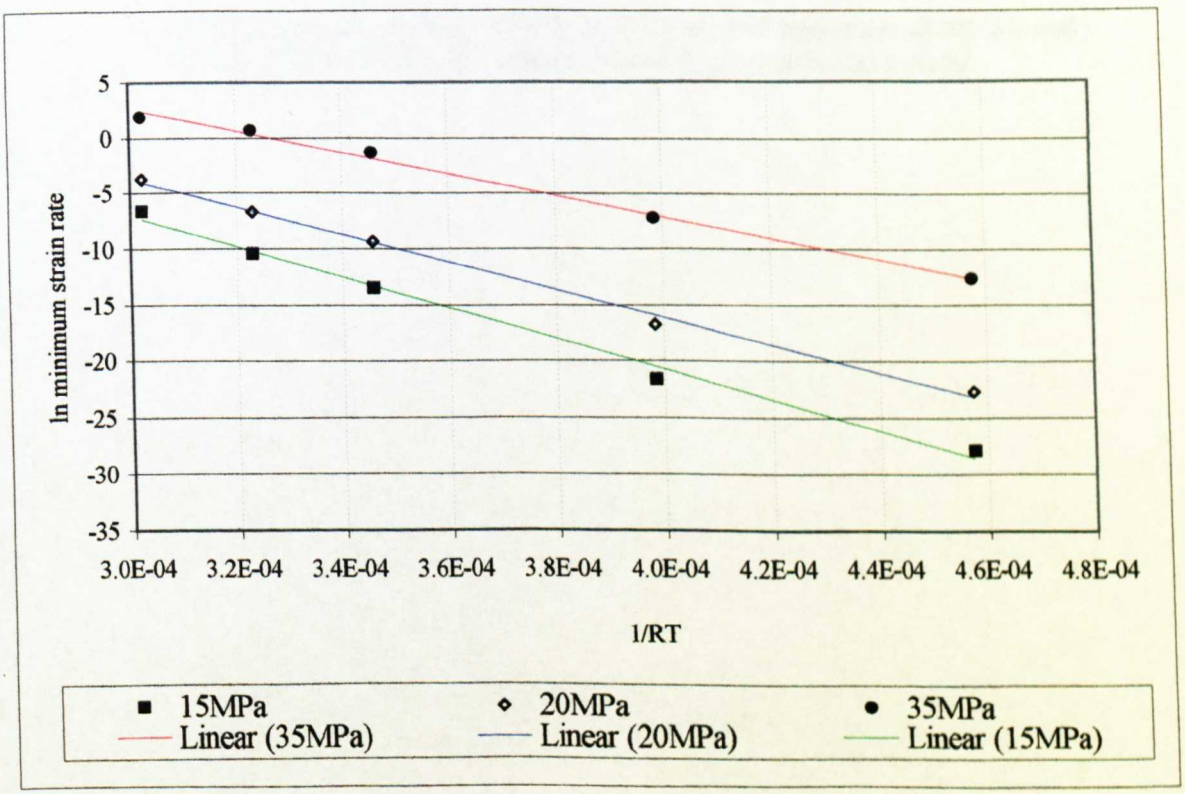


Figure 5.7 Determination of apparent activation energy for creep

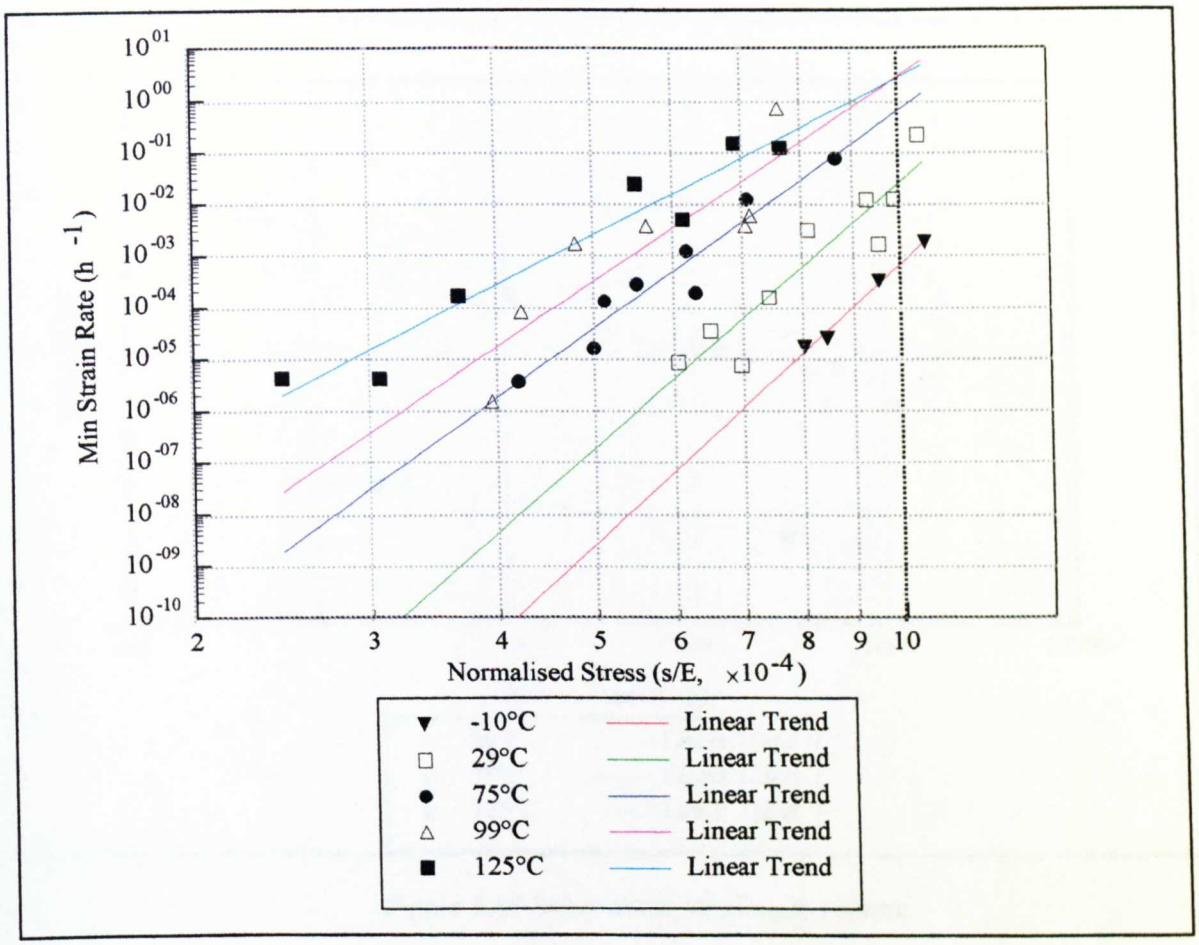


Figure 5.7b Normalised creep strength as a function of minimum strain rate and temperature – used in the determination of true activation energy

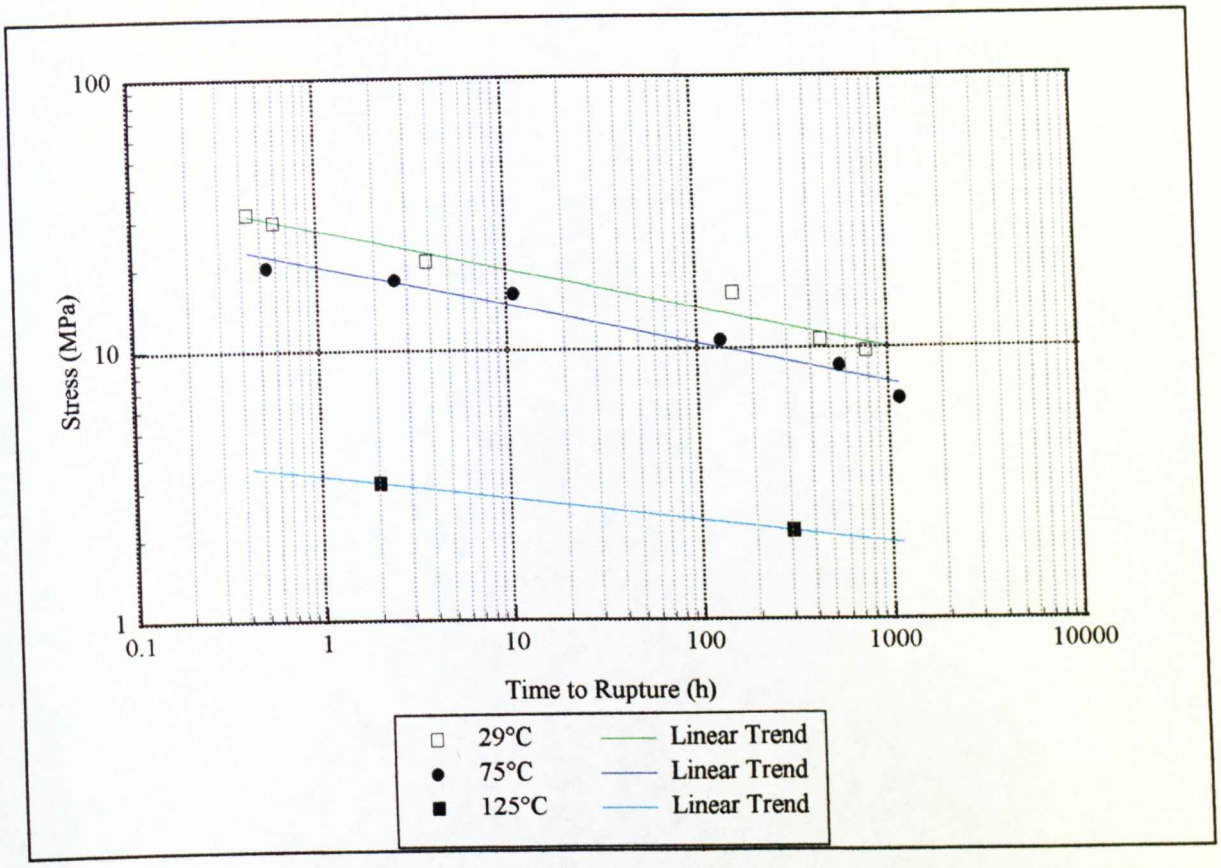


Figure 5.19 Shear stress vs. time to rupture

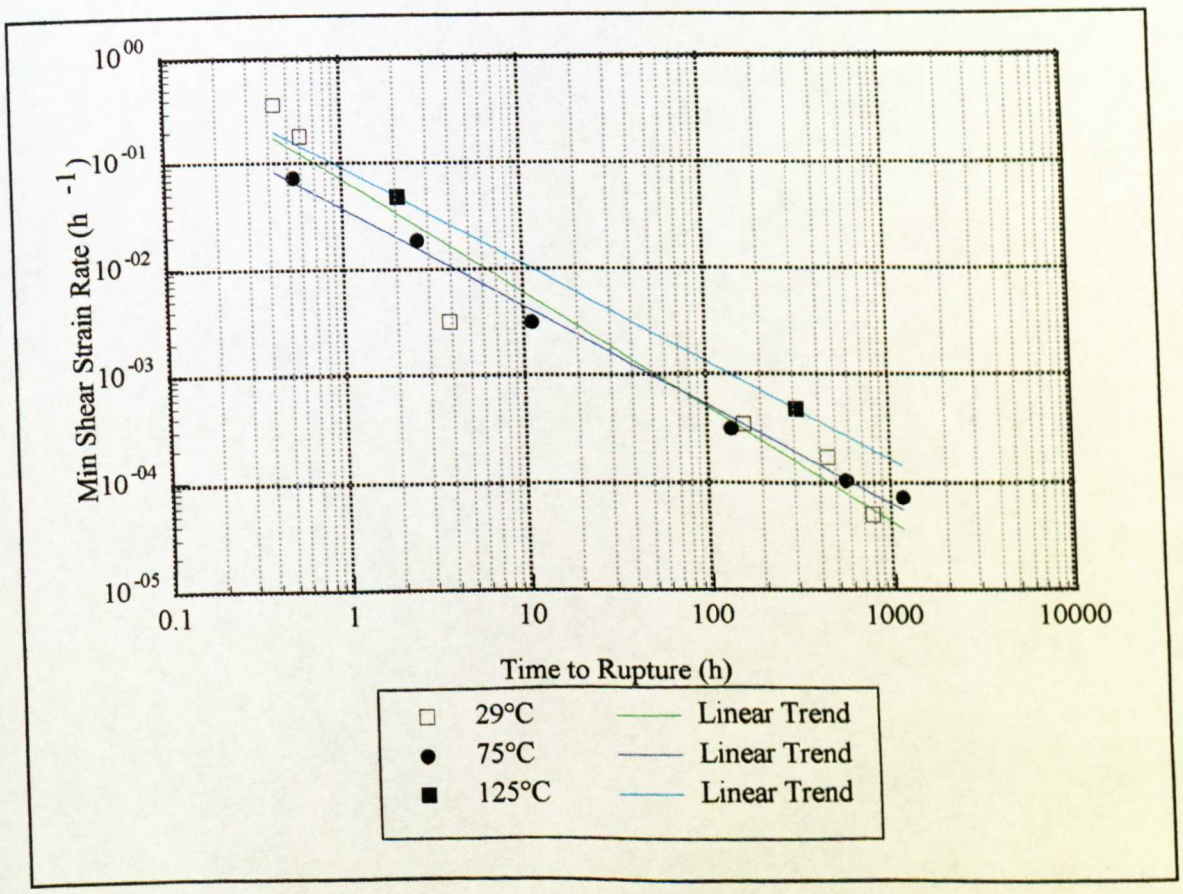


Figure 5.21 Monkman-Grant relationship at all test temperatures

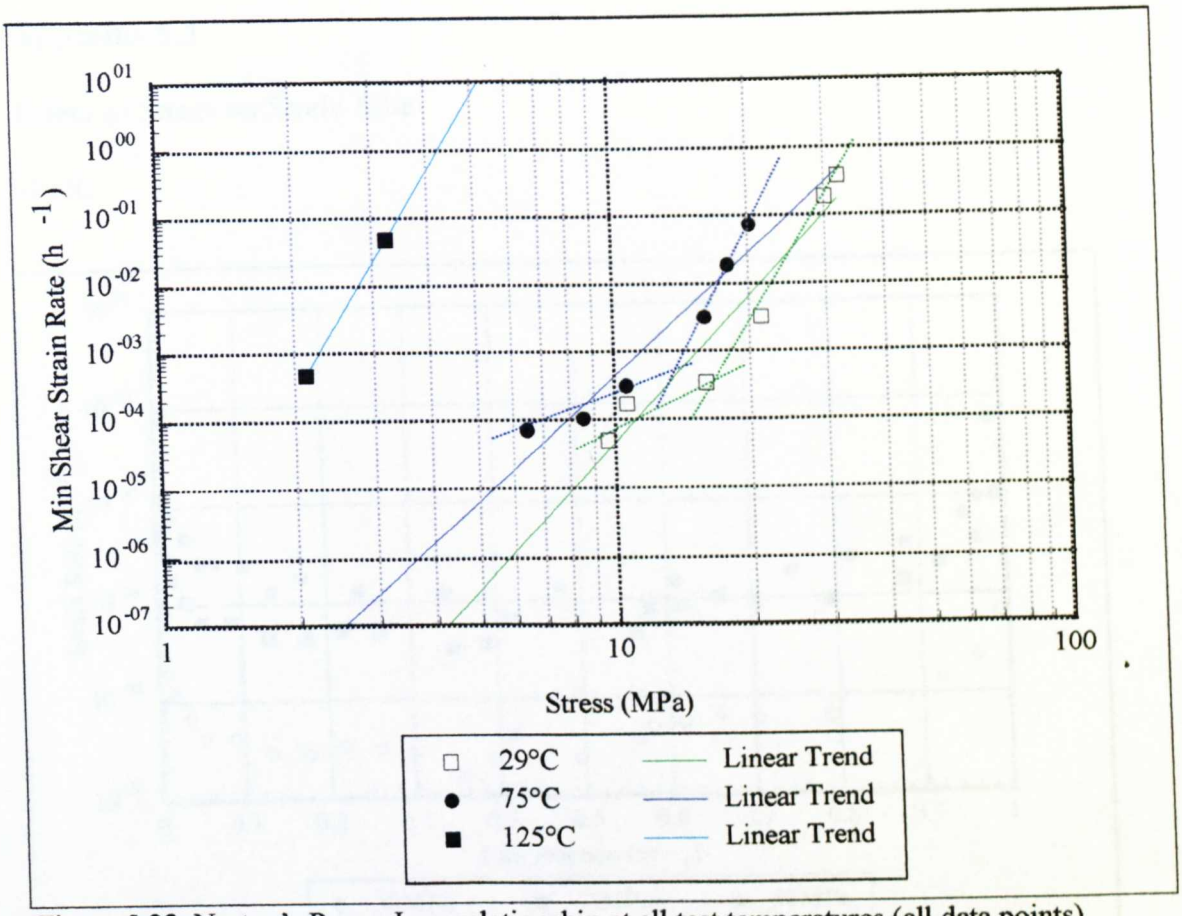


Figure 5.22 Norton's Power Law relationship at all test temperatures (all data points)

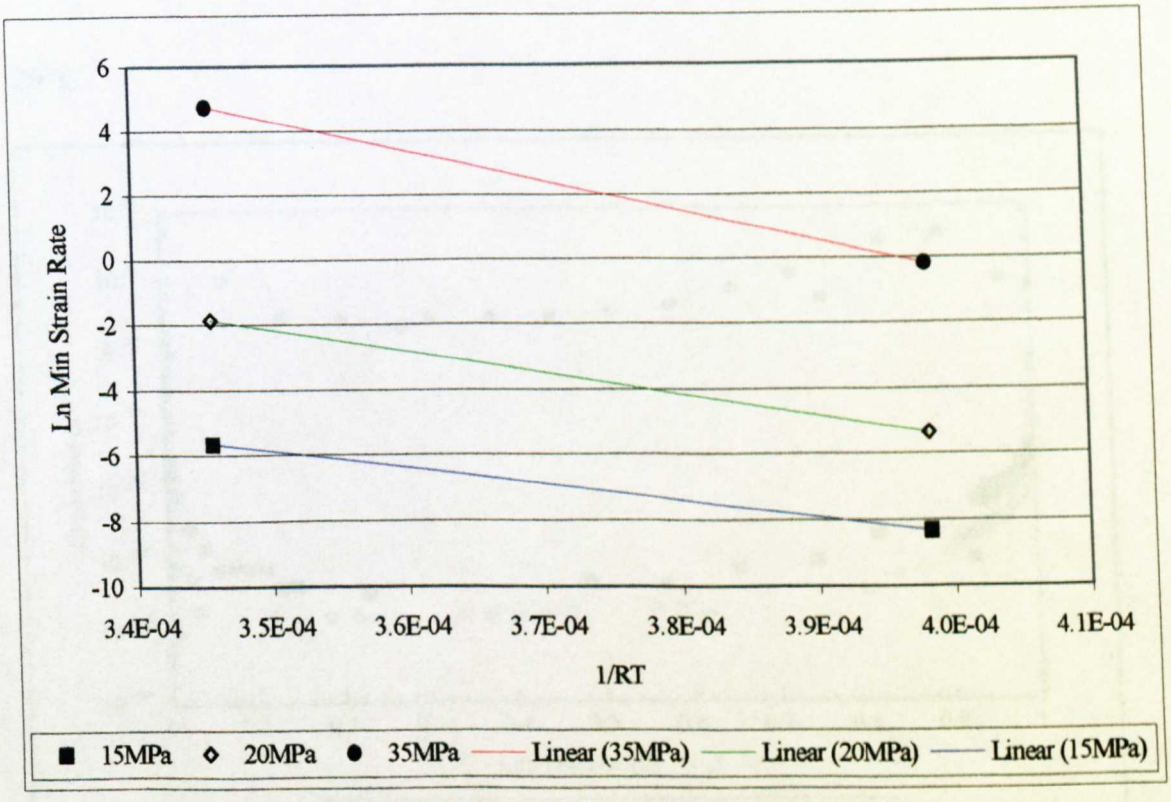


Figure 5.25 Determination of apparent activation energy for creep at high stress

## Appendix 5.3

Effect of Stress on Strain Rate

-10°C

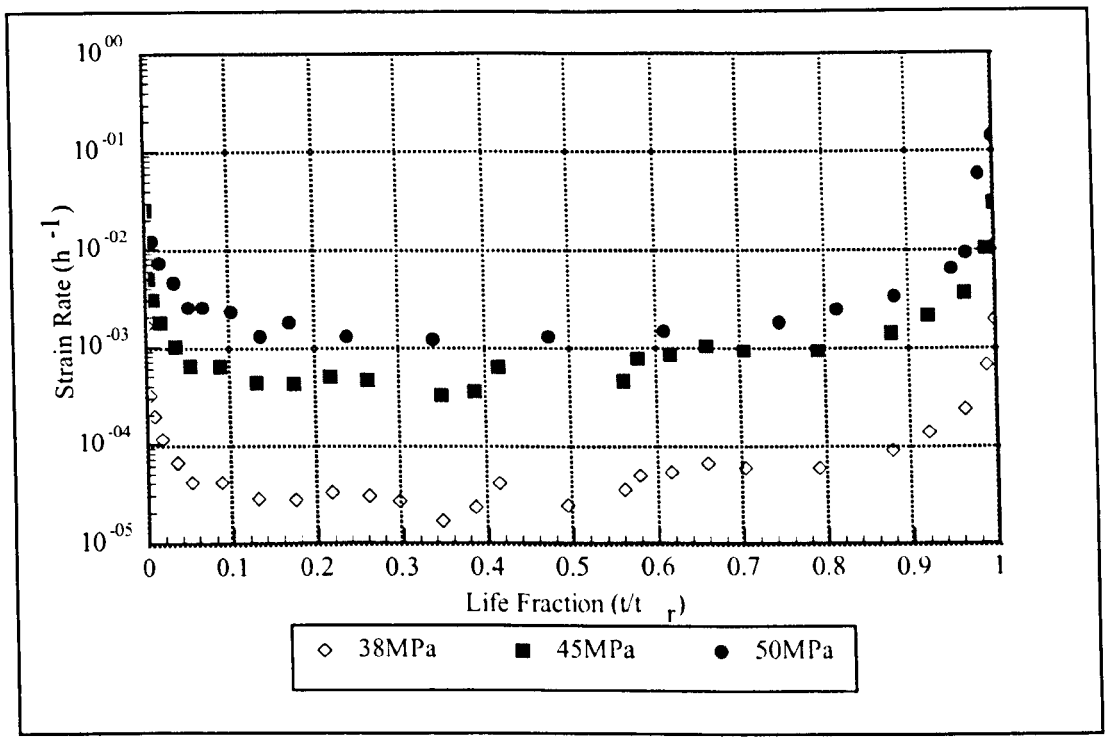


29°C

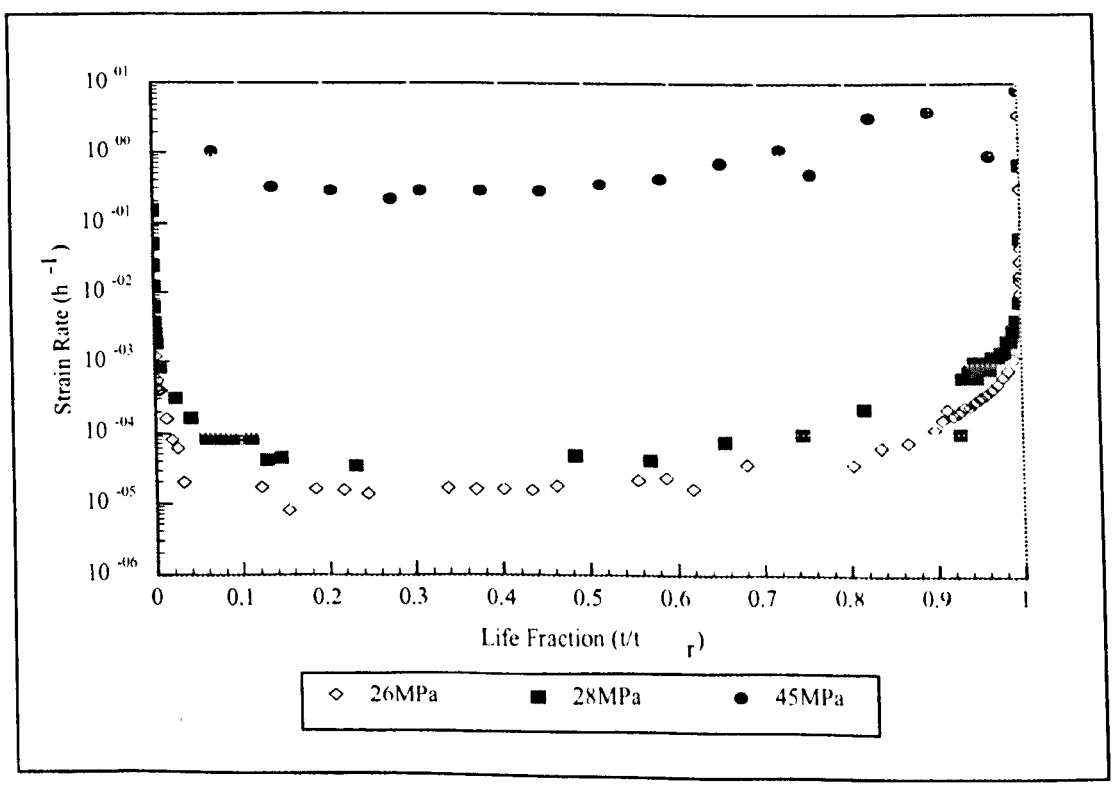

99.4°C

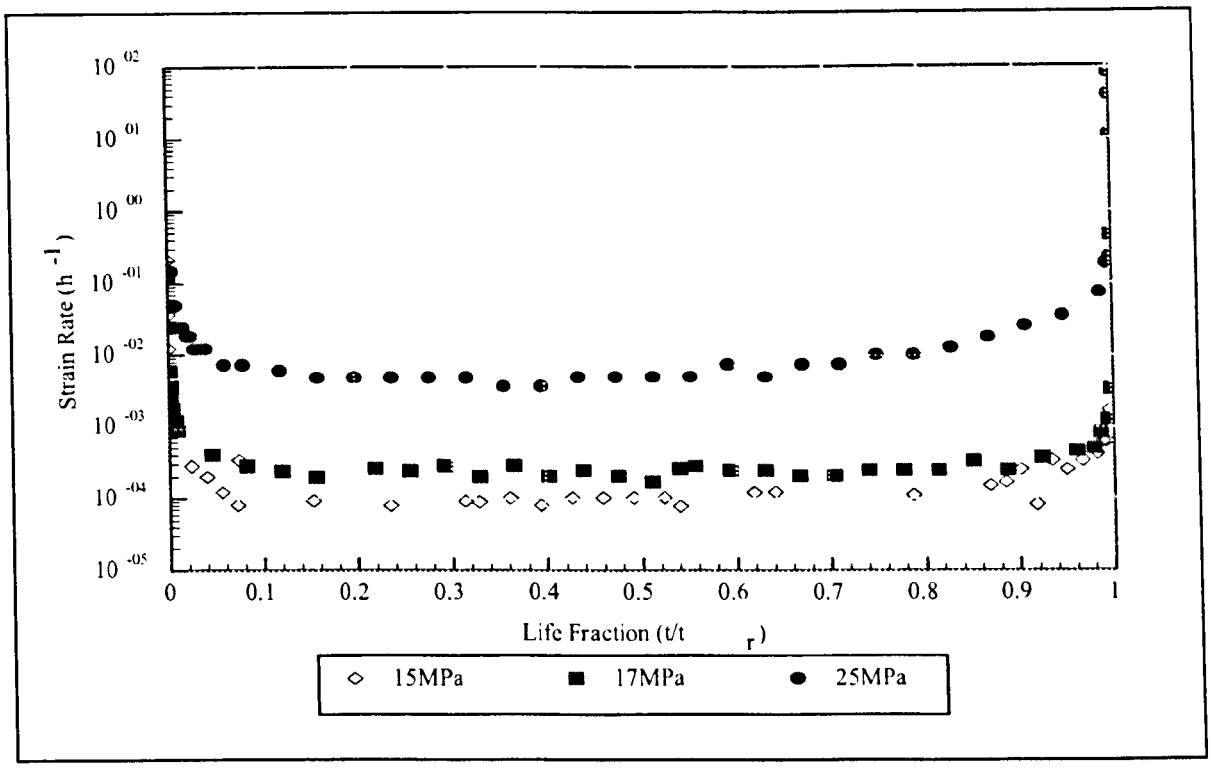
Strain Rate (h -1 )
Life Fraction (t/t r )
15MPa
17MPa
25MPa

125°C

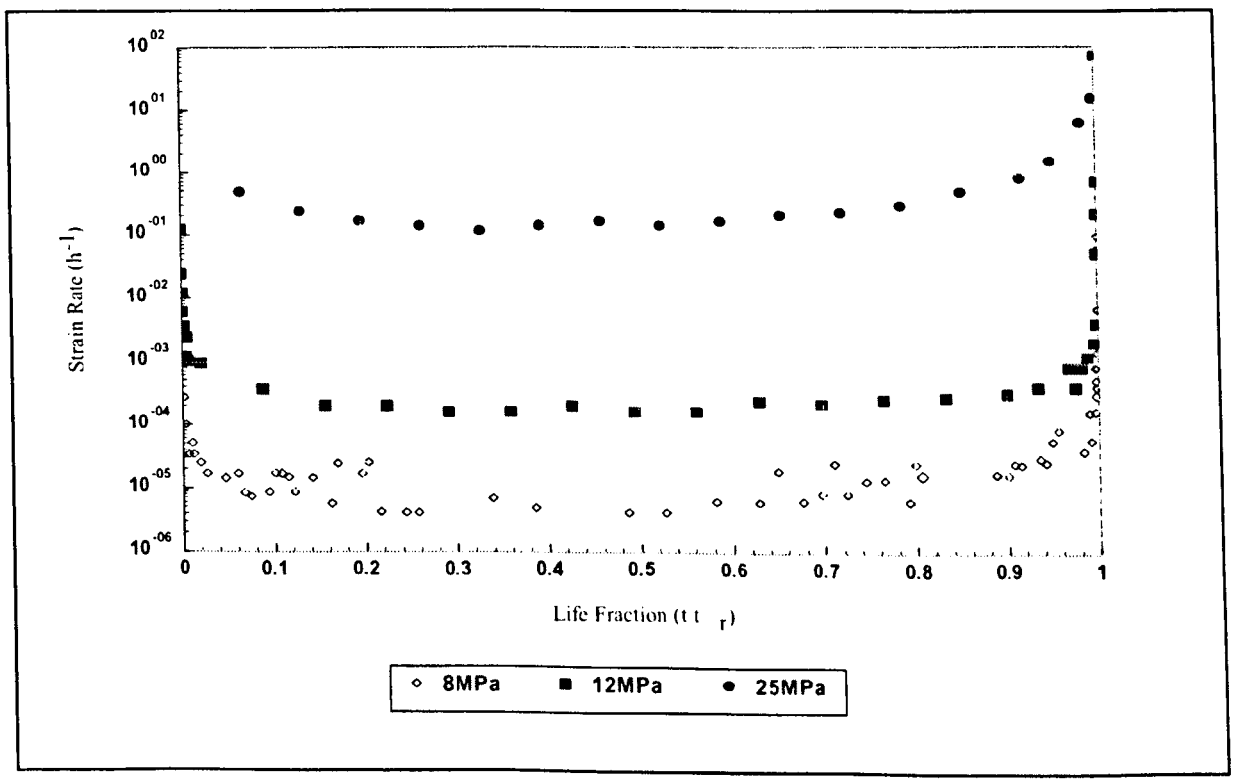
Strain Rate (h-1)
Life Fraction (t t r)
8MPa
12MPa
25MPa

## Appendix 5.4

| Temperature °C | Stress MPa | Separate measurements $\varepsilon_0$ | $\varepsilon_p$ | $\varepsilon_s$ | $\varepsilon_t$ |
|---|---|---|---|---|---|
| -10 | 38 | 0.0055 | 0.0125 | 0.024 | 0.17 |
| -10 | 40 | 0.0055 | 0.0083 | 0.022 | 0.16 |
| -10 | 45 | 0.019 | 0.015 | 0.031 | 0.13 |
| -10 | 50 | 0.011 | 0.011 | 0.018 | 0.14 |
| 29 | 40 | 0.006 | 0.006 | 0.015 | 0.203 |
| 29 | 41 | 0.009 | 0.004 | 0.009 | 0.171 |
| 29 | 30 | 0.009 | 0.007 | 0.007 | 0.153 |
| 29 | 45 | 0.0125 | 0.018 | 0.027 | 0.242 |
| 29 | 35 | 0.009 | 0.002 | 0.012 | 0.179 |
| 29 | 42.5 | 0.007 | 0.011 | 0.018 | 0.136 |
| 29 | 32 | 0.005 | 0.002 | 0.012 | 0.165 |
| 29 | 28 | 0.002 | 0.011 | 0.011 | 0.127 |
| 29 | 26 | 0.008 | 0.006 | 0.012 | 0.126 |
| 75 | 12 | - | - | - | - |
| 75 | 21 | 0.003 | 0.008 | 0.004 | 0.214 |
| 75 | 23.5 | 0.01 | 0.001 | 0.008 | 0.15 |
| 75 | 27 | 0.006 | 0.003 | 0.011 | 0.194 |
| 75 | 24 | 0.009 | 0.005 | 0.006 | 0.09 |
| 75 | 16 | 0.007 | 0.001 | 0.002 | 0.19 |
| 75 | 19.5 | 0.003 | 0.001 | 0.004 | 0.121 |
| 75 | 19 | 0.006 | 0.006 | 0.004 | 0.106 |
| 75 | 33 | 0.02 | 0.012 | 0.013 | 0.168 |
| 99.4 | 25 | 0.004 | 0.006 | 0.013 | 0.16 |
| 99.4 | 27 | 0.016 | - | 0.045 | 0.318 |
| 99.4 | 25.25 | 0.019 | 0.01 | 0.013 | 0.183 |
| 99.4 | 20 | 0.007 | 0.008 | 0.014 | 0.214 |
| 99.4 | 15 | 0.009 | 0.011 | 0.023 | 0.08 |
| 99.4 | 17 | 0.007 | 0.009 | 0.029 | 0.088 |
| 99.4 | 14 | 0.003 | 0.001 | 0.003 | 0.108 |
| 125 | 10 | 0.001 | 0.004 | 0.006 | 0.125 |
| 125 | 20 | 0.004 | 0.007 | 0.014 | 0.225 |
| 125 | 25 | 0.027 | 0.012 | 0.027 | 0.223 |
| 125 | 22.5 | 0.01 | - | 0.017 | 0.24 |
| 125 | 18 | 0.04 | 0.003 | 0.01 | 0.233 |
| 125 | 12 | 0.009 | 0.011 | 0.016 | 0.109 |
| 125 | 8 | 0.004 | 0.016 | 0.009 | 0.11 |

Separate measurements of creep strain occurring in each regime

| | | Accumulative Measurements | | |
|---|---|---|---|---|
| **Temperature** °C | **Stress** MPa | $e_0+e_p$ | $e_0+e_p+e_s$ | $e_0+e_p+e_s+e_t$ ($e_f$) |
| -10 | 38 | 0.018 | 0.042 | 0.212 |
| -10 | 40 | 0.0138 | 0.0358 | 0.1958 |
| -10 | 45 | 0.034 | 0.065 | 0.195 |
| -10 | 50 | 0.022 | 0.04 | 0.18 |
| 29 | 40 | 0.012 | 0.027 | 0.23 |
| 29 | 41 | 0.013 | 0.022 | 0.193 |
| 29 | 30 | 0.016 | 0.023 | 0.176 |
| 29 | 45 | 0.0305 | 0.0575 | 0.2995 |
| 29 | 35 | 0.011 | 0.023 | 0.202 |
| 29 | 42.5 | 0.018 | 0.036 | 0.172 |
| 29 | 32 | 0.007 | 0.019 | 0.184 |
| 29 | 28 | 0.013 | 0.024 | 0.151 |
| 29 | 26 | 0.014 | 0.026 | 0.152 |
| 75 | 12 | 0 | 0 | 0 |
| 75 | 21 | 0.011 | 0.015 | 0.229 |
| 75 | 23.5 | 0.011 | 0.019 | 0.169 |
| 75 | 27 | 0.009 | 0.02 | 0.214 |
| 75 | 24 | 0.014 | 0.02 | 0.11 |
| 75 | 16 | 0.008 | 0.01 | 0.2 |
| 75 | 19.5 | 0.004 | 0.008 | 0.129 |
| 75 | 19 | 0.012 | 0.016 | 0.122 |
| 75 | 33 | 0.032 | 0.045 | 0.213 |
| 99.4 | 25 | 0.01 | 0.023 | 0.183 |
| 99.4 | 27 | 0.016 | 0.061 | 0.379 |
| 99.4 | 25.25 | 0.029 | 0.042 | 0.225 |
| 99.4 | 20 | 0.015 | 0.029 | 0.243 |
| 99.4 | 15 | 0.02 | 0.043 | 0.123 |
| 99.4 | 17 | 0.016 | 0.045 | 0.133 |
| 99.4 | 14 | 0.004 | 0.007 | 0.115 |
| 125 | 10 | 0.005 | 0.011 | 0.136 |
| 125 | 20 | 0.011 | 0.025 | 0.25 |
| 125 | 25 | 0.039 | 0.066 | 0.289 |
| 125 | 22.5 | 0.01 | 0.027 | 0.267 |
| 125 | 18 | 0.043 | 0.053 | 0.286 |
| 125 | 12 | 0.02 | 0.036 | 0.145 |
| 125 | 8 | 0.02 | 0.029 | 0.139 |

Accumulative measurements of creep strain occurring in during creep life

## Appendix 5.5

| Temperature (°C) | Stress (MPa) | $\%\varepsilon_p$ | $\%\varepsilon_s$ | $\%\varepsilon_t$ |
|---|---|---|---|---|
| -10 | 38 | 6% | 12% | 82% |
| -10 | 40 | 4% | 12% | 84% |
| -10 | 45 | 9% | 18% | 74% |
| -10 | 50 | 7% | 11% | 83% |
| 29 | 40 | 3% | 7% | 91% |
| 29 | 41 | 2% | 5% | 93% |
| 29 | 30 | 4% | 4% | 92% |
| 29 | 45 | 6% | 9% | 84% |
| 29 | 35 | 1% | 6% | 93% |
| 29 | 42.5 | 7% | 11% | 82% |
| 29 | 32 | 1% | 7% | 92% |
| 29 | 28 | 7% | 7% | 85% |
| 29 | 26 | 4% | 8% | 88% |
| 75 | 12 | - | - | - |
| 75 | 21 | 4% | 2% | 95% |
| 75 | 23.5 | 1% | 5% | 94% |
| 75 | 27 | 1% | 5% | 93% |
| 75 | 24 | 5% | 6% | 89% |
| 75 | 16 | 1% | 1% | 98% |
| 75 | 19.5 | 1% | 3% | 96% |
| 75 | 19 | 5% | 3% | 91% |
| 75 | 33 | 6% | 7% | 87% |
| 99.4 | 25 | 3% | 7% | 89% |
| 99.4 | 27 | 0% | 12% | 88% |
| 99.4 | 25.25 | 5% | 6% | 89% |
| 99.4 | 20 | 3% | 6% | 91% |
| 99.4 | 15 | 10% | 20% | 70% |
| 99.4 | 17 | 7% | 23% | 70% |
| 99.4 | 14 | 1% | 3% | 96% |
| 125 | 10 | 3% | 4% | 93% |
| 125 | 20 | 3% | 6% | 91% |
| 125 | 25 | 5% | 10% | 85% |
| 125 | 22.5 | 0% | 7% | 93% |
| 125 | 18 | 1% | 4% | 95% |
| 125 | 12 | 8% | 12% | 80% |
| 125 | 8 | 12% | 7% | 81% |

Percentage of creep life in each regime as determined by creep strain (omitting instantaneous strain)

| Temperature °C | Shear Stress MPa | Time to Rupture (h) | Shear Strain to Failure | Min Shear Strain Rate (h -1) | Stress MPa | Strain to Failure | Min Strain Rate (h -1) |
|---|---|---|---|---|---|---|---|
| 29 | 31.8 | 0.42 | 4.145 | 0.36144000 | 55.08 | 2.393 | 0.20868100 |
| 29 | 29.7 | 0.58 | 3.361 | 0.18072200 | 51.44 | 1.940 | 0.10434000 |
| 29 | 21.2 | 3.75 | 1.510 | 0.00312500 | 36.72 | 0.872 | 0.00180400 |
| 29 | 15.9 | 154.73 | 1.930 | 0.00033784 | 27.54 | 1.114 | 0.00078000 |
| 29 | 10.6 | 441.27 | 3.293 | 0.00016670 | 18.36 | 1.901 | 0.00009620 |
| 29 | 9.6 | 767.40 | 3.600 | 0.00004900 | 16.63 | 2.078 | 0.00002860 |
| 75 | 10.6 | 132.53 | 1.810 | 0.00030488 | 18.36 | 1.045 | 0.00017600 |
| 75 | 15.9 | 10.83 | 1.232 | 0.00304880 | 27.54 | 0.711 | 0.00176000 |
| 75 | 18 | 2.55 | 2.096 | 0.01807229 | 31.18 | 1.210 | 0.01043400 |
| 75 | 6.4 | 1134.50 | 1.689 | 0.00006987 | 11.09 | 0.975 | 0.00003670 |
| 75 | 8.5 | 555.70 | 1.650 | 0.00010160 | 14.72 | 0.953 | 0.00005870 |
| 75 | 20.2 | 0.53 | 2.214 | 0.07142857 | 34.99 | 1.278 | 0.04123900 |
| 125 | 3.2 | 2.00 | 0.475 | 0.04687500 | 5.54 | 0.274 | 0.02706300 |
| 125 | 2.1 | 300.9 | 1.65 | 0.00046875 | 3.64 | 0.953 | 0.000271 |

# Appendix 5.6

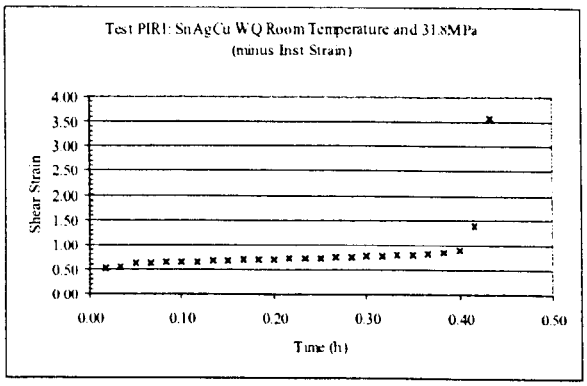
Test PIR1: SnAgCu WQ Room Temperature and 31.8MPa
(minus Inst Strain)
Shear Strain
Time (h)

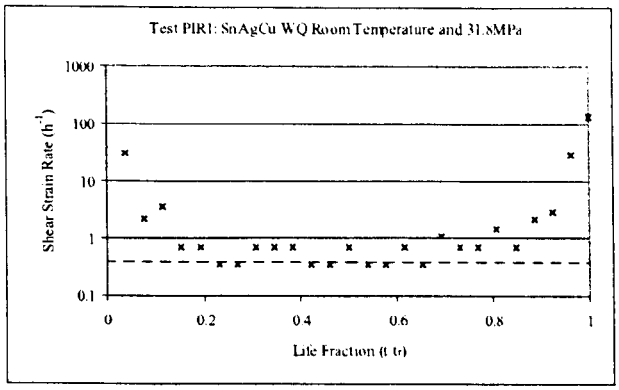
Test PIR1: SnAgCu WQ Room Temperature and 31.8MPa
Shear Strain Rate (h-1)
Life Fraction (t/tf)

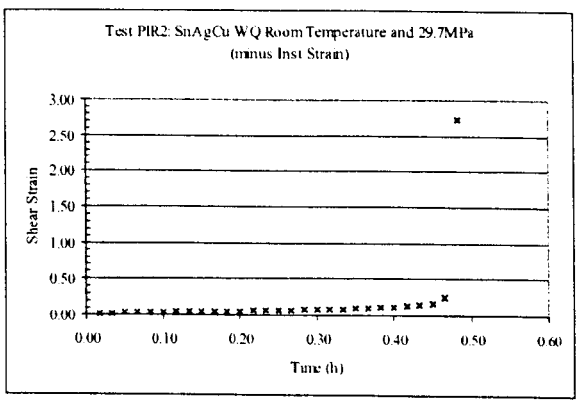
Test PIR2: SnAgCu WQ Room Temperature and 29.7MPa
(minus Inst Strain)
Shear Strain
Time (h)

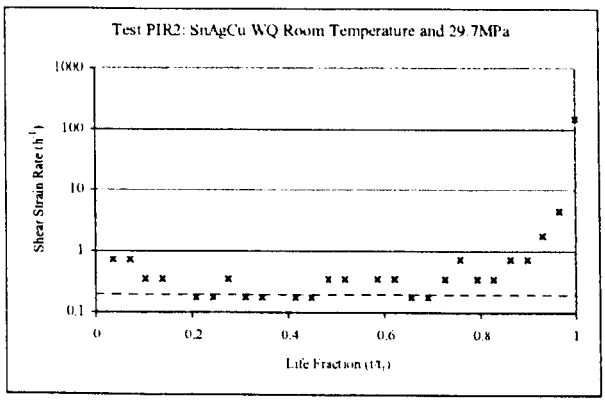
Test PIR2: SnAgCu WQ Room Temperature and 29.7MPa
Shear Strain Rate (h-1)
Life Fraction (t/tf)

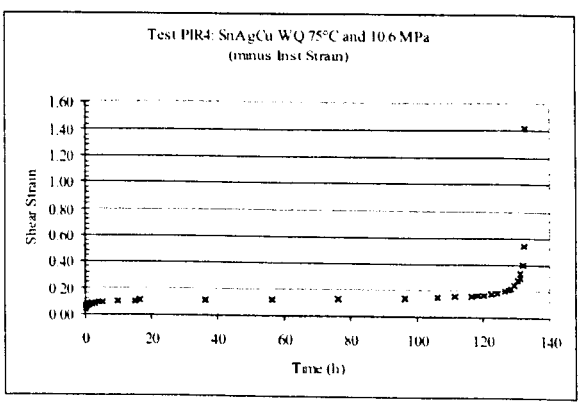
Test PIR4: SnAgCu WQ 75°C and 10.6MPa
(minus Inst Strain)
Shear Strain
Time (h)

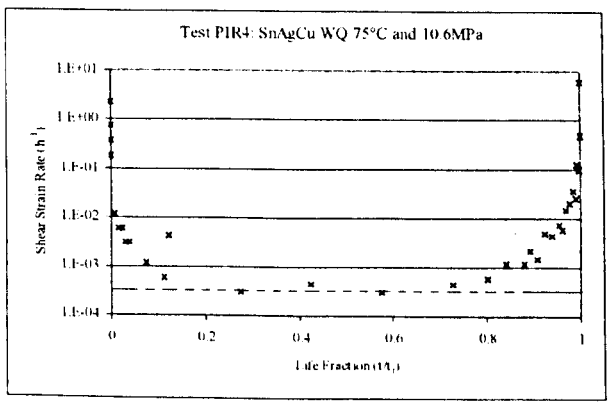
Test PIR4: SnAgCu WQ 75°C and 10.6MPa
Shear Strain Rate (h-1)
Life Fraction (t/tf)

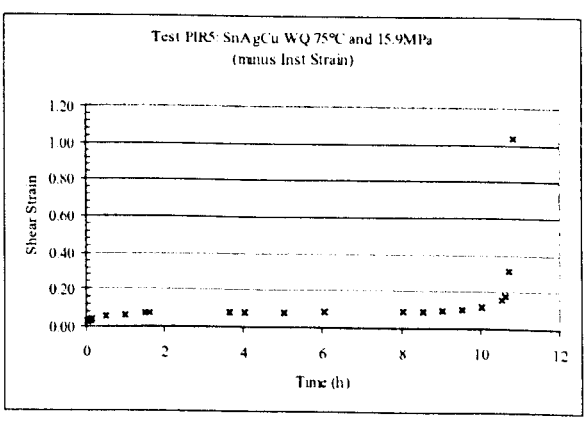
Test PIR5: SnAgCu WQ 75°C and 15.9MPa
(minus Inst Strain)
Shear Strain
Time (h)

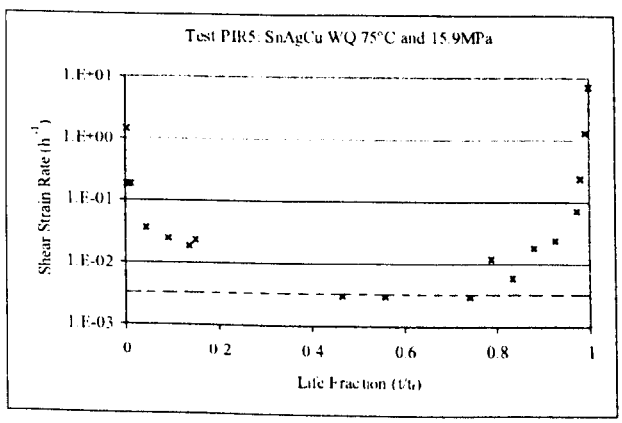
Test PIR5: SnAgCu WQ 75°C and 15.9MPa
Shear Strain Rate (h-1)
Life Fraction (t/tf)

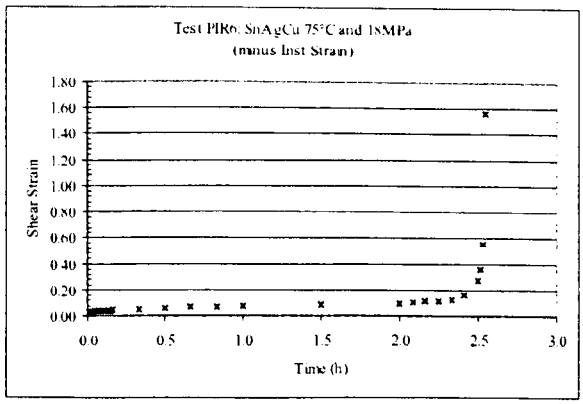
Test PIR6: SnAgCu 75°C and 18MPa
(minus Inst Strain)
Shear Strain
Time (h)

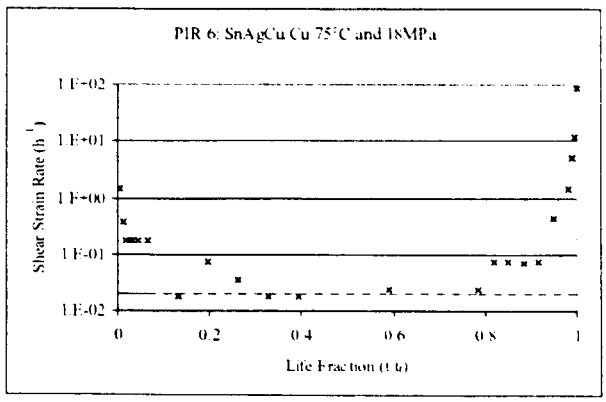
PIR 6: SnAgCu Cu 75°C and 18MPa
Shear Strain Rate (h⁻¹)
Life Fraction (t/tf)

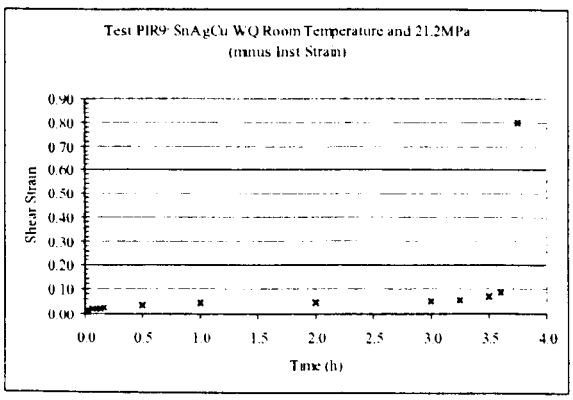
Test PIR9: SnAgCu WQ Room Temperature and 21.2MPa
(minus Inst Strain)
Shear Strain
Time (h)

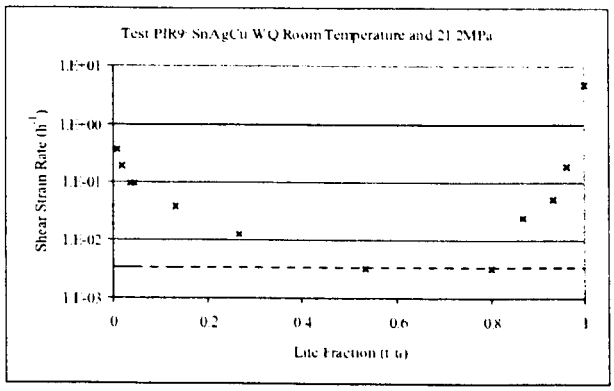
Test PIR9: SnAgCu WQ Room Temperature and 21.2MPa
Shear Strain Rate (h⁻¹)
Life Fraction (t/tf)

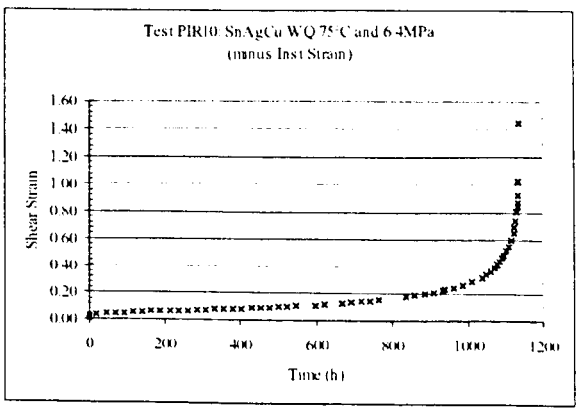
Test PIR10: SnAgCu WQ 75°C and 6.4MPa
(minus Inst Strain)
Shear Strain
Time (h)

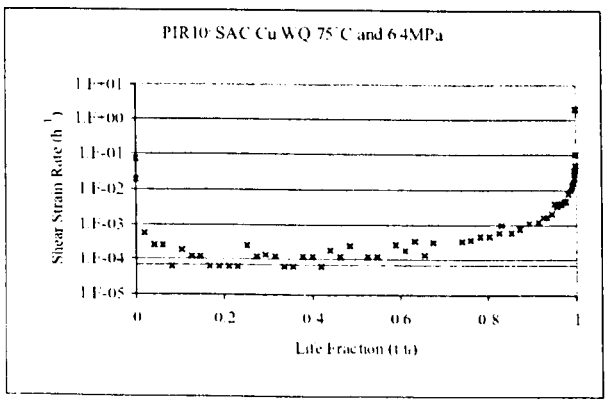
PIR10: SAC Cu WQ 75°C and 6.4MPa
Shear Strain Rate (h⁻¹)
Life Fraction (t/tf)

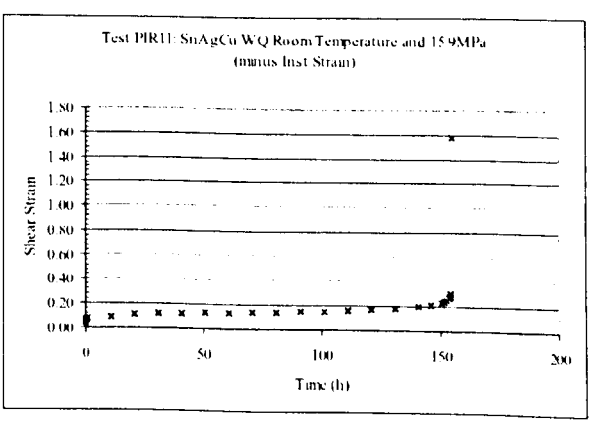
Test PIR11: SnAgCu WQ Room Temperature and 15.9MPa
(minus Inst Strain)
Shear Strain
Time (h)

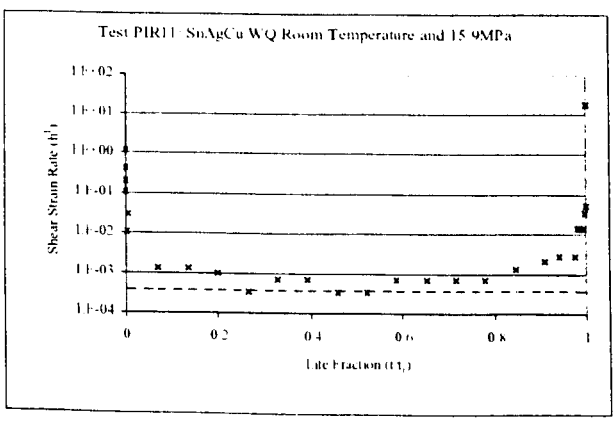
Test PIR11: SnAgCu WQ Room Temperature and 15.9MPa
Shear Strain Rate (h⁻¹)
Life Fraction (t/tf)

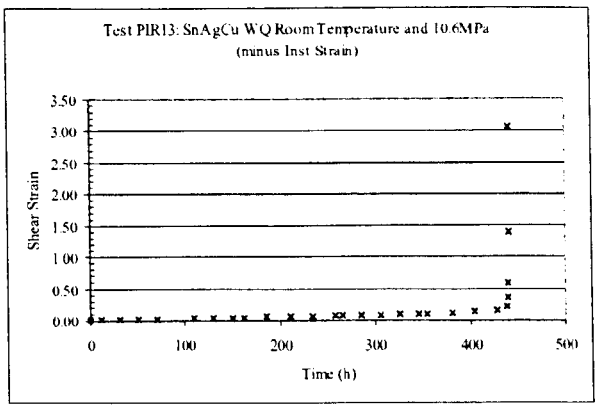
Test PIR13: SnAgCu WQ Room Temperature and 10.6MPa
(minus Inst Strain)
Shear Strain
Time (h)

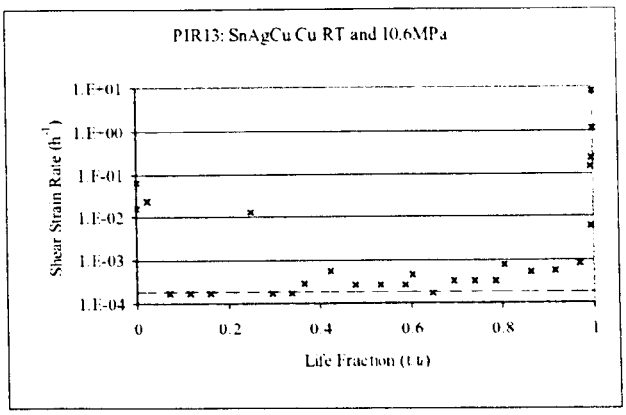
PIR13: SnAgCu Cu RT and 10.6MPa
Shear Strain Rate (h-1)
Life Fraction (Lf)

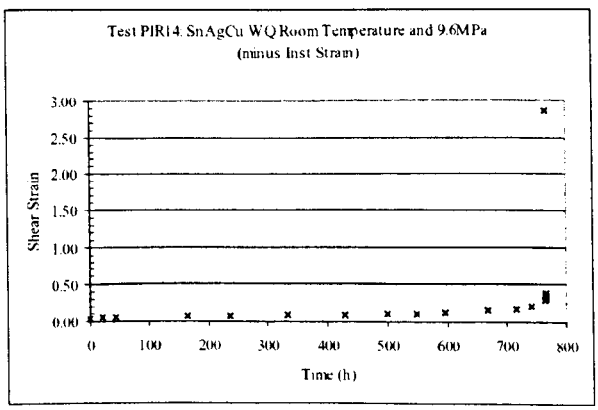
Test PIR14: SnAgCu WQ Room Temperature and 9.6MPa
(minus Inst Strain)
Shear Strain
Time (h)

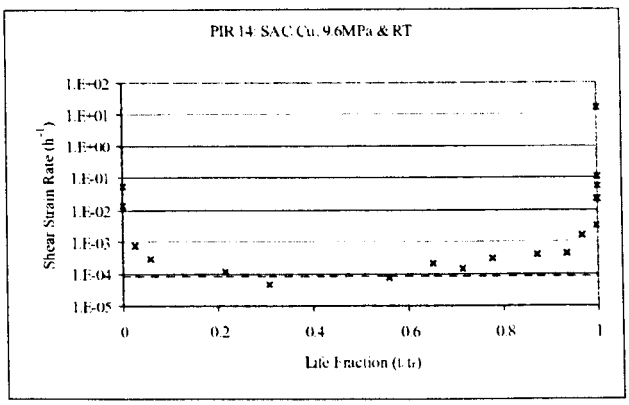
PIR 14: SAC Cu, 9.6MPa & RT
Shear Strain Rate (h-1)
Life Fraction (Lf)

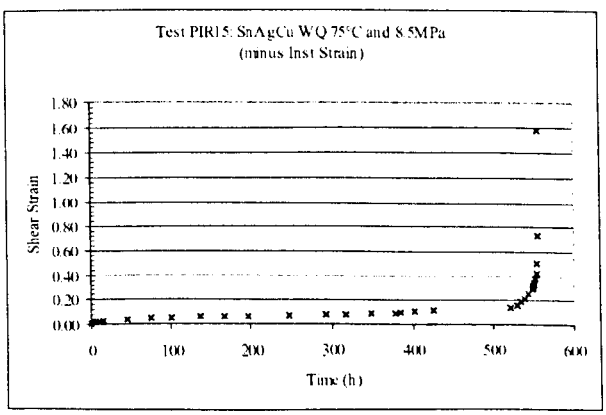
Test PIR15: SnAgCu WQ 75°C and 8.5MPa
(minus Inst Strain)
Shear Strain
Time (h)

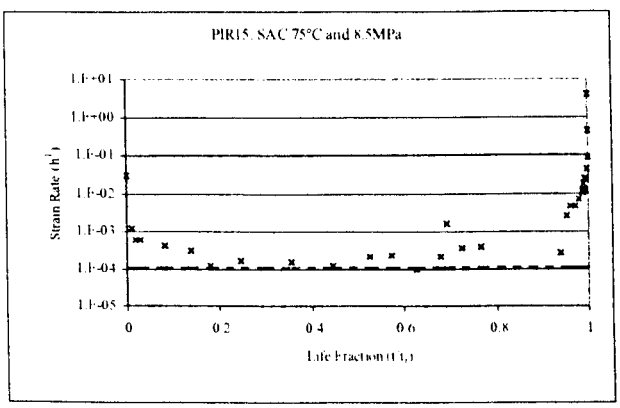
PIR15: SAC 75°C and 8.5MPa
Strain Rate (h-1)
Life Fraction (Lf)

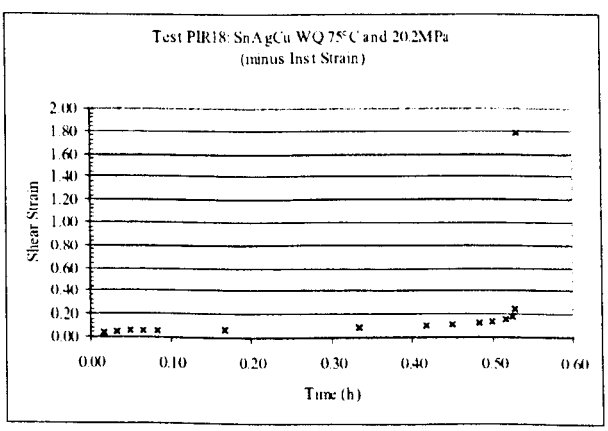
Test PIR18: SnAgCu WQ 75°C and 20.2MPa
(minus Inst Strain)
Shear Strain
Time (h)

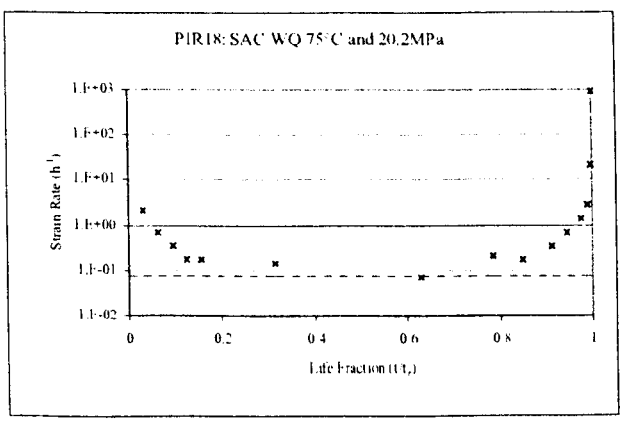
PIR18: SAC WQ 75°C and 20.2MPa
Strain Rate (h-1)
Life Fraction (Lf)

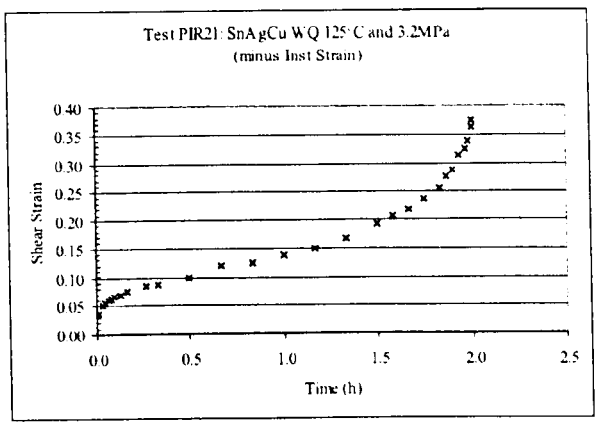
Test PIR21: SnAgCu WQ 125°C and 3.2MPa
(minus Inst Strain)
Shear Strain
0.40
0.35
0.30
0.25
0.20
0.15
0.10
0.05
0.00
0.0
0.5
1.0
1.5
2.0
2.5
Time (h)

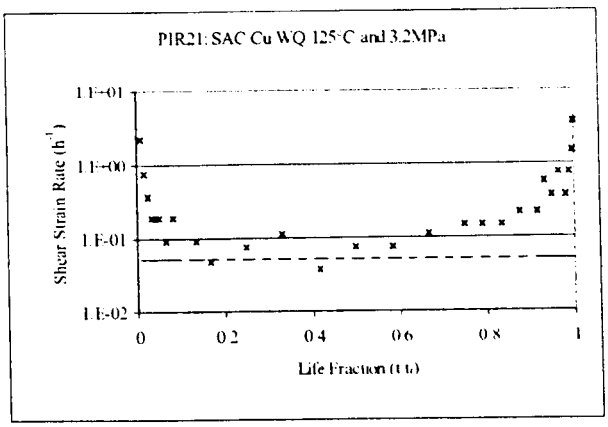
PIR21: SAC Cu WQ 125°C and 3.2MPa
Shear Strain Rate (h⁻¹)
1.E+01
1.E+00
1.E-01
1.E-02
0
0.2
0.4
0.6
0.8
1
Life Fraction (t/tf)

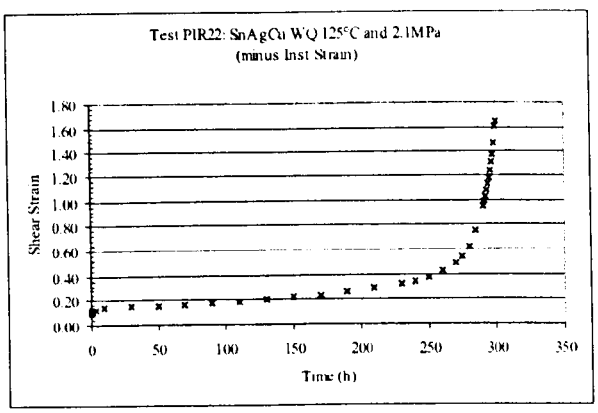
Test PIR22: SnAgCu WQ 125°C and 2.1MPa
(minus Inst Strain)
Shear Strain
1.80
1.60
1.40
1.20
1.00
0.80
0.60
0.40
0.20
0.00
0
50
100
150
200
250
300
350
Time (h)

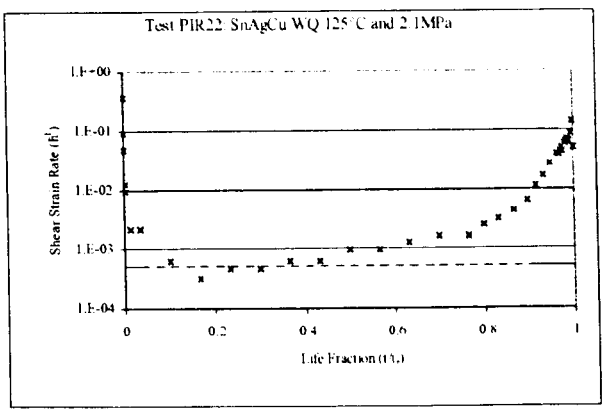
Test PIR22: SnAgCu WQ 125°C and 2.1MPa
Shear Strain Rate (h⁻¹)
1.E+00
1.E-01
1.E-02
1.E-03
1.E-04
0
0.2
0.4
0.6
0.8
1
Life Fraction (t/tf)

APPENDIX 5.7: SECTION OF CHART RECORDER PLOT OF SHEAR STRAIN VS. TIME (to illustrate the difficulty in measuring strain at failure)

(PIR15 - 8.5MPa @ 75°C $t_r$ ~ 555h)

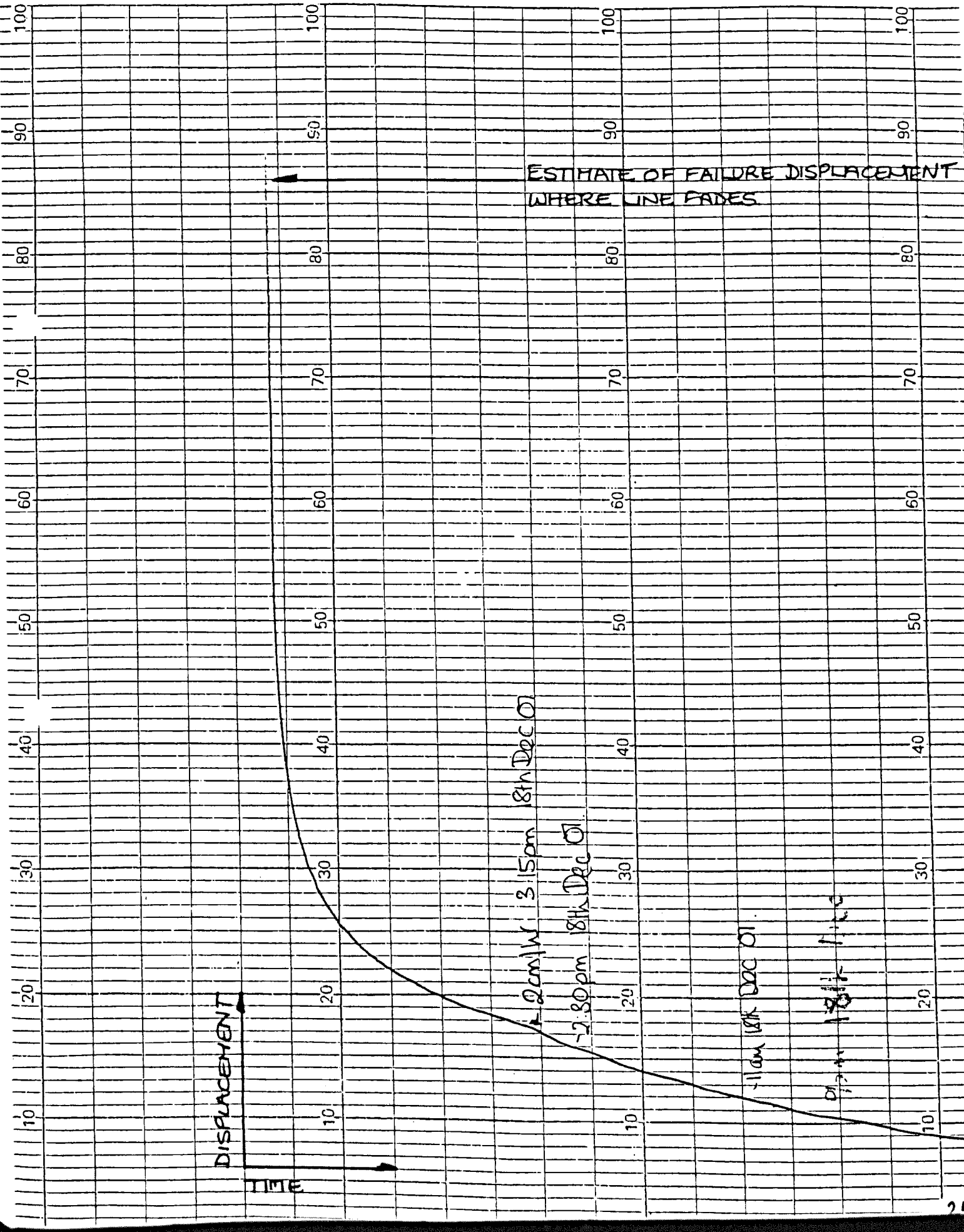

## Appendix 5.8

Effect of stress on strain rate at 29°C

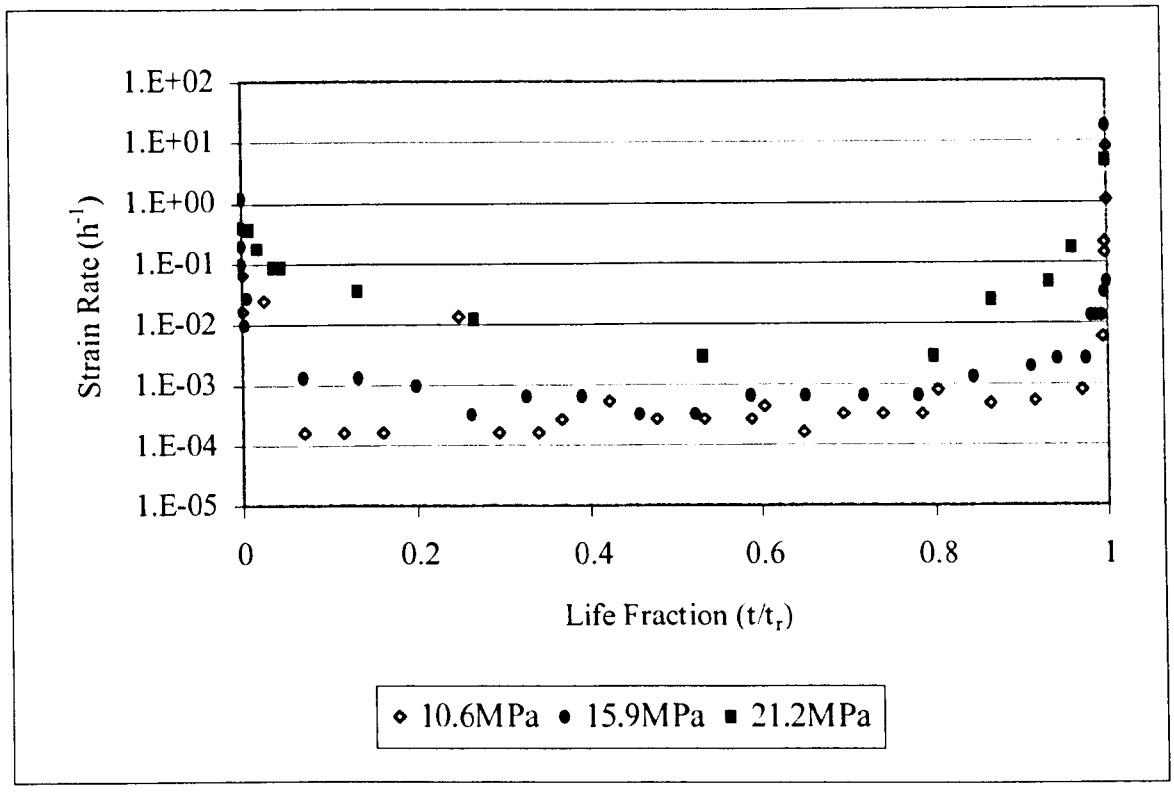


(Effect of stress on strain rate has not been examined at 125°C. This is because only two data points are currently available and data obtained at this temperature have proven to be unreliable when repeat tests were performed)

**Appendix 5.9**

| | | Separate Measurements | | |
|---|---|---|---|---|
| **Temperature** °C | **Stress** MPa | $e_p$ | $e_s$ | $e_t$ |
| 29 | 9.6 | 0.083 | 0.042 | 2.833 |
| 29 | 10.6 | 0.036 | 0.036 | 3.071 |
| 29 | 15.9 | 0.15 | 0.063 | 1.425 |
| 29 | 21.2 | 0.033 | 0.017 | 0.783 |
| 29 | 29.7 | 0.042 | 0.083 | 2.75 |
| 29 | 31.8 | 0.636 | 0.136 | 2.863 |
| 75 | 6.4 | 0.055 | 0.055 | 1.363 |
| 75 | 8.5 | 0.055 | 0.036 | 1.509 |
| 75 | 10.6 | 0.1 | 0.04 | 1.3 |
| 75 | 15.9 | 0.071 | 0.036 | 0.971 |
| 75 | 18 | 0.05 | 0.05 | 1.525 |
| 75 | 20.2 | 0.05 | 0.05 | 1.725 |
| 125 | 2.1 | 0.055 | 0.091 | 1.45 |
| 125 | 3.2 | 0.09 | 0.075 | 0.205 |

a) Separate measurements of creep strain occurring in each creep regime (omitting instantaneous strain)

| | | Accumulative Measurements | |
|---|---|---|---|
| **Temperature** °C | **Stress** MPa | $e_p+e_s$ | $e_p+e_s+e_t$ ($e_f$) |
| 29 | 9.6 | 0.125 | 2.958 |
| 29 | 10.6 | 0.072 | 3.143 |
| 29 | 15.9 | 0.213 | 1.638 |
| 29 | 21.2 | 0.05 | 0.833 |
| 29 | 29.7 | 0.125 | 2.875 |
| 29 | 31.8 | 0.772 | 3.635 |
| 75 | 6.4 | 0.11 | 1.473 |
| 75 | 8.5 | 0.091 | 1.6 |
| 75 | 10.6 | 0.14 | 1.44 |
| 75 | 15.9 | 0.107 | 1.078 |
| 75 | 18 | 0.1 | 1.625 |
| 75 | 20.2 | 0.1 | 1.825 |
| 125 | 2.1 | 0.146 | 1.596 |
| 125 | 3.2 | 0.165 | 0.37 |

b) Accumulative measurements of creep strain occurring during creep life (omitting instantaneous strain)

## Appendix 5.10

| Temperature °C | Stress MPa | $\%e_p$ | $\%e_s$ | $\%e_t$ |
|---|---|---|---|---|
| 29 | 9.6 | 3% | 1% | 96% |
| 29 | 10.6 | 1% | 1% | 98% |
| 29 | 15.9 | 9% | 4% | 87% |
| 29 | 21.2 | 4% | 2% | 94% |
| 29 | 29.7 | 1% | 3% | 96% |
| 29 | 31.8 | 17% | 4% | 79% |
| 75 | 6.4 | 4% | 4% | 93% |
| 75 | 8.5 | 3% | 2% | 94% |
| 75 | 10.6 | 7% | 3% | 90% |
| 75 | 15.9 | 7% | 3% | 90% |
| 75 | 18 | 3% | 3% | 94% |
| 75 | 20.2 | 3% | 3% | 95% |
| 125 | 2.1 | 3% | 6% | 91% |
| 125 | 3.2 | 24% | 20% | 55% |

Percentage of creep life in each regime as determined by creep strain (omitting instantaneous strain)

## Appendix 6.1 Trend lines for figures using a 'best fit' plot.

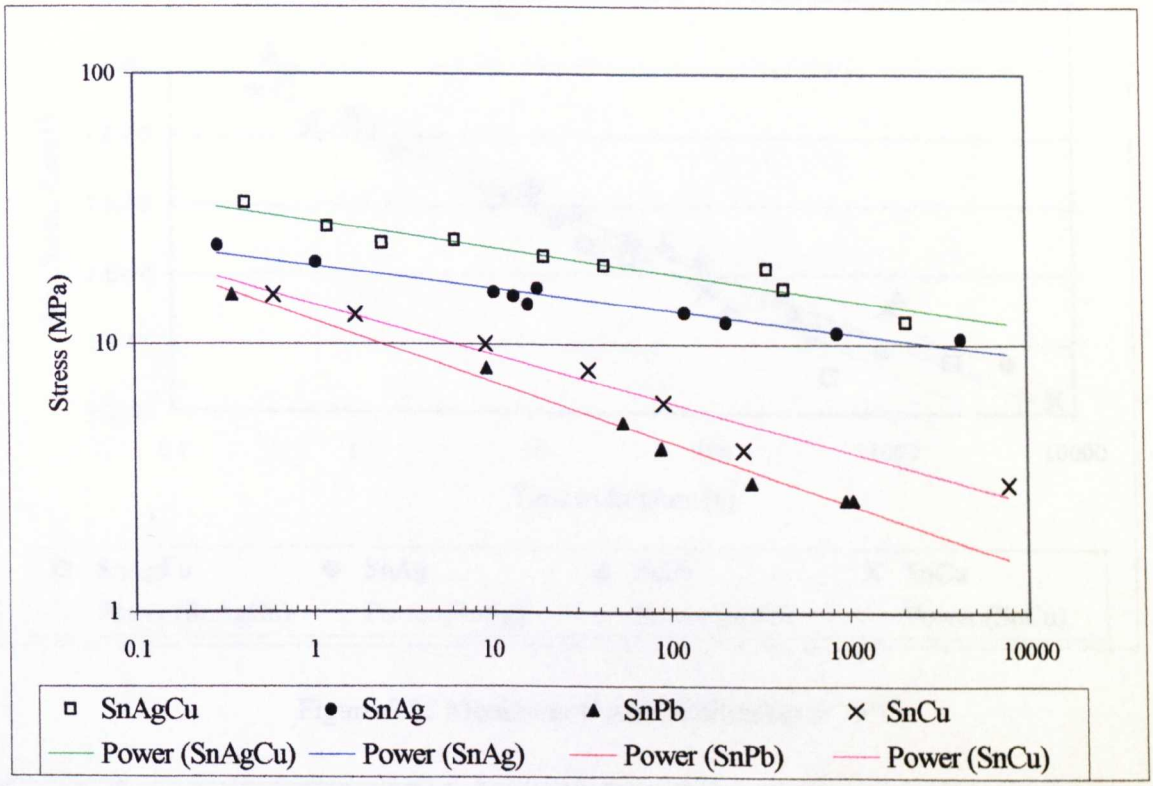


Figure 6.8 Time to rupture of solder alloys tested at 75°C

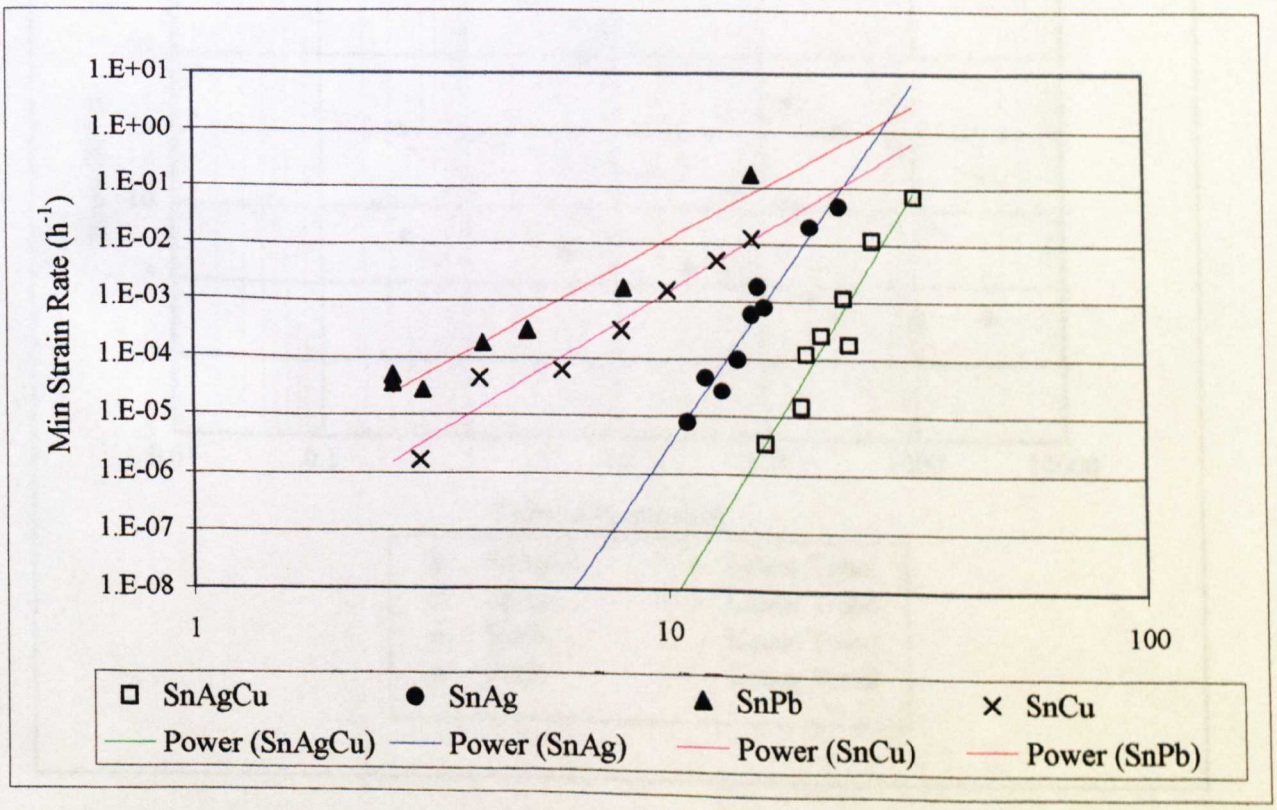


Figure 6.9 Minimum strain rate vs. stress plot at 75°C

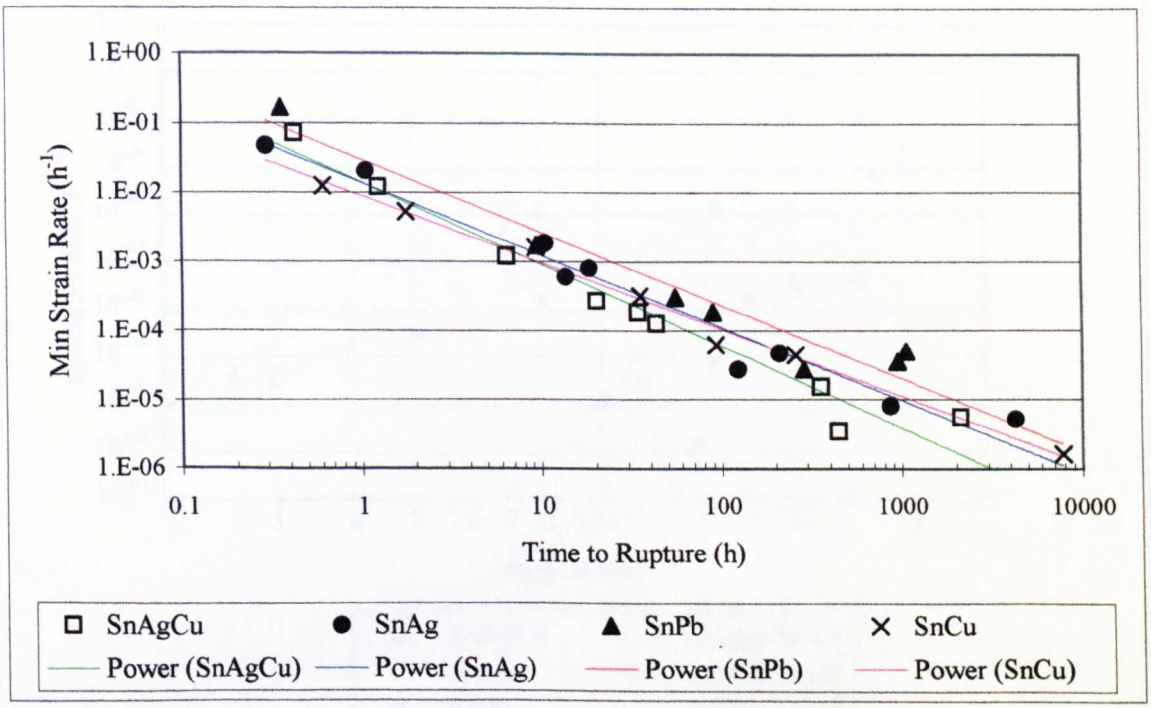


Figure 6.12 Monkman-Grant relationship at 75°C

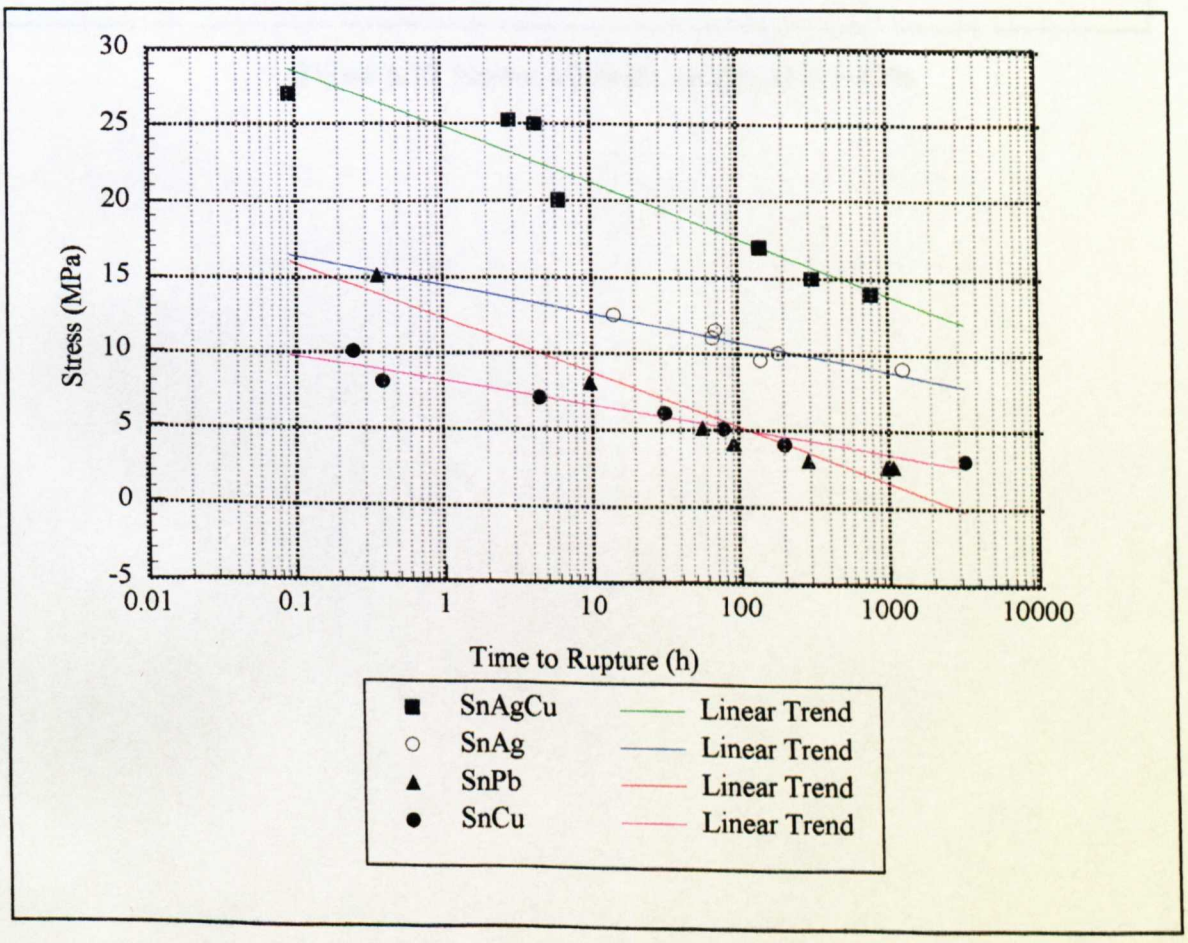


Figure 6.15 Time to rupture at $T_h = 0.76$

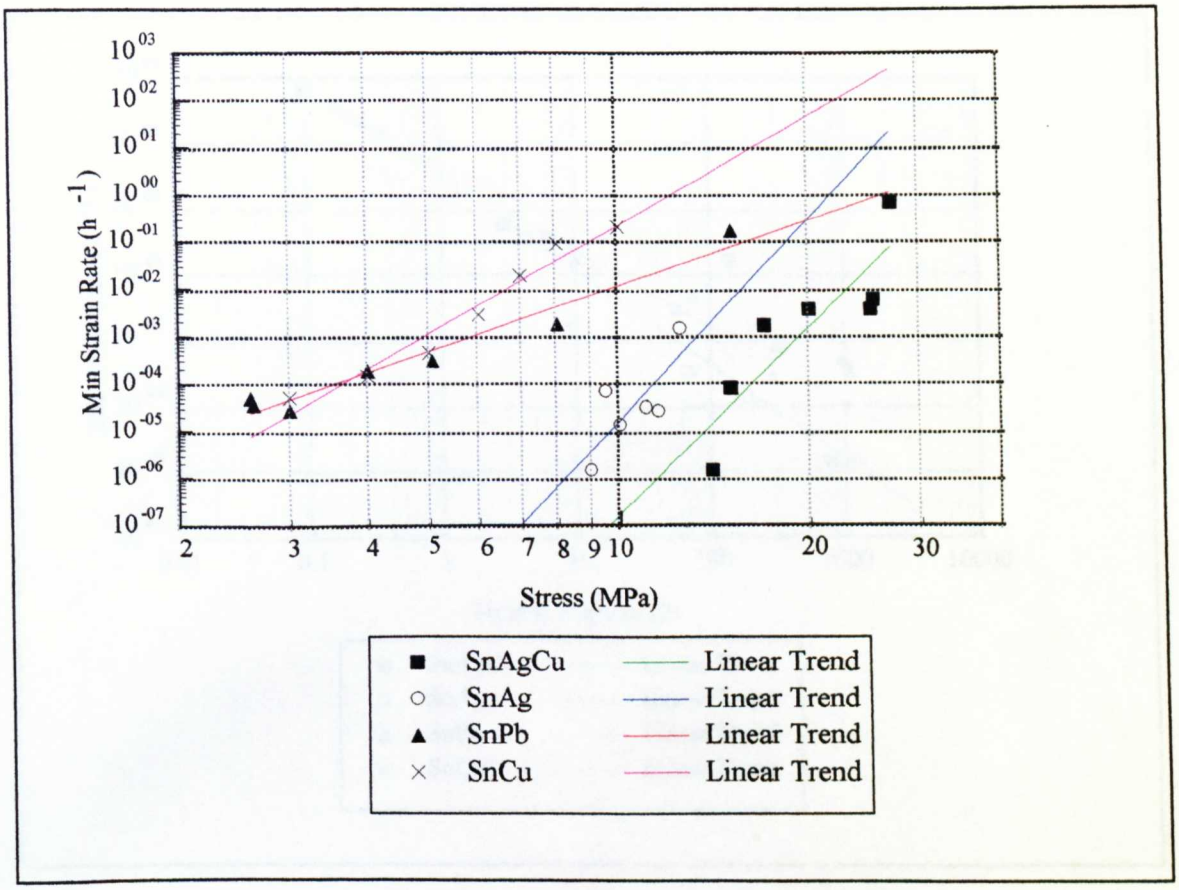


Figure 6.17 Norton's Power Law plot at $T_h = 0.76$

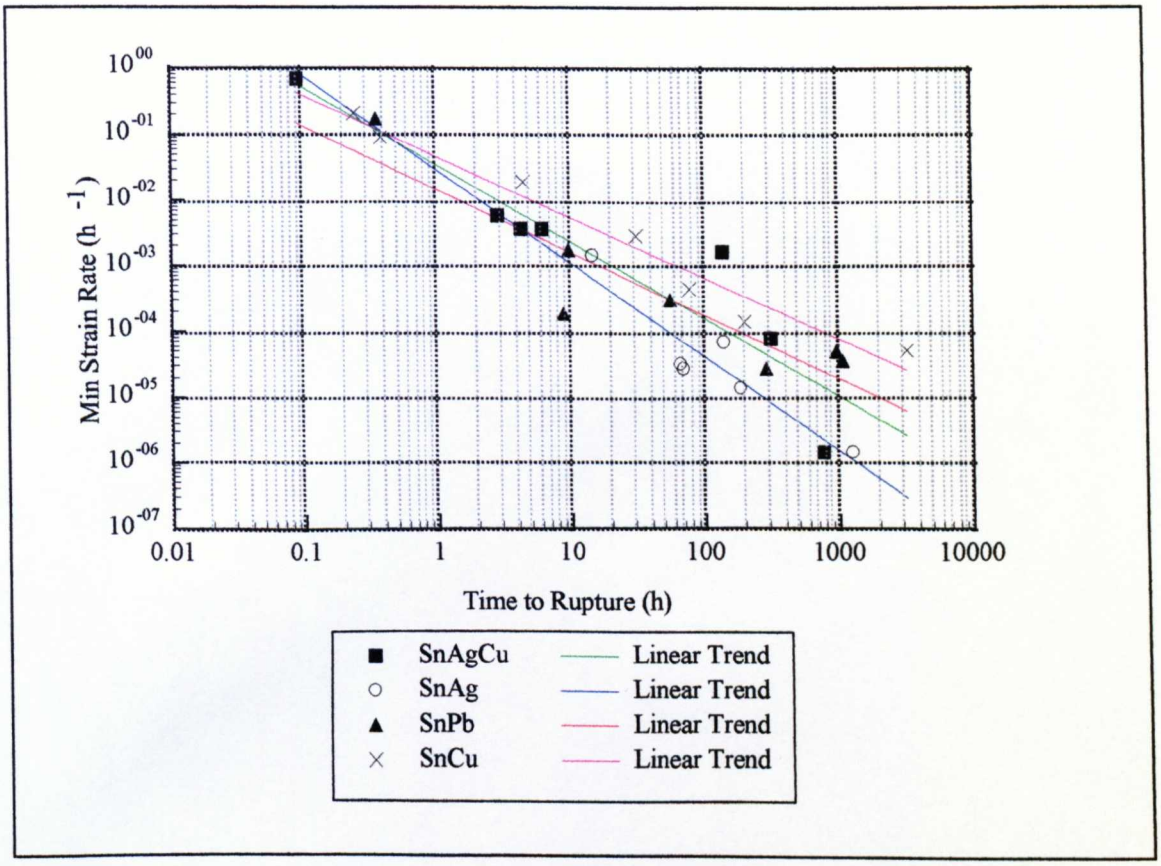


Figure 6.18 Monkman-Grant Plot at $T_h = 0.76$